Electronic Supporting Information

Hemiparetic Koneramine NNP Ligand Comprising Strategic Hard and Soft Donors: Transition Metal Complexes, CS_2 Activation and Therapeutic Potential

Archana Yadav,[a] Sayari Dewan,[a] Kajal Chaudhary,[a] Ray J. Butcher,[b] Ritika Gautam Singh[a] and Raja Angamuthu*[a]

[a] Department of Chemistry, Indian Institute of Technology Kanpur, Kanpur 208016, India.

[b] Department of Chemistry, Howard University, Washington, D.C, 20059, USA.

* All correspondence should be addressed to raja@iitk.ac.in

Table of contents:

Figure S 1. ^{1}H NMR spectrum of the (1) and (2) in $CDCl_3$ at 298 K. 26

Figure S 2. ^{31}P NMR spectrum of the (1) and (2) in $CDCl_3$ at 298 K. 27

Figure S 3.^{1}H NMR spectrum of the N^1-(2-(diphenylphosphaneyl)benzyl)-N^2-phenylethane-1,2-diamine (3) in $CDCl_3$ at 298 K. 28

Figure S 4. ^{13}C NMR spectrum of the N^1-(2-(diphenylphosphaneyl)benzyl)-N^2-phenylethane-1,2-diamine (3) in $CDCl_3$ at 298 K. 29

Figure S 5. ^{31}P NMR spectrum of the N^1-(2-(diphenylphosphaneyl)benzyl)-N^2-phenylethane-1,2-diamine (3) in $CDCl_3$ at 298 K. 30

Figure S 6. ^{1}H NMR spectrum of the NNP in $CDCl_3$ at 298 K. 31

Figure S 7. ^{13}C NMR spectrum of the NNP in $CDCl_3$ at 298 K. 32

Figure S 8. ^{31}P NMR spectrum of the NNP in $CDCl_3$ at 298 K. 33

Figure S 9. ESI-MS of NNP 34

Figure S 10. Simulated ESI-MS of NNP 35

Figure S 11. ^{1}H NMR of $[Zn(NNP)Cl_2]$ complex in $CDCl_3$ at 298 K. 36

Figure S 12. ^{13}C NMR of $[Zn(NNP)Cl_2]$ complex in $CDCl_3$ at 298 K. 37

Figure S 13. ^{31}P NMR of $[Zn(NNP)Cl_2]$ complex in $CDCl_3$ at 298 K. 38

Figure S 14. Elemental analysis of $[Zn(NNP)Cl_2]$ complex. 39

Figure S 15. ESI-MS of $[Zn(NNP)Cl_2]$ complex. 40

Figure S 16. ESI-MS of $[Ni(NNP)Cl_2]\cdot CH_3CN$ 41

Figure S 17. Simulated ESI-MS of $[Ni(NNP)Cl_2]\cdot CH_3CN$ complex. 42

Figure S 18. Elemental analysis of $[Ni(NNP)Cl_2]\cdot CH_3CN$ complex. 43

Figure S 19. Cyclic voltammogram of $[Ni(NNP)Cl_2]\cdot CH_3CN$ 44

Figure S 20. ^{1}H NMR spectrum of the [Pd(NNP)Cl][Cl] in $CDCl_3$ at 298 K. 45

Figure S 21. ^{13}C NMR spectrum of the [Pd(NNP)Cl][Cl] in $CDCl_3$ at 298 K. 46

Figure S 22. ^{31}P NMR spectrum of the [Pd(NNP)Cl][Cl] in $CDCl_3$ at 298 K. 47

Figure S 23. Elemental analysis of [Pd(NNP)Cl][Cl]. 48

Figure S 24. ESI-MS of [Pd(NNP)Cl][Cl].....49

Figure S 25. Simulated ESI-MS of [Pd(NNP)Cl][Cl] 50

Figure S 26. ^{1}H NMR spectrum of the [Pd(NNP)($SPhCH_3$)][Cl] in $CDCl_3$ at 298 K. 51

Figure S 27. ^{13}C NMR spectrum of the [Pd(NNP)($SPhCH_3$)][Cl] in $CDCl_3$ at 298 K. 52

Figure S 28. ^{31}P NMR spectrum of the [Pd(NNP)($SPhCH_3$)][Cl] in $CDCl_3$ at 298 K.....53

Figure S 29. ESI-MS of [Pd(NNP)($SPhCH_3$)][Cl] 54

Figure S 30. Simulated ESI-MS of [(NNP)Pd($SPhCH_3$)][Cl] 55

Figure S 31. ^{1}H NMR spectrum of the [Pd(NNP)($SPhCH_3$)][PF_6] in $CDCl_3$ at 298 K. 56

Figure S 32. ^{31}P NMR spectrum of the [Pd(NNP)($SPhCH_3$)][PF_6] in $CDCl_3$ at 298 K. 57

Figure S 33. ^{1}H NMR spectrum of [Ru(NNP)(PPh_3)Cl_2] complex in $CDCl_3$ at 298 K. 58

Figure S 34. ^{31}P NMR spectrum of [Ru(NNP)(PPh_3)Cl_2] complex in $CDCl_3$ at 298 K. 59

Figure S 35. Elemental analysis of [Ru(NNP)(PPh_3)Cl_2] complex. 60

Figure S 36. ESI-MS of [Ru(NNP)(PPh_3)Cl_2] 61

Figure S 37. Simulated ESI-MS of [Ru(NNP)(PPh_3)Cl_2]. 62

Figure S 38. ^{1}H NMR spectrum of the *rac*-[(NNP)Ru(H)(CO)Cl] (crude) in $CDCl_3$ at 298 K. 63

Figure S 39. ^{31}P NMR spectrum of the *rac*-[Ru(NNP)(H)Cl(CO)] (crude) in $CDCl_3$ at 298 K. 64

Figure S 40. ^{1}H NMR spectrum of the *anti-rac*-[Ru(NNP)(H)Cl(CO)] in $CDCl_3$ at 298 K. 65

Figure S 41. ^{31}P NMR spectrum of the *anti-rac*-[Ru(NNP)(H)Cl(CO)] in $CDCl_3$ at 298 K. 66

Figure S 42. ^{1}H NMR spectrum of the *syn-rac*-[Ru(NNP)(H)Cl(CO)] in $CDCl_3$ at 298 K. 67

Figure S 43. ^{31}P NMR spectrum of the *syn-rac*-[Ru(NNP)(H)Cl(CO)] in $CDCl_3$ at 298 K. 68

Figure S 44. Elemental analysis of [Ru(NNP)(H)Cl(CO)] 69

Figure S 45. FTIR of [Ru(H)Cl(CO)(PPh_3)$_3$] 70

Figure S 46. FTIR of *syn* and *anti-rac*-[Ru(NNP)(H)Cl(CO)] 71

Figure S 47. ESI-MS of [Ru(NNP)(H)Cl(CO)] 72

Figure S 48. Simulated ESI-MS of [Ru(NNP)(H)Cl(CO)] 73

Figure S 49. Absorption spectra of *syn* and *anti-rac*-[Ru(NNP)(H)Cl(CO)] 74

Figure S 50. Fluorescence spectrum of *syn* and *anti-rac*-[Ru(NNP)(H)Cl(CO)].....75

Figure S 51. ^{31}P NMR spectrum for *anti-rac*-[Ru(NNP)(H)Cl(CO)] after adding CS_2 in $CDCl_3$ at 298 K.....76

Figure S 52. ^{31}P NMR spectrum for *syn-rac*-[Ru(NNP)(H)Cl(CO)] after adding CS_2 in $CDCl_3$ at 298 K.....77

Figure S 53. ^{1}H NMR spectrum of *anti-rac*-[Ru(NNP)(H)(η^1-BH_4)(CO)] complex in $CDCl_3$ at 298 K. 78

Figure S 54. ^{31}P NMR spectrum of *anti-rac*-[Ru(NNP)(H)(η^1-BH_4)(CO)] complex in $CDCl_3$ at 298 K. 79

Figure S 55. ^{31}P NMR spectrum of *syn-rac*-[Ru(NNP)(H)(η^1-BH_4)(CO)] complex in $CDCl_3$ at 298 K. 80

Figure S 56. ESI-MS of [Ru(NNP)(H)(η^1-BH_4)(CO)] 81

Figure S 57. Simulated ESI-MS of [Ru(NNP)(H)(η^1-BH_4)(CO)].....82

Figure S 58. ^{1}H NMR spectrum of [Ru(NNP)(CS_2H)$_2$(CO)] complex in $CDCl_3$ at 298 K. 83

Figure S 59. ^{31}P NMR spectrum of [Ru(NNP)(CS_2H)$_2$(CO)] complex in $CDCl_3$ at 298 K. 84

Figure S 60. ESI-MS of [Ru(NNP)(CS_2H)$_2$(CO)] 85

Figure S 61. Simulated for [Ru(NNP)(CS_2H)$_2$(CO)].....86

Figure S 62. FTIR spectrum of [Ru(NNP)(CS_2H)$_2$(CO)] 87

Figure S 63. ^{1}H NMR spectrum of crude [Ru(NNP)(CS_2H)$_2$(CO)] and after the addition of MeI in $CDCl_3$ at 298 K. 88

Figure S 64. ^{31}P NMR spectrum of [Ru(NNP)I_2(CO)] complex in dichloromethane at 298 K.....89

Figure S 65. ESI-MS for [Ru(NNP)I_2(CO)] 90

Figure S 66. Simulated ESI-MS for [Ru(NNP)I_2(CO)] 91

Figure S 67. UV-Vis spectrum for [Ru(NNP)(CS_2H)$_2$(CO)] reaction with MeI. 92

Figure S 68. ^{1}H NMR spectrum of the [Cu(NNP)I] in $CDCl_3$ at 298 K. 93

Figure S 69. ^{31}P NMR spectrum of the [Cu(NNP)I] in $CDCl_3$ at 298 K. 94

Figure S 70. ESI-MS of [Cu(NNP)I] 95

Figure S 71. Simulated ESI-MS of [Cu(NNP)I] 96

Figure S 72. ^{1}H NMR spectrum of the [Cu(NNP)Cl] in $CDCl_3$ at 298 K. 97

Figure S 73. ^{31}P NMR spectrum of the [Cu(NNP)Cl] in $CDCl_3$ at 298 K. 98

Figure S 74. ^{1}H NMR spectrum of the [Cu(NNP)(CH_3CN)][BF_4] in $CDCl_3$ at 298 K. 99

Figure S 75. ^{31}P NMR spectrum of the [Cu(NNP)(CH_3CN)][BF_4] in $CDCl_3$ at 298 K. 100

Figure S 76. ^{1}H NMR spectrum of the [Cu(NNP)(CH_3CN)][PF_6] in $CDCl_3$ at 298 K. 101

Figure S 77. ^{31}P NMR spectrum of the [Cu(NNP)(CH_3CN)][PF_6] in $CDCl_3$ at 298 K. 102

Figure S 78. ^{1}H NMR spectrum of the [Cu(NNP)(CH_3CN)][OTf] in $CDCl_3$ at 298 K. 103

Figure S 79. ^{31}P NMR spectrum of the [Cu(NNP)(CH_3CN)](OTf) in $CDCl_3$ at 298 K. 104

Figure S 80. ^{1}H NMR spectrum of the [Cu(NNP)(PPh_3)][BF_4] in $CDCl_3$ at 298 K. 105

Figure S 81. ^{31}P NMR spectrum of the [Cu(NNP)(PPh_3)][BF_4] in $CDCl_3$ at 298 K. 106

Figure S 82. ESI-MS of [Cu_2(NNP)$_2$(μ-Cl)Cl_2][$CuCl_2$] 107

Figure S 83. Simulated ESI-MS of [Cu_2(NNP)$_2$(μ-Cl)Cl_2][$CuCl_2$], ... 108

Figure S 84. Reduction of Cu(II) to Cu(I) using ascorbic acid 109

Figure S 85. ^{1}H NMR titration for the transmetallation of Zn(II) by Cu(I) in $CDCl_3$:CD_3CN mixture at 298 K 110

Figure S 86. ^{31}P NMR titration for the transmetallation of Zn(II) by Cu(I) in $CDCl_3$:CD_3CN mixture at 298 K 111

Figure S 87. ESI-MS for the transmetallation of Zn(II) by Cu(I) 112

Figure S 88. Cyclic Voltammogram of [Cu(NNP)(CH_3CN)][OTf] 113

Figure S 89. Cyclic Voltammogram of [Cu(NNP)(CH_3CN)][PF_6] 114

Figure S 90. Cyclic Voltammogram of [Cu(NNP)I] 115

Figure S 91. Cyclic Voltammogram of [Cu(NNP)Cl] 116

Figure S 92. Cyclic Voltammogram of [Cu_2(NNP)$_2$(μ-Cl)Cl_2][$CuCl_2$] 117

Figure S 93. ORTEP of NNP 118

Figure S 94. ORTEP of [Zn(NNP)Cl_2] 119

Figure S 95. ORTEP of [Ni(NNP)Cl_2]·CH_3CN 120

Figure S 96. ORTEP of [Pd(NNP)Cl][Cl] 121

Figure S 97. ORTEP of [Pd(NNP)($SPhCH_3$)][PF_6] 122

Figure S 98. ORTEP of [Ru(NNP)(PPh_3)Cl_2] 123

Figure S 99. ORTEP of *anti-rac*-[Ru(NNP)(H)Cl(CO)] 124

Figure S 100. ORTEP of *syn-rac*-[Ru(NNP)(H)Cl(CO)] 125

Figure S 101. ORTEP of *anti-rac*-[Ru(NNP)(H)(η^1-BH_4)(CO)] 126

Figure S 102. ORTEP of [Ru(NNP)(CS_2H)$_2$(CO)] 127

Figure S 103. ORTEP of [Cu(NNP)I] 128

Figure S 104. ORTEP of [Cu(NNP)(PPh_3)][BF_4] 129

Figure S 105. ORTEP of [Cu(NNP)Cl] 130

Figure S 106. ORTEP of [Cu_2(NNP)$_2$(μ-Cl)Cl_2][$CuCl_2$] 131

Figure S 108. Cytotoxicity profiles 148

Table S 1. Crystal data and structure refinement for 10febc_0m (NNP) 132

Table S 2. Crystal data and structure refinement for 27octf [Zn(NNP)Cl_2] 133

Table S 3. Crystal data and structure refinement for 26maya_0m [Ni(NNP)Cl_2]·CH_3CN 134

Table S 4. Crystal data and structure refinement for 3febd [Pd(NNP)Cl][Cl]. 135

Table S 5. Crystal data and structure refinement for 1augb_0m [Pd(NNP)($SPhCH_3$)][PF_6]. 136

Table S 6. Crystal data and structure refinement for 23dece_0m [Ru(NNP)(PPh_3)Cl_2]. 137

Table S 7. Crystal data and structure refinement for 12mayd_0m *anti-rac*-[Ru(NNP)(H)Cl(CO)]. 138

Table S 8 Crystal data and structure refinement for 5jula_O_0m *syn-rac*-[Ru(NNP)(H)Cl(CO)]. 139

Table S 9. Crystal data and structure refinement for 31augb_a *anti-rac*-[Ru(NNP)(H)(η^1- BH_4)(CO)]. 140

Table S 10. Crystal data and structure refinement for 9marb_0m [Ru(NNP)(CS_2H)$_2$(CO)] 141

Table S 11. Crystal data and structure refinement for 25mayb [Cu(NNP)I]. 142

Table S 12. Crystal data and structure refinement for 13junb [(NNP)Cu(PPh_3)][BF_4]. 143

Table S 13. Crystal data and structure refinement for 16maya_0m_a [Cu(NNP)Cl].....144

Table S 14. Crystal data and structure refinement for 25mayb $[Cu_2(NNP)_2(\mu\text{-}Cl)Cl_2][CuCl_2]$. 145

Table S 15. MIC (μg/mL) of metal salts and hydride precursors against *S. aureus* ATCC29213. 146

Table S 16. MIC (μg/mL) of NNP copper complexes against *S. aureus* ATCC29213.....147

Experimental Section

Materials

Pyridine-2-carboxaldehyde (Sigma Aldrich), 2-(diphenylphosphino) benzaldehyde (TCI), *N*-phenylethylenediamine (TCI), formaldehyde (Emplura), 2-methoxyethanol (Spectrochem), $RuCl_3 \cdot 3H_2O$ (Sigma Aldrich), $CDCl_3$ (Merck), anhydrous Na_2SO_4 (FINAR), CS_2 (Fisher Scientific), $NiCl_2$ (RANKEM), $[Pd(CH_3CN)_2Cl_2]$ (TCI), $ZnCl_2$ (FINAR), CuI (TCI), MeI (Sigma- Aldrich), ferrocene (Spectrochem), tetrabutylammonium hexafluorophosphate (TCI) and $NaBH_4$ (SRL).

Methods

Elemental analyses were carried out on a Perkin-Elmer CHNS/O analyser. NMR spectra were recorded on JEOL 500 MHz and JEOL 400 MHz spectrometers. The temperature was kept constant usinga variable temperature unit within the error limit of ±1 K. The software MestReNova was used to process the NMR spectra. Tetramethylsilane (TMS) or the deuterated solvent residual peaks were used for calibration. Mass spectrometry experiments were performed on an Agilent 6546 LC/Q-TOF equipped with an electrospray interface. Spectra were collected by a constant infusion of the sample dissolved in methanol or acetonitrile with 0.1% formic acid. The freeware mMass was used to simulate the calculated isotopic distributions. UV-Vis spectra were recorded on a Shimadzu UV-2450. Fluorescence spectra were recorded on a HORIBA Fluromax-4.

Crystal Structure Determinations

Single-crystal X-ray data were collected at either 293 K or 123 K on a Bruker SMART APEXCCD diffractometer using graphite-monochromated Mo Kα radiation (λ= 0.71073 Å). The linear absorption coefficients, the scattering factors for the atoms, and the anomalous dispersion corrections were taken from International Tables for X-ray Crystallography. Data integration and reduction wereconducted with SAINT. An empirical absorption correction was applied to the collected reflections withSADABS using XPREP. Structures were determined by a direct method using SHELXTL and refinedon F2 by a full-matrix least-squares technique using the SHELXL-97 program package. The lattice parameters and structural data are listed at the end of this Supporting Information.

Electrochemical studies

Cyclic Voltammetry (CV) analysis was performed on the AUT50405 Autolab electrochemical analyser under N_2 conditions. The system comprised three electrodes: a

static glassy Carbon working electrode with Ag/AgCl reference electrode, and a Pt wire auxiliary. The supporting electrolyte was 0.1 M tetrabutylammonium hexafluorophosphate ($TBAPF_6$).

Synthesis of N^1-(2-(diphenylphosphaneyl)benzyl)-N^2-phenylethane-1,2-diamine (3)

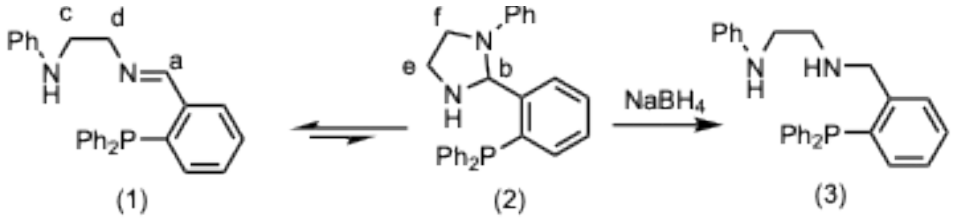

In a 100 mL Schlenk flask, 2-(diphenylphosphino)benzaldehyde (0.551 g, 1.9 mmol) was dissolved in 25 mL of methanol, and *N*-phenylethylenediamine (0.272 g, 2.0 mmol) was added to it. The white suspension was refluxed at 60 ºC for 4 h under an N_2 atmosphere. A white precipitate was obtained. The white precipitate was filtered, washed with methanol, and dried under a vacuum. Yield: (0.633 g, 82%, Schiff base: cyclized product = 1:0.4). ^{1}H NMR of crude product (400 MHz, $CDCl_3$) δ = 8.76 (d, *J* = 4.1 Hz, 1H, a), 7.85 (dd, *J* = 7.6, 4.0 Hz, 1H, Ph), 7.43 – 7.37 (m, 3H, Ph), 7.36 – 7.25 (m, 14H, Ph), 7.17 – 7.11 (m, 2H, Ph), 7.04 – 6.99 (m, 0.4H, Ph, cyclized), 6.97 (d, *J* = 7.9 Hz, 0.4H, Ph, cyclized), 6.89 (dd, *J* = 7.6, 4.6 Hz, 1H, Ph), 6.68 (t, *J* = 7.3 Hz, 1H, Ph), 6.58 (t, *J* = 7.3 Hz, 0.5H, Ph, c), 6.53 (d, *J* = 8.5 Hz, 2H, Ph), 6.21 (d, *J* = 8.2 Hz, 1H, Ph), 5.97 (d, *J* = 4.2 Hz, 0.4H, b, cyclized), 3.78 – 3.73 (m, 0.4H, f, cyclized), 3.69 (d, *J* = 5.5 Hz, 2H, d), 3.45 – 3.39 (m, 0.5H, f, cyclized), 3.33 – 3.27 (m, 0.4H, e, cyclized), 3.25 – 3.20 (m, 2.4H, e, c). ^{31}P NMR (200 MHz, $CDCl_3$) δ = -11.13 (s, a), -16.43 (s, b).

Note: The spectrum was recorded for the crude product. Both Schiff base and cyclized forms are present in equilibrium (1:0.4 ratio). Signals assigned to the minor cyclized species are indicated and appear as fractional integrals (0.4H, 0.5H), consistent with the observed 1:0.4 mixture of Schiff base to cyclized product. Where peaks for the two species are merged, combined integrals are reported.

The white precipitate (0.630 g, 1.5 mmol) was dissolved in a mixture of methanol and dichloromethane (20 mL, 1:1). $NaBH_4$ (0.293 g, 7.5 mmol) was added to it and stirred for 16 h under an N_2 atmosphere. The volatiles were evaporated under reduced pressure. A colorless residue was obtained and dissolved in 20 mL of distilled water. The desired compound was extracted with dichloromethane (4 x 20 mL). The combined organic layer was dried with Na_2SO_4 and evaporated under reduced pressure, resulting in a yellow oily compound (3). Yield: (0.470 g, 76%). ^{1}H NMR (500 MHz, $CDCl_3$) δ = 7.42 (dd, *J* = 7.2, 4.9 Hz, 1H, Ph), 7.33 (dd,

J = 12.5, 4.7 Hz, 8H, Ph), 7.27 (dd, *J* = 7.4, 0.9 Hz, 3H, Ph), 7.18 – 7.12 (m, 3H, Ph), 6.92 – 6.90 (dd, *J* = 7.0, 5.1 Hz, 1H, Ph), 6.68 – 6.66 (t, *J* = 7.3 Hz, 1H, Ph), 6.55 (d, *J* = 7.6 Hz, 2H, Ph), 3.99 (s, 2H, Bn, benzylic), 3.04 – 3.02 (t, 2H, -CH_2), 2.77 – 2.74 (t, 2H, -CH_2). ^{13}C NMR (100 MHz, $CDCl_3$) δ = 148.55, 144.47, 144.28, 136.79, 135.97, 129.45, 129.19, 129.08, 128.96, 128.63, 127.49, 117.23, 52.25, 47.91, 43.34. ^{31}P NMR (200 MHz, $CDCl_3$) δ = −15.45 (s).

Synthesis of NNP ligand

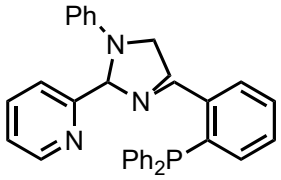

NNP

In a 100 mL Schlenk flask, 2-pyridinecarboxaldehyde (0.117 g, 1.1 mmol) was dissolved in 10 mL methanol. *N*^{1}-(2-(diphenylphosphaneyl)benzyl)-*N*^{2}-phenylethane-1,2-diamine (0.460 g, 1.1 mmol) was dissolved in 10 mL of methanol and added dropwise. The resulting yellow solution was stirred for 15 h under an N_2 atmosphere. All volatiles were evaporated under reduced pressure. A white precipitate was obtained, which was dried under a vacuum. XRD quality crystals were formed by slow diffusion of diethyl ether into a concentrated chloroform solution of NNP at 5 ºC after 2 days. Yield: (0.38 g, 69%). ^{1}H NMR (500 MHz, $CDCl_3$) δ = 8.57 (d, *J* = 6.5 Hz, 1H, Ph), 7.58 – 7.55 (m, 1H, Ph), 7.34 – 7.31 (m, 1H, Ph), 7.25 – 7.04 (m, 16H, Ph), 6.89 (dd, *J* = 8.1, 3.7 Hz, 1H, Ph), 6.61 (t, *J* = 6.8 Hz, 1H, Ph), 6.37 (d, *J* = 8.5 Hz, 2H, Ph), 5.10 (s, 1H, C*H, stereogenic chiral carbon), 4.03 (d, *J* = 15.4 Hz, 1H, Bn), 3.78 (d, *J* = 13.2 Hz, 1H, Bn), 3.39 – 3.35 (d, *J* = 6.3 Hz, 1H, CH_2-Im), 2.98 – 2.92 (m, 2H, CH_2-Im), 2.63 – 2.60 (m, 1H, CH_2-Im, imidazolidinyl proton). ^{13}C NMR (100 MHz, $CDCl_3$) δ = 160.86, 148.69, 146.00, 143.63, 138.01, 136.87, 136.65, 134.40, 133.79, 133.46, 129.37, 129.33, 128.89, 128.67, 127.38, 122.89, 122.44, 116.41, 112.39, 82.08, 54.69, 49.32, 47.07. ^{31}P NMR (200 MHz, $CDCl_3$) δ = −15.21 (s). High resolution ESI-MS: *m/z* for $[M+H]^+$ = 500.2274 (calcd. 500.2256) = $[C_{33}H_{31}N_3P]^+$.

Synthesis of [Zn(NNP)Cl_2] complex

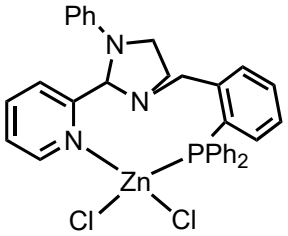

In a 50 mL Schlenk flask, anhydrous zinc (II) chloride (0.013 g, 0.1 mmol) was dissolved in 3 mL methanol. NNP (0.054 g, 0.1 mmol) was dissolved in 4 mL methanol and 1 mL dichloromethane and added dropwise to the zinc (II) chloride solution. A white precipitate appeared after 5 minutes. The reaction mixture was stirred for 3 h under an N_2 atmosphere. All volatiles were evaporated under reduced pressure. A white precipitate was obtained, washed with diethyl ether, and dried under a vacuum. XRD quality crystals were formed by slow diffusion of diethyl ether into a concentrated dichloromethane solution of [Zn(NNP)Cl_2] at 5 ºC after 3 days. Yield: (0.06 g, 94%). ^{1}H NMR (400 MHz, $CDCl_3$) δ = 9.54 (d, *J* = 5.3 Hz, 1H, Ph), 7.76 (t, *J* = 7.7 Hz, 1H, Ph), 7.54 – 7.36 (m, 8H, Ph), 7.30 – 7.22 (m, 9H, Ph) , 7.08 (t, *J* = 8.1 Hz, 1H. Ph), 6.83 (t, *J* = 7.3 Hz, 1H, Ph), 6.61 (d, *J* = 8.1 Hz, 2H, Ph), 6.19 (s, 1H, C*H), 5.22 (d, *J* = 13.5 Hz, 1H, Bn), 3.79 – 3.65 (m, 2H, Bn, CH_2-Im), 3.28 (t, *J* = 8.2 Hz, 1H, CH_2-Im), 2.86 (dd, *J* = 13.1, 6.7 Hz, 1H, CH_2-Im), 2.28 – 2.16 (m, 1H, CH_2-Im). ^{13}C NMR (100 MHz, $CDCl_3$) δ = 157.13, 150.81, 146.21, 140.39, 136.67, 134.18, 133.66, 131.53, 130.65, 130.42, 129.90, 129.06, 128.97, 128.70, 128.60, 124.55, 123.26, 118.19, 111.71, 81.78, 57.73, 47.93, 43.49. ^{31}P NMR (200 MHz, $CDCl_3$) δ = −13.85 (s). Elemental analysis calculated (%) for $C_{33}H_{30}Cl_2N_3PZn$: C, 62.33; H, 4.76; N, 6.61. Found: C, 62.35; H, 4.49; N, 6.62. High resolution ESI-MS: *m/z* for $[M\text{-}Cl]^+$ = 598.1149 (calcd. 598.1157) = $[ZnC_{33}H_{30}N_3PCl]^+$, [NNP+H] = 500.2268 (calcd. 500.2256) = $[C_{33}H_{31}N_3P]^+$.

Synthesis of [Ni(NNP)Cl_2]·CH_3CN complex

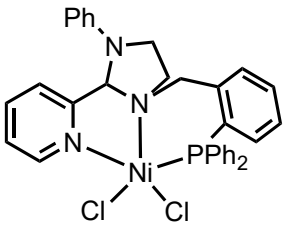

In a 50 mL Schlenk flask, anhydrous nickel (II) chloride (0.012 g, 0.1 mmol) and NNP (0.05 g, 0.1 mmol) were dissolved in 5 mL dry acetonitrile. The reaction mixture was stirred for 3 h at room temperature under an N_2 atmosphere. The color of the solution turned green. The solvent

was evaporated under reduced pressure. A green residue was washed with diethyl ether and dried under a vacuum. XRD quality crystals were obtained by dissolving the complex in acetonitrile at room temperature after 1 day. Yield: (0.062 g, 96%). High resolution ESI-MS: *m/z* for $[M-Cl]^+$ = 592.1221 (calcd. 592.1219) = $[NiC_{33}H_{30}N_3ClP]^+$. Elemental analysis calculated (%) for $C_{33}H_{30}Cl_2N_3PNi$ + (1 CH_3CN): C, 62.72; H, 4.96; N, 8.36. Found: C, 62.77; H, 4.88; N, 8.66.

Synthesis of [Pd(NNP)Cl][Cl] complex

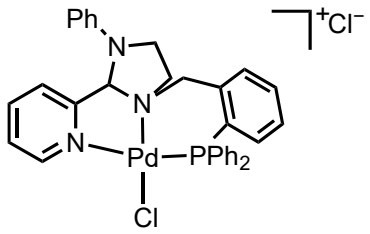

In a 50 mL Schlenk flask, bis-acetonitrile palladium (II) chloride (0.008 g, 0.05 mmol) was dissolved in 2 mL dichloromethane. NNP (0.025 g, 0.05 mmol) was dissolved in 3 mL dichloromethane and added dropwise. The reaction mixture was stirred for 3 h under an N_2 atmosphere. The solvent was evaporated under reduced pressure. A yellow residue was obtained, washed with diethyl ether, and dried under a vacuum. XRD quality crystals were formed by slow diffusion of diethyl ether into a concentrated dichloromethane solution of [Pd(NNP)Cl][Cl] at 5 ºC after 2 days. Yield: (0.03 g, 96%). ^{1}H NMR (500 MHz, $CDCl_3$) δ = 9.05 (t, *J* = 3.9 Hz, 1H, Ph), 8.02 (t, *J* = 8.5 Hz, 2H, Ph), 7.89 (dd, *J* = 12.0, 7.9 Hz, 1H, Ph), 7.71 – 7.59 (m, 6H, Ph), 7.53 (d, *J* = 5.6 Hz, 6H, Ph), 7.46 (d, *J* = 7.5 Hz, 1H, Ph), 7.39 (dd, *J* = 8.5, 7.5 Hz, 2H, Ph), 7.08 (d, *J* = 25.4 Hz, 1H, Ph), 7.02 (d, *J* = 8.1 Hz, 2H, Ph), 6.95 (d, *J* = 7.4 Hz, 1H, C*H), 4.81 (d, *J* = 13.3 Hz, 1H, Bn), 3.94 (t, *J* = 8.7 Hz, 1H, CH_2-Im), 3.80 (ddd, *J* = 21.5, 11.8, 7.7 Hz, 2H, CH_2-Im, Bn), 3.66 (dd, *J* = 20.0, 11.6 Hz, 1H, CH_2-Im), 3.54 – 3.48 (m, 1H, CH_2-Im). ^{13}C NMR (100 MHz, $CDCl_3$) δ = 158.52, 148.42, 146.04, 141.65, 137.52, 135.01, 134.27, 134.03, 132.95, 132.41, 131.44, 130.40, 129.78, 129.18, 127.05, 126.52, 124.88, 120.12, 112.47, 87.98, 60.05, 52.87, 44.22. ^{31}P NMR (200 MHz, $CDCl_3$) δ = 24.07 (s). Elemental analysis calculated (%) for $C_{33}H_{30}Cl_2N_3PPd \cdot 0.8CH_2Cl_2$: C, 54.50; H, 4.28; N, 5.64. Found: C, 54.59; H, 4.74; N, 5.55. High resolution ESI-MS: *m/z* for $[M-Cl]^+$ = 640.0891 (calcd. 640.0901) = $[PdC_{33}H_{30}ClN_3P]^+$.

Synthesis of [Pd(NNP)(SPhCH$_3$)][Cl]

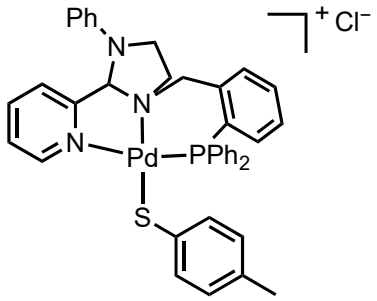

In a 50 mL round bottom flask, *p*-Toluenethiol (0.011 g, 0.096 mmol) was dissolved in 5 mL methanol, and a few drops of triethylamine were added, stirred for 5 minutes. Then [Pd(NNP)Cl][Cl] (0.065 g, 0.096 mmol) was added to it. The orange color reaction mixture was stirred for 6 h at room temperature. The desired compound was extracted with dichloromethane and water. The combined organic layer was dried with Na_2SO_4 and evaporated under reduced pressure, resulting in the orange solid compound. Yield = (0.072 g, 98%). ^{1}H NMR (400 MHz, $CDCl_3$) δ = 8.80 (s, 1H, Ph), 7.91 – 7.84 (m, 3H, Ph), 7.60 – 7.55 (m, 1H, Ph), 7.52 (d, *J* = 4.3 Hz, 4H, Ph), 7.48 – 7.42 (m, 4H, Ph), 7.38 (d, *J* = 8.4 Hz, 9H, Ph), 7.06 (d, *J* = 8.5 Hz, 3H, Ph), 6.94 (t, *J* = 7.3 Hz, 1H, Ph), 6.77 (d, *J* = 8.1 Hz, 2H, C*H, Ph), 5.18 (d, *J* = 13.2 Hz, 1H, Bn), 3.84 – 3.73 (m, 3H, Bn, CH_2-Im), 3.41 – 3.34 (m, 2H, CH_2-Im), 2.16 (s, 3H, CH_3). ^{13}C NMR (100 MHz, $CDCl_3$) δ = 159.54, 149.65, 146.30, 140.84, 138.50, 137.48, 135.07, 134.46, 133.90, 133.49, 133.20, 132.12, 131.68, 130.92, 130.31, 129.65, 129.16, 129.128.90, 125.56, 124.87, 119.72, 112.53, 86.38 (C*H), 59.57, 51.18, 44.07, 29.81 (grease), 20.94 (CH_3). ^{31}P NMR (200 MHz, $CDCl_3$) δ = 27.44 (s). High resolution ESI-MS: *m/z* for $[M-Cl]^+$ = 728.1477 (calcd. 728.1481) = $[PdC_{40}H_{37}N_3SP]^+$.

Synthesis of [Pd(NNP)(SPhCH$_3$)][PF$_6$]

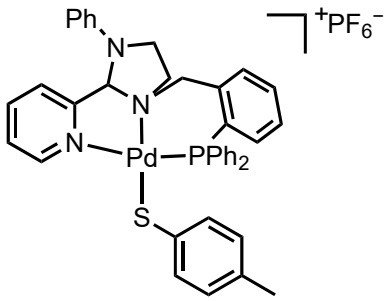

In a 50 mL round-bottom flask, [Pd(NNP)(SPhCH$_3$)][Cl] (0.072 g, 0.08 mmol) was dissolved in 5 mL of methanol, a few drops of triethylamine were added and stirred for 5 minutes. Then KPF_6 (0.014 g, 0.08 mmol) was added to it. The orange color reaction mixture was stirred for 6 h at room temperature. The solvent evaporated under reduced pressure, resulting in the orange solid compound. XRD quality crystals were formed by slow diffusion of diethyl ether into a concentrated chloroform solution of [Pd(NNP)(SPhCH$_3$)][PF_6] at 5 ºC after 4 days. Yield: (0.068 g, 97%). ^{1}H NMR (400 MHz, $CDCl_3$) δ = 8.84 (d, *J* = 5.8 Hz, 1H, Ph), 7.90 (t, *J* = 7.7 Hz, 1H, Ph), 7.79 (dd, *J* = 12.4, 7.4 Hz, 2H, Ph), 7.61 (d, *J* = 7.6 Hz, 1H, Ph), 7.55 (t, *J* = 7.4 Hz, 2H, Ph), 7.47 (dd, *J* = 7.1, 4.0 Hz, 4H, Ph), 7.36 (dd, *J* = 16.1, 7.5 Hz, 8H, Ph), 7.18 (d, *J* = 8.1 Hz, 2H, Ph), 7.07 – 7.02 (m, 1H, Ph), 6.98 – 6.92 (m, 3H, Ph), 6.76 (d, *J* = 8.1 Hz, 2H, Ph), 6.43 (s, 1H, C*H), 4.58 (d, *J* = 13.0 Hz, 1H, Bn), 3.81 (dd, *J* = 13.0, 5.9 Hz, 1H, Bn), 3.76 – 3.70 (m, 1H, CH_2), 3.67 – 3.60 (m, 1H, CH_2), 3.35 (dd, *J* = 8.7, 5.0 Hz, 2H, CH_2), 2.17 (s, 3H, CH_3). ^{31}P NMR (200 MHz, $CDCl_3$) δ = 27.66 (s), (−137.22) – (−151.06) (quintet).

Synthesis of [Ru(NNP)(PPh_3)Cl_2] complex

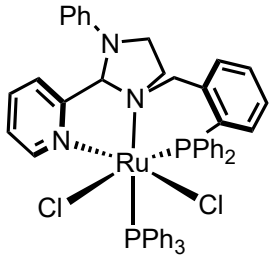

- In a 50 mL Schlenk flask, [$RuCl_2(PPh_3)_3$] (0.038 g, 0.04 mmol) was dissolved in 3 mL dichloromethane. NNP (0.020 g, 0.04 mmol) was dissolved in 2 mL of methanol and added dropwise to the [$RuCl_2(PPh_3)_3$] solution under an N_2 atmosphere. A yellow precipitate was formed after 5 minutes. The reaction mixture was stirred for 3 h under an N_2 atmosphere. The solvent was evaporated under reduced pressure. The yellow solid was washed with diethyl ether and dried under a vacuum. XRD quality crystals were formed by slow diffusion of diethyl ether into a concentrated chloroform solution of [Ru(NNP)(PPh_3)Cl_2] at 5 ºC after 2 days. Yield: (0.035 g, 93%). ^{1}H NMR (500 MHz, $CDCl_3$) δ = 9.00 – 8.89 (m, 1H, Ph), 8.42 (s, 1H, C*H), 8.24 (d, *J* = 5.5 Hz, 1H, Ph), 7.47 (t, *J* = 7.3 Hz, 1H, Ph), 7.38 (s, 3H, Ph), 7.30 (t, *J* = 7.9 Hz, 3H, Ph), 7.26 – 7.11 (m, 10H, Ph), 7.09 – 6.96 (m, 9H, Ph), 6.91 (t, *J* = 7.0 Hz, 4H, Ph), 6.74 (t, *J* = 7.0 Hz, 3H, Ph), 6.52 (t, *J* = 8.7 Hz, 1H, Ph), 6.37 – 6.32 (m, 1H, Ph), 6.23 (t, *J* = 6.4 Hz, 1H, Ph), 4.51 (dt, *J* = 9.7, 6.8 Hz,1H, Bn), 4.38 (dt, *J* = 12.8, 4.5 Hz,1H, Bn), 4.09 (q, *J* =

10.4 Hz, 1H, CH_2-Im), 3.52 (d, *J* = 9.1 Hz, 1H, CH_2-Im), 3.24 (dd, *J* = 12.6, 6.3 Hz, 1H, CH_2-Im), 3.11 (d, *J* = 12.9 Hz, 1H, CH_2-Im). ^{31}P NMR (200 MHz, $CDCl_3$) δ = 46.64, 46.48, 42.78, 42.61. Elemental analysis calculated (%) for $C_{51}H_{45}Cl_2N_3P_2Ru \cdot 0.6\ CH_2Cl_2$: C, 63.93; H, 4.73; N, 4.27. Found: C, 63.97; H, 4.72; N, 4.48. High resolution ESI-MS: *m/z* for $[M\text{-}Cl]^+$ = 898.1814 (calcd. 898.1821) = $[RuC_{51}H_{45}ClN_3P_2]^+$; *m/z* = 636.0896 (calcd. 636.0909) = $[M\text{-}(PPh_3+Cl)]^+$; *m/z* = 516.2188 (calcd. 516.2205) = $[NNP{=}O+H]^+$; *m/z* = 263.0976 (calcd. 263.0990) = $[PPh_3+H]^+$; *m/z* = 938.2200 (calcd. 938.2214) = $[Ru(NNP)(O{=}PPh_3)\text{-}2Cl+CH_3COO]^+$. The CH_3COO^- likely originates from the formic acid used to infuse the sample during measurement.

Synthesis of [Ru(NNP)(H)Cl(CO)] complex

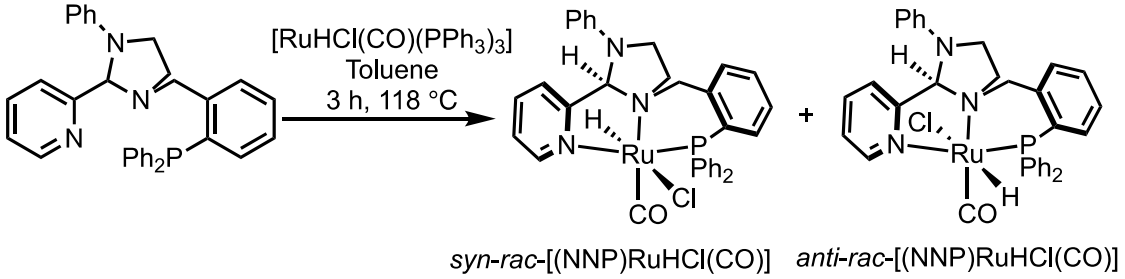

syn-rac-[(NNP)RuHCl(CO)] *anti-rac*-[(NNP)RuHCl(CO)]

In a 50 mL Schlenk flask, NNP (0.100 g, 0.20 mmol) and [Ru(H)Cl(CO)(PPh_3)$_3$] (0.190 g, 0.20 mmol) were dissolved in dry toluene (5 mL) and refluxed for 3 h under N_2 atmosphere at 118 °C. The reaction mixture was filtered via cannula. The solid residue was washed several times with diethyl ether and dried under vacuum to afford *anti-rac*-[Ru(NNP)(H)(CO)Cl] as a white solid (0.061 g, 45%). Single crystals suitable for X-ray diffraction were obtained by slow diffusion of diethyl ether into a concentrated dichloromethane solution at 5 °C after 2 days.

The yellow filtrate was concentrated, and diethyl ether was added to induce precipitation. The resulting solid was collected and dried under vacuum to afford *syn-rac*-[Ru(NNP)(H)(CO)Cl] as a white solid (0.054 g, 40%). Single crystals suitable for X-ray diffraction were obtained by slow diffusion of diethyl ether into a concentrated dichloromethane solution at room temperature over one week.

***anti-rac*-[Ru(NNP)(H)(CO)Cl]**: ^{1}H NMR (500 MHz, $CDCl_3$) δ = 9.00 (d, *J* = 5.4 Hz, 1H, Ph), 7.67 (td, *J* = 7.8, 1.5 Hz, 1H, Ph), 7.55 (dd, *J* = 10.7, 7.6 Hz, 2H, Ph), 7.38 (t, *J* = 11.4 Hz, 12H, Ph), 7.32 (d, *J* = 7.5 Hz, 2H, Ph), 7.23 (d, *J* = 6.6 Hz, 1H, Ph), 6.95 (t, *J* = 8.0 Hz, 1H, Ph), 6.88 (t, *J* = 7.3 Hz, 1H, Ph), 6.82 (d, *J* = 8.2 Hz, 2H, Ph), 6.76 (s, 1H, C*H), 5.38 (d, *J* = 12.6 Hz, 1H, Bn), 3.55 – 3.49 (m, 1H, CH_2-Im), 3.44 (dd, *J* = 12.6, 4.2 Hz, 1H, CH_2-Im), 3.34 (t, *J* = 8.3 Hz, 1H, CH_2-Im), 3.21 (dd, *J* = 13.1, 6.6 Hz, 1H, Bn), 3.13 – 3.05 (m, 1H, CH_2-Im), −13.77 (d, *J* = 25.3 Hz, 1H, Ru-H). ^{31}P NMR (200 MHz, $CDCl_3$) δ = 66.61 (d, *J* = 17.1 Hz).

***syn-rac*-[Ru(NNP)(H)(CO)Cl]**: ^{1}H NMR (500 MHz, $CDCl_3$) δ = 9.08 – 9.04 (m, 1H, Ph), 7.67 (td, *J* = 7.8, 1.6 Hz, 1H, Ph), 7.48 – 7.28 (m, 15H, Ph), 7.25 (t, *J* = 4.6 Hz, 1H, Ph), 7.00 – 6.94 (m, 1H, Ph), 6.89 (t, *J* = 7.3 Hz, 1H, Ph), 6.76 (d, *J* = 8.1 Hz, 2H, Ph), 5.87 (s, 1H, C*H), 4.40 (d, *J* = 11.9 Hz, 1H, Bn), 3.77 (dd, *J* = 12.0, 4.5 Hz, 1H, Bn), 3.69 – 3.62 (m, 1H, CH_2-Im), 3.51 – 3.39 (m, 1H, CH_2-Im), 3.31 (t, *J* = 8.4 Hz, 1H, CH_2-Im), 2.89 (d, *J* = 7.4 Hz, 1H, CH_2-

Im), −13.89 (d, J = 26.1 Hz, 1H, RuH). ^{31}P NMR (202 MHz, $CDCl_3$) δ = 57.06 (d, J = 20.8 Hz).

Elemental analysis calculated (%) for $C_{34}H_{31}ClN_3OPRu \cdot 0.5CH_2Cl_2$: C, 58.56; H, 4.56; N, 5.94. Found: C, 58.77; H, 4.96; N, 5.79. High resolution ESI-MS: *m/z* for = $[M-Cl]^+$ = 630.1234 (calcd. 630.1248) = $[RuC_{34}H_{31}N_3OP]^+$. FT-IR (KBr pellet) [Ru(H)Cl(CO)(PPh_3)$_3$]: ν $_{Ru-H}$ = 2014 cm^{-1}, ν $_{CO}$ = 1923 cm^{-1}. FT-IR (KBr pellet) *syn-rac*-[Ru(NNP)(H)(CO)Cl]: ν_{Ru-H} = 1989 cm^{-1}, ν_{CO} = 1914 cm^{-1} FT-IR (KBr pellet) *anti-rac*-[Ru(NNP)(H)(CO)Cl]: ν_{Ru-H} = 1999 cm^{-1}, ν_{CO} = 1913 cm^{-1}.

Synthesis of *anti-rac*-[Ru(NNP)(H)(η^1-BH_4)(CO)] complex

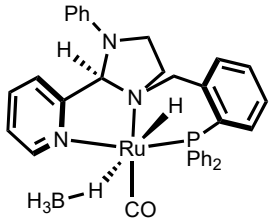

In a 50 mL Schlenk flask, *anti-rac*-[Ru(NNP)(H)Cl(CO)] (0.02 g, 0.03 mmol) was dissolved in 3 mL dichloromethane. $NaBH_4$ (0.011 g, 0.30 mmol) was dissolved in 2 mL of ethanol and added dropwise to the *anti-rac*-[Ru(NNP)(H)Cl(CO)] solution. The reaction mixture was stirred under an N_2 atmosphere for 12 h. The solvent was evaporated under reduced pressure. Then, it was dissolved in dichloromethane and passed through celite to get a clear solution. The solvent was evaporated to get the white solid compound. XRD quality crystals were formed by slow diffusion of diethyl ether into a concentrated dichloromethane solution of *anti-rac*-[Ru(NNP)(H)(η^1-BH_4)(CO)] at 5 ºC after 3 days. Yield: (0.018 g, 93%). ^{1}H NMR (400 MHz, $CDCl_3$) δ = 8.96 (d, J = 5.4 Hz, 1H, Ph), 7.67 (t, J = 7.4 Hz, 2H, Ph), 7.57 – 7.52 (m, 2H, Ph), 7.42 (m, 4H, Ph), 7.38 (m, 6H, Ph), 7.31 (m, J = 12.5 Hz, 3H, Ph), 7.00 (d, J = 8.7 Hz, 1H, Ph), 6.88 (t, J = 7.3 Hz, 1H, Ph), 6.81 (d, J = 8.2 Hz, 2H, Ph), 6.53 (s, 1H, C*H), 4.82 (d, J = 12.5 Hz, 1H, Bn), 3.61 (dd, J = 12.6, 4.3 Hz, 1H, Bn), 3.51 (m, 1H, CH_2-Im), 3.34 – 3.28 (m, 1H, CH_2-Im), 3.16 (d, J = 13.1 Hz, 1H, CH_2-Im), 3.03 (dd, J = 14.5, 10.1 Hz, 1H, CH_2-Im), −1.56 (s, 4H, -BH_4), −11.86 (d, J = 24.0 Hz, 1H, Ru-H). ^{31}P NMR (200 MHz, $CDCl_3$) δ = 63.67 (s). High resolution ESI-MS: *m/z* for = $[M-BH_4]^+$ = 630.1249 (calcd. 630.1248) = $[RuC_{34}H_{31}N_3OP]^+$.

Reactivity of *anti-rac*-[Ru(NNP)(H)(η^1-BH_4)(CO)] with CS_2

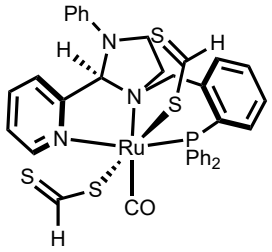

In a 50 mL Schlenk flask, *anti-rac*-[Ru(NNP)(H)(η^1-BH_4)(CO)] (0.02 g, 0.03 mmol) was dissolved in 10 mL dichloromethane and ethanol. Then, CS_2 (0.5 mL) was added to the same reaction mixture. The color of the solution immediately turned yellow. A yellow color precipitate was formed within 5 min. The reaction mixture was stirred for 3 h under an N_2 atmosphere. The solvent was evaporated under reduced pressure, and the yellow residue was redissolved in dichloromethane and passed through celite. The solvent was evaporated to get a yellow color precipitate, which was dried under a vacuum. XRD quality crystals were formed by slow diffusion of diethyl ether into a concentrated dichloromethane solution of [Ru(NNP)(CO)(CS_2H)$_2$] at 5 ºC after 2 days. Yield: (0.018 g, 76%). ^{1}H NMR (400 MHz, $CDCl_3$) δ = 11.43 (s, 1H, -CS_2H), 11.05 (s, 1H, -CS_2H), 9.36 (s, 1H, Ph), 7.73 (t, *J* = 6.0 Hz, 2H, Ph), 7.56 (m, 1H, Ph), 7.48 (m, 1H, Ph), 7.41 (m, 5H, Ph), 7.32 (m, 2H, Ph), 7.18 (m, 2H, Ph), 7.00 (m, 2H, Ph), 6.94 (m, 2H, Ph), 6.73 (d, *J* = 8.2 Hz, 2H, Ph), 6.47 (s, 1H, C*H), 4.65 (d, *J* = 12.8 Hz, 1H, Bn), 3.70 (d, *J* = 3.6 Hz, 1H, Bn), 3.43 (m, 1H, CH_2-Im), 3.18 – 3.10 (m, 2H, CH_2-Im), 3.06 – 3.00 (m, 1H, CH_2-Im). ^{31}P NMR (200 MHz, $CDCl_3$) δ = 50.23 (s). High resolution ESI-MS: *m/z* for = $[M-CS_2H]^+$ = 706.0686 (calcd. 706.0690) = $[RuC_{35}H_{31}N_3OPS_2]^+$; *m/z* = 798.0446 (calcd. 798.0080) = $[Ru(NNP{=}O)(CS_2H)(CS_2)]^+$. FT-IR (KBr pellet) [Ru(NNP)(CO)(CS_2H)$_2$]: ν_{C-H} = 2930-2920 cm^{-1}, ν_{CO} = 1977 cm^{-1}, ν_{S-C-S} = 996 cm^{-1}, $\nu_{C=S}$ = 692 cm^{-1}.

Reaction of [Ru(NNP)(CO)(CS_2H)$_2$] with MeI

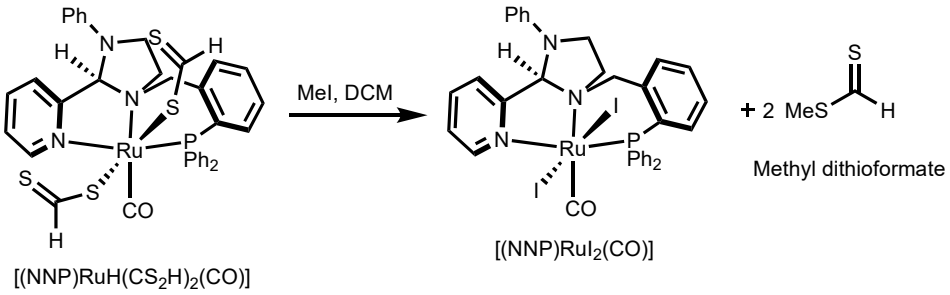

[(NNP)RuH(CS_2H)$_2$(CO)] [(NNP)RuI$_2$(CO)]

In a 50 mL round-bottom flask, [Ru(NNP)(CO)(CS_2H)$_2$] (0.01 g, 0.01 mmol) was dissolved in 5 mL dichloromethane, and MeI (0.018 g, 0.10 mmol) was added to it. The color of the reaction mixture was changed from yellow to orange within 5 minutes. The reaction mixture was stirred for 2 h at room temperature. The solvent was evaporated, and orange color compound was dried under vacuum. ^{31}P NMR (200 MHz, $CDCl_3$) δ = 46.39 (s). High resolution ESI-MS: *m/z* for = $[M-I]^+$ = 756.0218 (calcd. 756.0215) = $[RuC_{34}H_{30}N_3OPI]^+$.

Synthesis of [Cu(NNP)I] complex

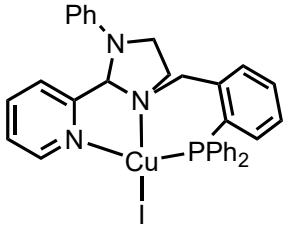

In a 50 mL Schlenk flask, CuI (0.009 g, 0.05 mmol) and NNP (0.025 g, 0.05 mmol) were dissolved in 4 mL dry acetonitrile under N_2 atm. The pale-yellow reaction mixture was stirred for 3 h at room temperature under N_2 atm. The solvent was evaporated under reduced pressure. A pale-yellow solid compound was obtained. XRD quality crystals were formed by slow diffusion of diethyl ether into a concentrated acetonitrile solution of [Cu(NNP)I] at 5 ºC after 2 days. Yield: (0.034 g, 98%). ^{1}H NMR (500 MHz, $CDCl_3$) δ = 8.95 (d, *J* = 4.6 Hz, 1H, Ph), 7.85 – 7.80 (m, 2H, Ph), 7.65 (t, *J* = 7.7 Hz, 1H, Ph), 7.44 (d, *J* = 1.7 Hz, 4H, Ph), 7.36 (d, *J* = 9.9 Hz, 5H, Ph), 7.28 – 7.16 (m, 6H, Ph), 6.93 (t, *J* = 8.5 Hz, 1H, Ph), 6.84 (d, *J* = 7.3 Hz, 1H, Ph), 6.79 – 6.76 (m, 1H, Ph), 6.55 (d, *J* = 8.0 Hz, 2H, Ph), 5.27 (s, 1H, C*H), 4.12 (d, *J* = 12.2 Hz, 1H, Bn), 3.80 (dd, *J* = 17.8, 8.2 Hz, 1H, Bn), 3.69 (dd, *J* = 21.5, 9.7 Hz, 1H, CH_2-Im), 3.51 (d, *J* = 12.3 Hz, 1H, CH_2-Im), 3.46 (t, *J* = 7.8 Hz, 1H, CH_2-Im), 3.37 (dd, *J* = 13.0, 6.6 Hz, 1H, CH_2-Im). ^{31}P NMR (200 MHz, $CDCl_3$) δ = −13.08 (s). High resolution ESI-MS: *m/z* for $[M-I]^+$ = 562.1472 (calcd. 562.1473) = $[CuC_{33}H_{30}N_3P]^+$; *m/z* = 1253.1977 (calcd. 1253.1973) = $Cu_2(NNP)_2I]^+$; *m/z* = 500.2249 (calcd. 500.2256) = $[NNP+H]^+$.

Synthesis of [Cu(NNP)Cl]

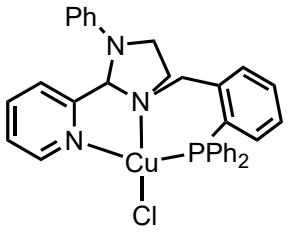

In a 50 mL Schlenk flask, CuCl (0.006 g, 0.05 mmol) and NNP (0.025 g, 0.05 mmol) were dissolved in 5 mL of CH_3CN under N_2 atm. The yellow reaction mixture was stirred for 5 h at room temperature under N_2 atm. The solvent was evaporated under reduced pressure and dried under vacuum. A yellow color solid compound was obtained. XRD-quality crystals were formed by slow diffusion of diethyl ether into a concentrated acetonitrile solution of [Cu(NNP)Cl] after 2 weeks. Yield: (0.03 g, 100%). ^{1}H NMR (400 MHz, $CDCl_3$) δ = 8.88 (d, *J* = 4.8 Hz, 1H, Ph), 7.85 – 7.79 (m, 2H, Ph), 7.65 (t, *J* = 7.7 Hz, 1H, Ph), 7.45 (m, 3H, Ph), 7.37 (d, *J* = 5.1 Hz, 7H, Ph), 7.28 (m, 1H, Ph), 7.24 (m, 1H, Ph), 7.21 (d, *J* = 7.1 Hz, 2H, Ph), 6.92 (t, *J* = 7.4 Hz, 1H, Ph), 6.83 (t, *J* = 7.3 Hz, 2H, Ph), 6.58 (d, *J* = 8.1 Hz, 2H, Ph), 5.29 (s, 1H, C*H), 4.03 (d, *J* = 12.2 Hz, 1H, Bn), 3.79 (dd, *J* = 17.8, 8.2 Hz, 1H, Bn), 3.60 (d, *J* = 5.6 Hz, 1H, CH_2-Im), 3.55 (d, *J* = 12.1 Hz, 1H, CH_2-Im), 3.48 (d, *J* = 8.0 Hz, 1H, CH_2-Im), 3.35 (dd, *J* = 13.2, 6.8 Hz, 1H, CH_2-Im). ^{31}P NMR (200 MHz, $CDCl_3$) δ = −11.78 (s). High resolution ESI-MS: *m/z* for $[M-Cl]^+$ = 562.1476 (calcd. 562.1473) = $[CuC_{33}H_{30}N_3P]^+$.

Synthesis of [Cu(NNP)(CH_3CN)][X] complexes

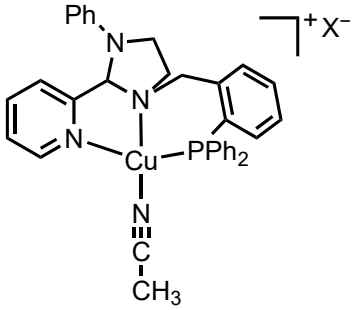

In a 50 mL Schlenk flask, $[Cu(CH_3CN)_4][X]$ (X = BF_4, PF_6, OTf) (0.05 mmol) and NNP (0.025 g, 0.05 mmol) were dissolved in 5 mL dry acetonitrile under N_2 atm. The colorless reaction mixture was stirred for 5 h at room temperature under N_2 atm. The solvent was evaporated under reduced pressure. A colorless solid compound was obtained.

[Cu(NNP)(CH_3CN)][BF_4]: Yield: (0.032 g, 92%), ^{1}H NMR (500 MHz, $CDCl_3$) δ = 8.69 (d, *J* = 3.9 Hz, 1H, Ph), 7.79 (t, *J* = 7.6 Hz, 1H, Ph), 7.48 (d, *J* = 5.9 Hz, 8H, Ph), 7.41 (t, *J* = 11.2

Hz, 4H, Ph), 7.33 (d, *J* = 18.4 Hz, 3H, Ph), 7.25 (m, 1H, Ph), 6.91 (d, *J* = 8.8 Hz, 1H, Ph), 6.83 (m, 2H, Ph), 6.57 (d, *J* = 8.2 Hz, 2H, Ph), 5.25 (s, 1H, C*H), 4.02 (d, *J* = 12.4 Hz, 1H, Bn), 3.84 (dd, *J* = 17.0, 9.4 Hz, 1H, Bn), 3.61 – 3.55 (m, 2H, CH_2-Im), 3.48 (dd, *J* = 12.8, 6.7 Hz, 1H, CH_2-Im), 3.35 (dd, *J* = 19.7, 11.4 Hz, 1H, CH_2-Im), 2.19 (s, 3H, -CH_3). ^{31}P NMR (200 MHz, $CDCl_3$) δ = −8.12 (s).

[Cu(NNP)(CH_3CN)][PF_6]: Yield: (0.035 g, 93%), ^{1}H NMR (400 MHz, $CDCl_3$) δ = 8.68 (s, 1H, Ph), 7.79 (t, *J* = 7.6 Hz, 1H, Ph), 7.44 (dd, *J* = 19.0, 10.6 Hz, 11H, Ph), 7.37 – 7.28 (m, 3H), 6.91 (m, 1H, Ph), 6.87 – 6.80 (m, 2H, Ph), 6.56 (d, *J* = 8.1 Hz, 2H, Ph), 5.24 (s, 1H, C*H), 4.03 (d, *J* = 12.4 Hz, 1H, Bn), 3.85 (dd, *J* = 17.1, 9.2 Hz, 1H, Bn), 3.59 (dd, *J* = 19.5, 10.4 Hz, 2H, CH_2-Im), 3.50 – 3.43 (m, 1H, CH_2-Im), 3.39 – 3.30 (m, 1H, CH_2-Im), 2.19 (s, 3H, -CH_3). ^{31}P NMR (200 MHz, $CDCl_3$) δ = −8.21 (s), −(137.80) −140.72, −145.29, −147.32, −152.27 (quintet).

[Cu(NNP)(CH_3CN)][OTf]: Yield: (0.036 g, 95%), ^{1}H NMR (400 MHz, $CDCl_3$) δ = 8.85 (d, *J* = 4.8 Hz, 1H, Ph), 7.75 (t, *J* = 7.3 Hz, 1H, Ph), 7.64 – 7.59 (m, 2H, Ph), 7.45 (dd, *J* = 21.2, 5.5 Hz, 11H, Ph), 7.29 (d, *J* = 8.4 Hz, 3H, Ph), 6.87 (dd, *J* = 18.1, 11.4 Hz, 3H, Ph), 6.59 (d, *J* = 8.1 Hz, 2H, Ph), 5.27 (s, 1H, C*H), 3.95 (d, *J* = 12.4 Hz, 1H, Bn), 3.80 (dd, *J* = 17.6, 8.5 Hz, 1H, Bn), 3.60 (d, *J* = 12.4 Hz, 1H, CH_2-Im), 3.55 – 3.49 (m, 1H, CH_2-Im), 3.45 – 3.32 (m, 2H, CH_2-Im), 2.06 (s, 3H, -CH_3). ^{31}P NMR (200 MHz, $CDCl_3$) δ = −7.14 (s).

Synthesis of [Cu_2(NNP)$_2$(μ-Cl)Cl_2][$CuCl_2$]

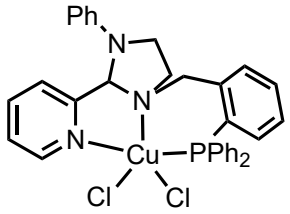

In a 50 mL Schlenk flask, $CuCl_2$ (0.006 g, 0.05 mmol) and NNP (0.025 g, 0.05 mmol) were dissolved in 5 mL dichloromethane under N_2 atm. The green reaction mixture was stirred for 5 h at room temperature under N_2 atm. The solvent was evaporated under reduced pressure. A green color solid compound was obtained. XRD quality crystals were formed by slow diffusion of diethyl ether into a concentrated dichloromethane solution of [Cu_2(NNP)$_2$(μ-Cl)Cl_2][$CuCl_2$] after 5 days. Yield: (0.060 g, 87%). High resolution ESI-MS: *m/z* for $[M-Cl]^+$ = 597.1164 (calcd. 597.1162) = $[CuC_{33}H_{30}N_3PCl]^+$; $[M-2Cl]^+$ = 562.1472 (calcd. 562.1473) =

$[CuC_{33}H_{30}N_3P]^+$; *m/z* = 500.2257 (calcd. 500.2256) = $[NNP+H]^+$; *m/z* = 1231.1998 (calcd. 1231.1983 (96.0%)) = $[Cu_2(NNP)_2(\mu\text{-}Cl)Cl_2]^+$.

Reduction of Cu (II) to Cu(I) using ascorbic acid:

A stock solution of ascorbic acid (5mM) in 5% H_2O in CH_3CN and $[Cu_2(NNP)_2(\mu\text{-}Cl)Cl_2][CuCl_2]$, (1mM) in 10 mL CH_3CN were prepared.

In a 50 mL Schlenk flask, 10 mL solution of $[Cu_2(NNP)_2(\mu\text{-}Cl)Cl_2][CuCl_2]$ was taken. Ascorbic acid (520 µL, 2.6 eq.) was added to it. The color of the reaction immediately changed from green to colorless. It was stirred for 2 h under a N_2 atmosphere. The solvent was evaporated under reduced pressure and dried under a vacuum. The progress of the reaction was monitored by UV-vis spectroscopy, which showed a reduction of the Cu (II) complex (λ_{max} around 600-800 nm corresponding to a d–d transition band of d^9 Cu (II) species) to Cu(I) species (no d–d transition band). The formation of $[Cu_2(NNP)_2(\mu\text{-}Cl)Cl_2][CuCl_2]$ was confirmed by ^1H and ^{31}P NMR.

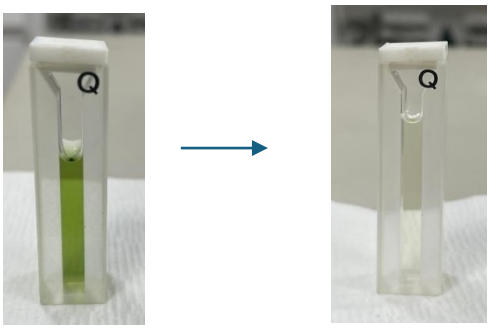

Reaction of $[Cu(NNP)(CH_3CN)][BF_4]$ with PPh_3

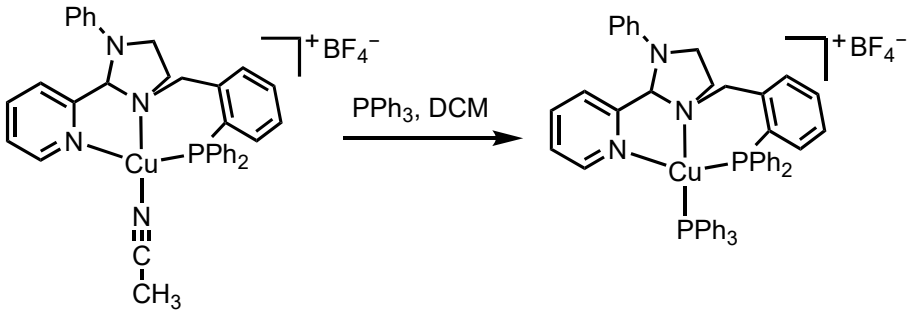

In a 50 mL Schenk flask, [Cu(NNP)(CH_3CN)][BF_4] (0.07 g, 0.1 mmol) was dissolved in 5 mL dichloromethane. PPh_3 (0.026 g, 0.1 mmol) was added to it. The colorless reaction mixture was stirred for 6 h under N_2 atmosphere. The solvent was evaporated under reduced pressure and dried under vacuum. A colorless solid compound was obtained after adding diethyl ether. XRD quality crystals were formed by slow diffusion of diethyl ether into a concentrated dichloromethane solution of [Cu(NNP)(PPh_3)][BF_4] at room temperature after 2 days. Yield: (0.09 g, 98%). ^{1}H NMR (500 MHz, $CDCl_3$) δ = 8.20 (d, *J* = 4.8 Hz, 1H, Ph), 7.82 (t, *J* = 7.5 Hz, 1H, Ph), 7.58 (d, *J* = 6.8 Hz, 1H, Ph), 7.51 (d, *J* = 6.6 Hz, 2H, Ph), 7.43 (d, *J* = 7.9 Hz, 1H, Ph), 7.39 (m, 5H, Ph), 7.31 (m, 3H, Ph), 7.26 – 7.22 (m, 2H, Ph), 7.19 (t, *J* = 8.5 Hz, 7H, Ph), 7.05 (t, *J* = 6.9 Hz, 2H, Ph), 6.98 – 6.93 (m, 7H, Ph), 6.86 (t, *J* = 12.6 Hz, 2H, Ph), 6.68 – 6.62 (m, 2H, Ph), 6.49 (d, *J* = 8.1 Hz, 2H, Ph), 5.30 (s, 1H, C*H), 4.40 (d, *J* = 12.7 Hz, 1H, Bn), 3.90 (d, *J* = 7.2 Hz, 1H, Bn), 3.74 (d, *J* = 12.7 Hz, 1H, CH_2-Im), 3.51 (t, *J* = 8.1 Hz, 1H, CH_2-Im), 3.30 – 3.23 (m, 1H, CH_2-Im), 3.10 (d, *J* = 10.2 Hz, 1H, CH_2-Im). ^{31}P NMR (200 MHz, $CDCl_3$) δ = 2.82 (d, *J* = 108.3 Hz), −9.63 (d, *J* = 85.7 Hz). High resolution ESI-MS: *m/z* for [M−BF_4-PPh_3]$^+$ = 562.1461 (calcd. 562.1473) = [$CuC_{33}H_{30}N_3P$]$^+$.

Transmetallation Reaction

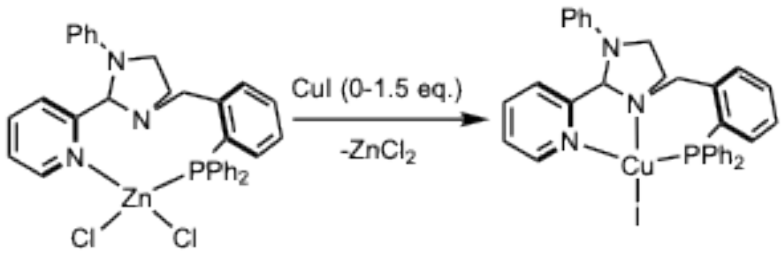

In an NMR tube, [(NNP)$ZnCl_2$] (0.010 g, 0.030 mmol) was dissolved in 300 µL of $CDCl_3$, while CuI (0.008 g, 0.045 mmol, 1.5 equiv.) was separately dissolved in 300 µL of CD_3CN. Aliquots of 100 µL from the CuI solution were sequentially added to the Zn(II) solution, and the reaction was monitored by ^{1}H and ^{31}P NMR spectroscopy. With each addition, the resonance corresponding to the Zn(II) complex gradually diminished, accompanied by the appearance of a new signal consistent with the formation of the [(NNP)CuI] complex. The product was further characterized by high-resolution ESI-MS, which showed a peak at m/z 562.1477 for [M–I]$^+$, in excellent agreement with the calculated value (562.1473) for [$CuC_{33}H_{30}N_3P$]$^+$.

Biological Activity

Antibacterial Activity

The broth microdilution assay was used to measure the antimicrobial activity of the synthesized compounds. Overnight grown S. aureus ATCC29213 culture was diluted to 10^6 CFU//mL in MHB media. Two-fold serial dilution of the compounds from the DMSO stock was prepared in 96-well plates (100 µL), followed by the addition of 100 µL bacterial culture. The plates were then kept in an incubator for 18-24 h at 37 °C. The MIC (Minimum Inhibitory Concentration) was identified as the minimum concentration at which no apparent growth was observed. For all the compounds, MIC was determined in biological replicates.

Anticancer Activity

Cell Lines and Culture Conditions:

Breast adenocarcinoma cell lines MDA-MB-231 and MCF-7, Human lung adenocarcinoma cell line A549, and Human embryonic kidney cell line HEK-293 were obtained from the National Centre for Cell Science (NCCS Pune, India). The cell lines were maintained in RPMI 1640 (MDA-MB-231, MCF-7 and A549) or DMEM medium (HEK-293), supplemented with 10% fetal bovine serum, 10,000 Units/mL penicillin and 10,000 µg/mL streptomycin, at 37 °C humidified atmosphere with 5% CO_2. Compound stocks were prepared in DMSO.

MTT assay:

The cytotoxicity of the compounds was determined by the MTT assay. The cells were trypsinized and seeded into 96-well microculture plates at a seeding density of 2,500 cells per well. After 24 h, they were treated with drugs at different concentrations in the media for 72 h. Cisplatin was taken as a positive control. Then the cells were incubated with MTT solution for 4 h in the dark, and the absorbance was taken at 570 nm by SpectraMax M5e microplate reader. All procedures were carried out in triplicate in three independent experiments. IC_{50} values were calculated using GraphPad Prism 8.0 software, and the results were presented as a mean ± SD.

Figure S 1. ^{1}H NMR spectrum of the (1) and (2) in $CDCl_3$ at 298 K.

The Schiff base compound was found to be in equilibrium with the cyclized compound which was confirmed by ^{1}H NMR and ^{31}P NMR.

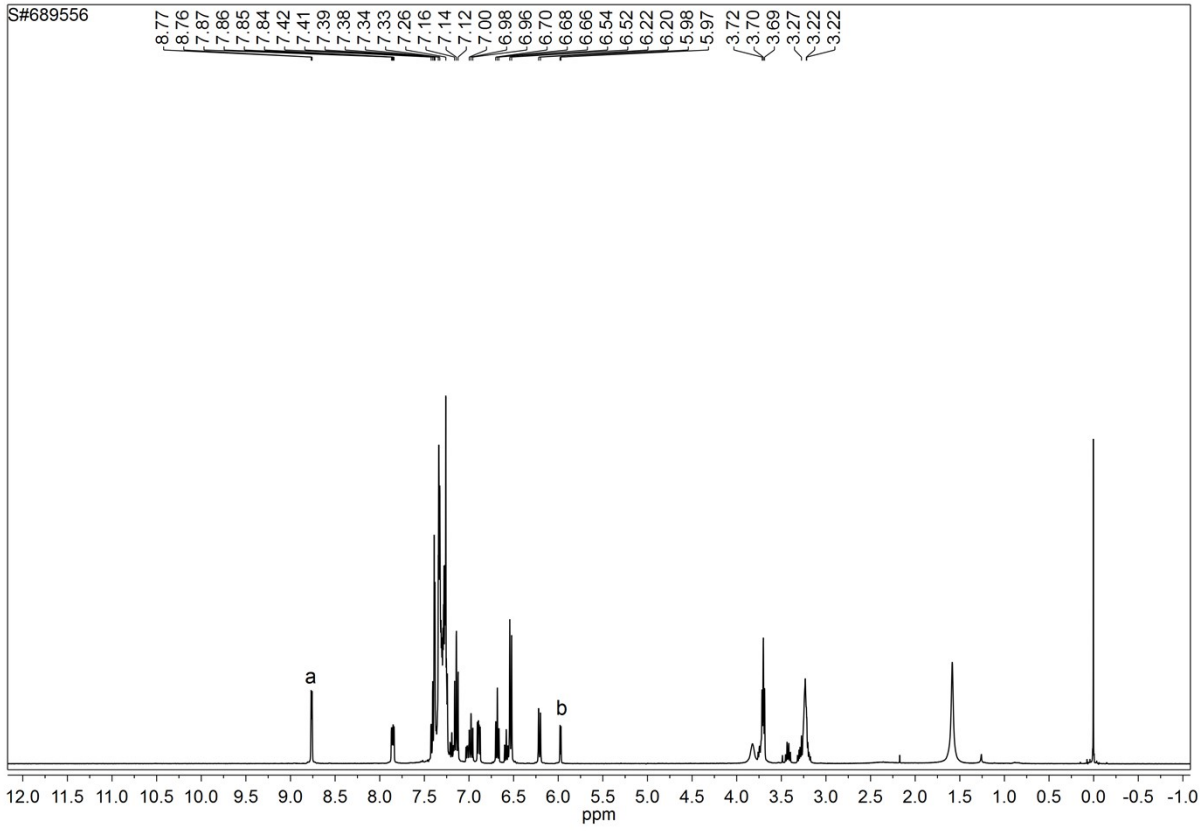

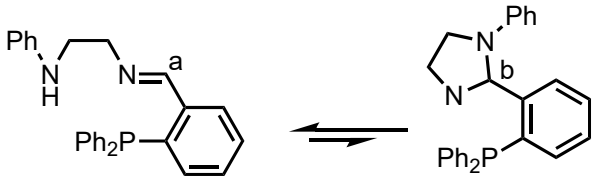

(1) (2)

Figure S 2. ^{31}P NMR spectrum of the (1) and (2) in $CDCl_3$ at 298 K.

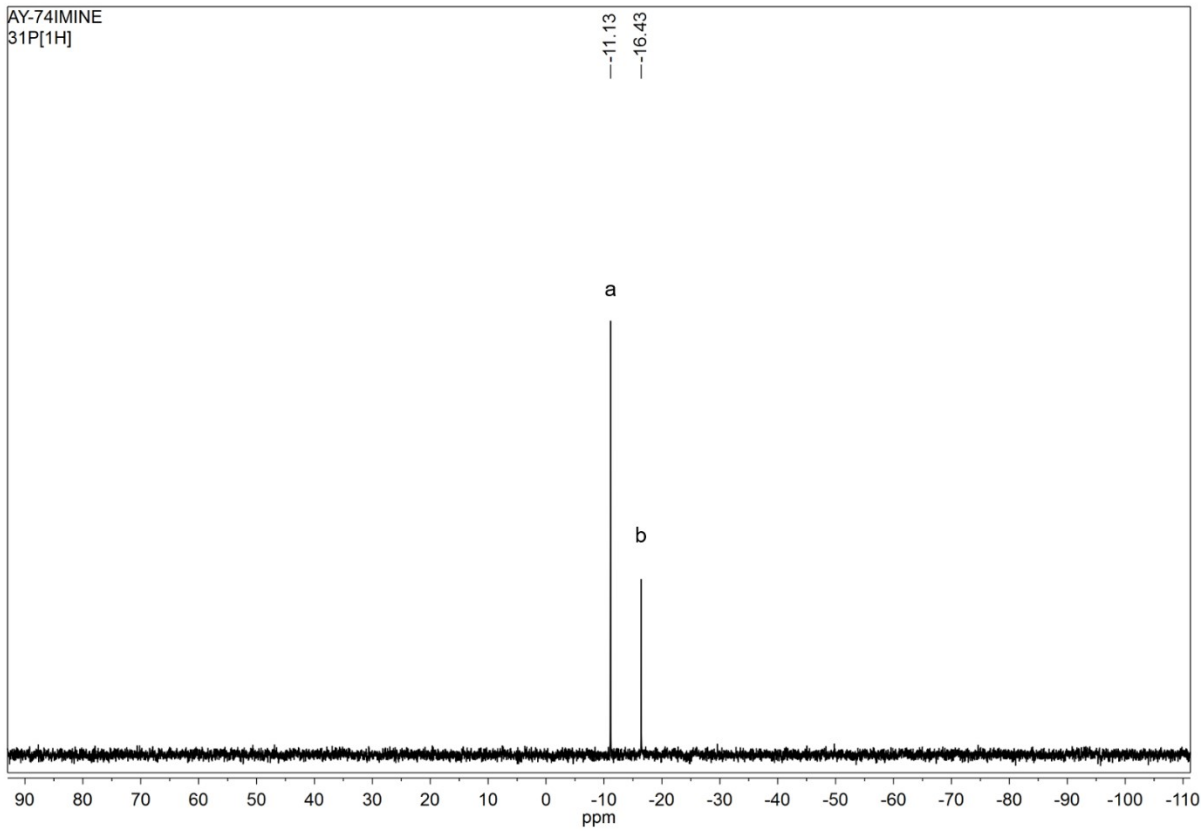

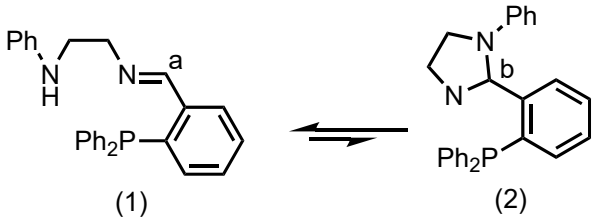

Figure S 3.[1]H NMR spectrum of the N^1-(2-(diphenylphosphaneyl)benzyl)-N^2-phenylethane-1,2-diamine (3) in $CDCl_3$ at 298 K.

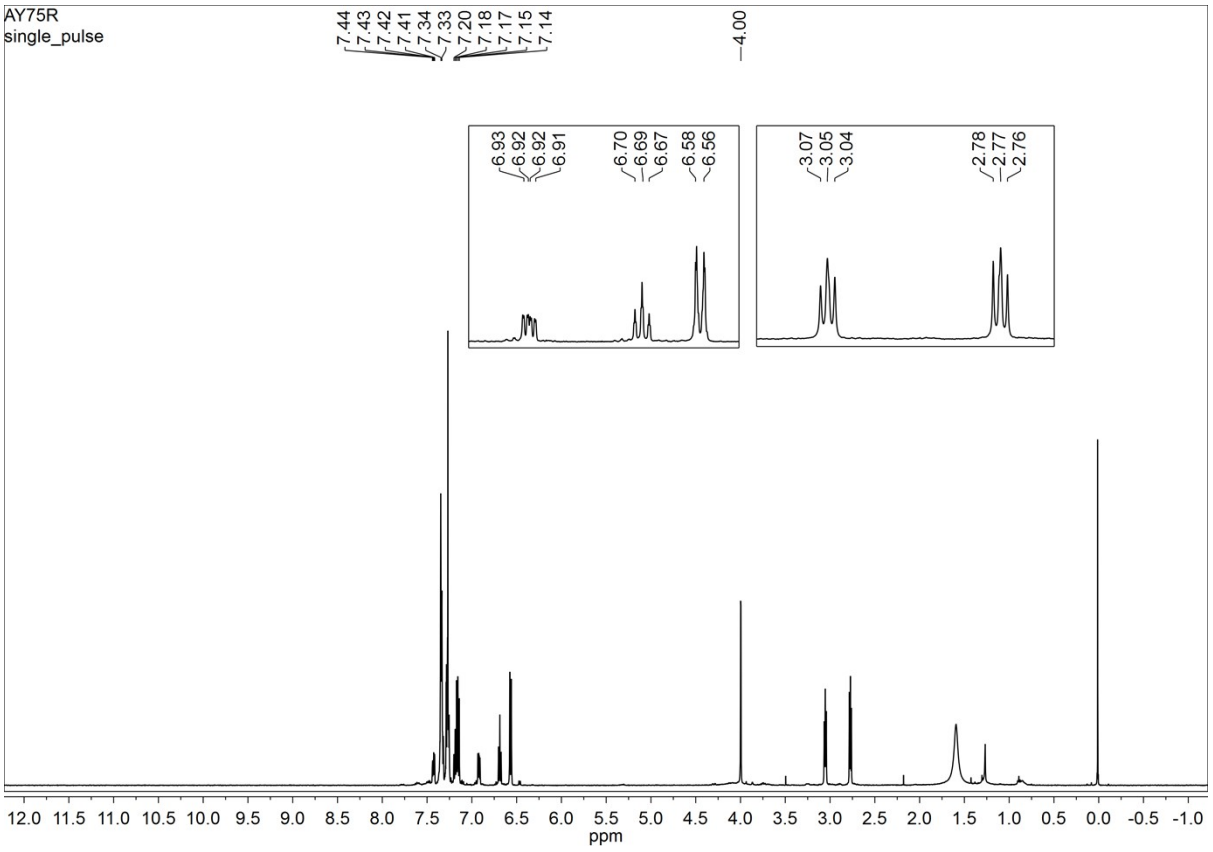

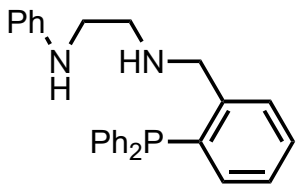

Figure S 4. ^{13}C NMR spectrum of the N^1-(2-(diphenylphosphaneyl)benzyl)-N^2-phenylethane-1,2-diamine (3) in $CDCl_3$ at 298 K.

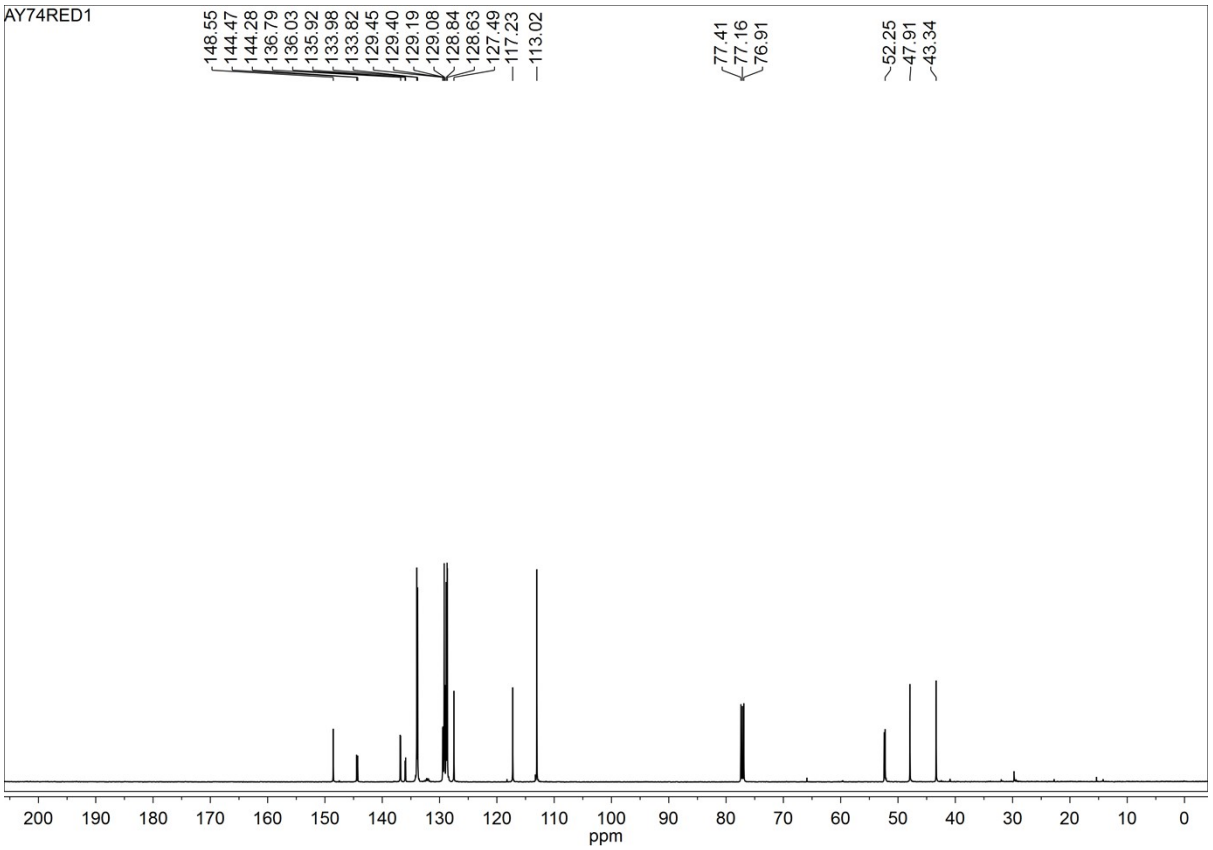

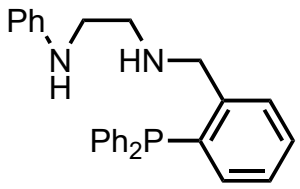

Figure S 5. ^{31}P NMR spectrum of the N^1-(2-(diphenylphosphaneyl)benzyl)-N^2-phenylethane-1,2-diamine (3) in $CDCl_3$ at 298 K.

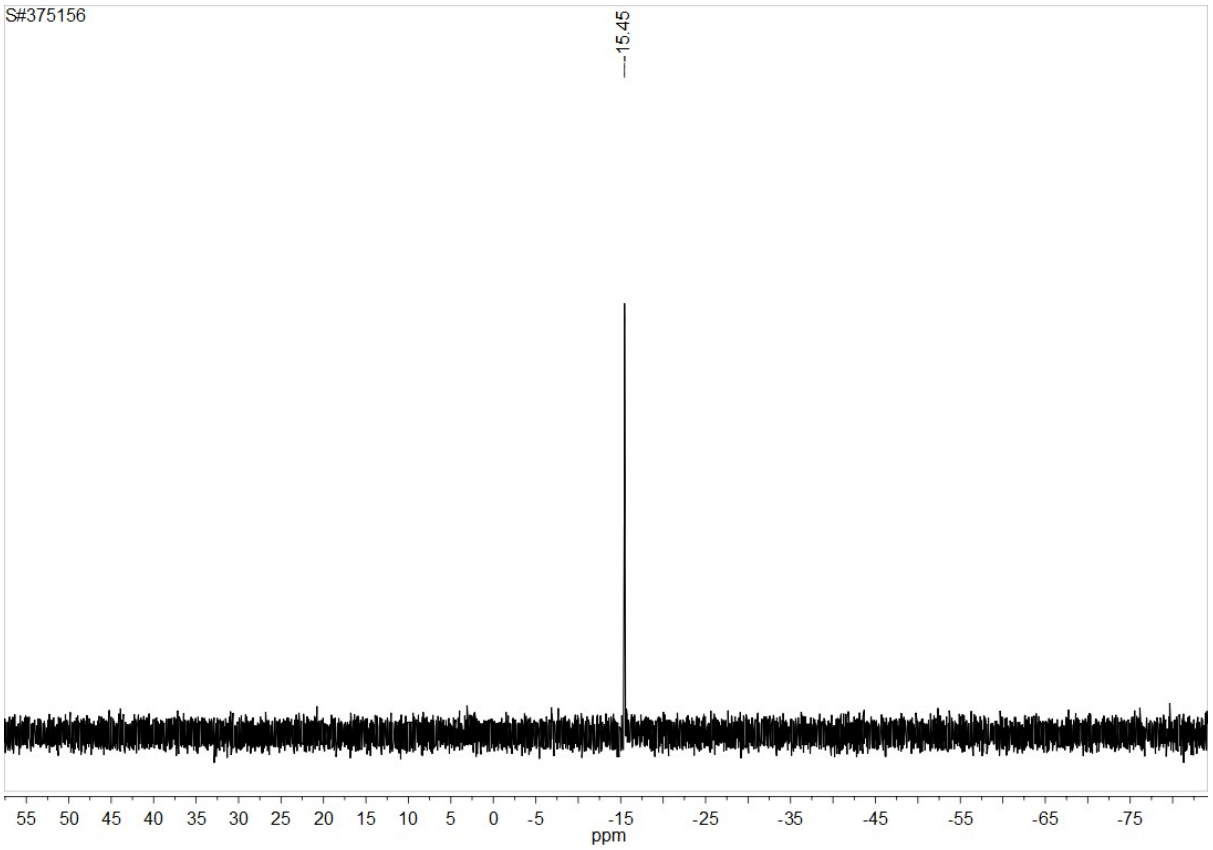

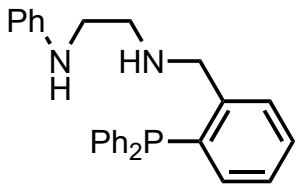

Figure S 6. ^{1}H NMR spectrum of the NNP in $CDCl_3$ at 298 K.

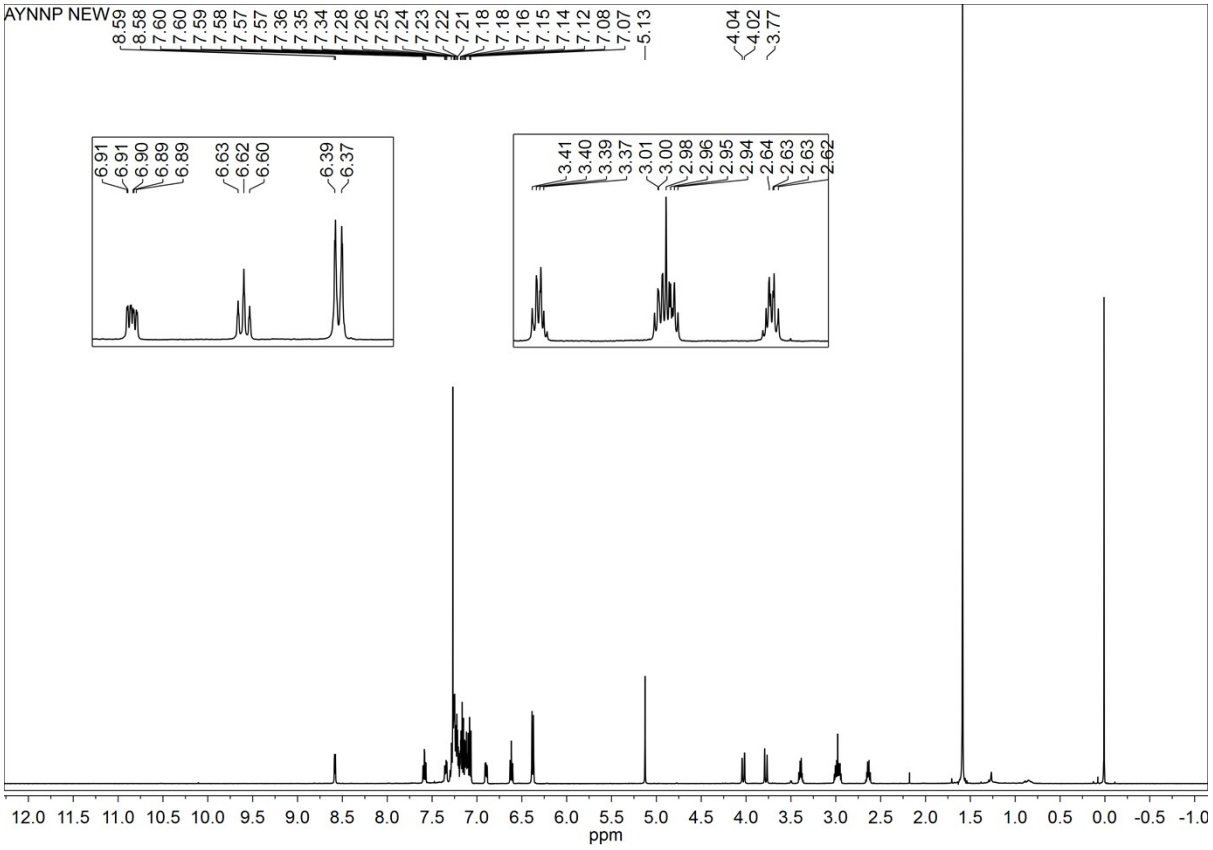

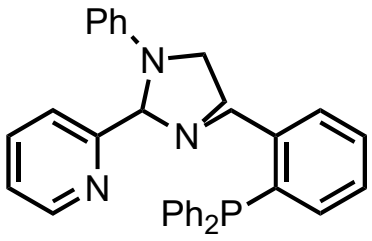

Figure S 7. ^{13}C NMR spectrum of the NNP in $CDCl_3$ at 298 K.

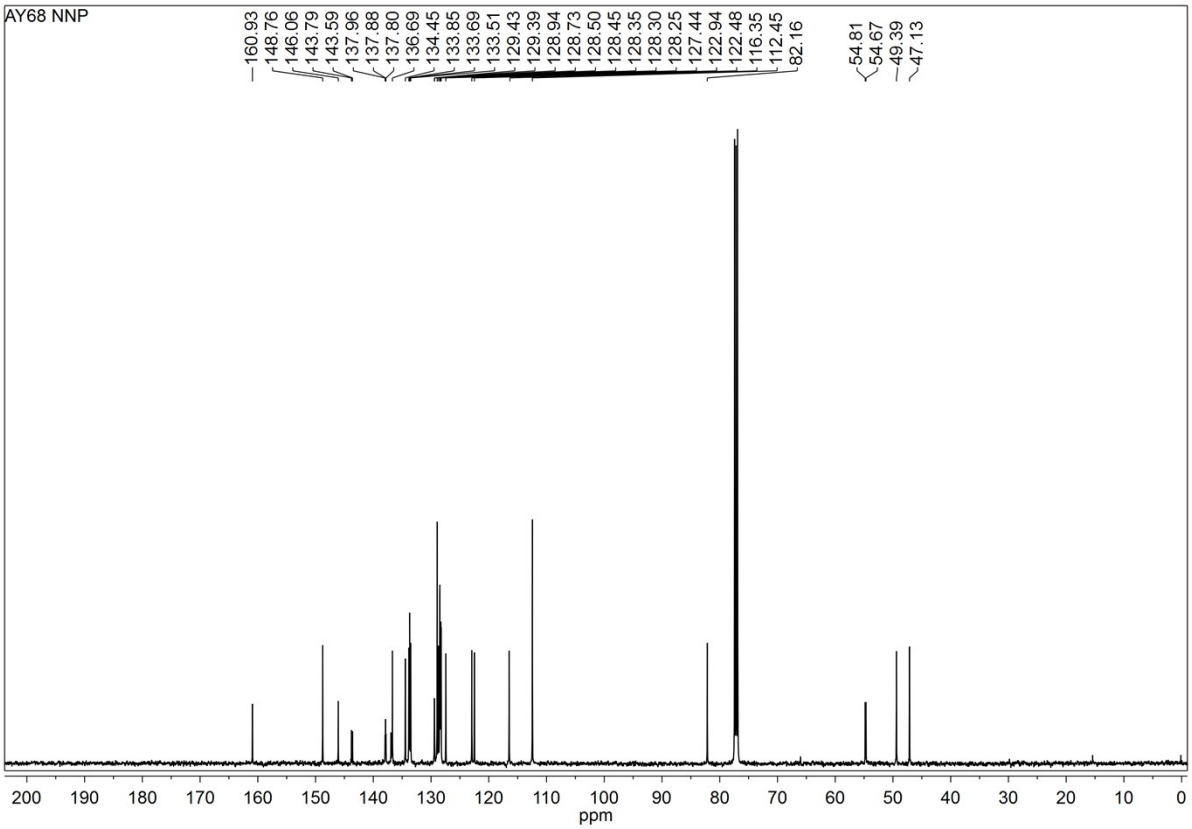

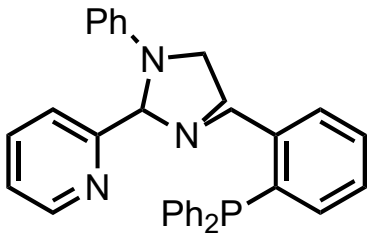

Figure S 8. ^{31}P NMR spectrum of the NNP in $CDCl_3$ at 298 K.

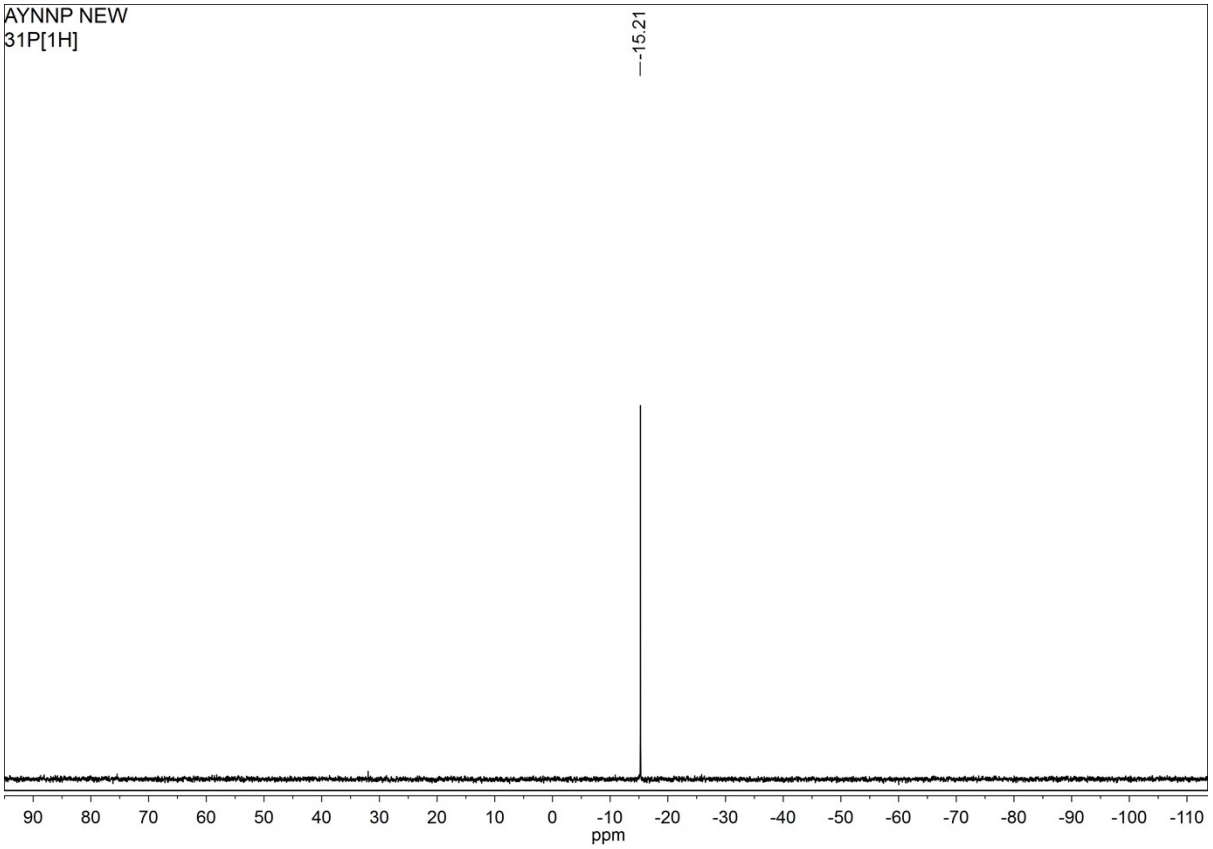

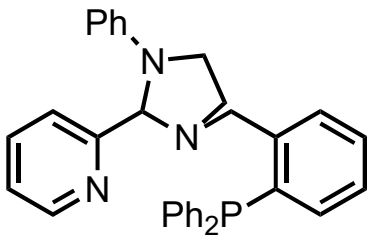

Figure S 9. ESI-MS of NNP

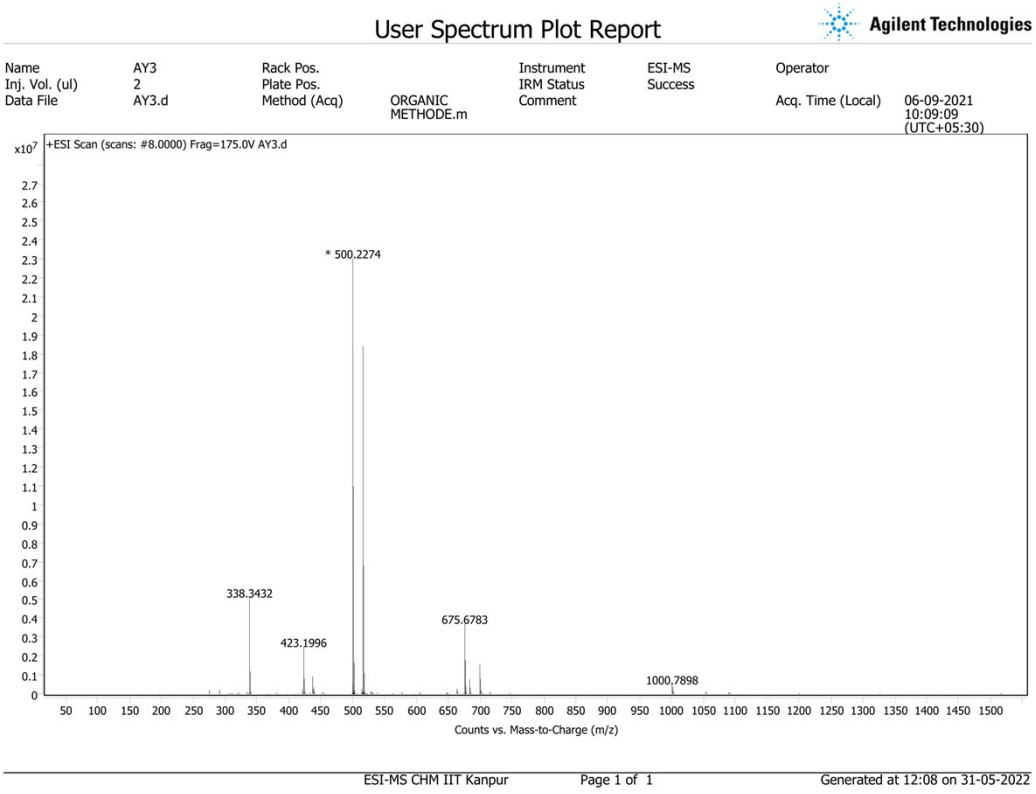

High resolution ESI-MS: *m/z* for $[M+H]^+$ = 500.2274 (calcd. 500.2256) = $[C_{33}H_{31}N_3P]^+$.

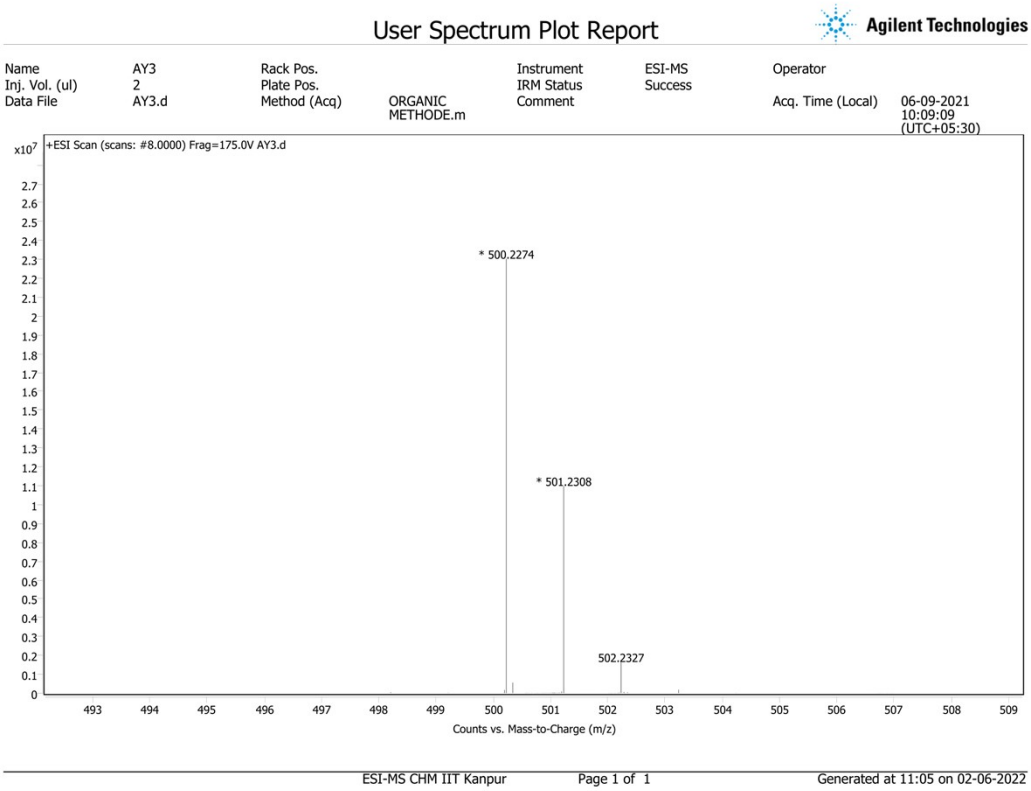

Figure S 10. Simulated ESI-MS of NNP

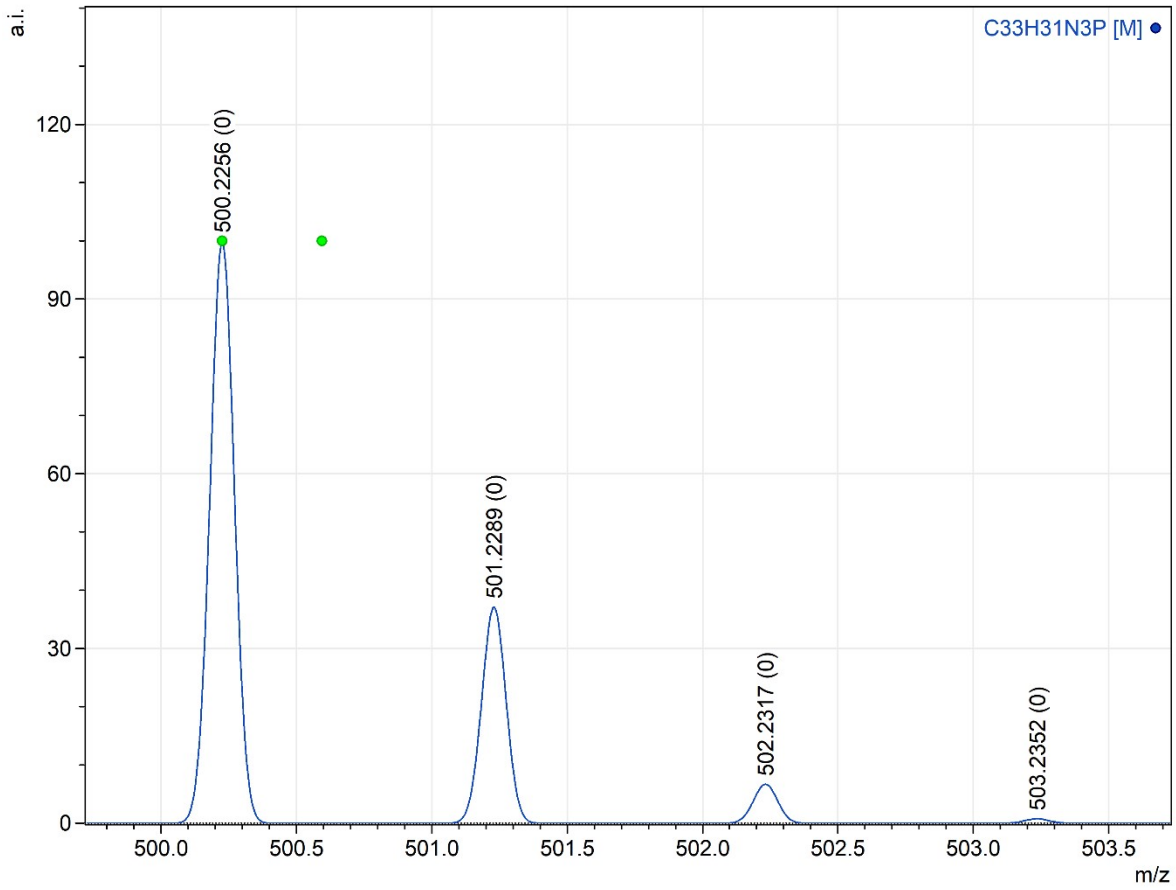

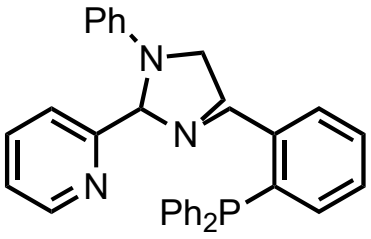

Figure S 11. ^{1}H NMR of $[Zn(NNP)Cl_2]$ complex in $CDCl_3$ at 298 K.

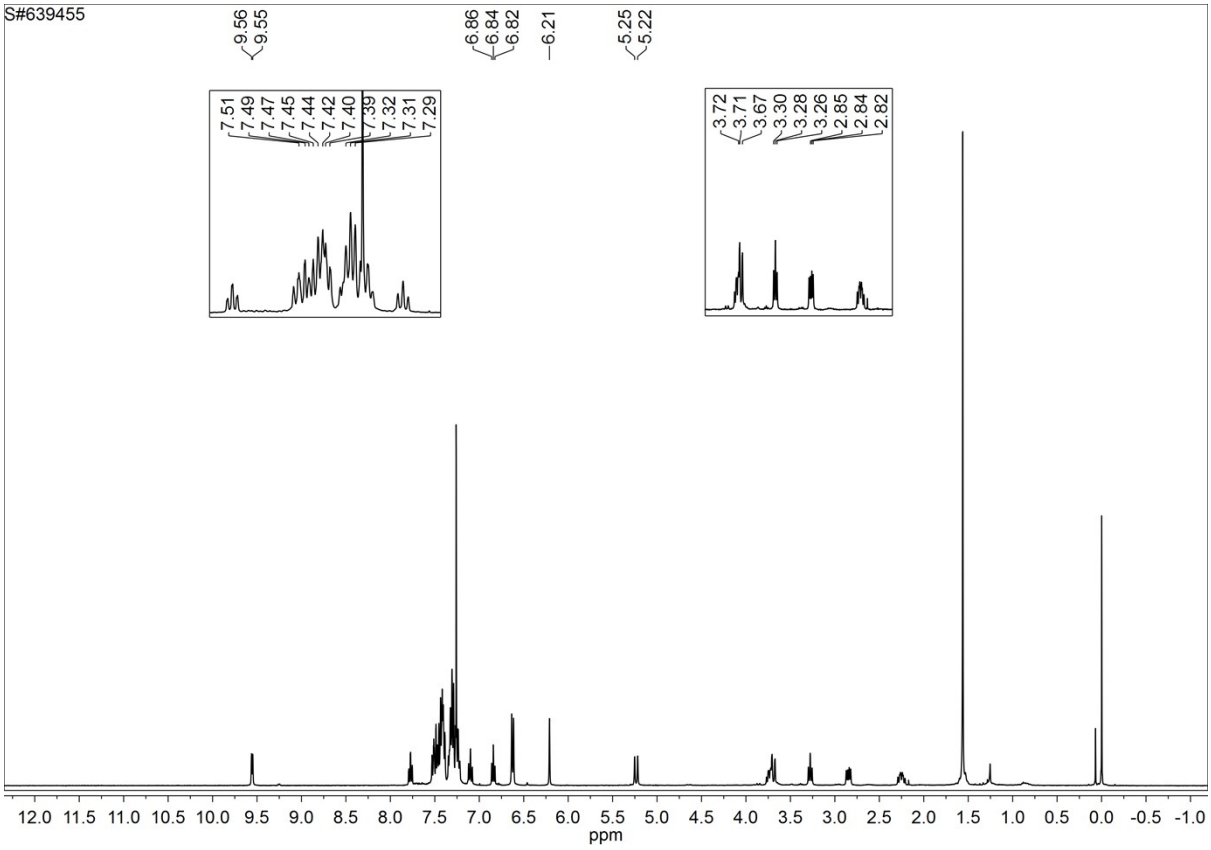

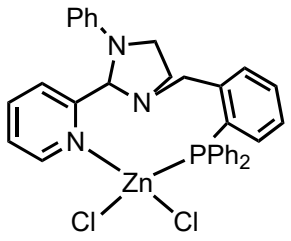

Figure S 12. ^{13}C NMR of $[Zn(NNP)Cl_2]$ complex in $CDCl_3$ at 298 K.

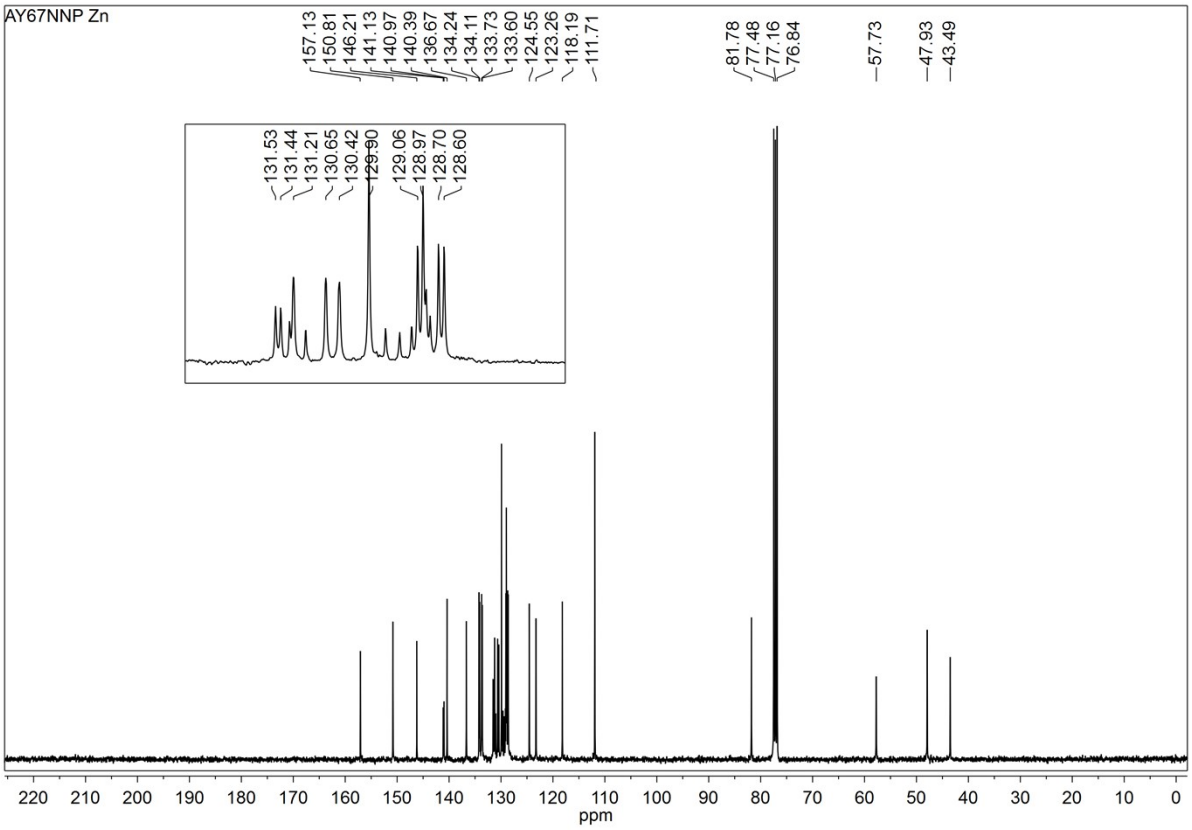

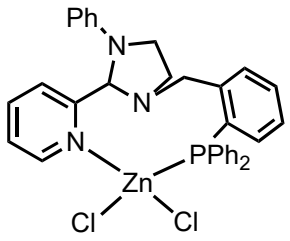

Figure S 13. ^{31}P NMR of $[Zn(NNP)Cl_2]$ complex in $CDCl_3$ at 298 K.

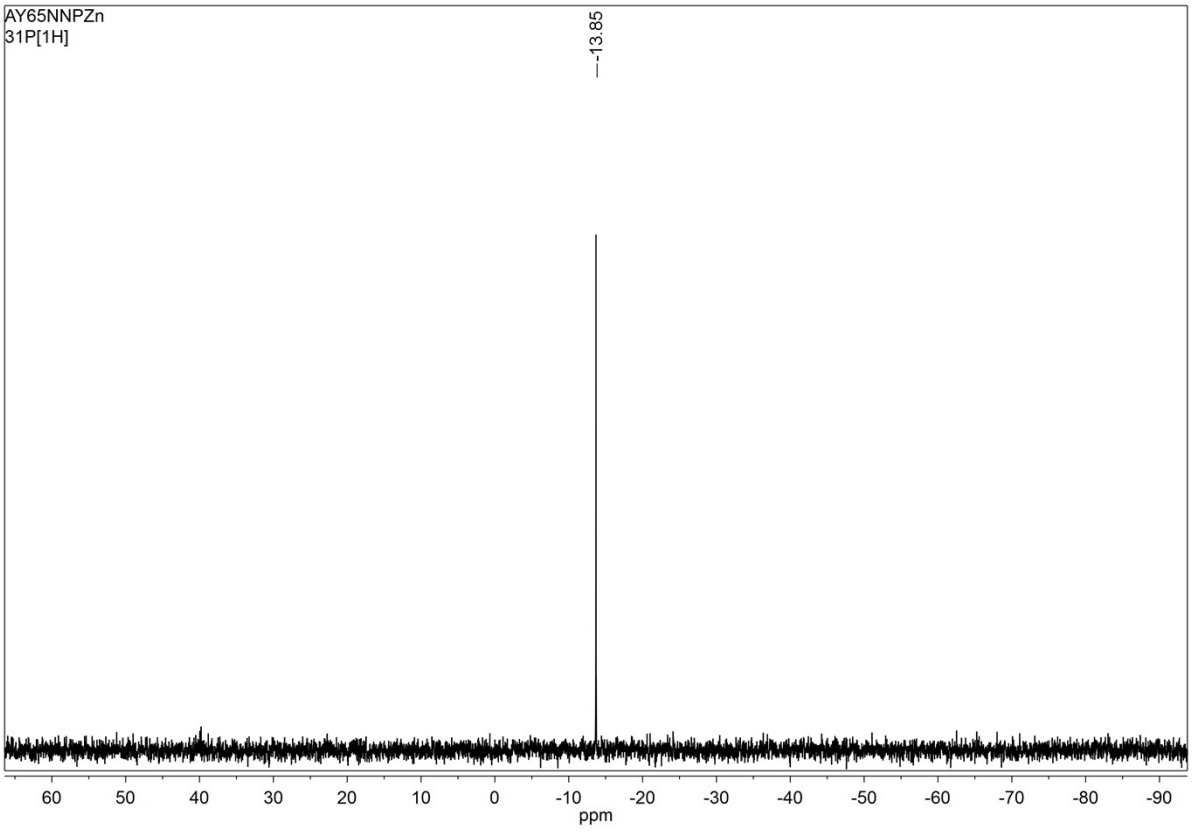

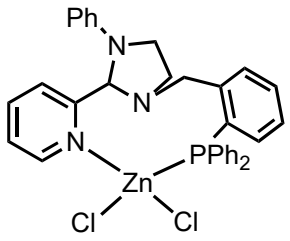

Figure S 14. Elemental analysis of [Zn(NNP)Cl_2] complex.

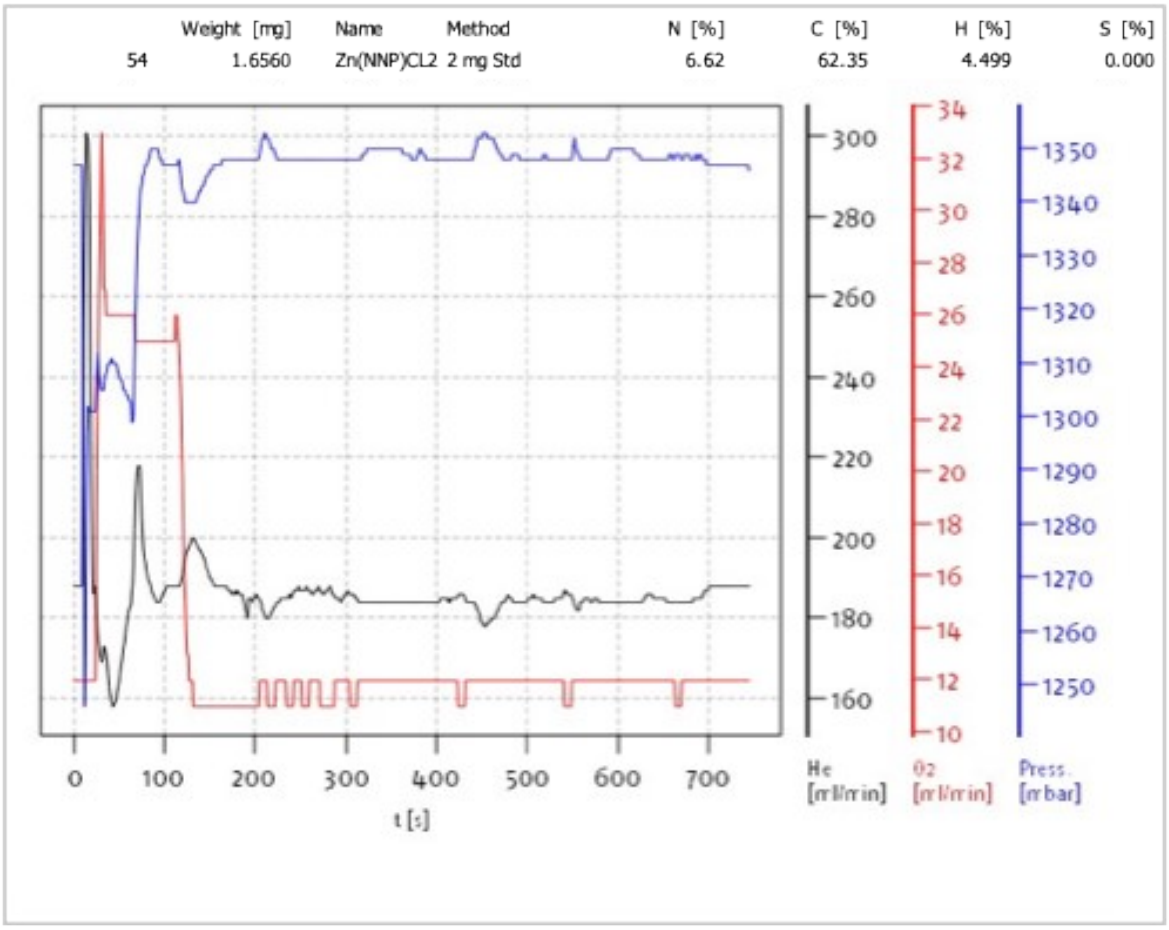

Elemental analysis calculated (%) for $C_{33}H_{30}Cl_2N_3PZn$: C, 62.33; H, 4.76; N, 6.61. Found: C, 62.35; H, 4.49; N, 6.62.

Figure S 15. ESI-MS of $[Zn(NNP)Cl_2]$ complex.

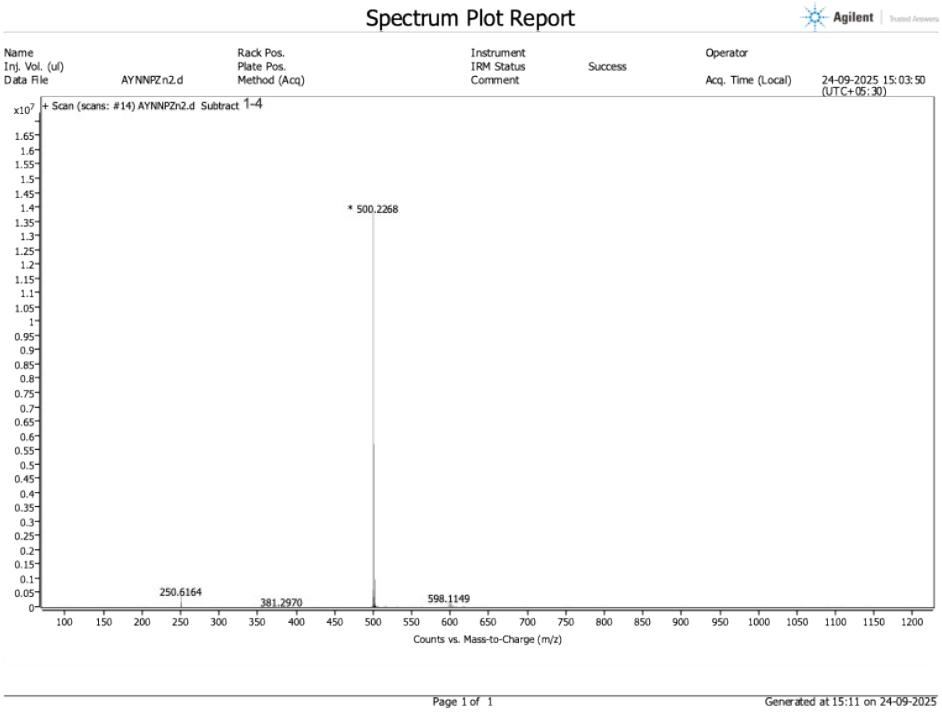

High resolution ESI-MS: *m/z* for $[M\text{-}Cl]^+$ = 598.1149 (calcd. 598.1157) = $[ZnC_{33}H_{30}N_3PCl]^+$, $[NNP+H]$ = 500.2268 (calcd. 500.2256) = $[C_{33}H_{31}N_3P]^+$.

Spectrum Plot Report

Agilent | Trusted Answers

Name		Rack Pos.		Instrument	Operator
Inj. Vol. (ul)		Plate Pos.		IRM Status Success	
Data File	AYNNPZn2.d	Method (Acq)		Comment	Acq. Time (Local) 24-09-2025 15:03:50 (UTC+05:30)

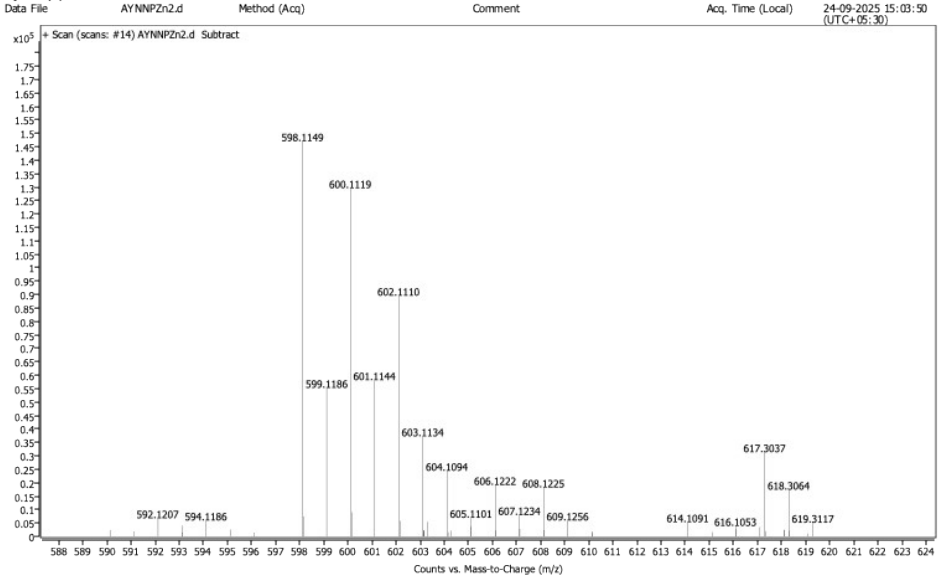

Generated at 15:12 on 24-09-2025

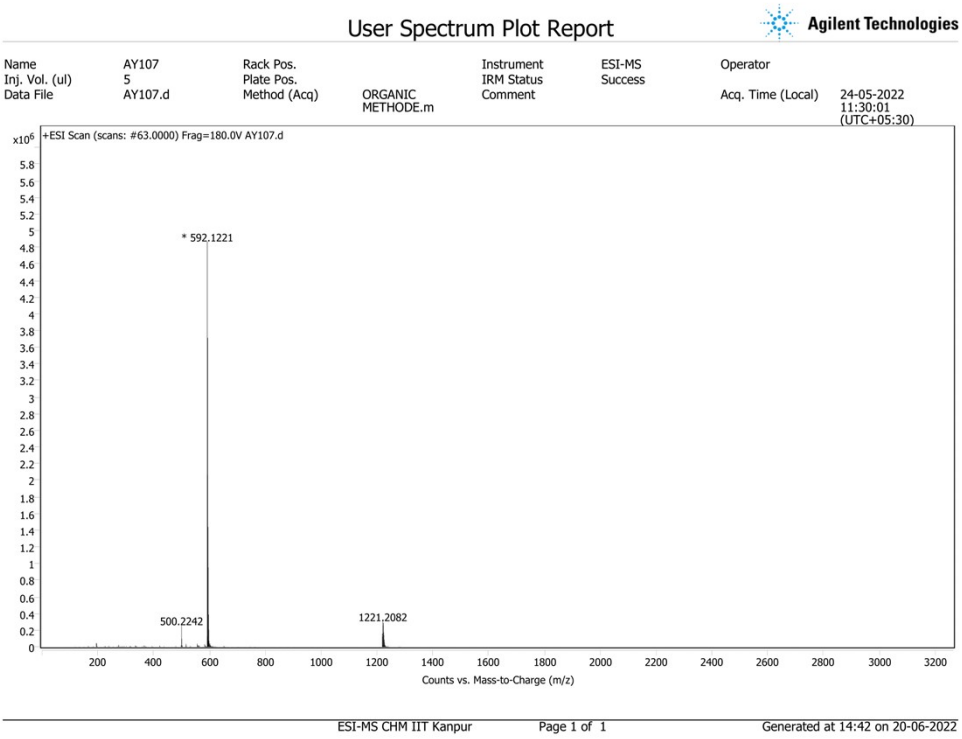

Figure S 16. ESI-MS of $[Ni(NNP)Cl_2]\cdot CH_3CN$

High resolution ESI-MS: m/z for $[M-Cl]^+$ = 592.1221 (calcd. 592.1219) = $[NiC_{33}H_{30}N_3ClP]^+$.

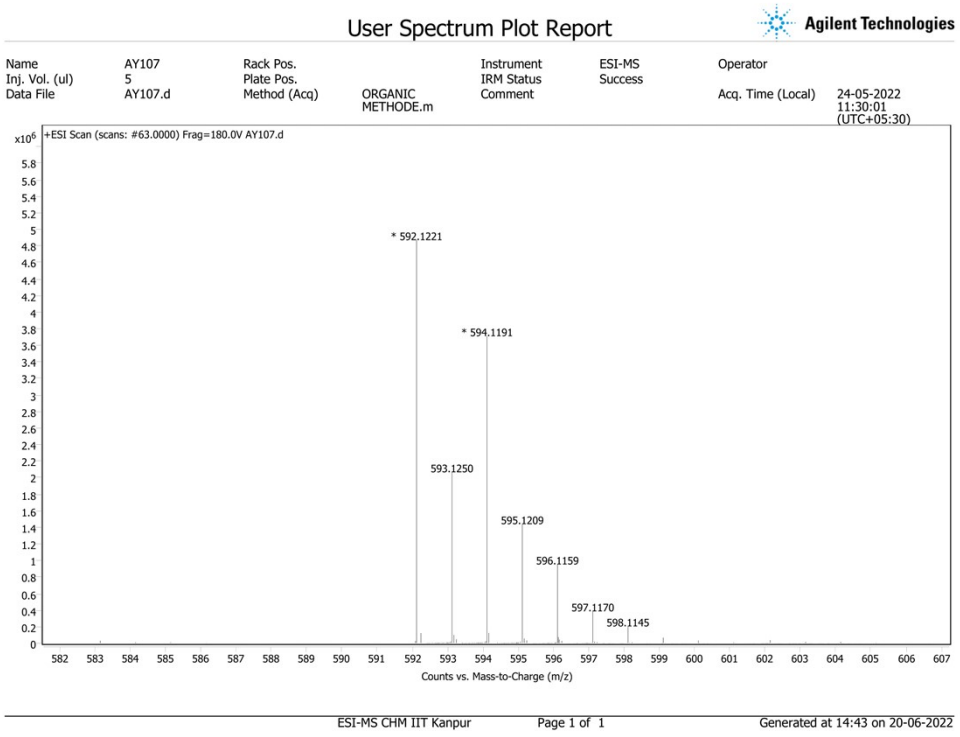

Figure S 17. Simulated ESI-MS of $[Ni(NNP)Cl_2]\cdot CH_3CN$ complex.

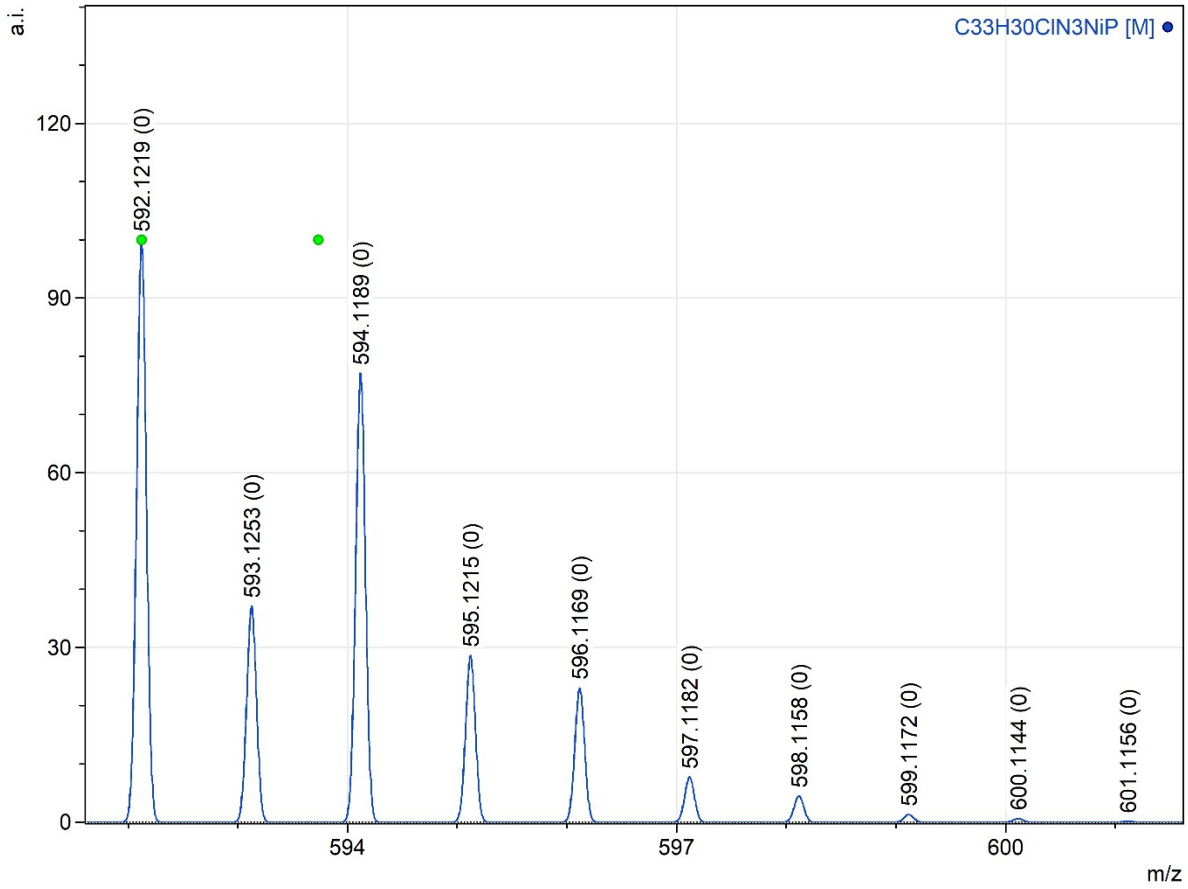

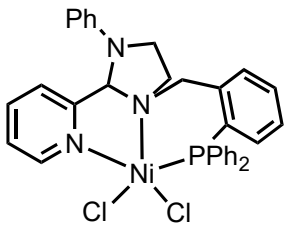

Figure S 18. Elemental analysis of $[Ni(NNP)Cl_2]\cdot CH_3CN$ complex.

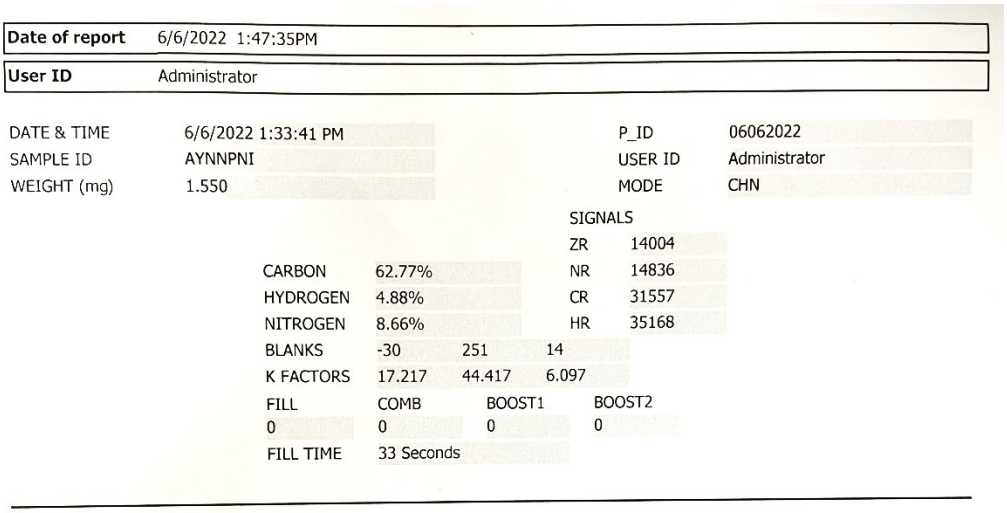

Date of report	6/6/2022 1:47:35PM
User ID	Administrator

DATE & TIME	6/6/2022 1:33:41 PM	P_ID	06062022
SAMPLE ID	AYNNPNI	USER ID	Administrator
WEIGHT (mg)	1.550	MODE	CHN

		SIGNALS	
		ZR	14004
CARBON	62.77%	NR	14836
HYDROGEN	4.88%	CR	31557
NITROGEN	8.66%	HR	35168

BLANKS	-30	251	14
K FACTORS	17.217	44.417	6.097

FILL	COMB	BOOST1	BOOST2
0	0	0	0
FILL TIME	33 Seconds		

Figure S 19. Cyclic voltammogram of $[Ni(NNP)Cl_2]\cdot CH_3CN$

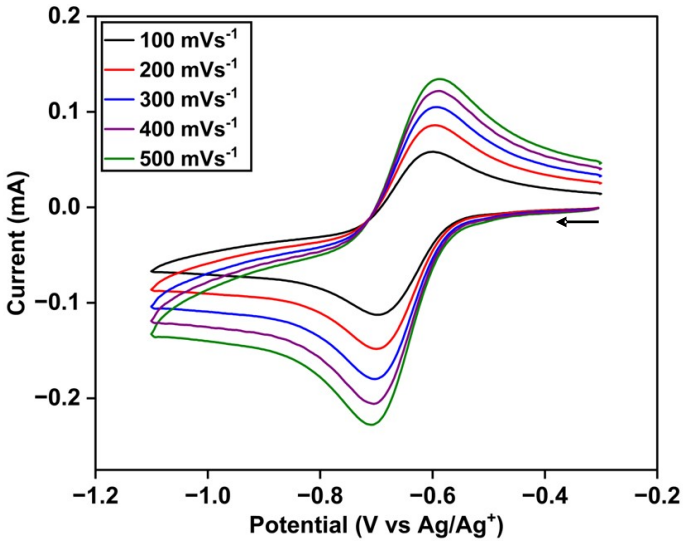

Cyclic Voltammograms of 1mM of $[Ni(NNP)Cl_2]\cdot CH_3CN$ complex at a static glassy Carbon working electrode with Ag/AgCl reference electrode, and a Pt wire auxiliary electrode at 25 °C in CH_3CN solution containing 0.1 M $TBAPF_6$ (supporting electrolyte) at different scan rates under nitrogen atmosphere.

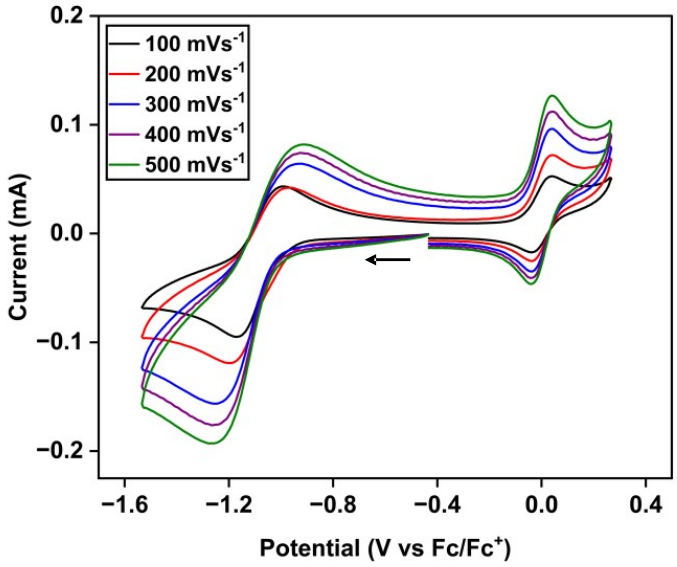

Cyclic Voltammograms of 1mM of $[Ni(NNP)Cl_2]\cdot CH_3CN$ complex after the addition of 1 mM ferrocene at a static glassy Carbon working electrode with Ag/AgCl reference electrode, and a Pt wire auxiliary electrode at 25 °C in CH_3CN solution containing 0.1 M $TBAPF_6$ (supporting electrolyte) at different scan rates under nitrogen atmosphere.

Figure S 20. ^{1}H NMR spectrum of the [Pd(NNP)Cl][Cl] in $CDCl_3$ at 298 K.

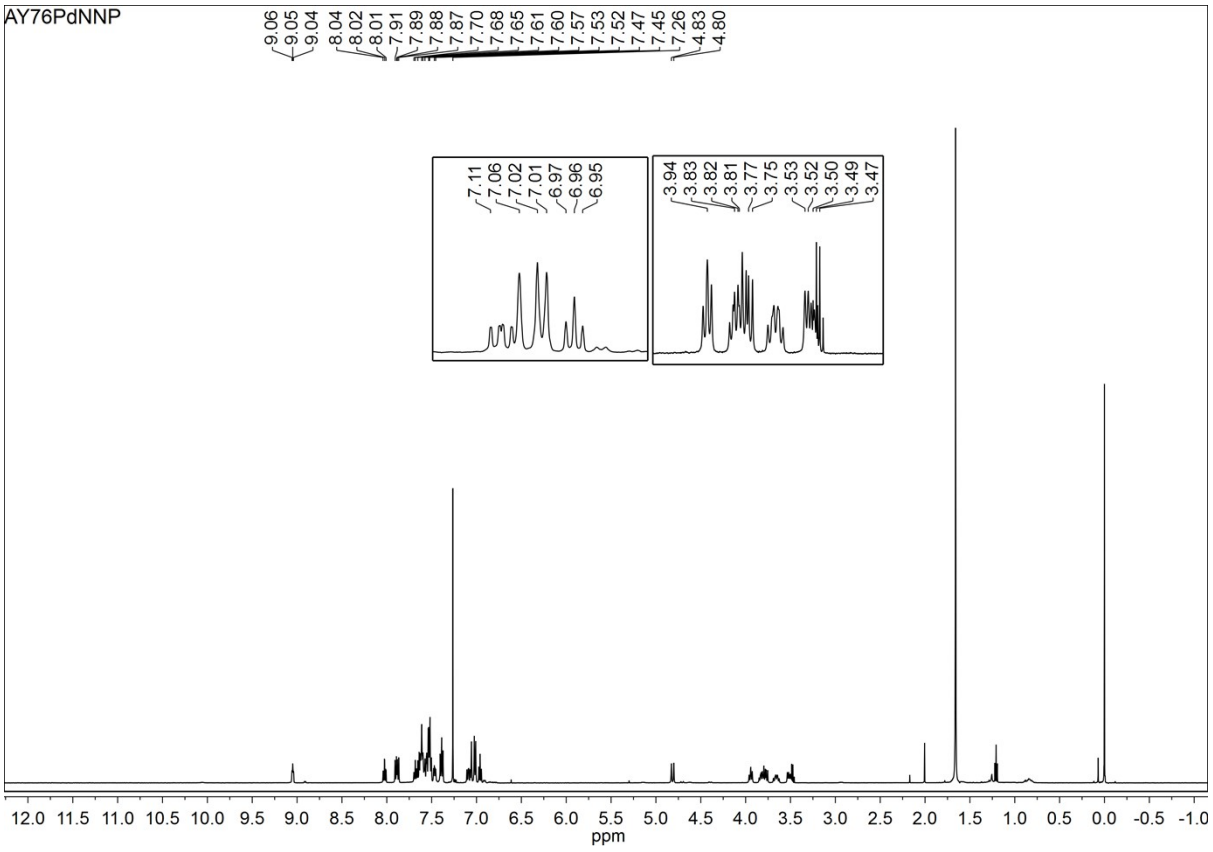

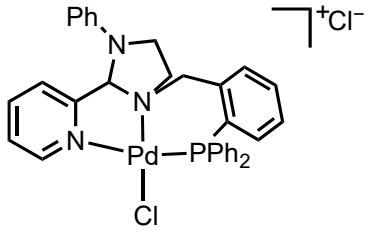

Figure S 21. ^{13}C NMR spectrum of the [Pd(NNP)Cl][Cl] in $CDCl_3$ at 298 K.

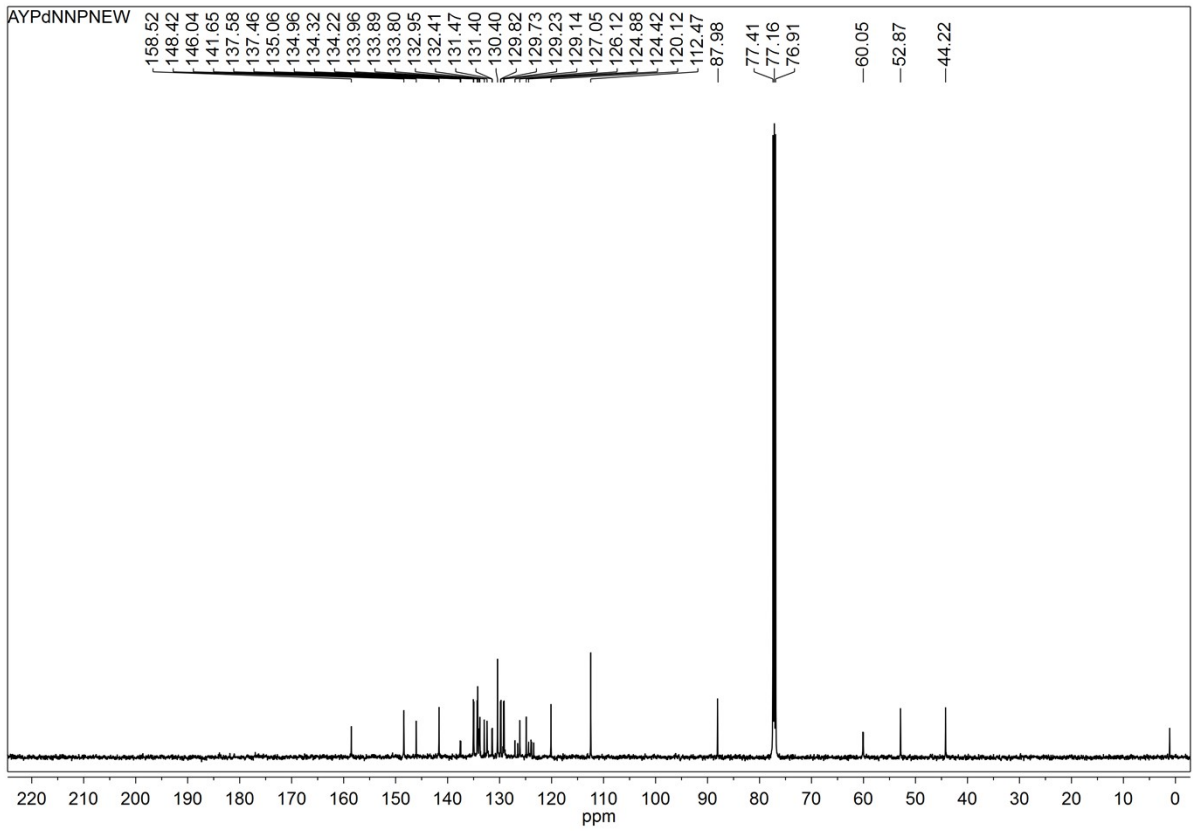

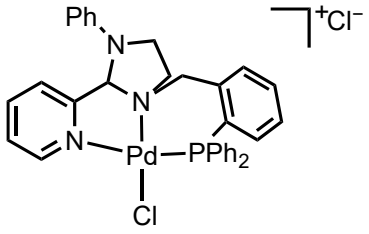

Figure S 22. ^{31}P NMR spectrum of the [Pd(NNP)Cl][Cl] in $CDCl_3$ at 298 K.

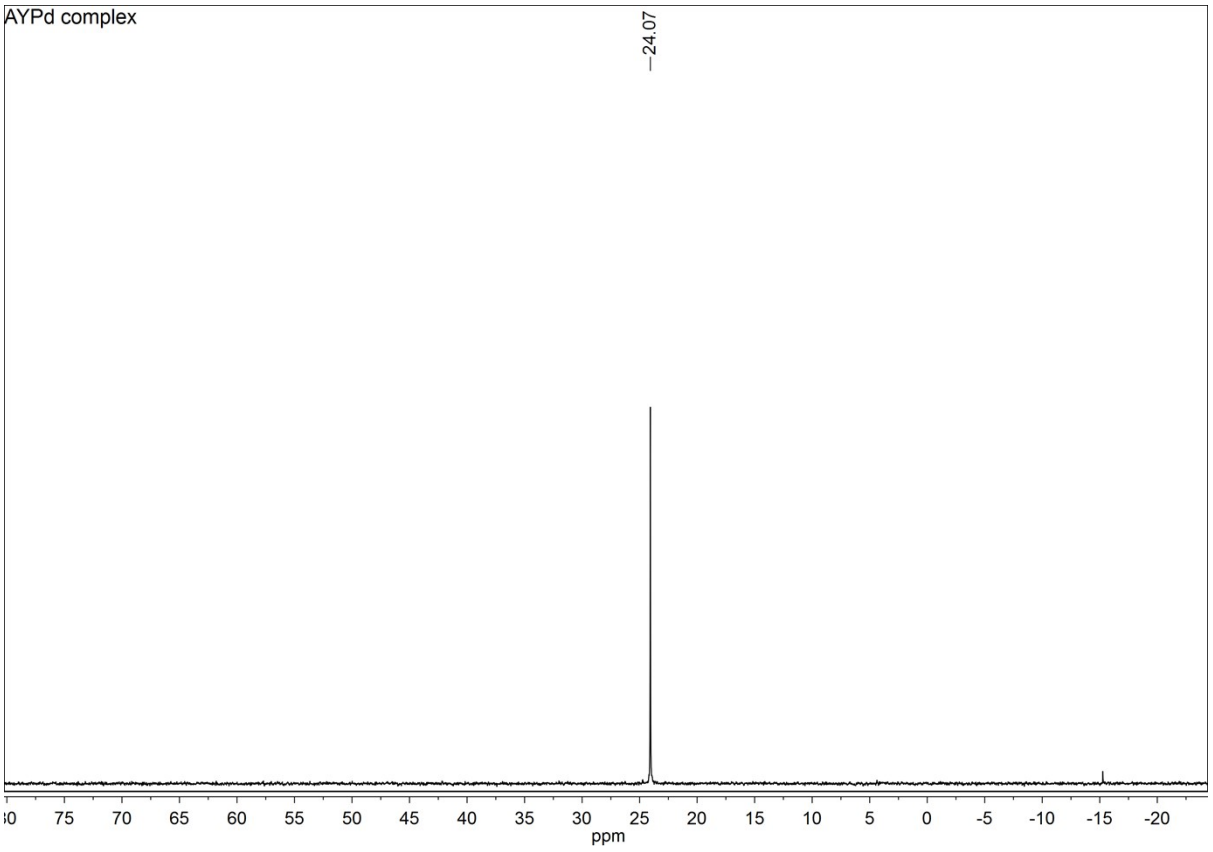

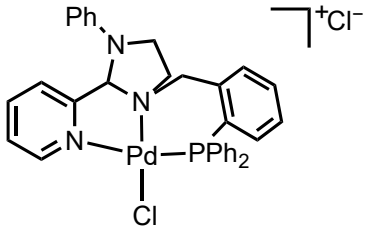

Figure S 23. Elemental analysis of [Pd(NNP)Cl][Cl].

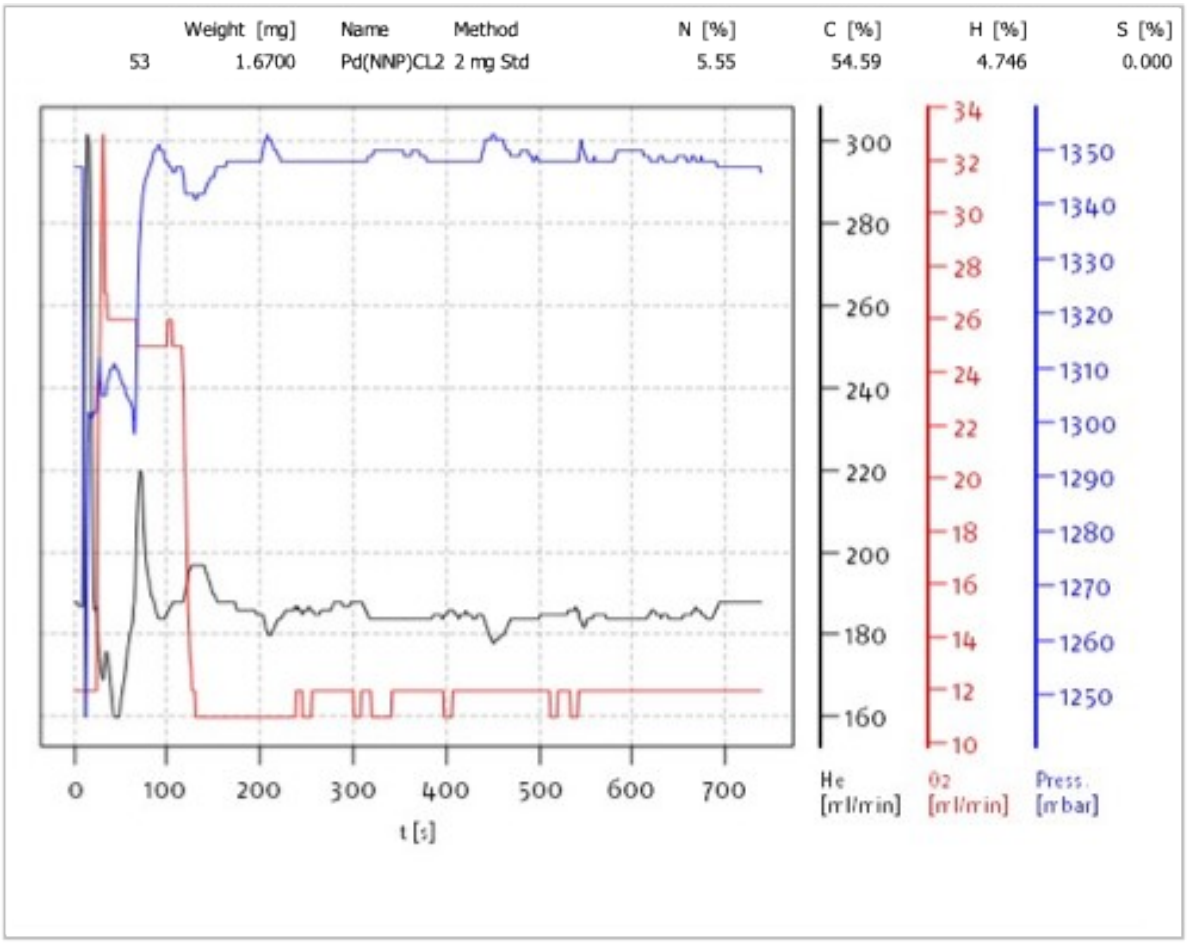

Elemental analysis calculated (%) for $C_{33}H_{30}Cl_2N_3PPd \cdot 0.8CH_2Cl_2$: C, 54.50; H, 4.28; N, 5.64. Found: C, 54.59; H, 4.74; N, 5.55.

Figure S 24. ESI-MS of [Pd(NNP)Cl][Cl]

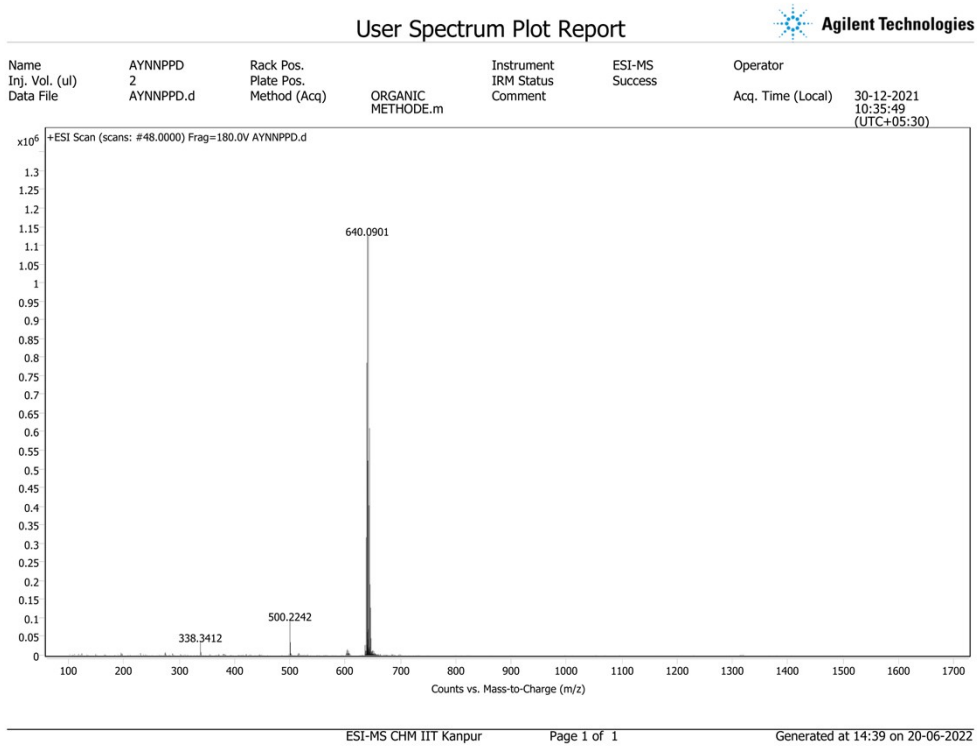

High resolution ESI-MS: m/z for $[M-Cl]^+$ = 640.0891 (calcd. 640.091) = $[PdC_{33}H_{30}ClN_3P]^+$.

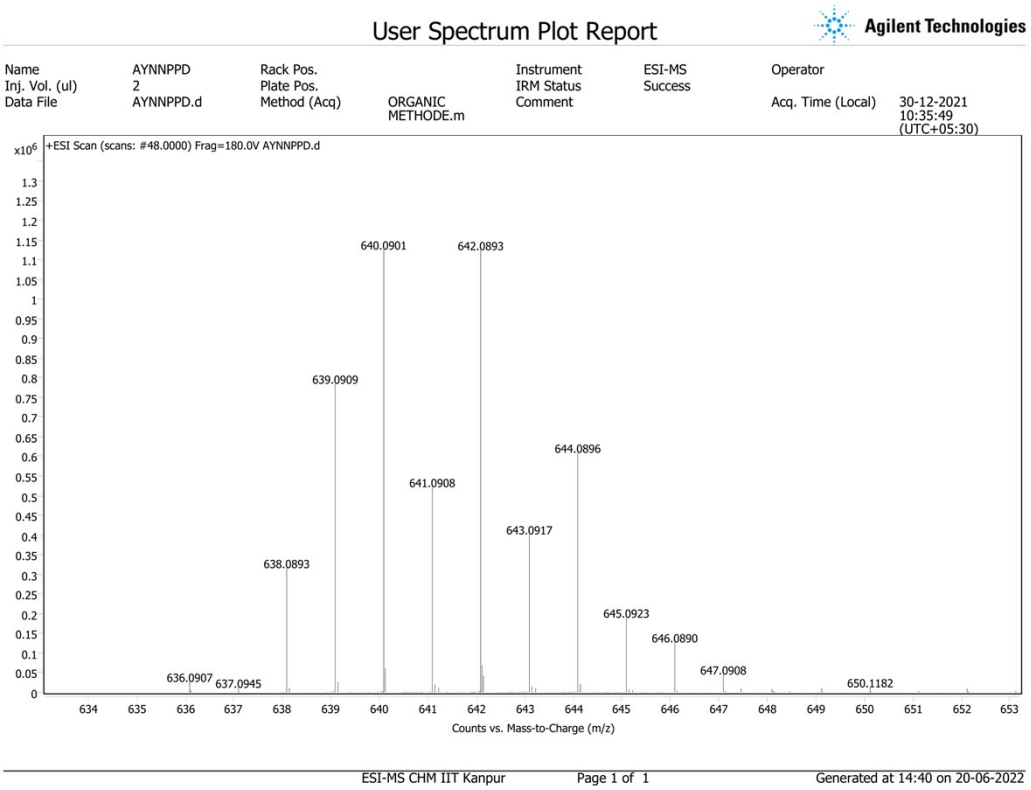

Figure S 25. Simulated ESI-MS of [Pd(NNP)Cl][Cl]

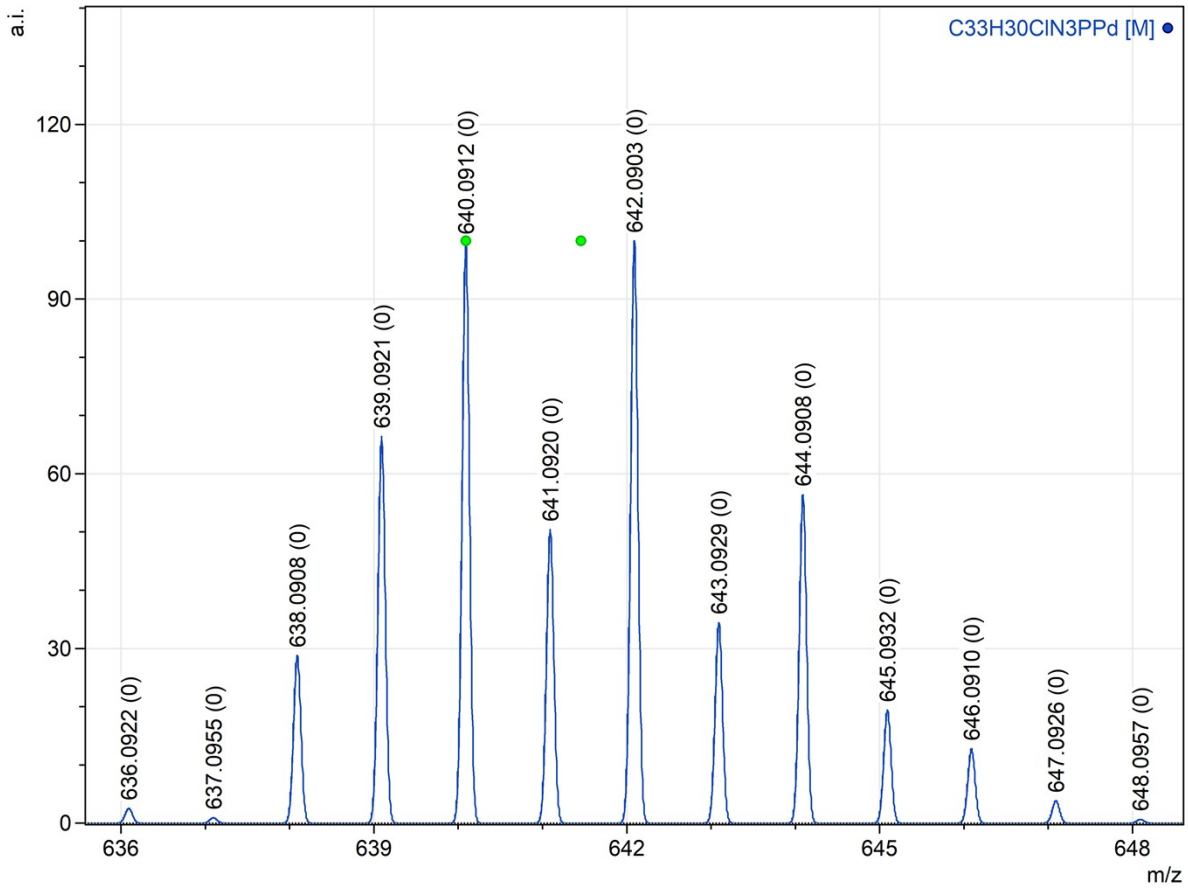

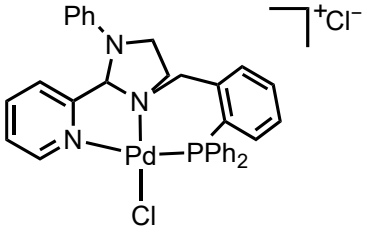

Figure S 26. ^{1}H NMR spectrum of the [Pd(NNP)($SPhCH_3$)][Cl] in $CDCl_3$ at 298 K.

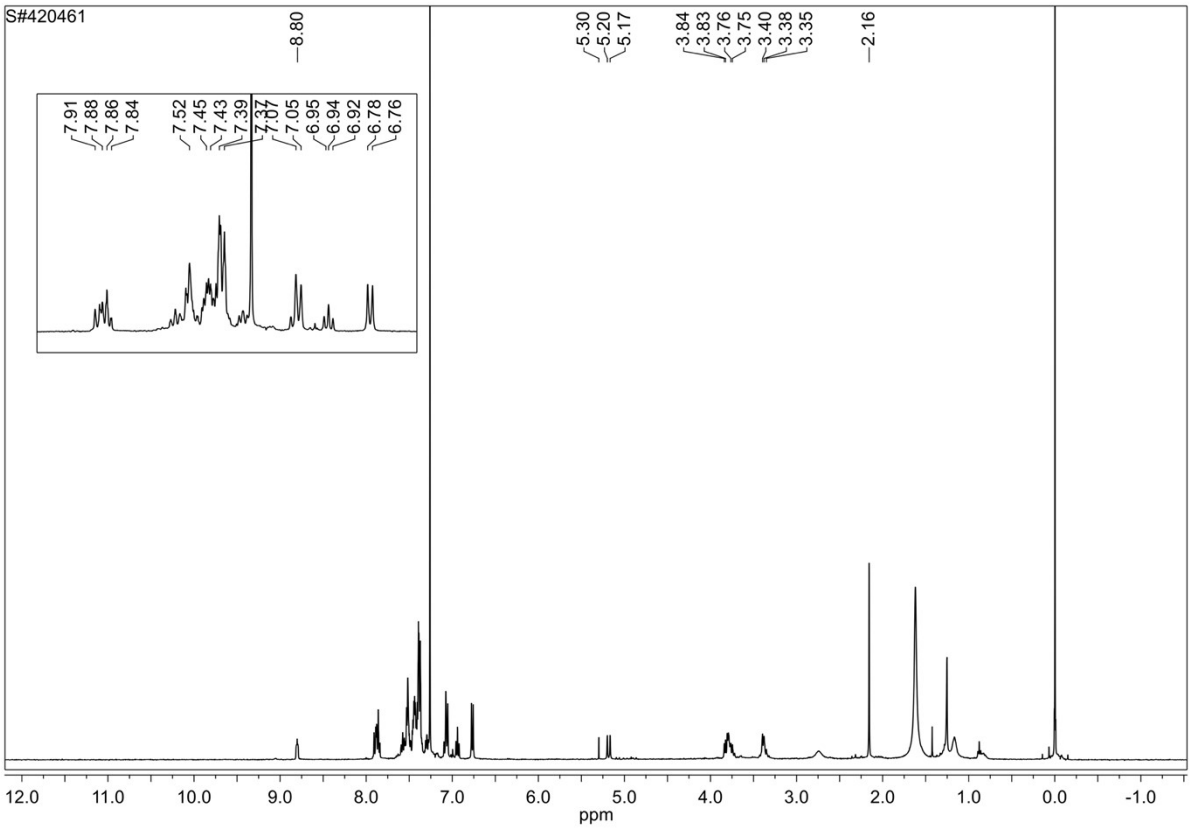

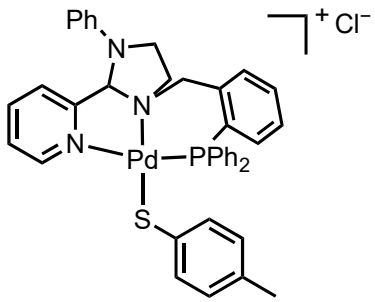

Figure S 27. ^{13}C NMR spectrum of the [Pd(NNP)($SPhCH_3$)][Cl] in $CDCl_3$ at 298 K.

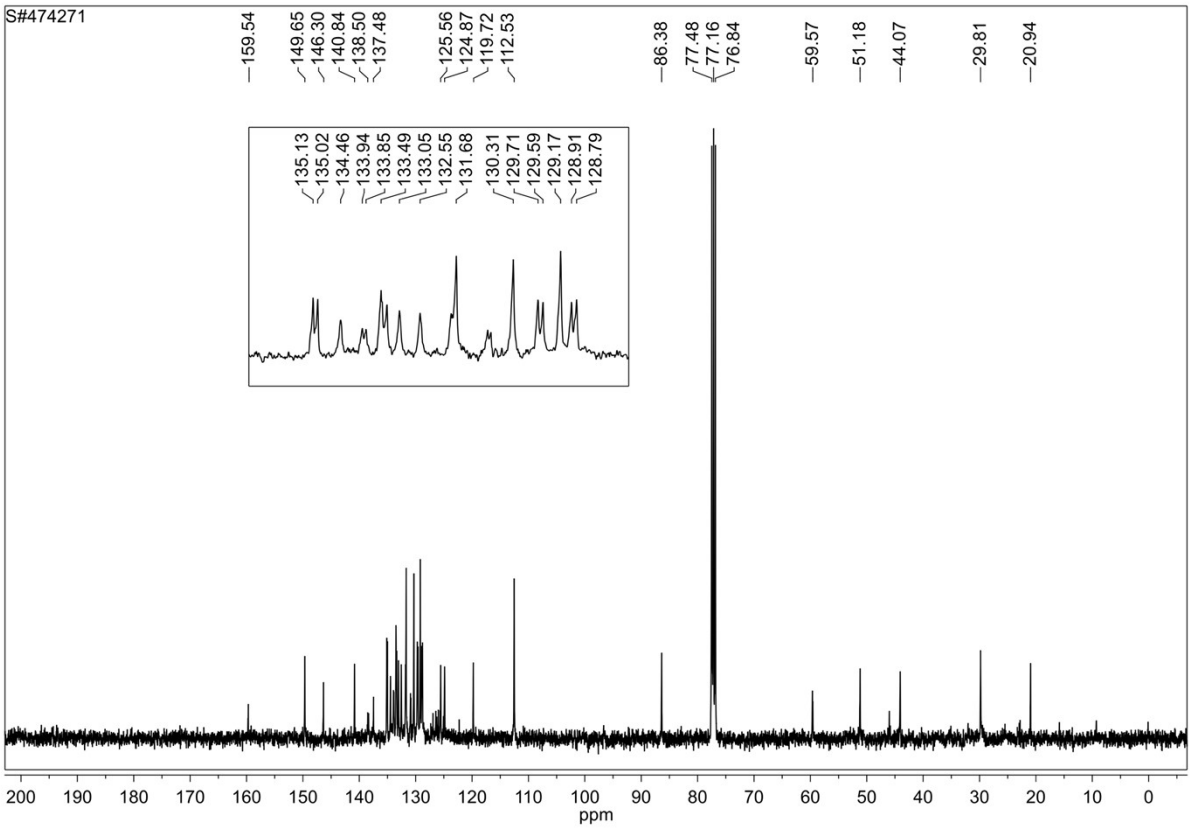

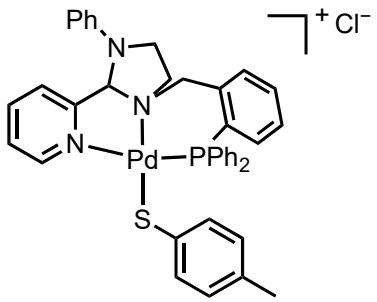

Figure S 28. ^{31}P NMR spectrum of the [Pd(NNP)(SPhCH$_3$)][Cl] in $CDCl_3$ at 298 K.

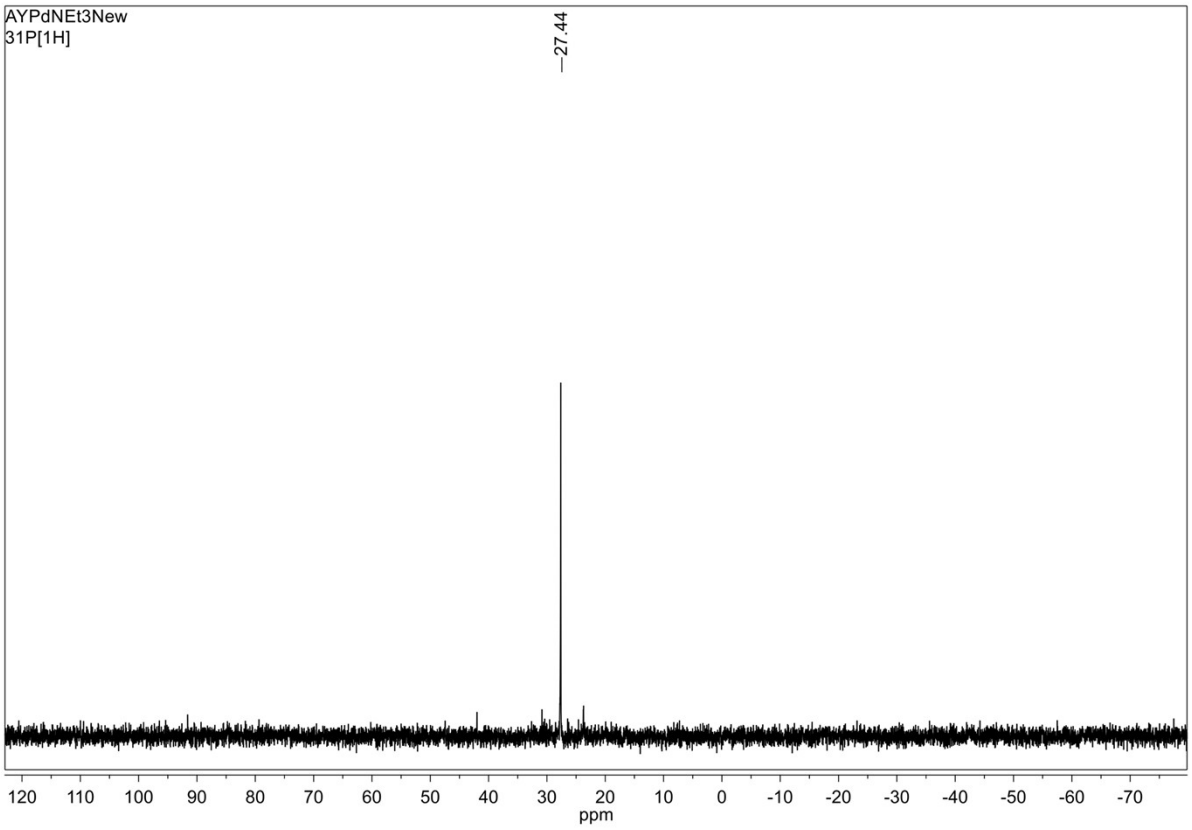

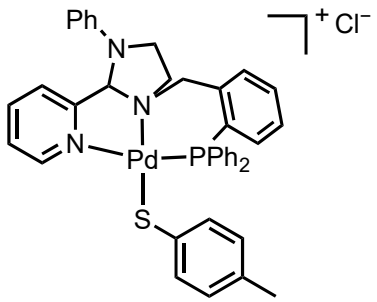

Figure S 29. ESI-MS of [Pd(NNP)(SPhCH$_3$)][Cl]

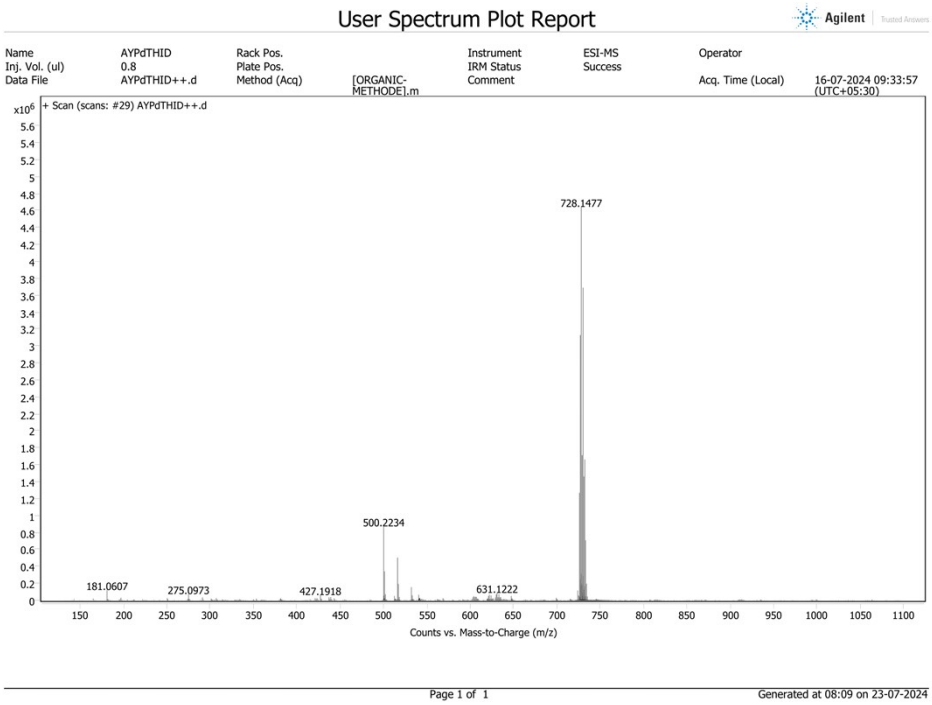

High resolution ESI-MS: *m/z* for $[M-Cl]^+$ = 728.1477 (calcd. 728.1481) = $[PdC_{40}H_{37}N_3SP]^+$.

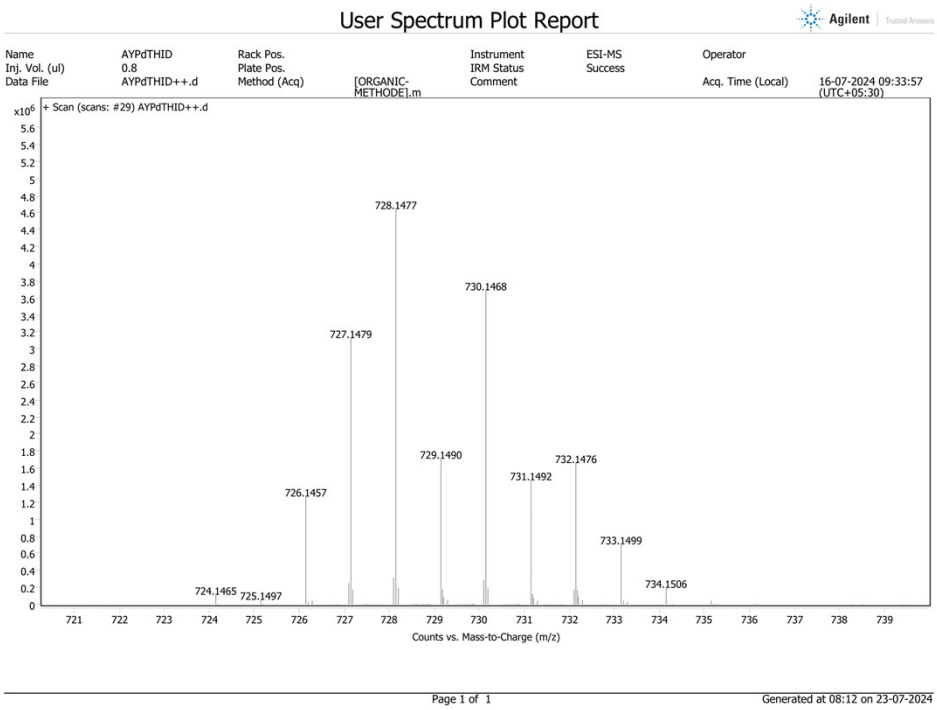

Figure S 30. Simulated ESI-MS of [(NNP)Pd(SPhCH$_3$)][Cl]

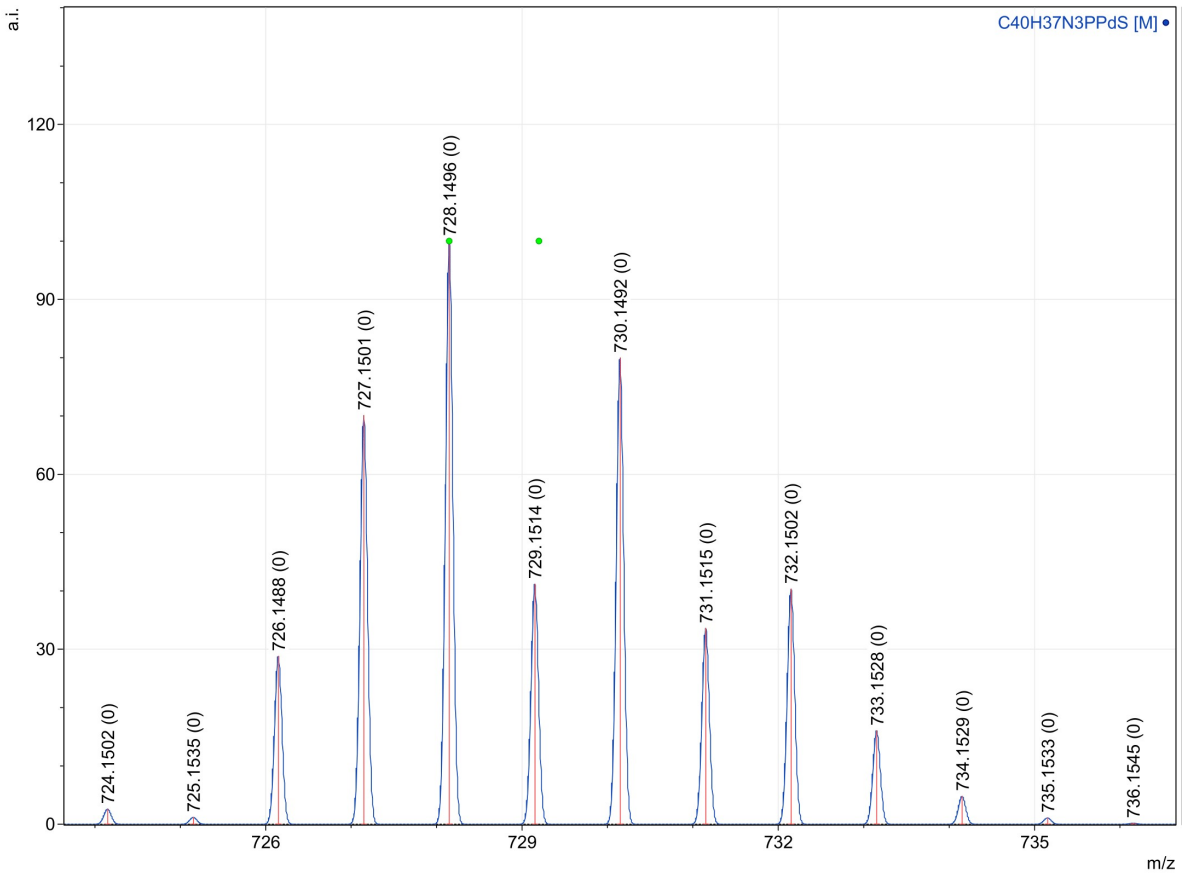

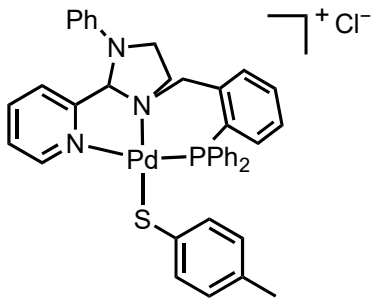

Figure S 31. ^{1}H NMR spectrum of the $[Pd(NNP)(SPhCH_3)][PF_6]$ in $CDCl_3$ at 298 K.

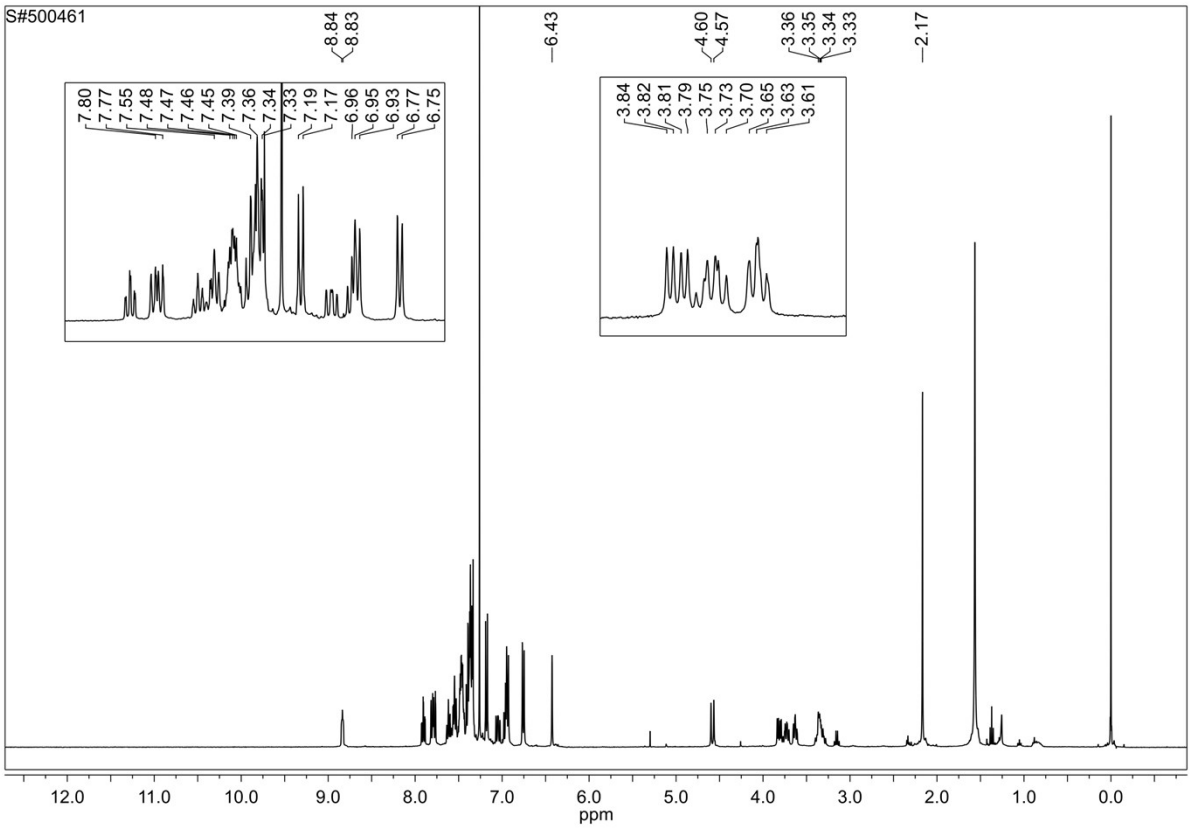

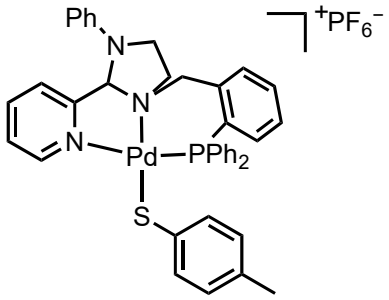

Figure S 32. ^{31}P NMR spectrum of the $[Pd(NNP)(SPhCH_3)][PF_6]$ in $CDCl_3$ at 298 K.

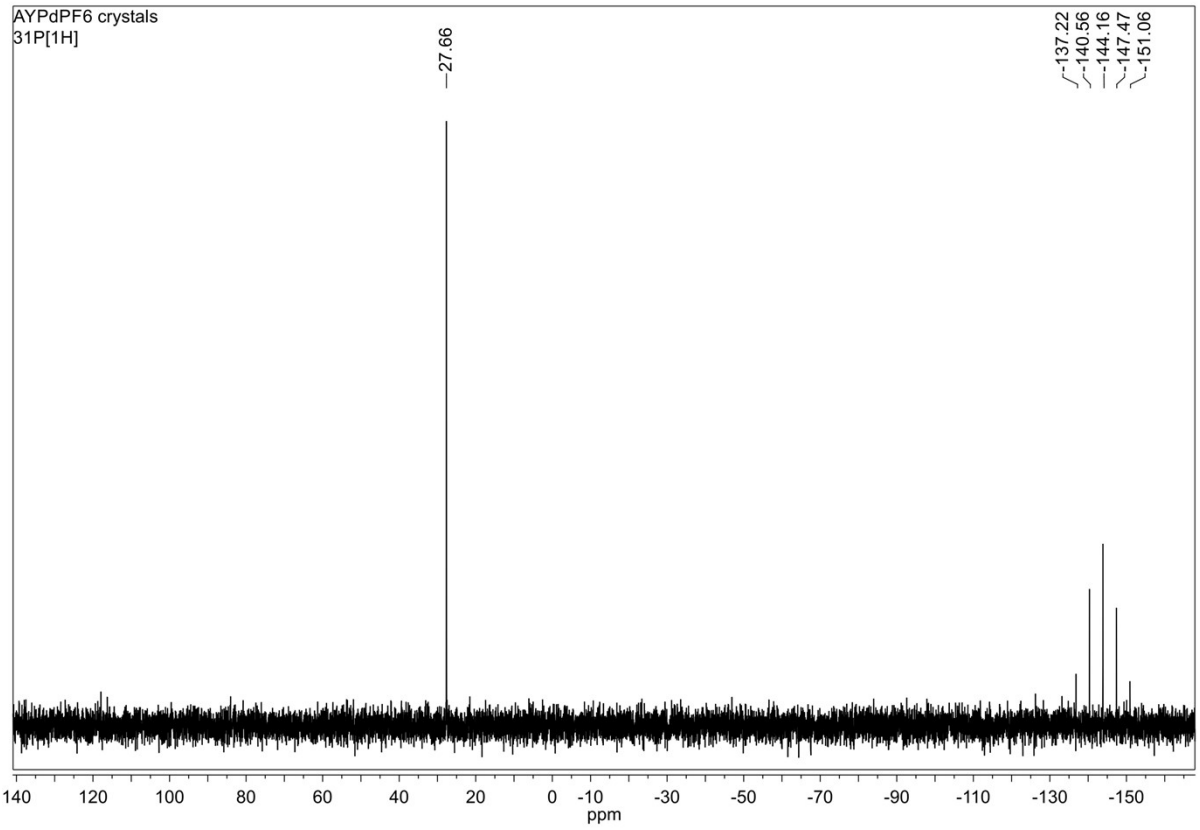

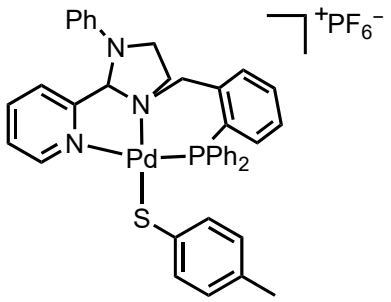

Figure S 33. ^{1}H NMR spectrum of $[Ru(NNP)(PPh_3)Cl_2]$ complex in $CDCl_3$ at 298 K.

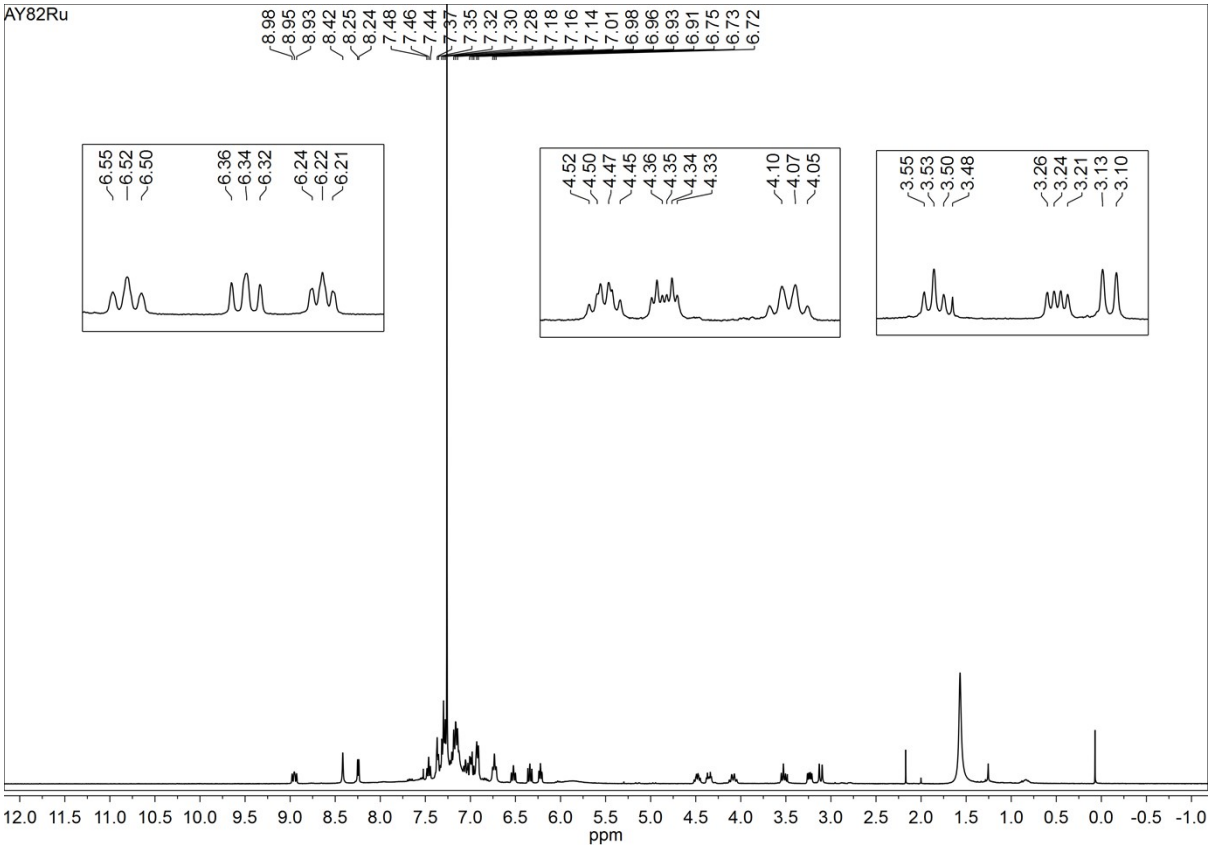

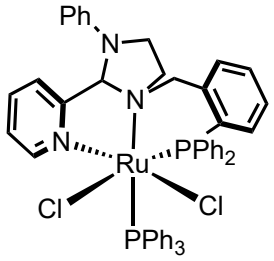

Figure S 34. ^{31}P NMR spectrum of $[Ru(NNP)(PPh_3)Cl_2]$ complex in $CDCl_3$ at 298 K.

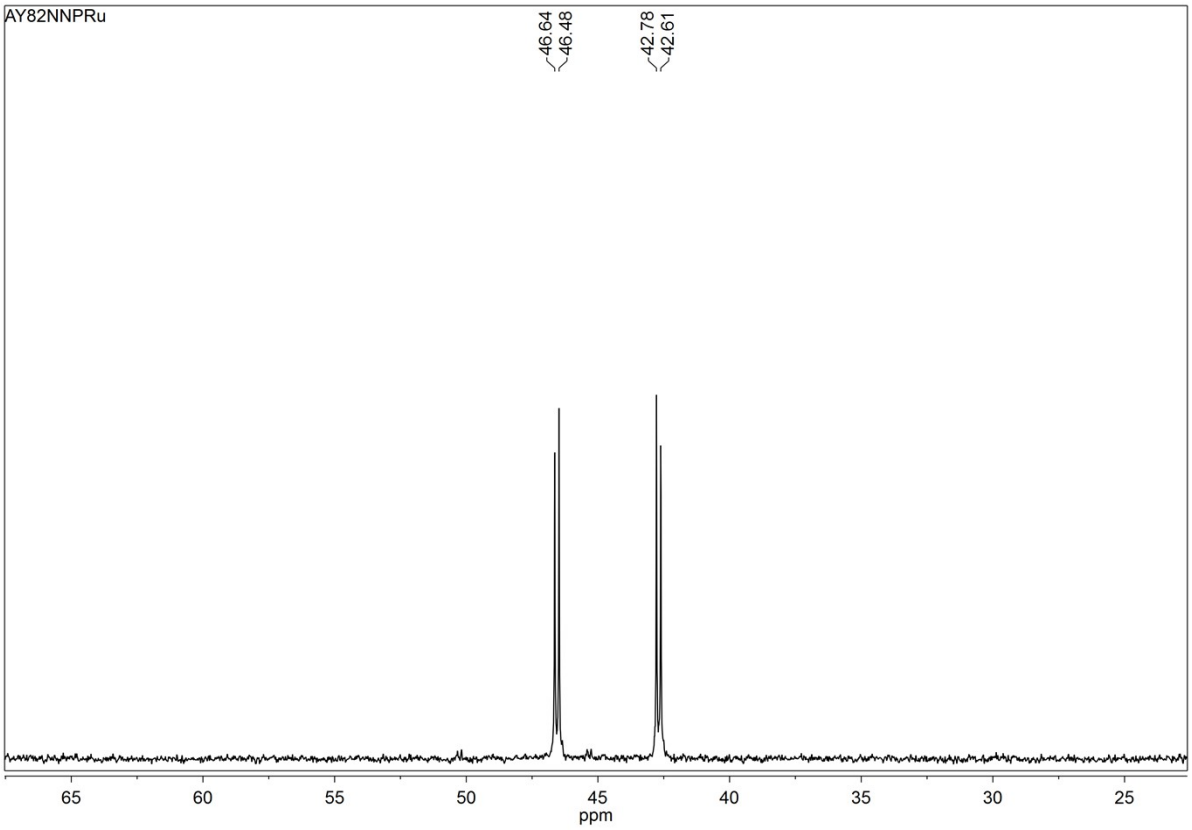

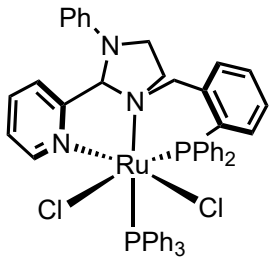

Figure S 35. Elemental analysis of [Ru(NNP)(PPh_3)Cl_2] complex.

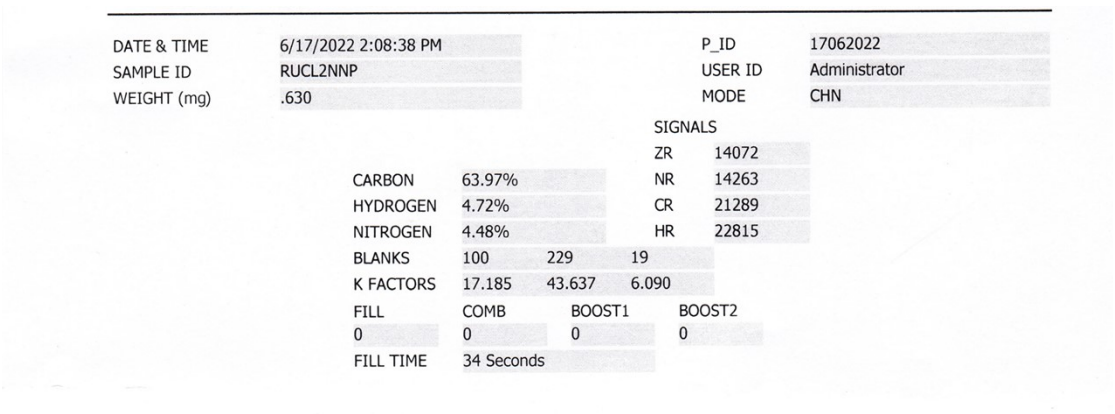

DATE & TIME	6/17/2022 2:08:38 PM			P_ID	17062022
SAMPLE ID	RUCL2NNP			USER ID	Administrator
WEIGHT (mg)	.630			MODE	CHN
				SIGNALS	
				ZR	14072
CARBON	63.97%			NR	14263
HYDROGEN	4.72%			CR	21289
NITROGEN	4.48%			HR	22815
BLANKS	100	229	19		
K FACTORS	17.185	43.637	6.090		
FILL	COMB	BOOST1	BOOST2		
0	0	0	0		
FILL TIME	34 Seconds				

Elemental analysis calculated (%) for $C_{51}H_{45}Cl_2N_3P_2Ru \cdot 0.6\ CH_2Cl_2$: C, 63.93; H, 4.73; N, 4.27. Found: C, 63.97; H, 4.72; N, 4.48.

Figure S 36. ESI-MS of $[Ru(NNP)(PPh_3)Cl_2]$

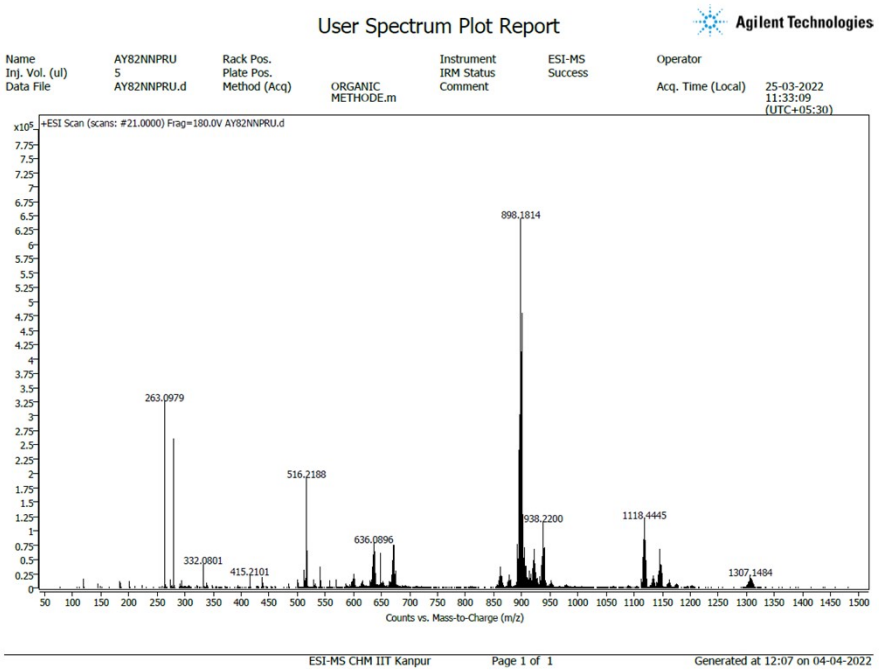

High resolution ESI-MS: *m/z* for $[M\text{-}Cl]^+$ = 898.1814 (calcd. 898.1821) = $[RuC_{51}H_{45}ClN_3P_2]^+$; *m/z* = 636.0896 (calcd. 636.0909) = $[M\text{-}(PPh_3+Cl]^+$; *m/z* = 516.2188 (calcd. 516.2205) = $[NNP{=}O+H]^+$; *m/z* = 263.0976 (calcd. 263.0990) = $[PPh_3+H]^+$; *m/z* = 938.2200 (calcd. 938.2214) = $[Ru(NNP)(O{=}PPh_3)\text{-}2Cl+CH_3COO]^+$. The CH_3COO^- likely originates from the formic acid used to infuse the sample during measurement.

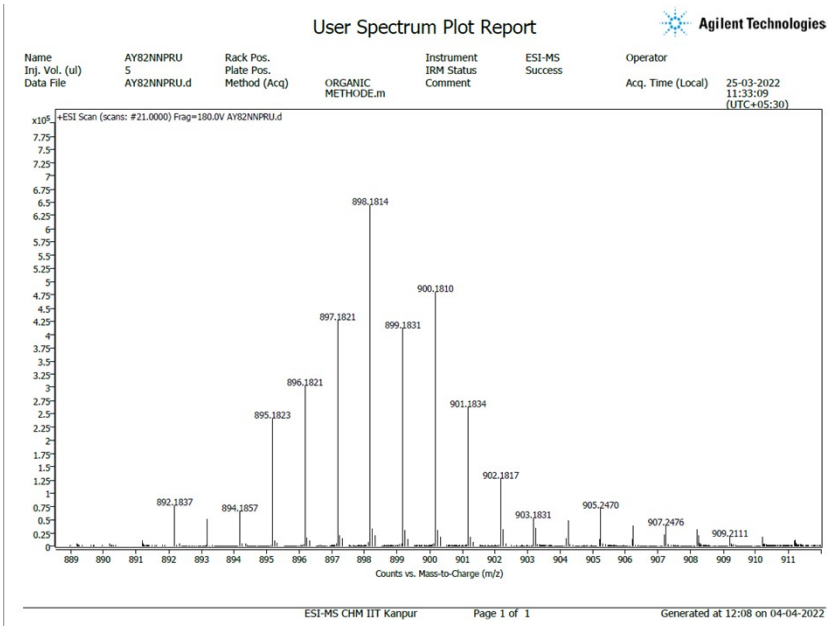

Figure S 37. Simulated ESI-MS of [Ru(NNP)(PPh_3)Cl_2].

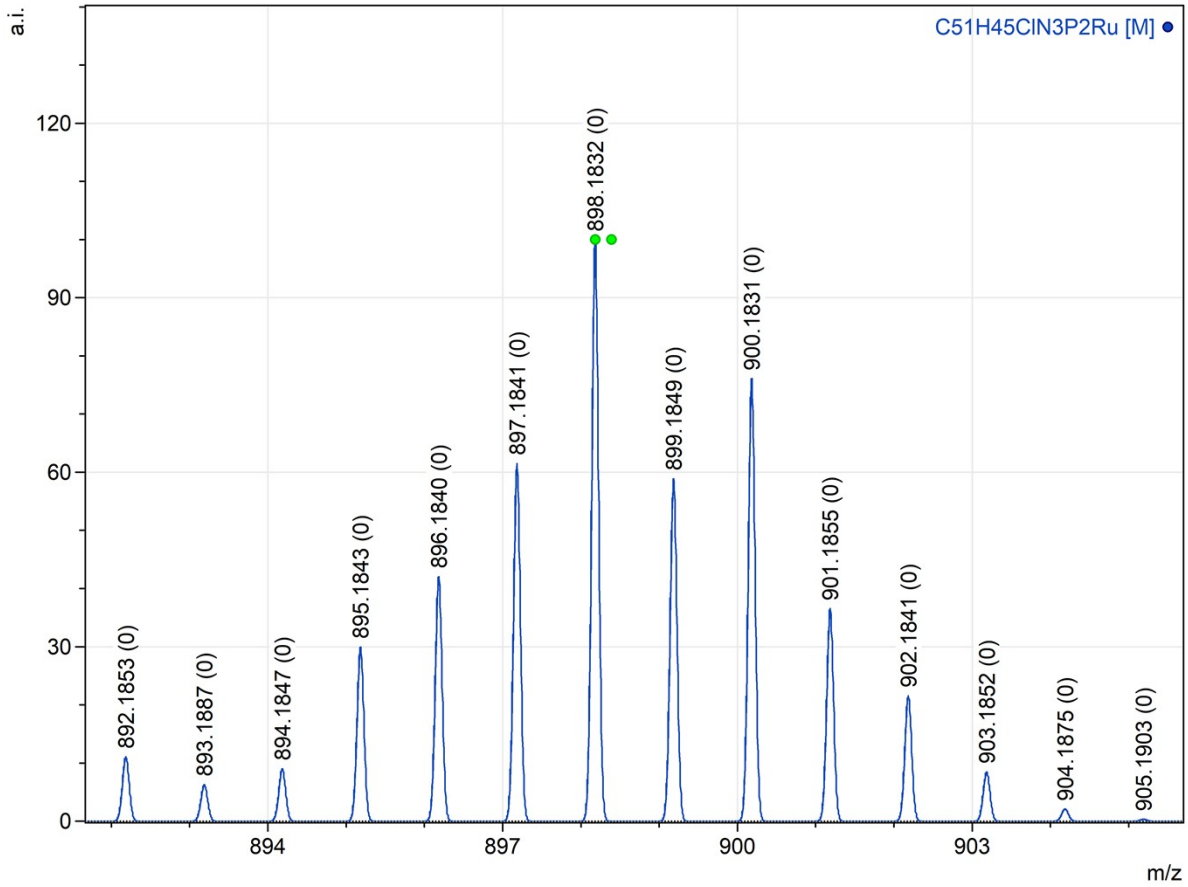

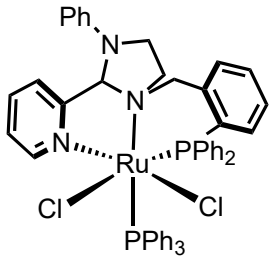

Figure S 38. ^{1}H NMR spectrum of the *rac*-[(NNP)Ru(H)(CO)Cl] (crude) in $CDCl_3$ at 298 K.

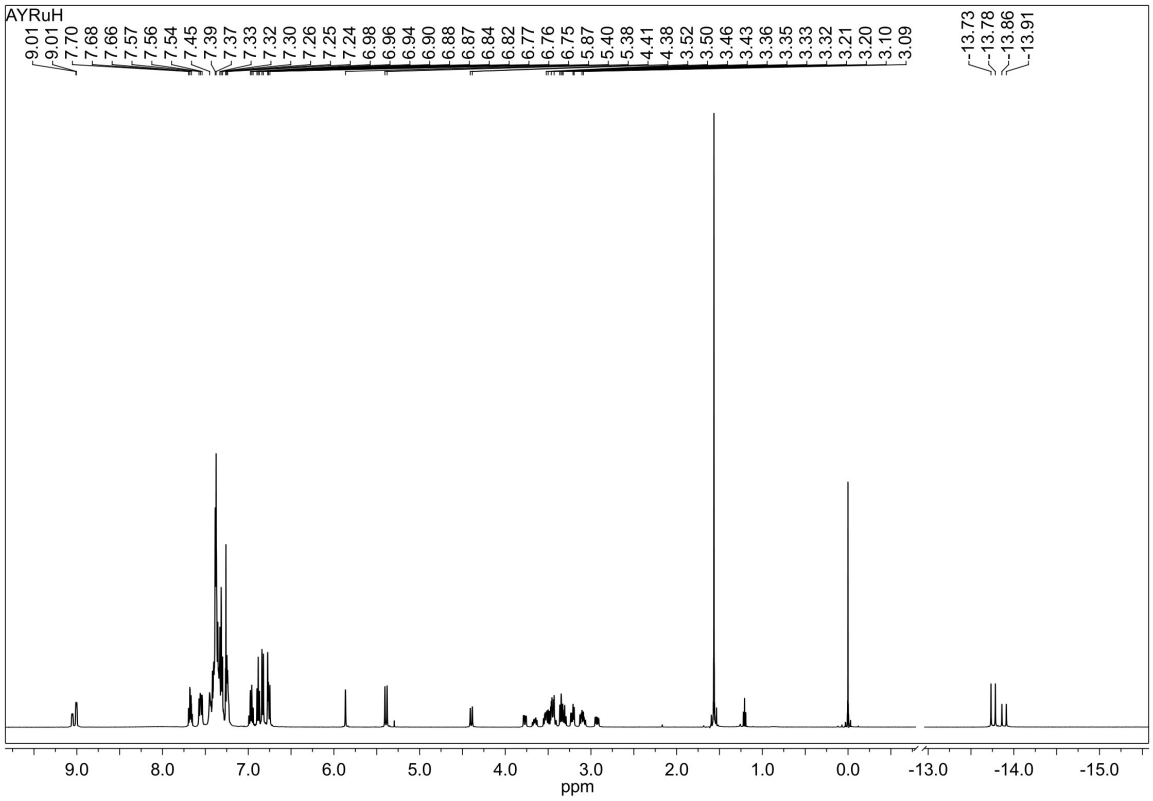

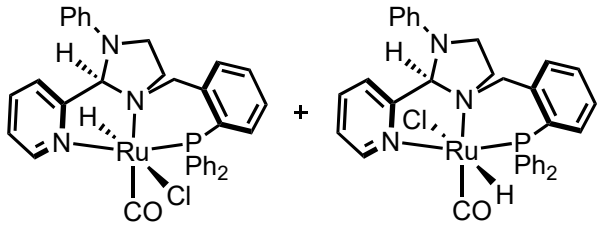

syn-rac-[(NNP)RuHCl(CO)] *anti-rac*-[(NNP)RuHCl(CO)]

Figure S 39. ^{31}P NMR spectrum of the *rac*-[Ru(NNP)(H)Cl(CO)] (crude) in $CDCl_3$ at 298 K.

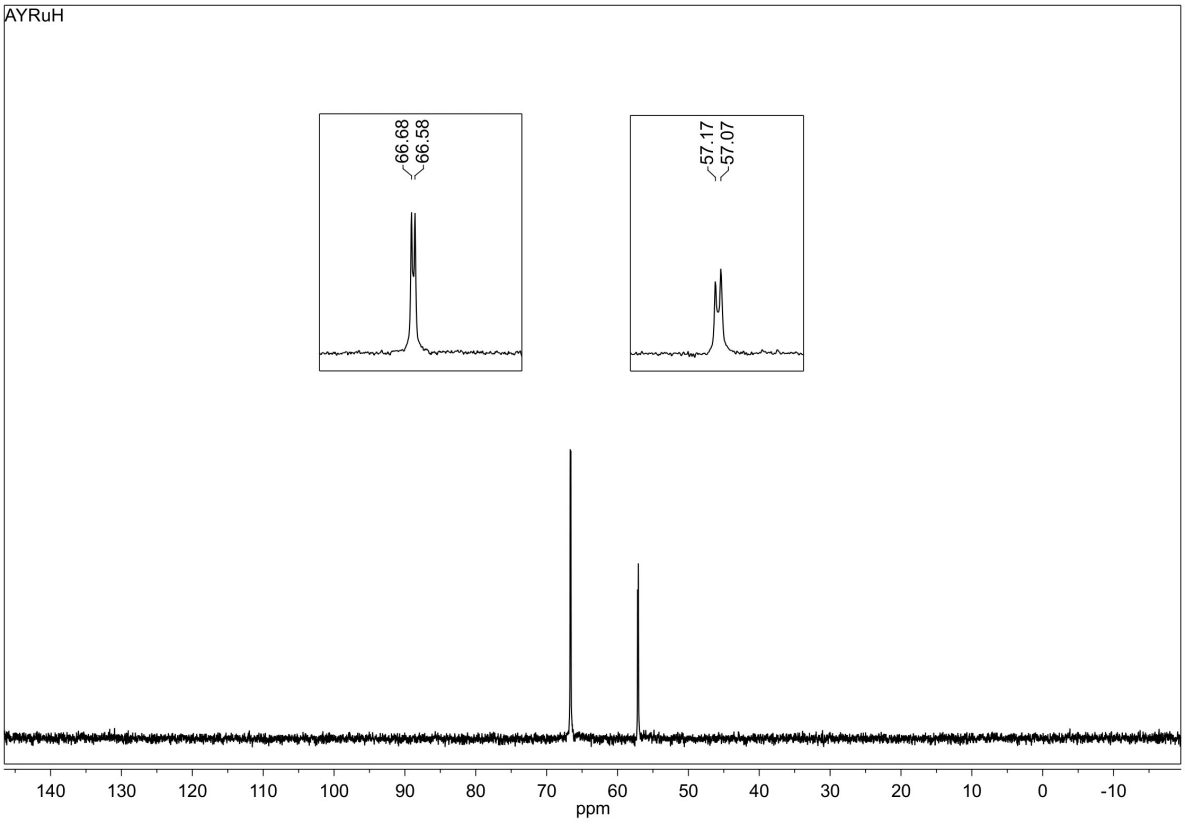

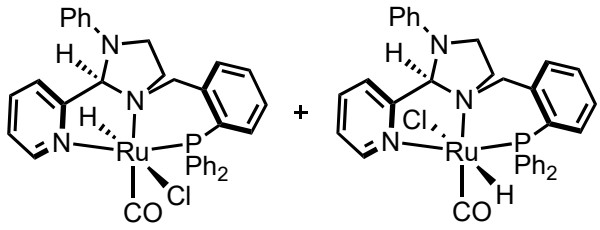

syn-rac-[(NNP)RuHCl(CO)] *anti-rac*-[(NNP)RuHCl(CO)]

Figure S 40. ^{1}H NMR spectrum of the *anti-rac*-[Ru(NNP)(H)Cl(CO)] in $CDCl_3$ at 298 K.

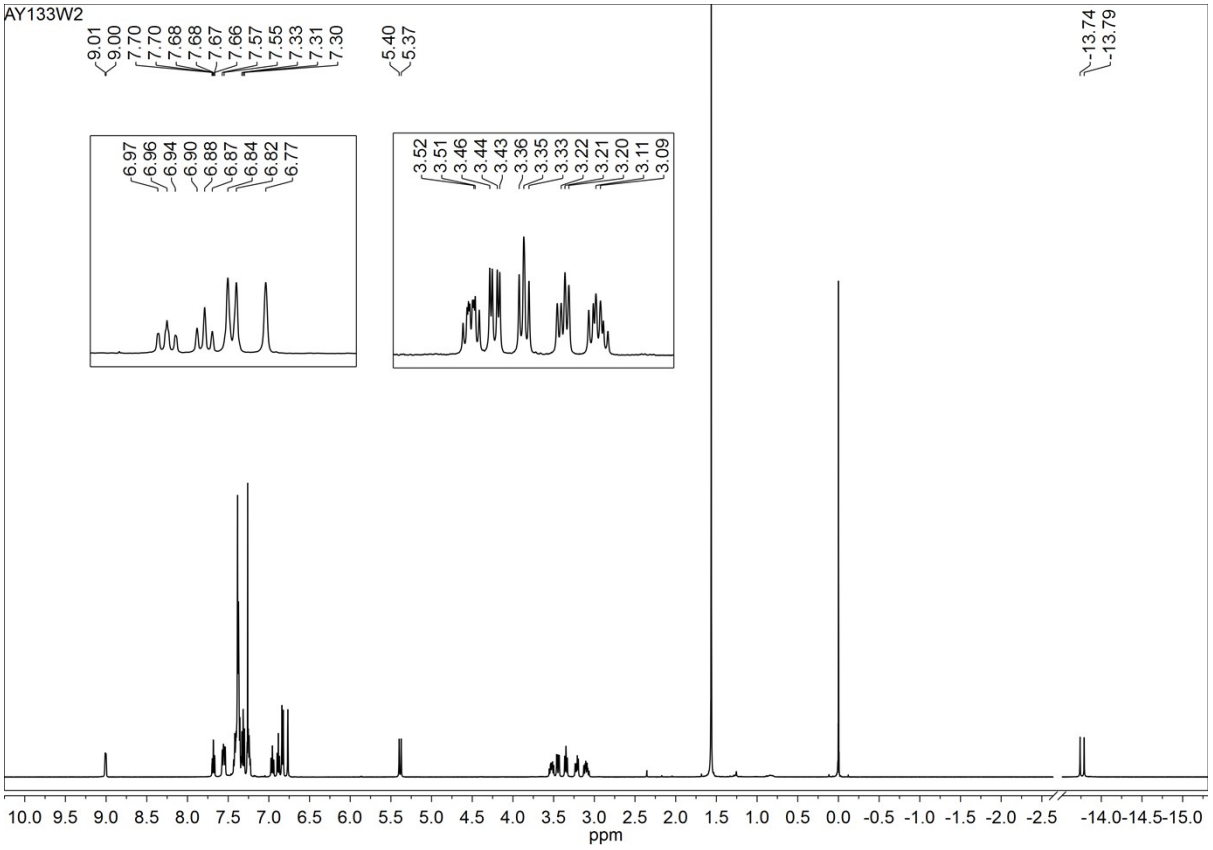

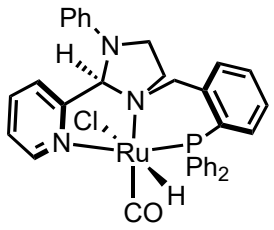

Figure S 41. ^{31}P NMR spectrum of the *anti-rac*-[Ru(NNP)(H)Cl(CO)] in $CDCl_3$ at 298 K.

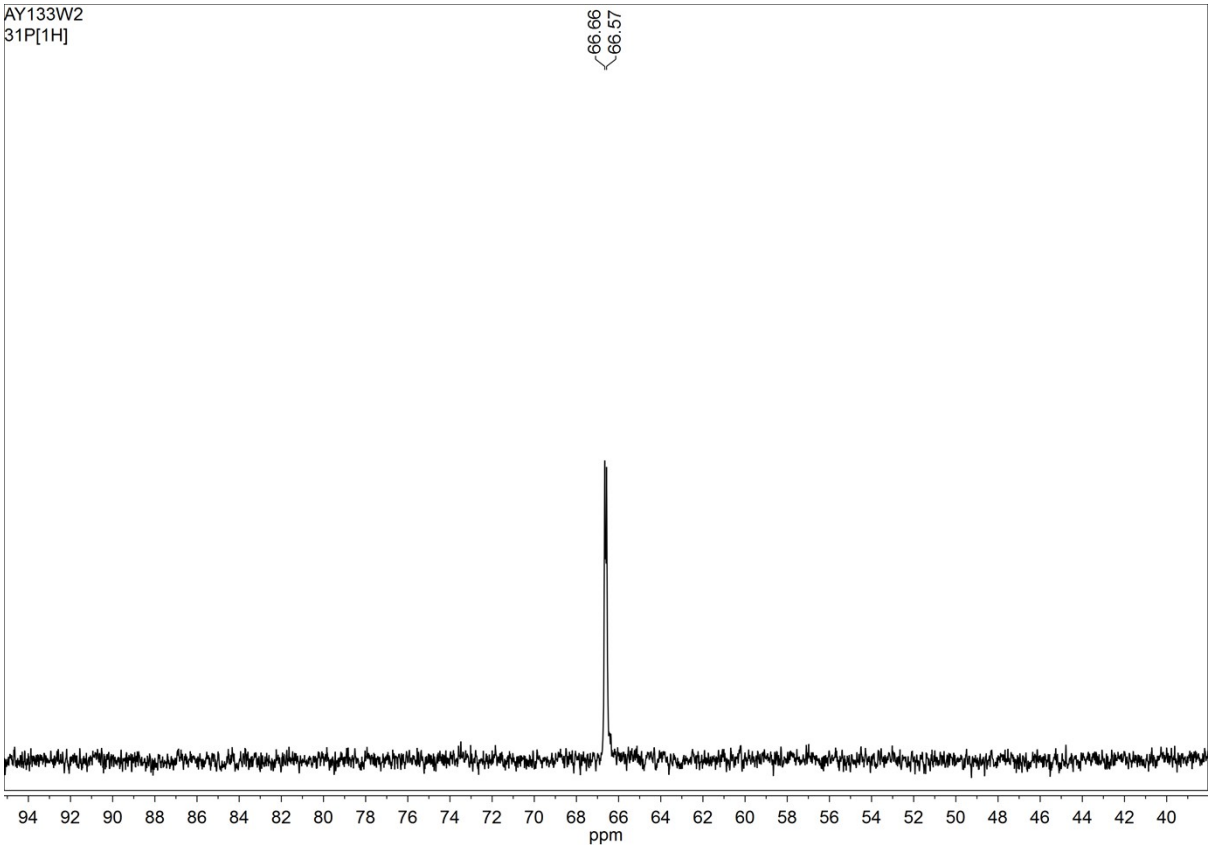

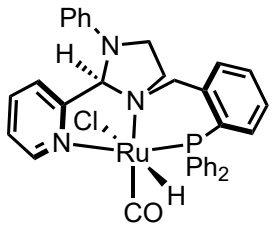

Figure S 42. ^{1}H NMR spectrum of the *syn-rac*-[Ru(NNP)(H)Cl(CO)] in $CDCl_3$ at 298 K.

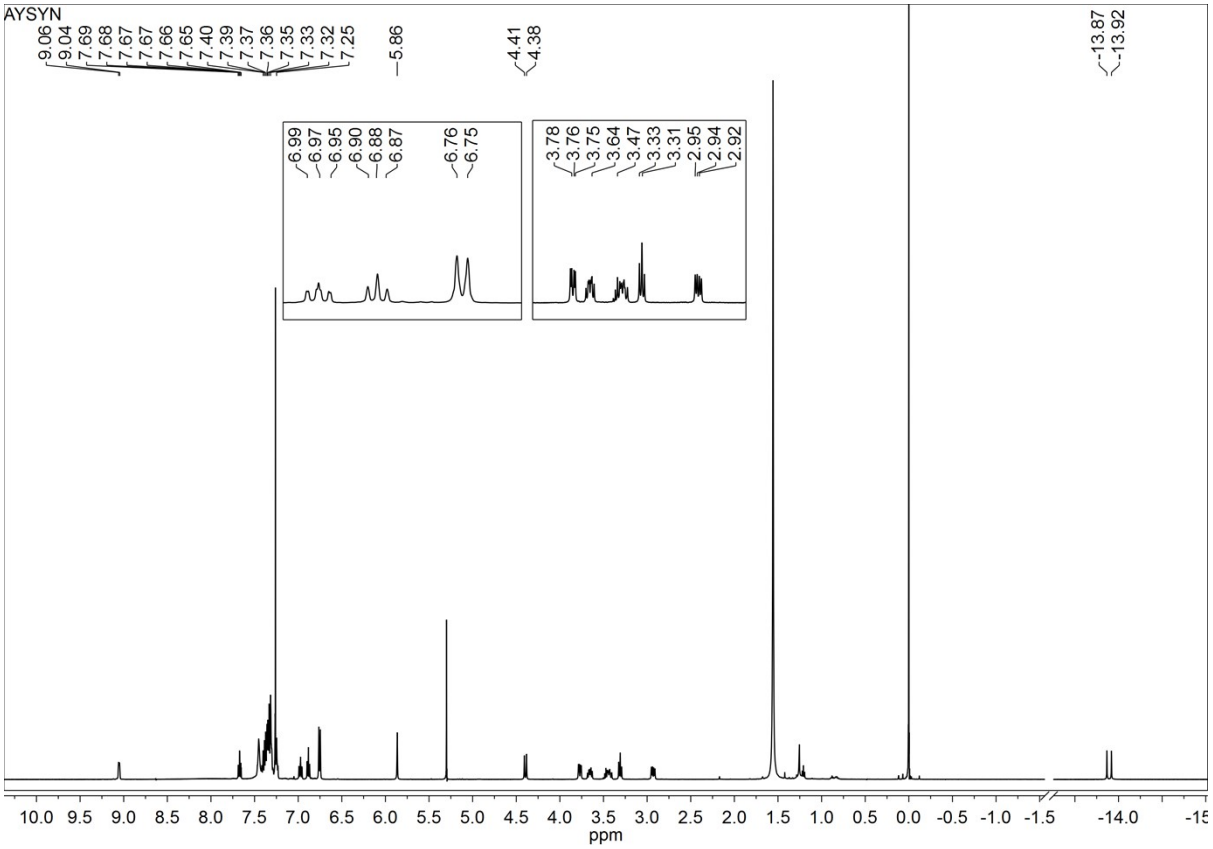

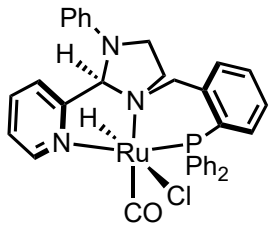

Figure S 43. ^{31}P NMR spectrum of the *syn-rac*-[Ru(NNP)(H)Cl(CO)] in $CDCl_3$ at 298 K.

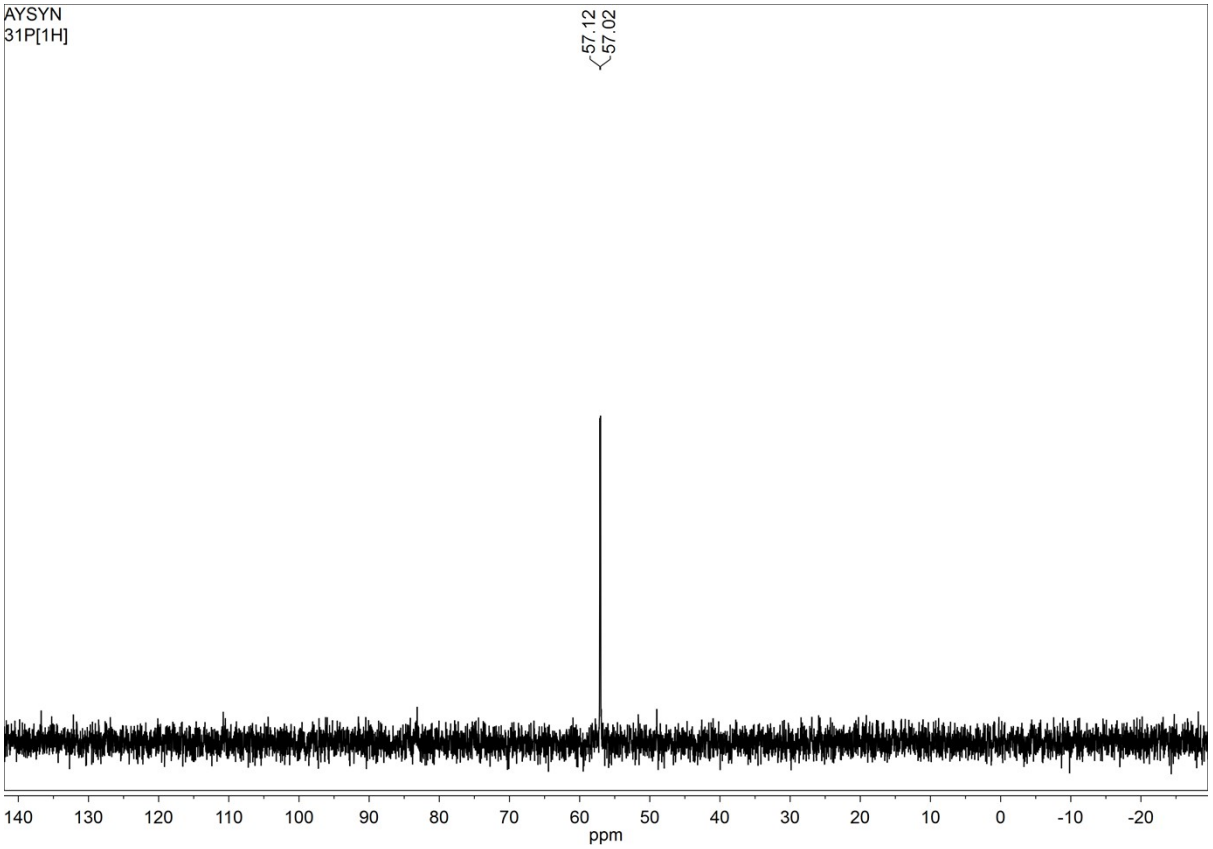

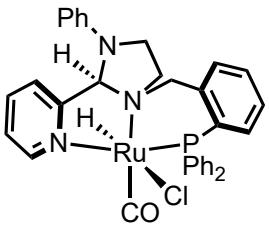

Figure S 44. Elemental analysis of [Ru(NNP)(H)Cl(CO)]

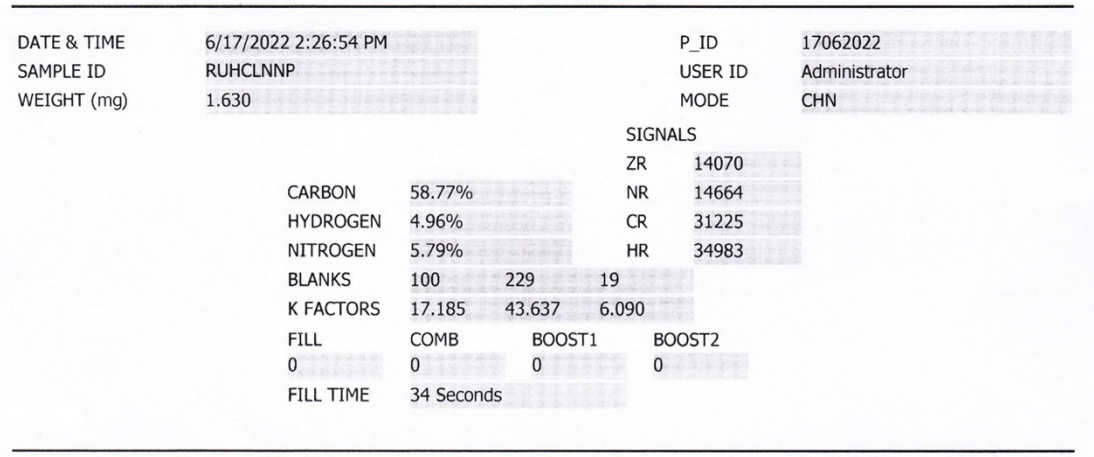

DATE & TIME	6/17/2022 2:26:54 PM			P_ID	17062022
SAMPLE ID	RUHCLNNP			USER ID	Administrator
WEIGHT (mg)	1.630			MODE	CHN
				SIGNALS	
				ZR	14070
	CARBON	58.77%		NR	14664
	HYDROGEN	4.96%		CR	31225
	NITROGEN	5.79%		HR	34983
	BLANKS	100	229	19	
	K FACTORS	17.185	43.637	6.090	
	FILL	COMB	BOOST1	BOOST2	
	0	0	0	0	
	FILL TIME	34 Seconds			

Elemental analysis calculated (%) for $C_{34}H_{31}ClN_3OPRu \cdot 0.5CH_2Cl_2$: C, 58.56; H, 4.56; N, 5.94. Found: C, 58.77; H, 4.96; N, 5.79.

Figure S 45. FTIR of [Ru(H)Cl(CO)(PPh_3)$_3$]

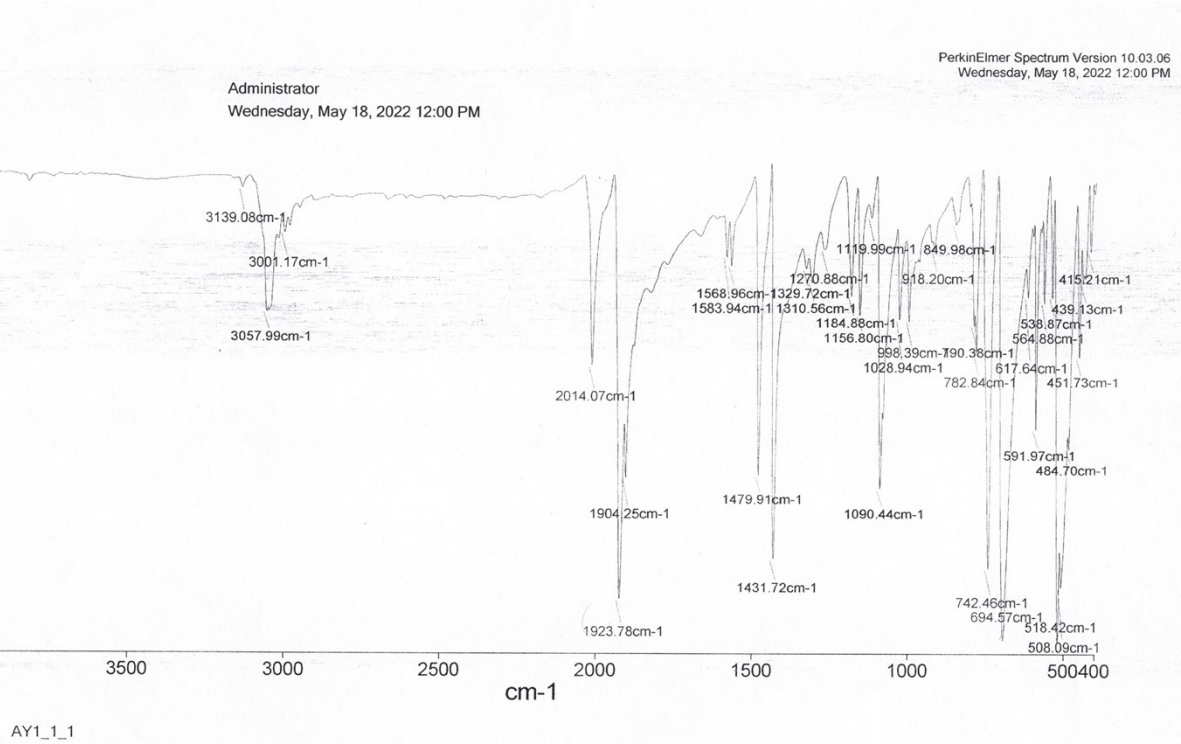

FTIR (KBr pellet) [Ru(H)Cl(CO)(PPh_3)$_3$]: ν_{Ru-H} = 2014 cm^{-1}, ν_{CO} = 1923 cm^{-1}.

Figure S 46. FTIR of *syn* and *anti-rac*-[Ru(NNP)(H)Cl(CO)]

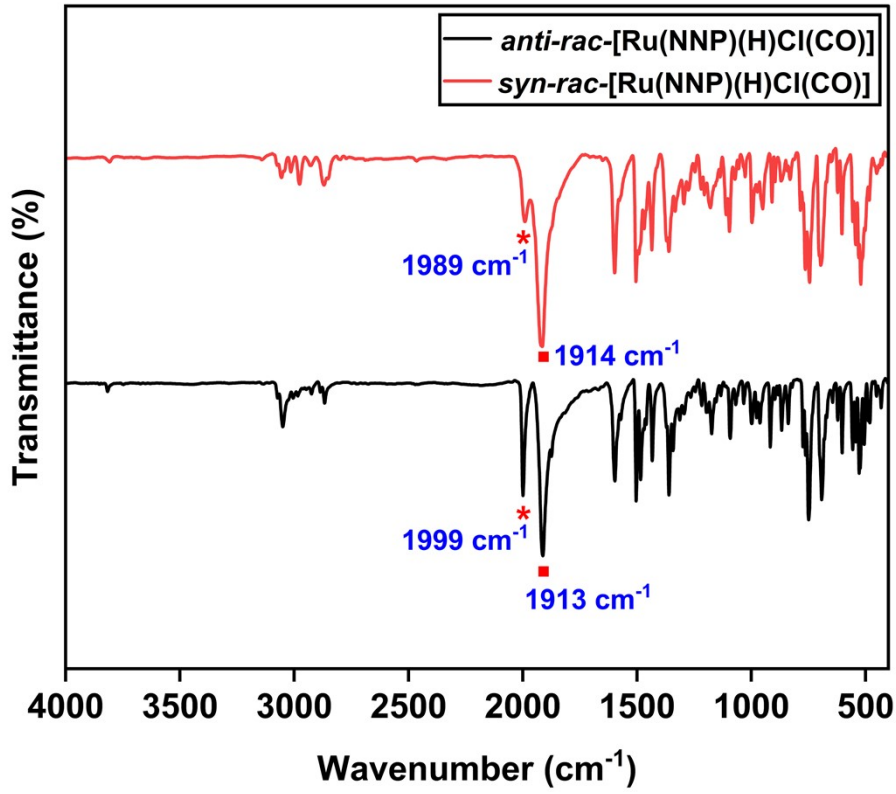

FTIR (KBr pellet) *syn-rac*-[Ru(NNP)(H)(CO)Cl]: $\nu_{\text{Ru-H}}$ = 1989 cm^{-1}, ν_{CO} = 1914 cm^{-1}.

FTIR (KBr pellet) *anti-rac*-[Ru(NNP)(H)(CO)Cl]: $\nu_{\text{Ru-H}}$ = 1999 cm^{-1}, ν_{CO} = 1913 cm^{-1}.

Figure S 47. ESI-MS of [Ru(NNP)(H)Cl(CO)]

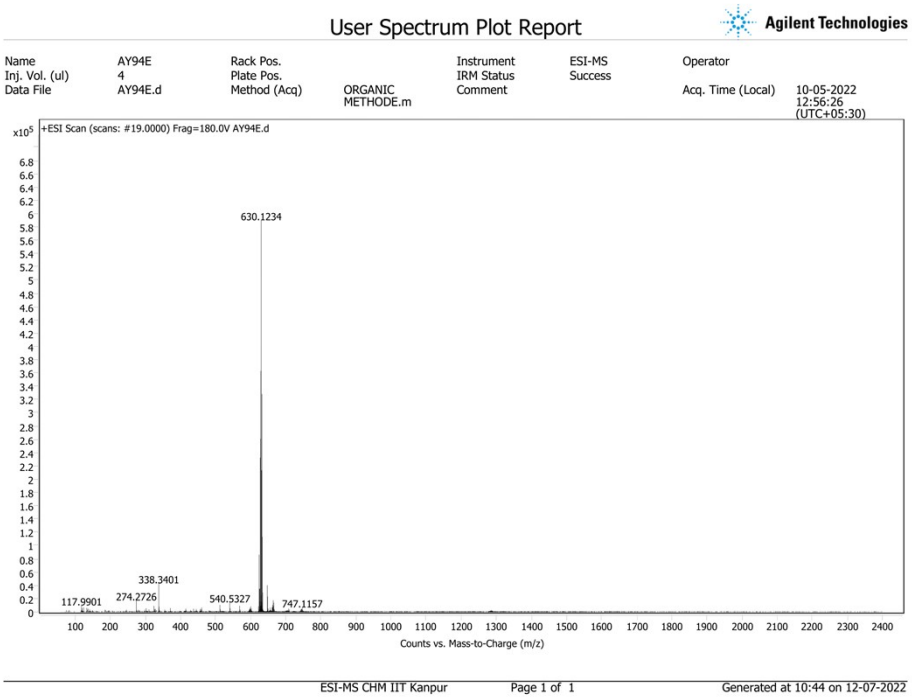

High resolution ESI-MS: *m/z* for = $[M-Cl]^+$ = 630.1234 (calcd. 630.1248) = $[RuC_{34}H_{31}N_3OP]^+$.

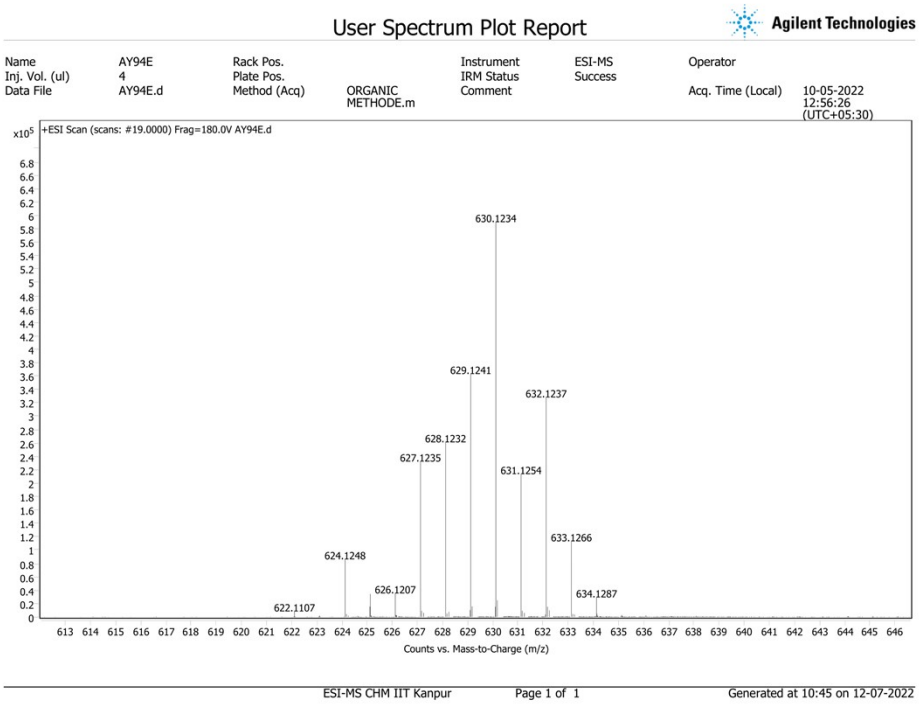

Figure S 48. Simulated ESI-MS of [Ru(NNP)(H)Cl(CO)]

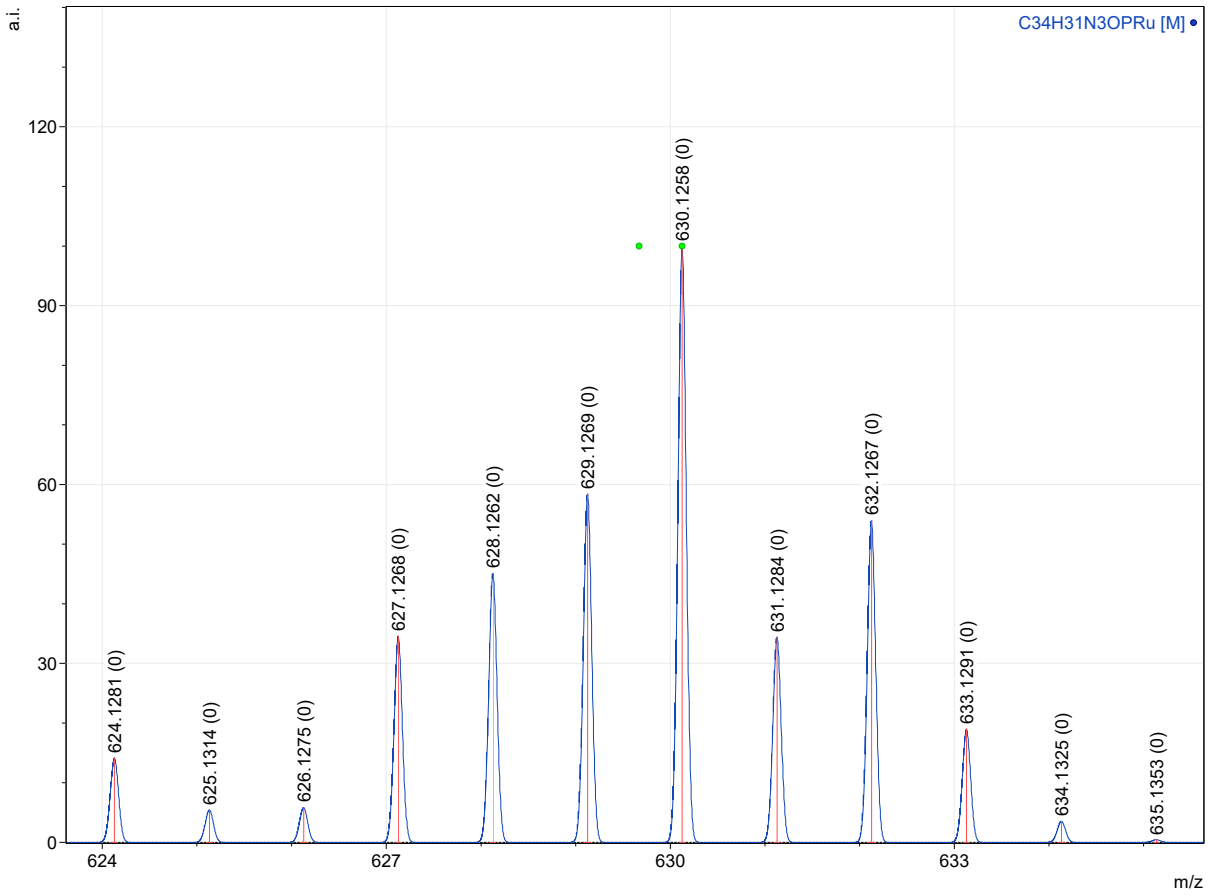

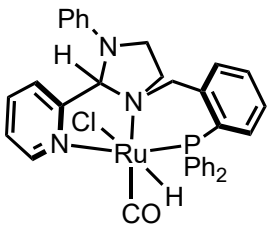

Figure S 49. Absorption spectra of *syn* and *anti-rac*-[Ru(NNP)(H)Cl(CO)]

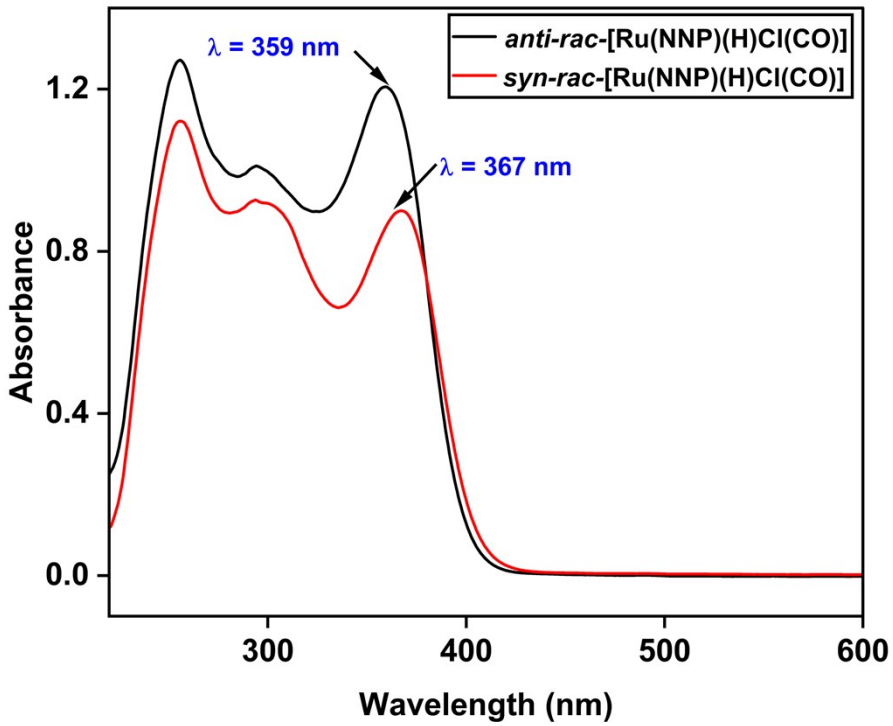

Absorption spectra of *syn* and *anti-rac*-[Ru(NNP)(H)Cl(CO)] in CH_2Cl_2 at 0.125 mM concentration.

Figure S 50. Fluorescence spectrum of *syn and anti-rac*-[Ru(NNP)(H)Cl(CO)]

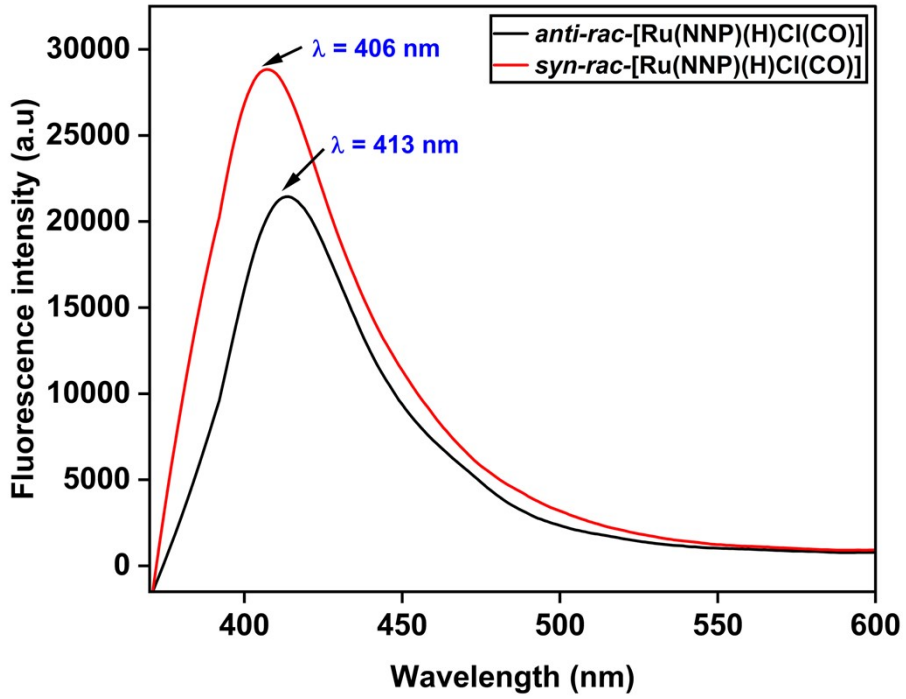

For *anti-rac*-[Ru(NNP)(H)Cl(CO)], upon excitation at λ_{ex} = 370 nm in dichloromethane at 0.125 mM concentration at rt, gives rise to an emission band at λ_{em} = 406 nm.

For *syn-rac*-[Ru(NNP)(H)Cl(CO)], upon excitation at λ_{ex} = 380 nm in dichloromethane at 0.125 mM concentration at rt, gives rise to an emission band at λ_{em} = 413 nm.

Figure S 51. ^{31}P NMR spectrum for *anti-rac*-[Ru(NNP)(H)Cl(CO)] after adding CS_2 in $CDCl_3$ at 298 K.

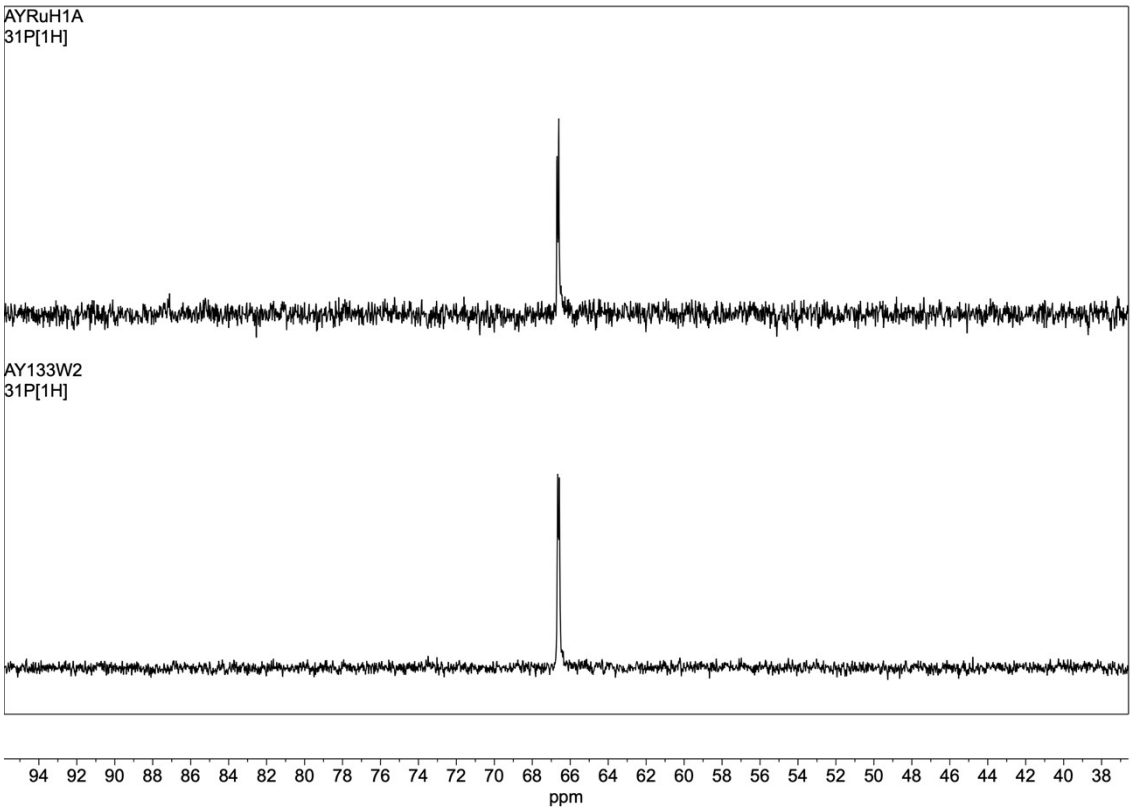

^{31}P NMR spectrum for *anti-rac*-[Ru(NNP)(H)Cl(CO)] (bottom) and after the addition of CS_2 (top). No peak shifting was observed.

Figure S 52. ^{31}P NMR spectrum for *syn-rac*-[Ru(NNP)(H)Cl(CO)] after adding CS_2 in $CDCl_3$ at 298 K.

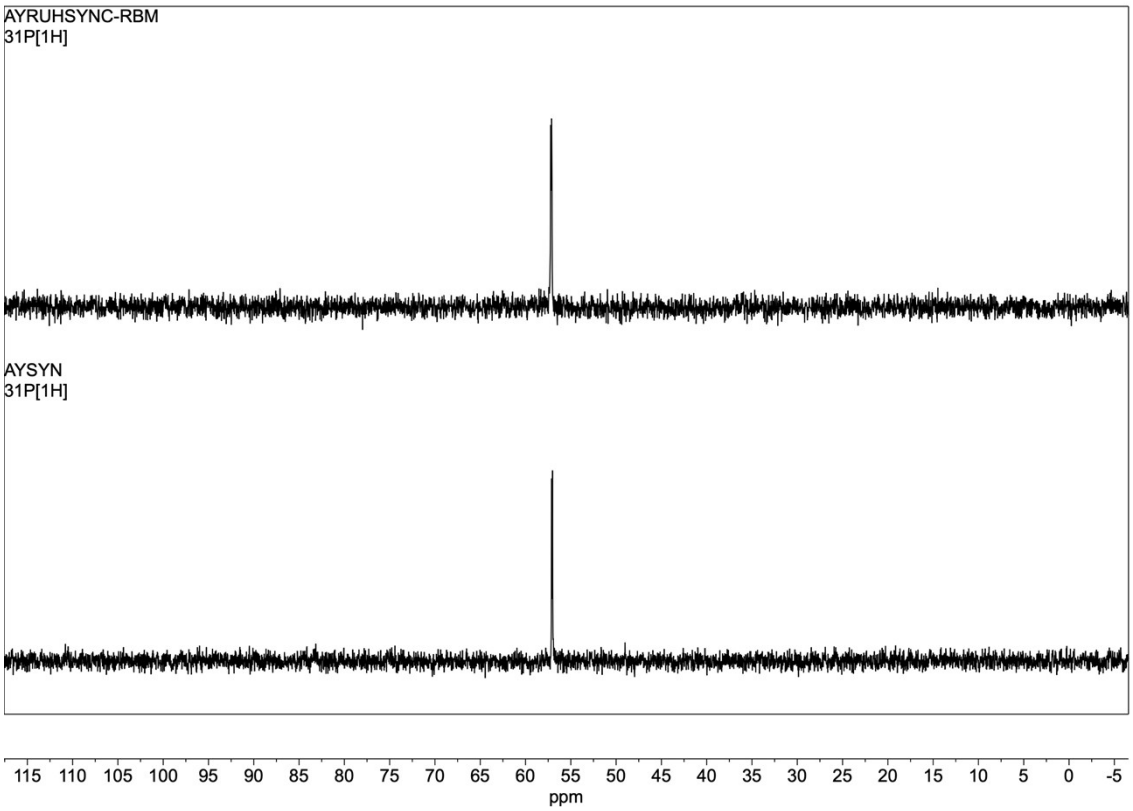

^{31}P NMR spectrum for *syn-rac*-[Ru(NNP)(H)Cl(CO)] (bottom) and after the addition of CS_2 (top). No peak shifting was observed.

Figure S 53. ^{1}H NMR spectrum of *anti-rac*-[Ru(NNP)(H)(η^{1}-BH_4)(CO)] complex in $CDCl_3$ at 298 K.

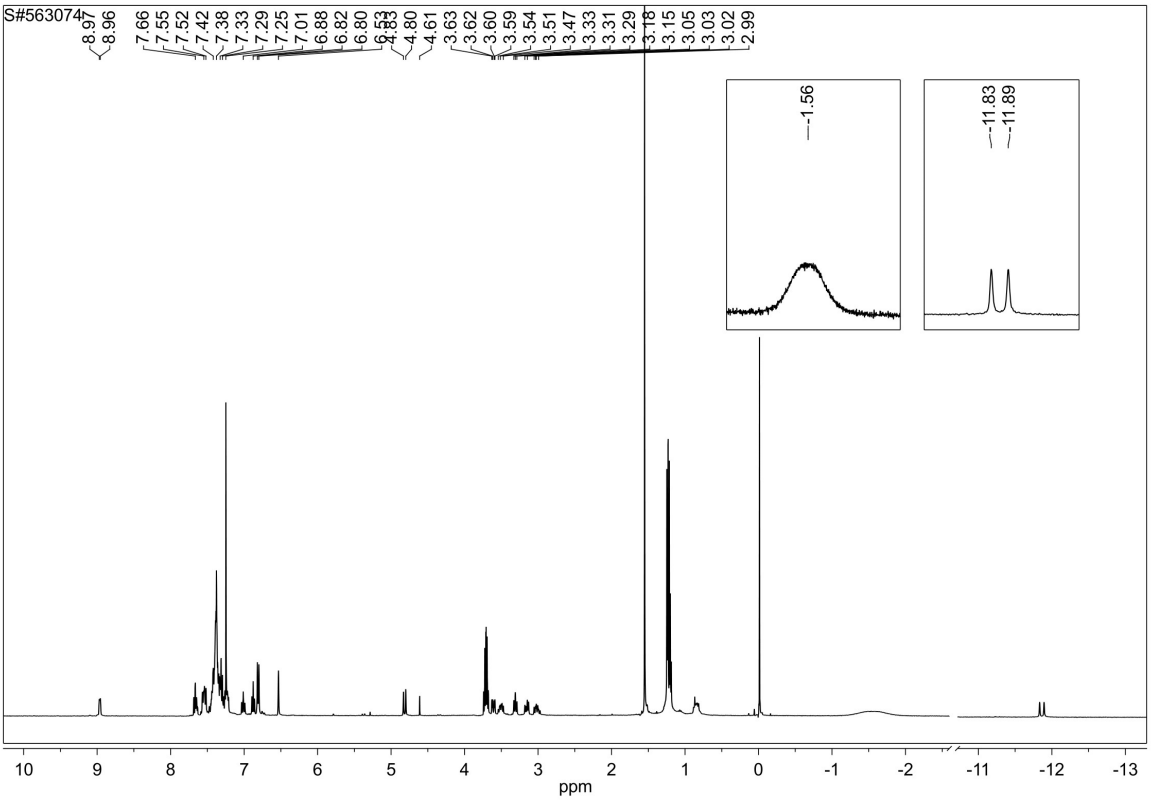

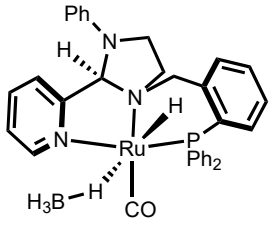

Figure S 54. ^{31}P NMR spectrum of *anti-rac*-[Ru(NNP)(H)(η^1-BH_4)(CO)] complex in $CDCl_3$ at 298 K.

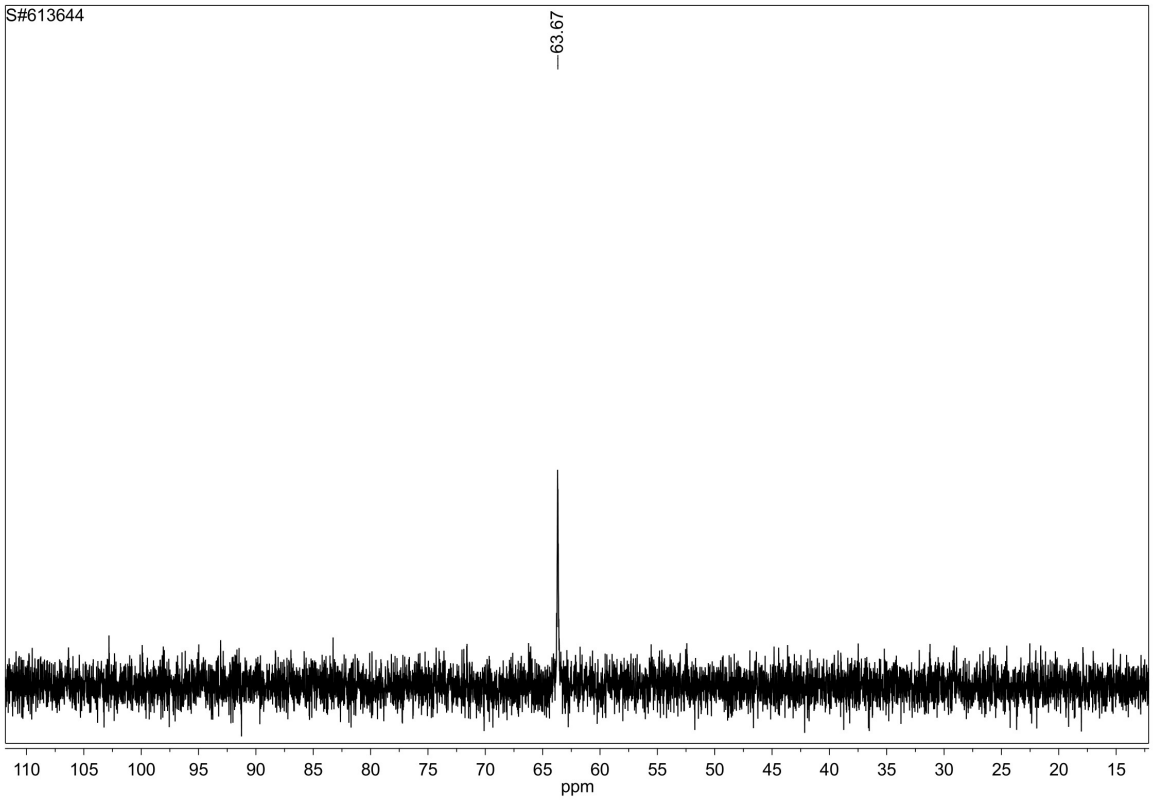

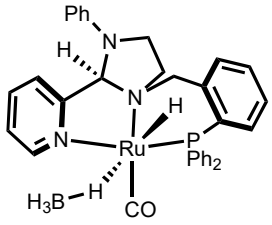

Figure S 55. ^{31}P NMR spectrum of *syn-rac*-[Ru(NNP)(H)(η^1-BH_4)(CO)] complex in $CDCl_3$ at 298 K.

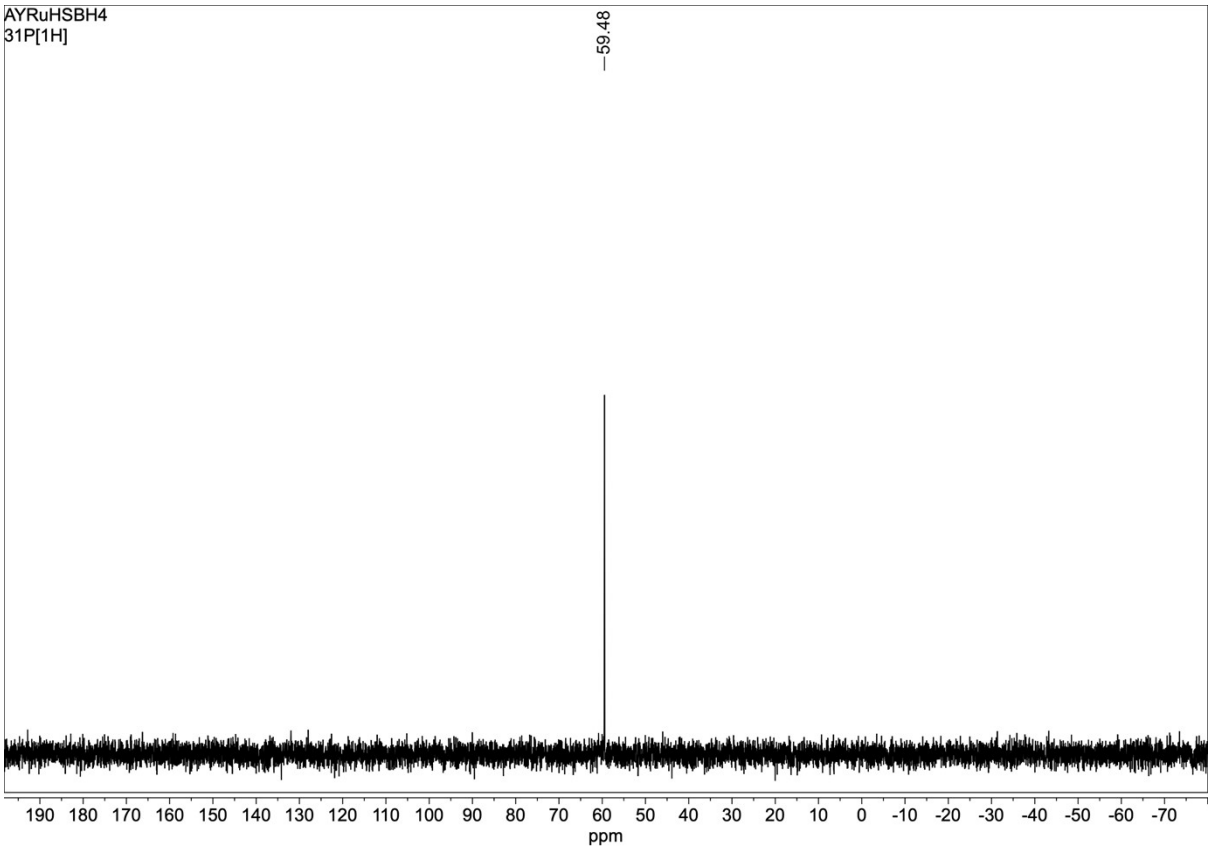

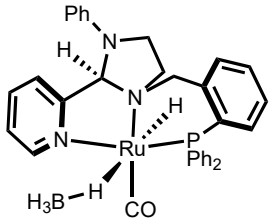

Figure S 56. ESI-MS of [Ru(NNP)(H)(η^1-BH_4)(CO)]

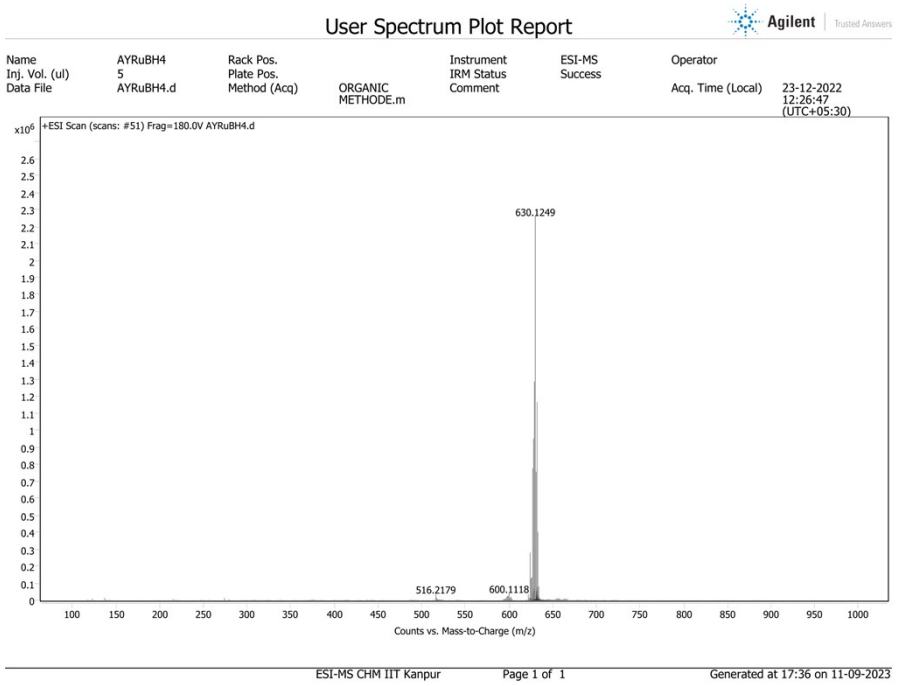

High resolution ESI-MS: m/z for = $[M-BH_4]^+$ = 630.1249 (calcd. 630.1248) = $[RuC_{34}H_{31}N_3OP]^+$.

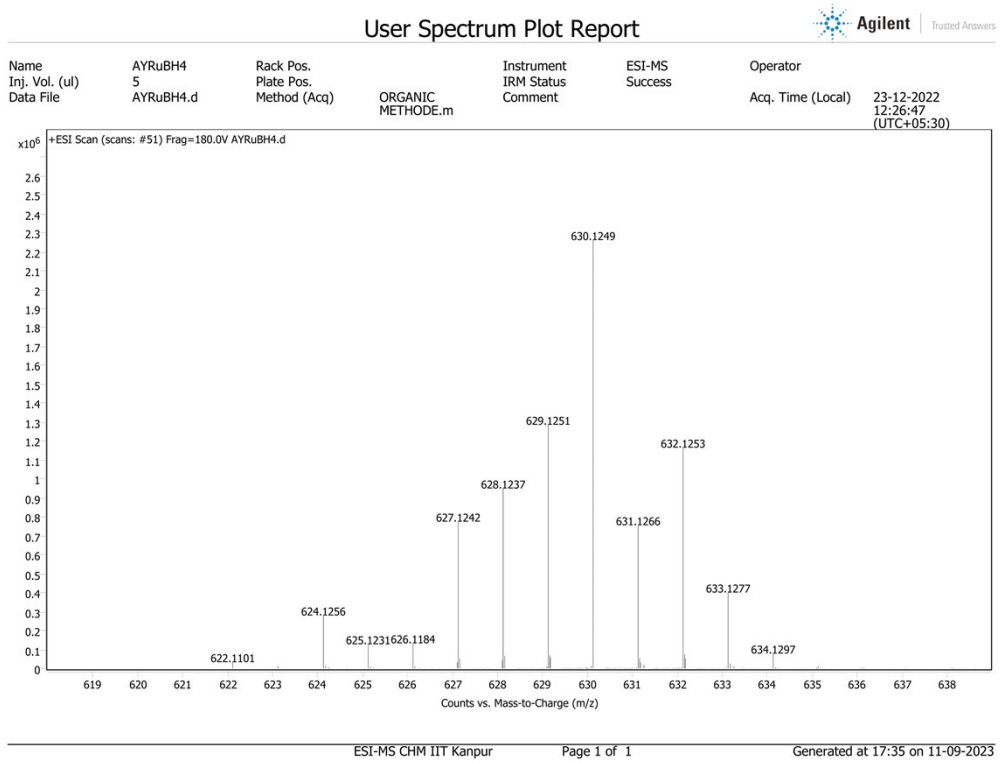

Figure S 57. Simulated ESI-MS of [Ru(NNP)(H)(η^1-BH_4)(CO)]

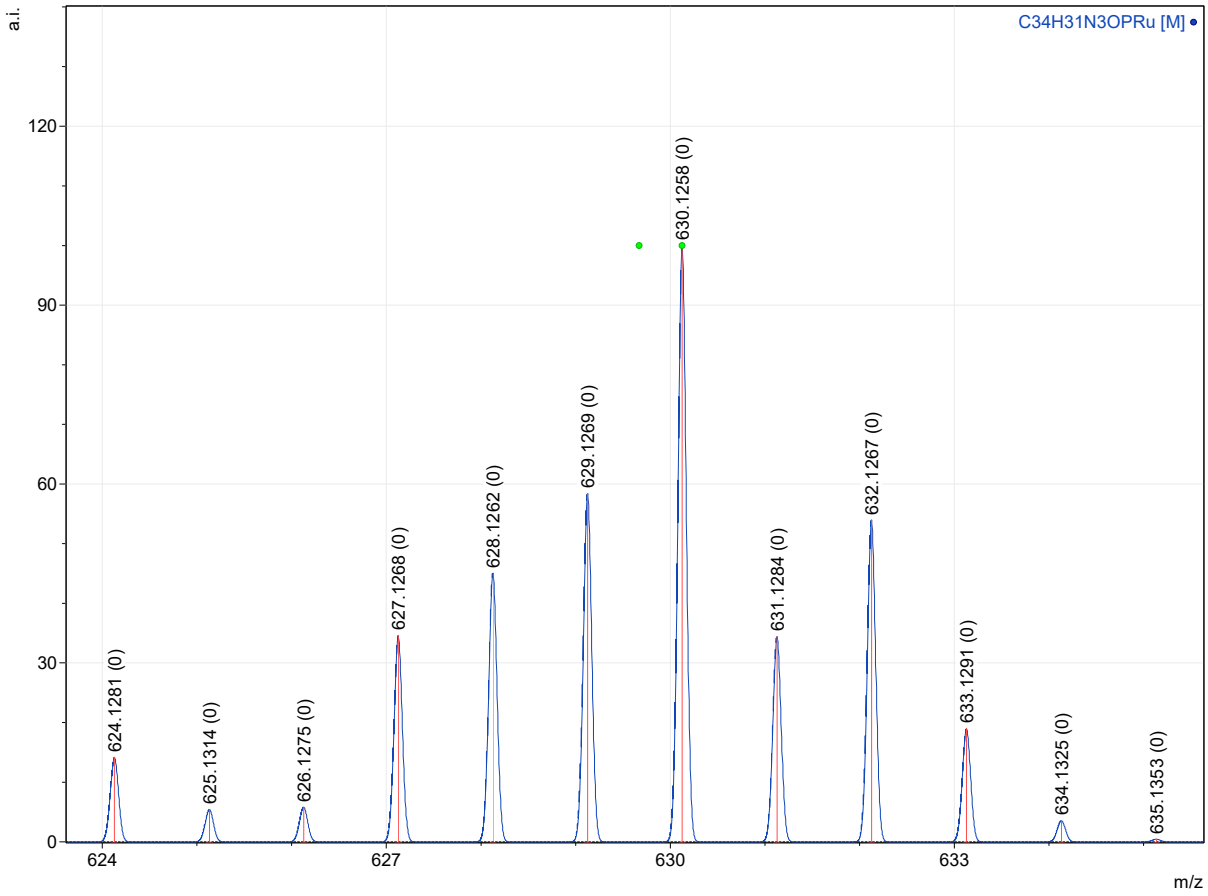

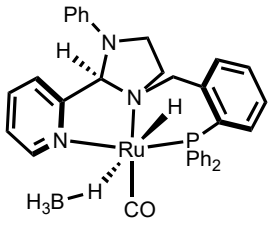

Figure S 58. ^{1}H NMR spectrum of [Ru(NNP)$(CS_2H)_2$(CO)] complex in $CDCl_3$ at 298 K.

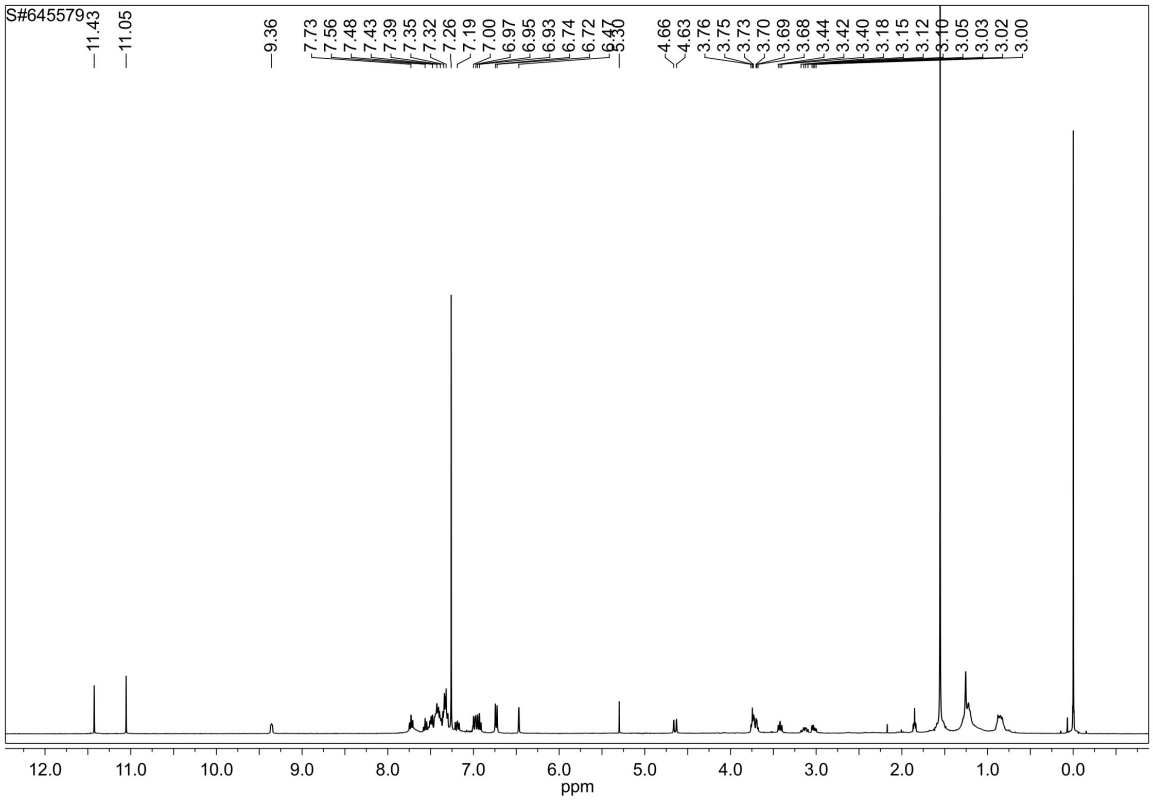

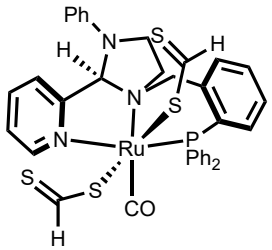

Figure S 59. ^{31}P NMR spectrum of $[Ru(NNP)(CS_2H)_2(CO)]$ complex in $CDCl_3$ at 298 K.

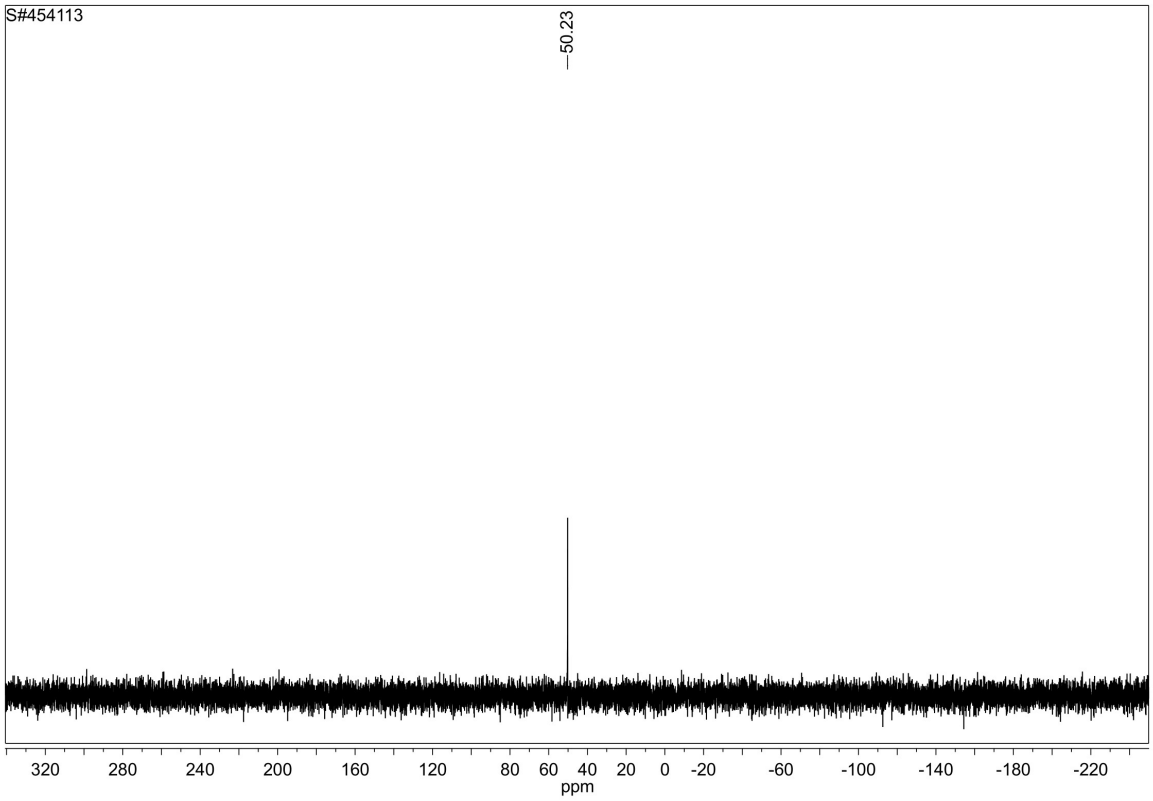

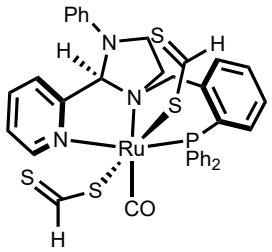

Figure S 60. ESI-MS of $[Ru(NNP)(CS_2H)_2(CO)]$

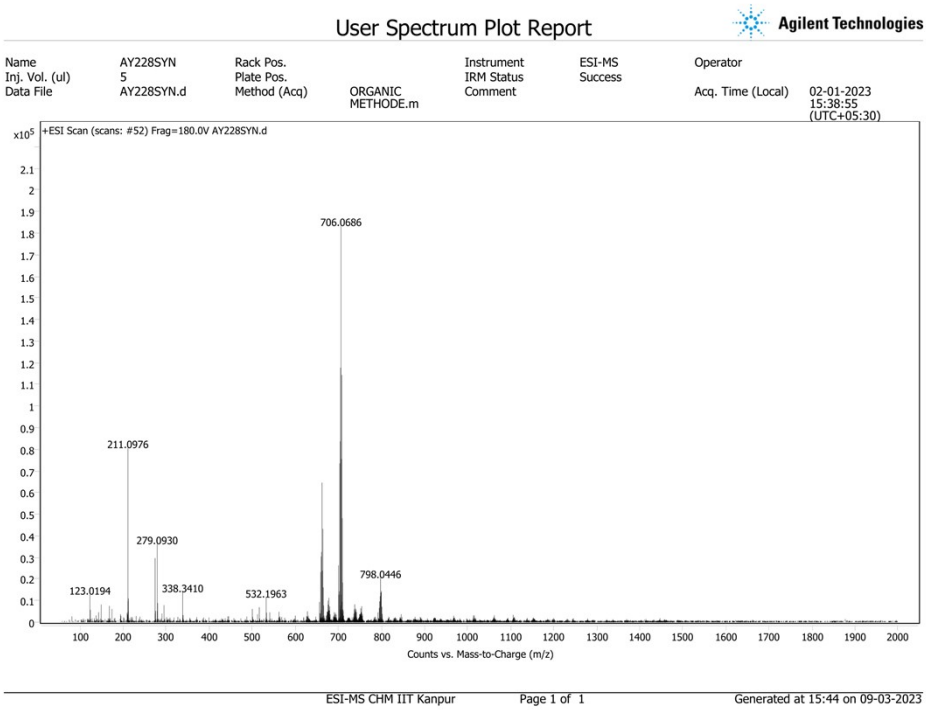

High resolution ESI-MS: *m/z* for = $[M-CS_2H]^+$ = 706.0686 (calcd. 706.0690) = $[RuC_{35}H_{31}N_3OPS_2]^+$; *m/z* = 798.0446 (calcd. 798.0080) = $[Ru(NNP{=}O)(CS_2H)(CS_2)]^+$.

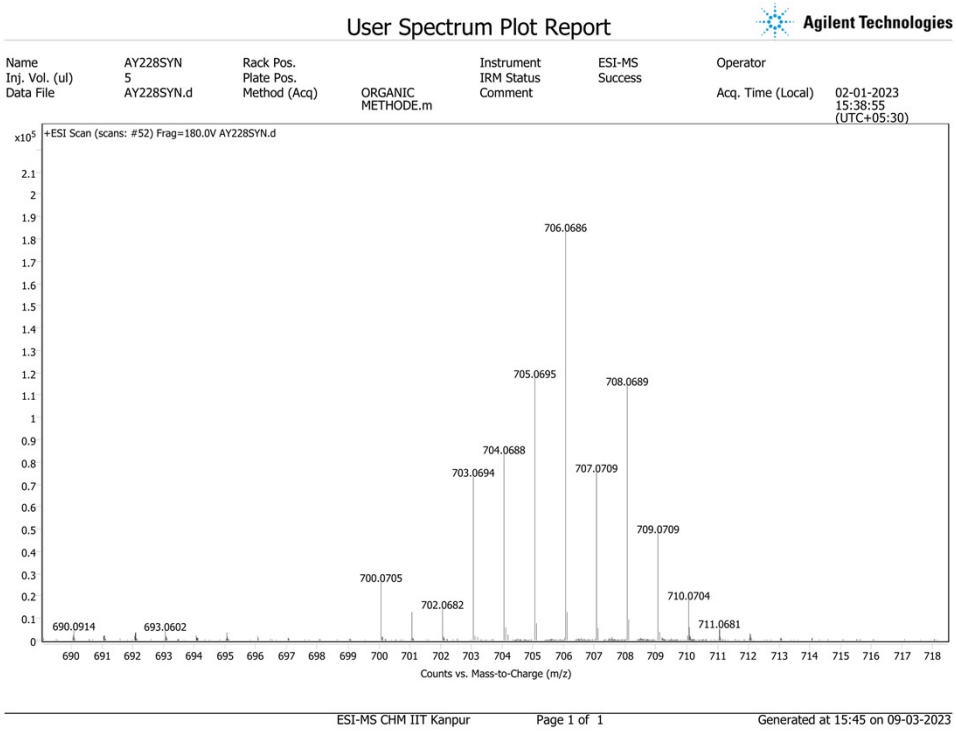

Figure S 61. Simulated for [Ru(NNP)($CS_2H)_2$(CO)]

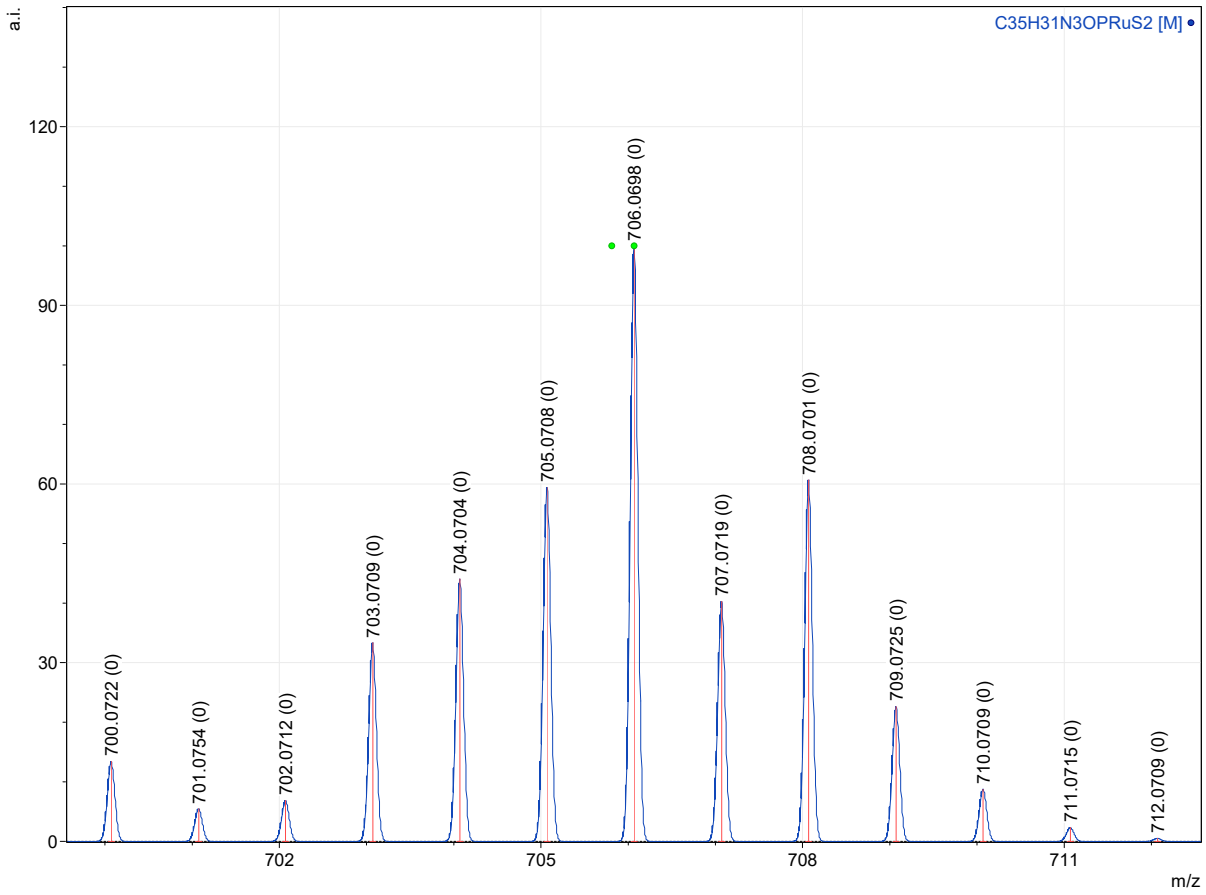

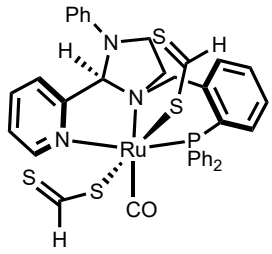

Figure S 62. FTIR spectrum of [Ru(NNP)(CS_2H)$_2$(CO)]

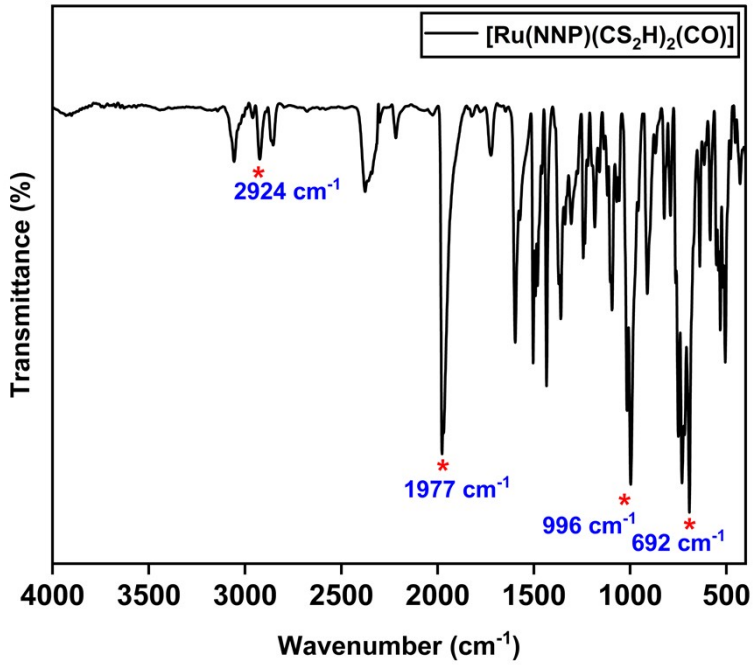

FTIR (KBr pellet) [Ru(NNP)(CS_2H)$_2$(CO)]: ν_{C-H} = 2930-2920 cm^{-1}, ν_{CO} = 1977 cm^{-1}, ν_{S-C-S} = 996 cm^{-1}, $\nu_{C=S}$ = 692 cm^{-1}.

Figure S 63. ^{1}H NMR spectrum of crude [Ru(NNP)$(CS_2H)_2$(CO)] and after the addition of MeI in $CDCl_3$ at 298 K.

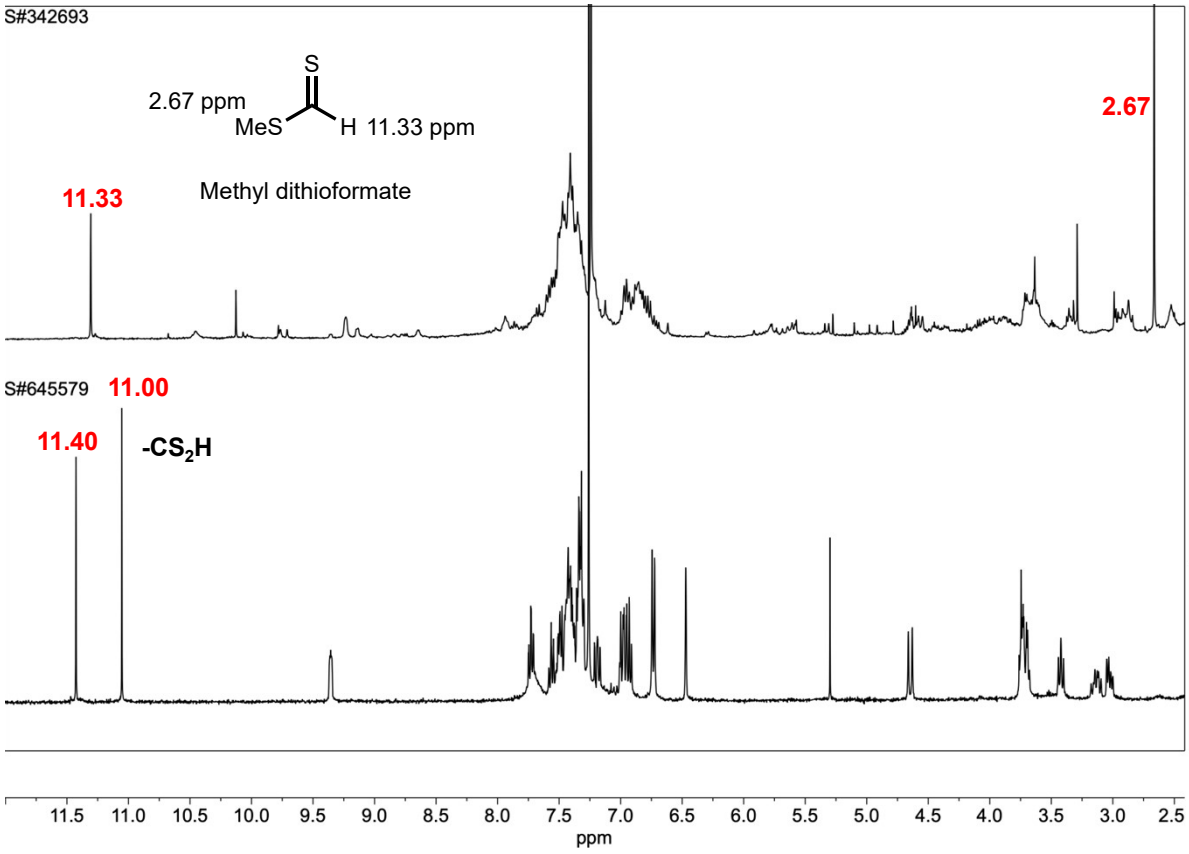

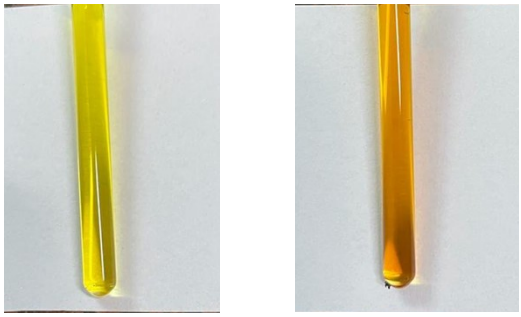

[Ru(NNP)$(CS_2H)_2$(CO)] **[Ru(NNP)$(CS_2H)_2$(CO)] + MeI**

^{1}H NMR spectrum of crude [Ru(NNP)$(CS_2H)_2$(CO)] (bottom) and after the addition of MeI (top).

Figure S 64. ^{31}P NMR spectrum of [Ru(NNP)I_2(CO)] complex in dichloromethane at 298 K.

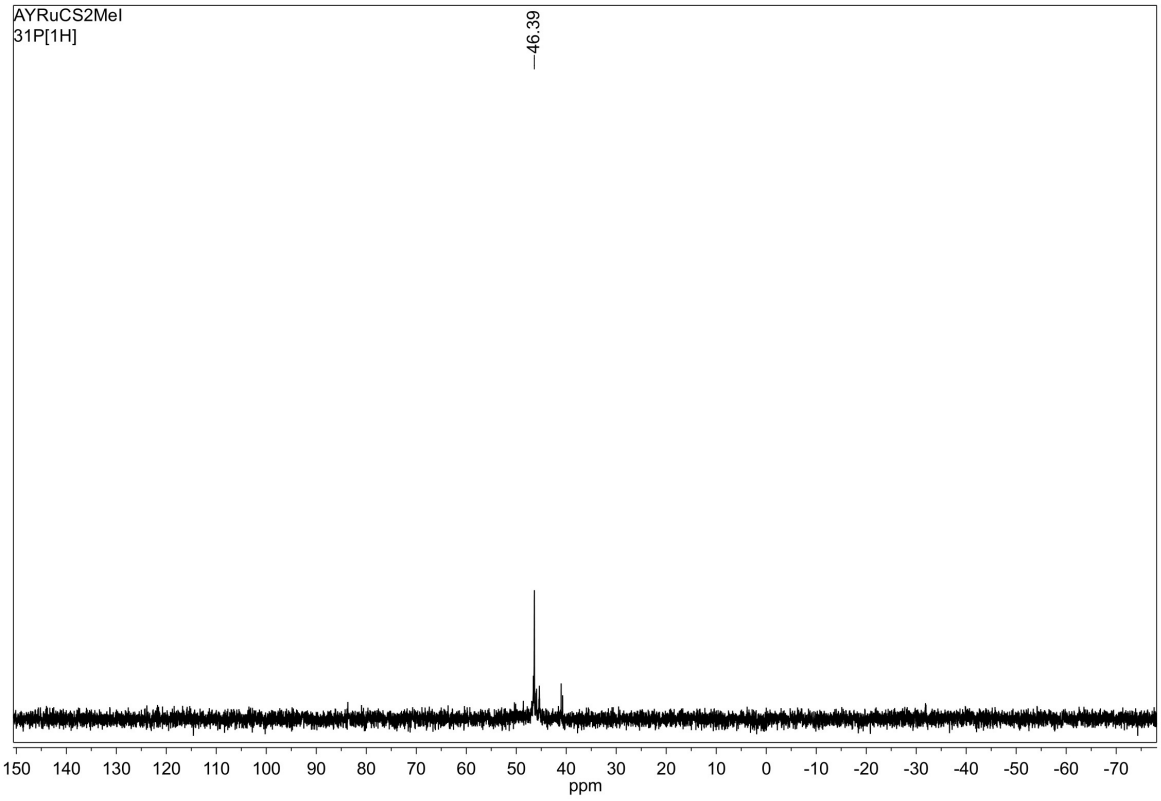

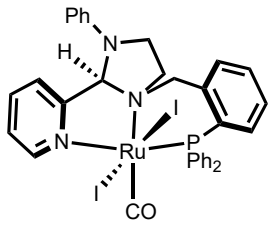

Figure S 65. ESI-MS for [Ru(NNP)I_2(CO)]

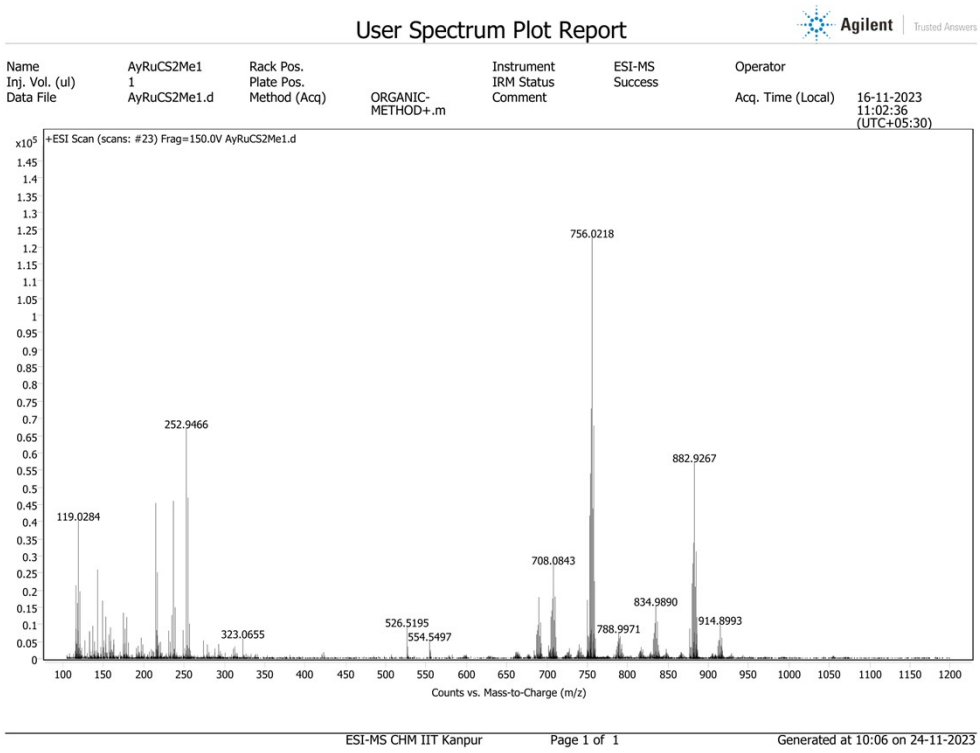

High resolution ESI-MS: *m/z* for = $[M-I]^+$ = 756.0218 (calcd. 756.0215) = $[C_{34}H_{30}N_3OPRuI]^+$.

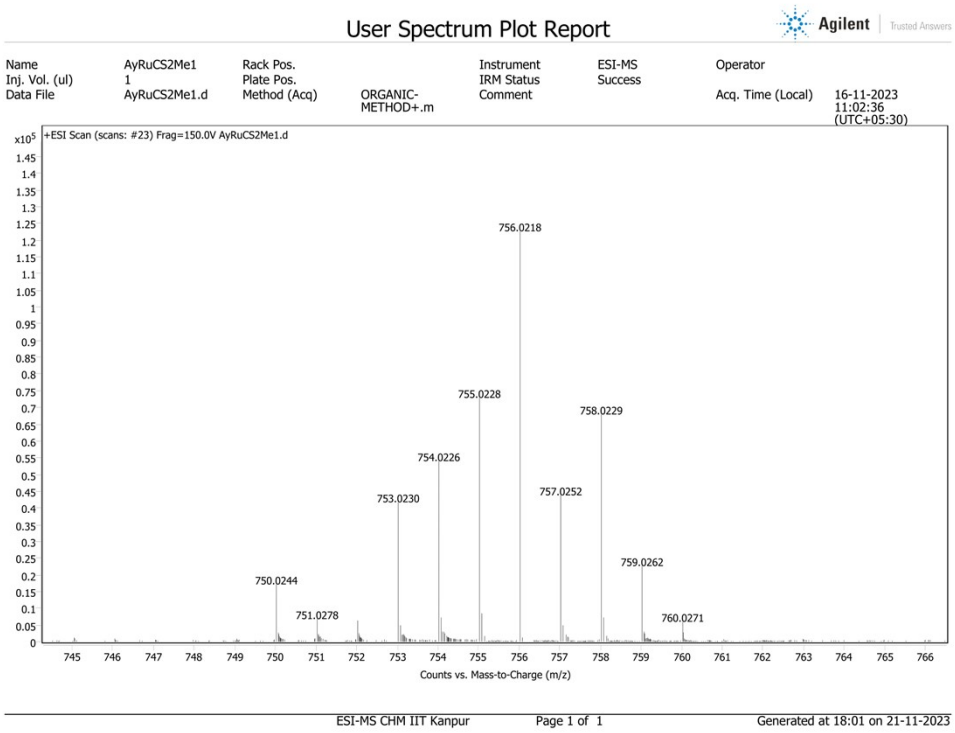

Figure S 66. Simulated ESI-MS for [Ru(NNP)I_2(CO)]

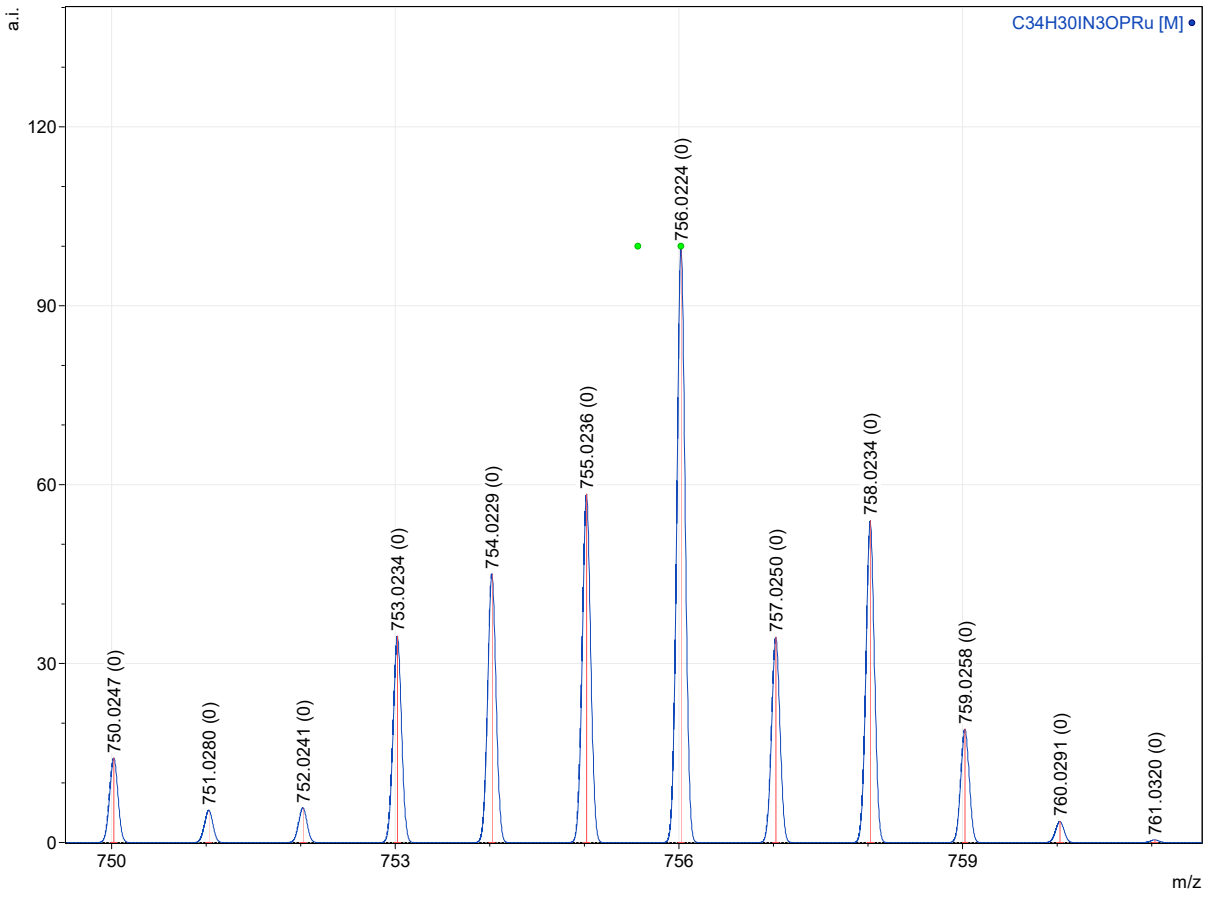

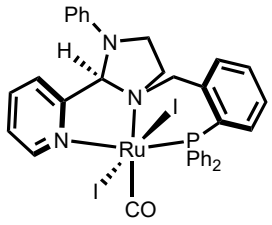

Figure S 67. UV-Vis spectrum for [Ru(NNP)(CS_2H)$_2$(CO)] reaction with MeI.

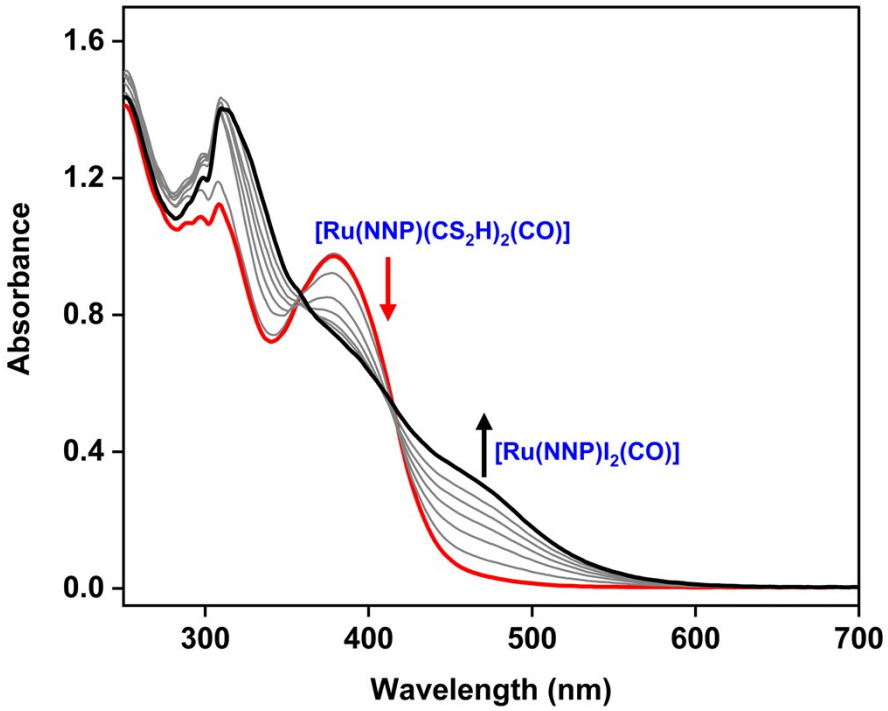

Absorption spectra of [Ru(NNP)(CS_2H)$_2$(CO)] reaction with MeI in CH_2Cl_2 at 0.125 mM concentration.

Figure S 68. ^{1}H NMR spectrum of the [Cu(NNP)I] in $CDCl_3$ at 298 K.

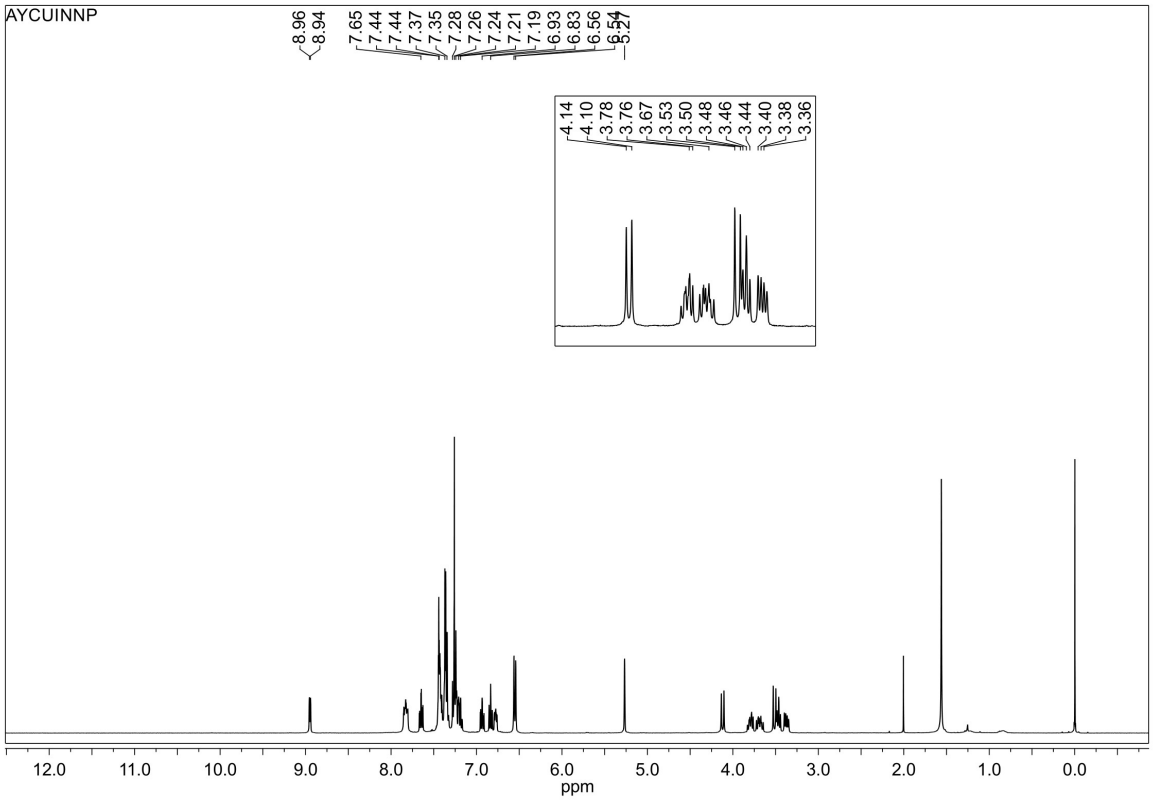

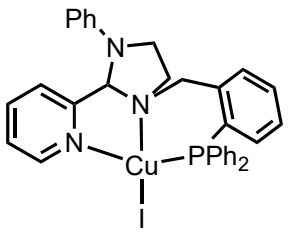

Figure S 69. ^{31}P NMR spectrum of the [Cu(NNP)I] in $CDCl_3$ at 298 K.

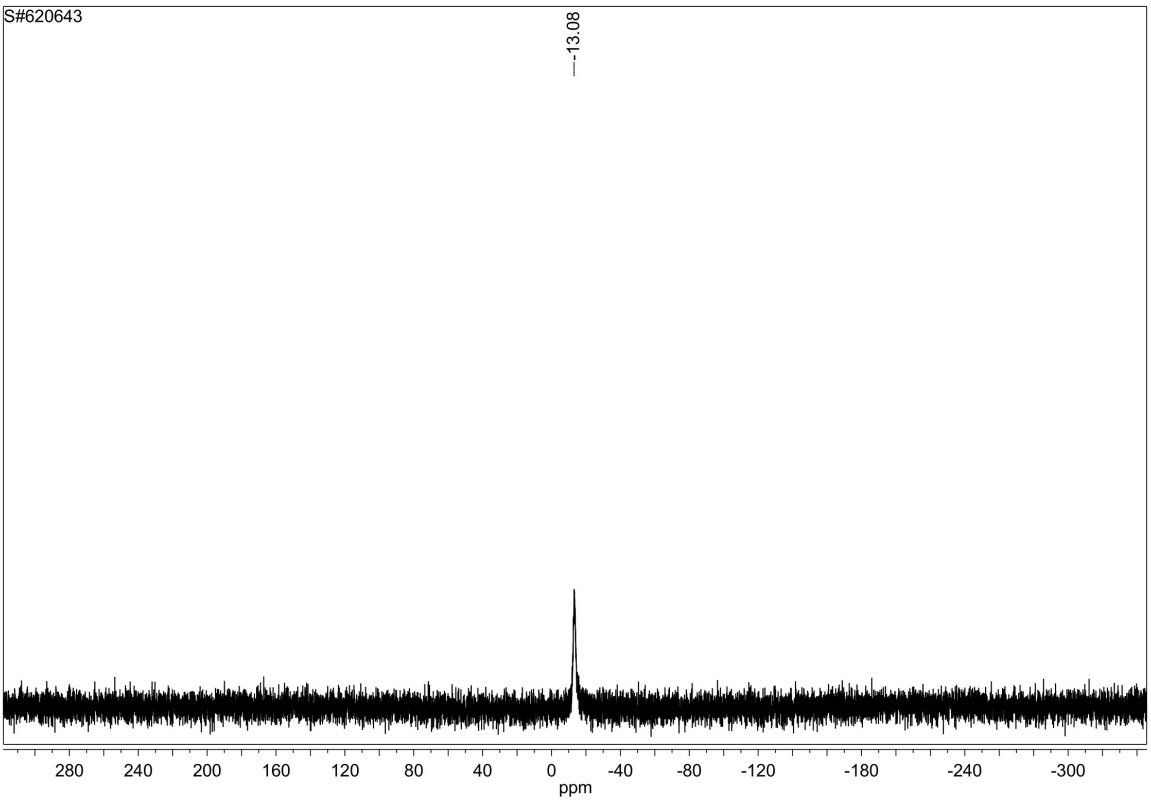

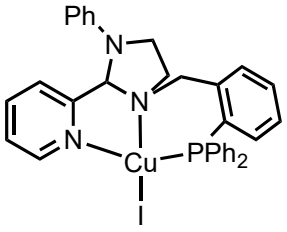

Figure S 70. ESI-MS of [Cu(NNP)I]

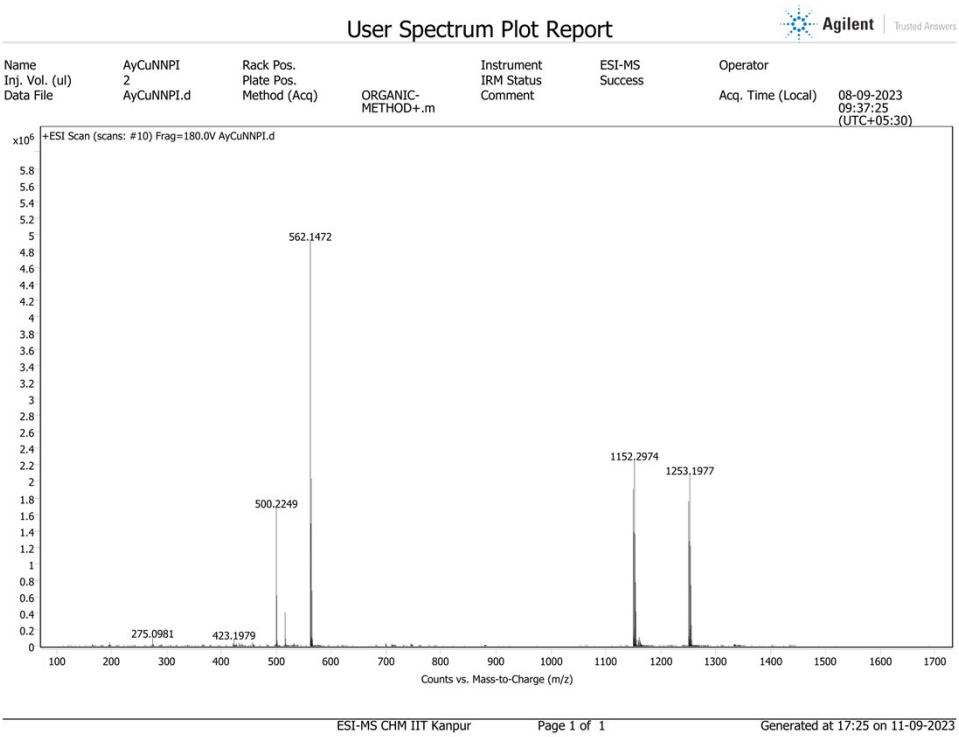

High resolution ESI-MS: m/z for $[M-I]^+$ = 562.1472 (calcd. 562.1473) = $[CuC_{33}H_{30}N_3P]^+$; *m/z* = 1253.1977 (calcd. 1253.1973) = $Cu_2(NNP)_2I]^+$; *m/z* = 500.2249 (calcd. 500.2256) = $[NNP+H]^+$.

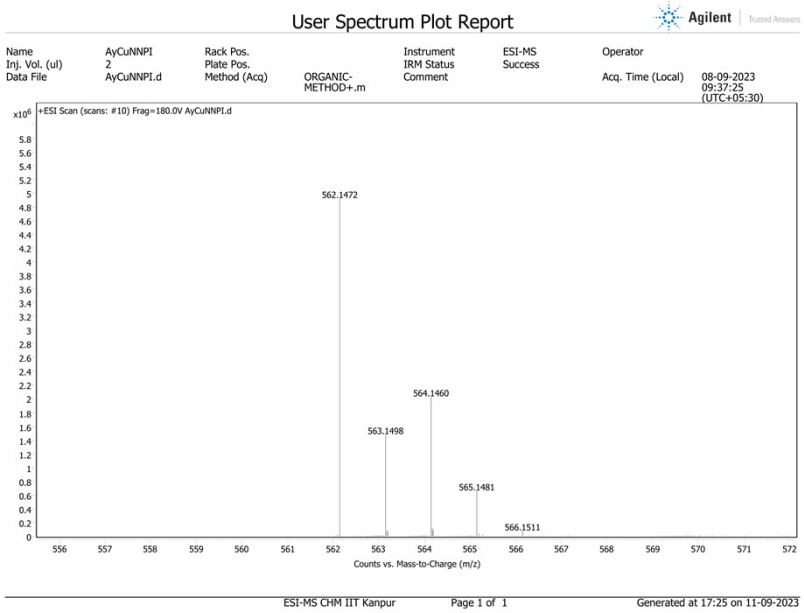

Figure S 71. Simulated ESI-MS of [Cu(NNP)I]

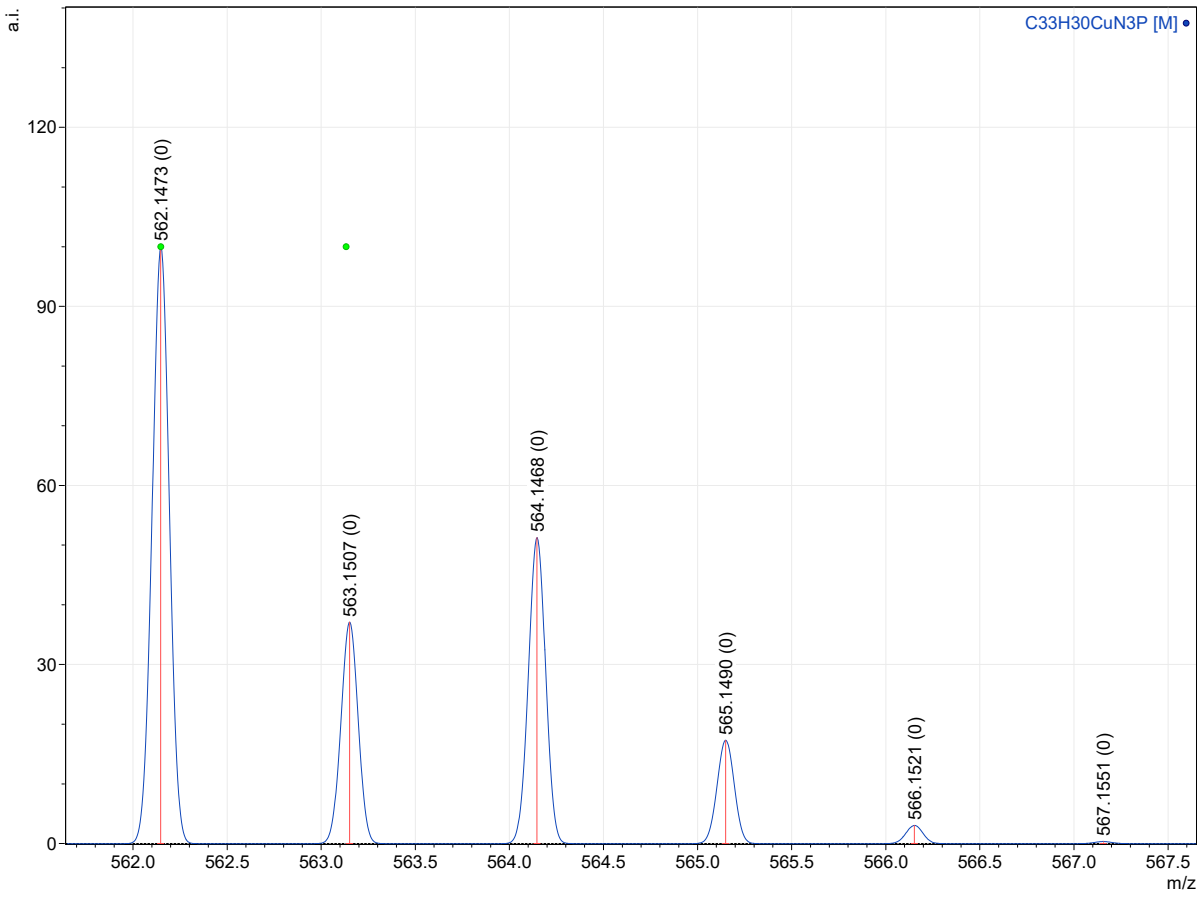

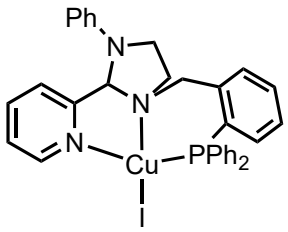

Figure S 72. ^{1}H NMR spectrum of the [Cu(NNP)Cl] in $CDCl_3$ at 298 K.

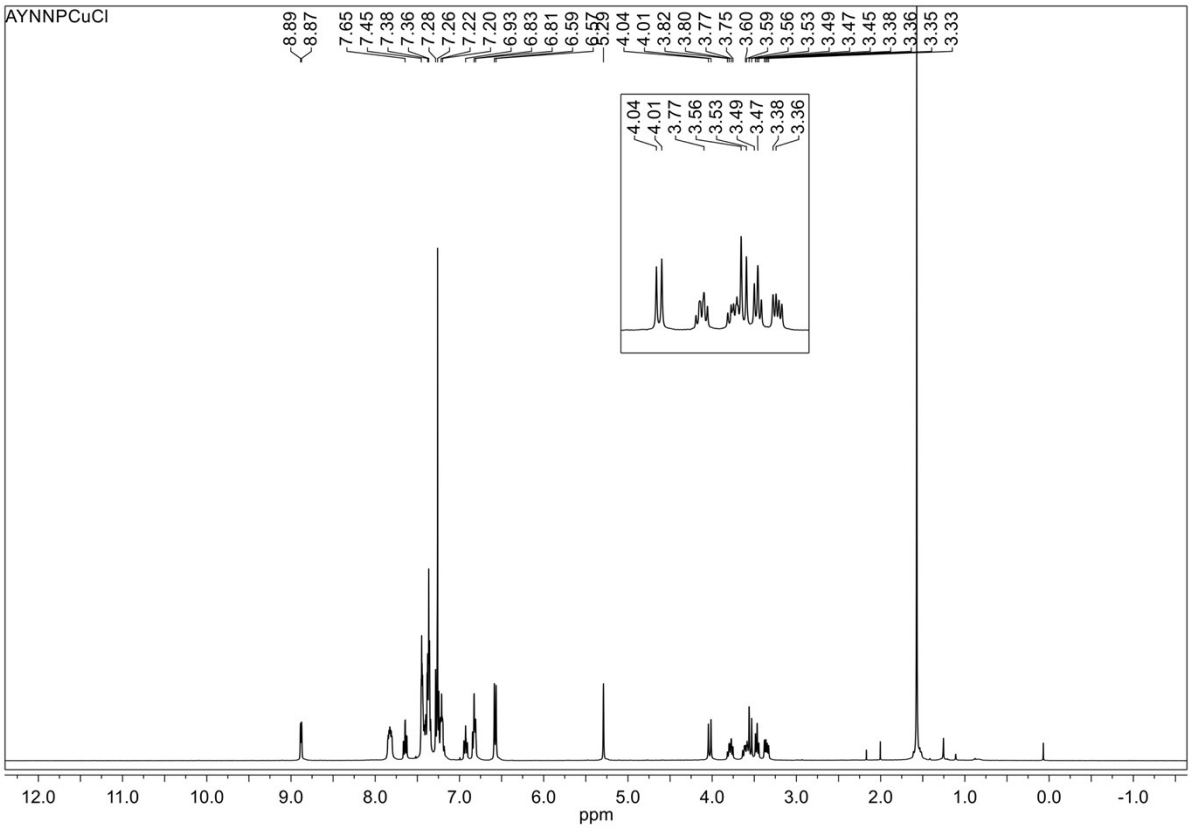

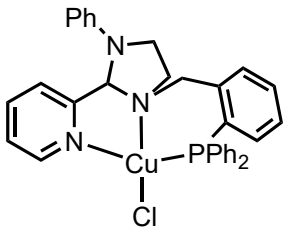

Figure S 73. ^{31}P NMR spectrum of the [Cu(NNP)Cl] in $CDCl_3$ at 298 K.

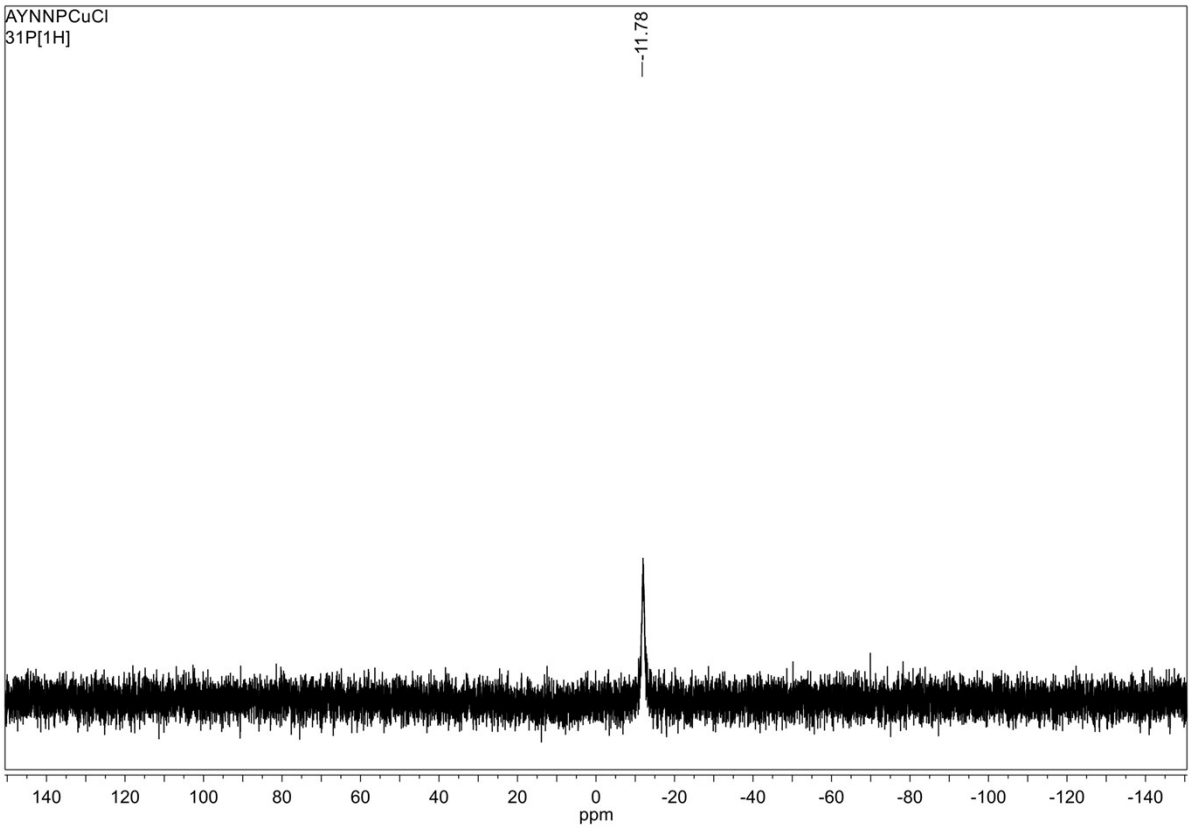

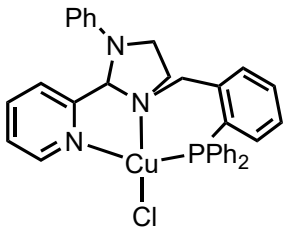

Figure S 74. ^{1}H NMR spectrum of the $[Cu(NNP)(CH_3CN)][BF_4]$ in $CDCl_3$ at 298 K.

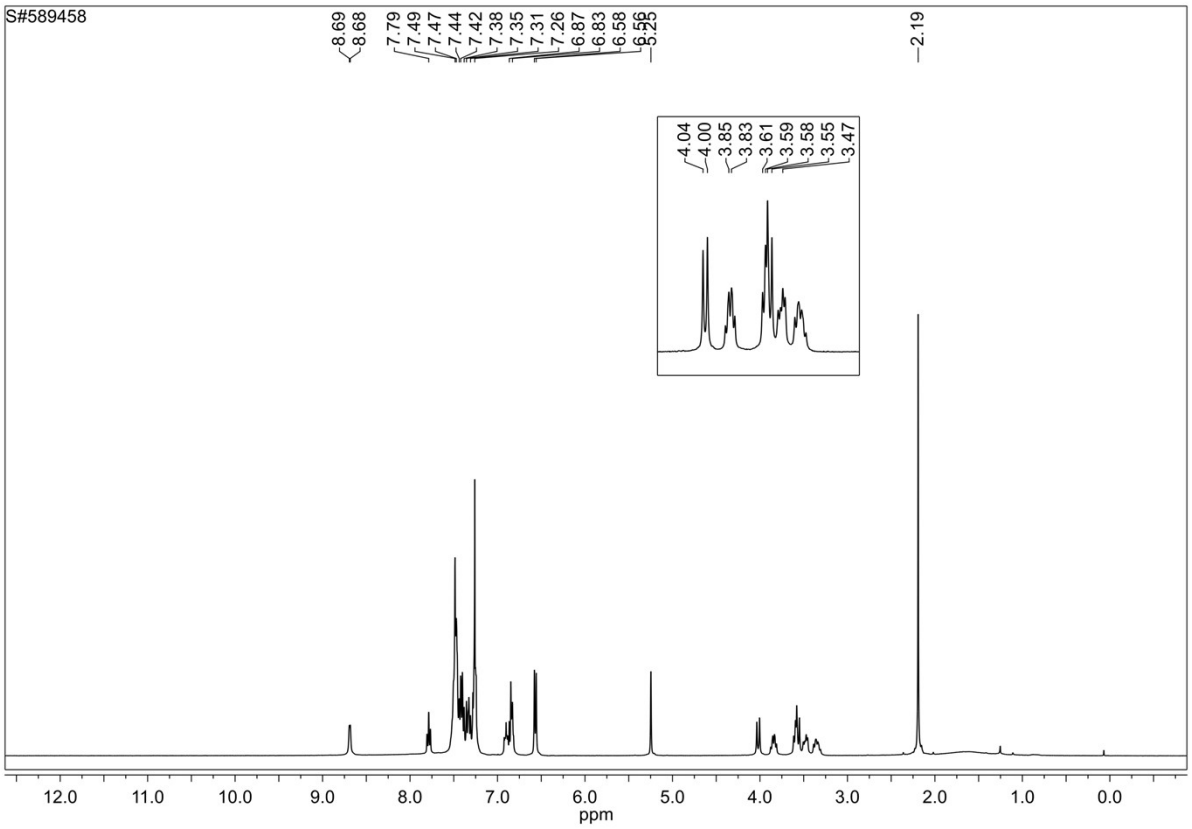

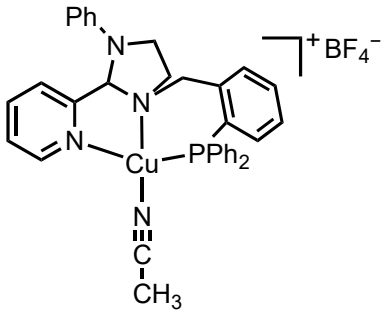

Figure S 75. ^{31}P NMR spectrum of the [Cu(NNP)(CH_3CN)][BF_4] in $CDCl_3$ at 298 K.

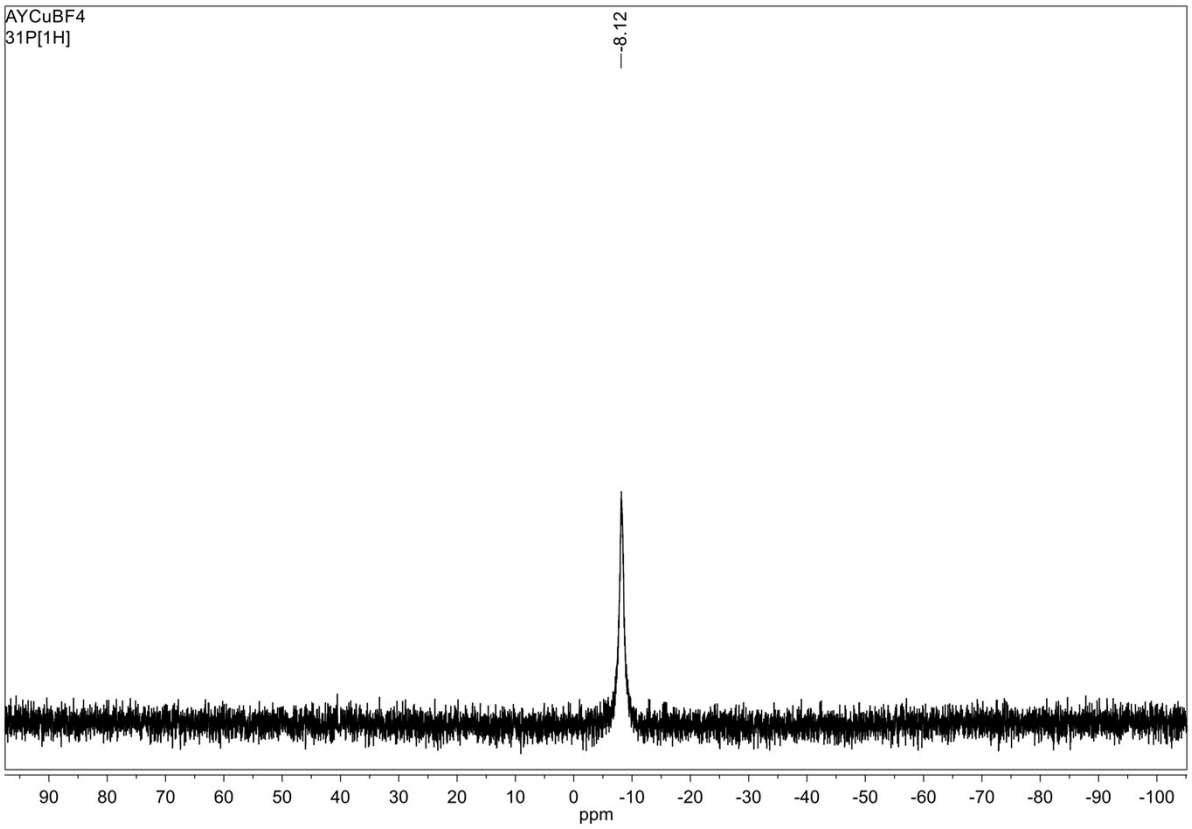

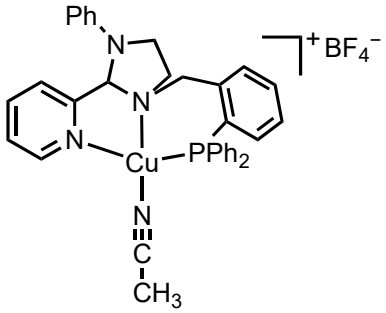

Figure S 76. ^{1}H NMR spectrum of the $[Cu(NNP)(CH_3CN)][PF_6]$ in $CDCl_3$ at 298 K.

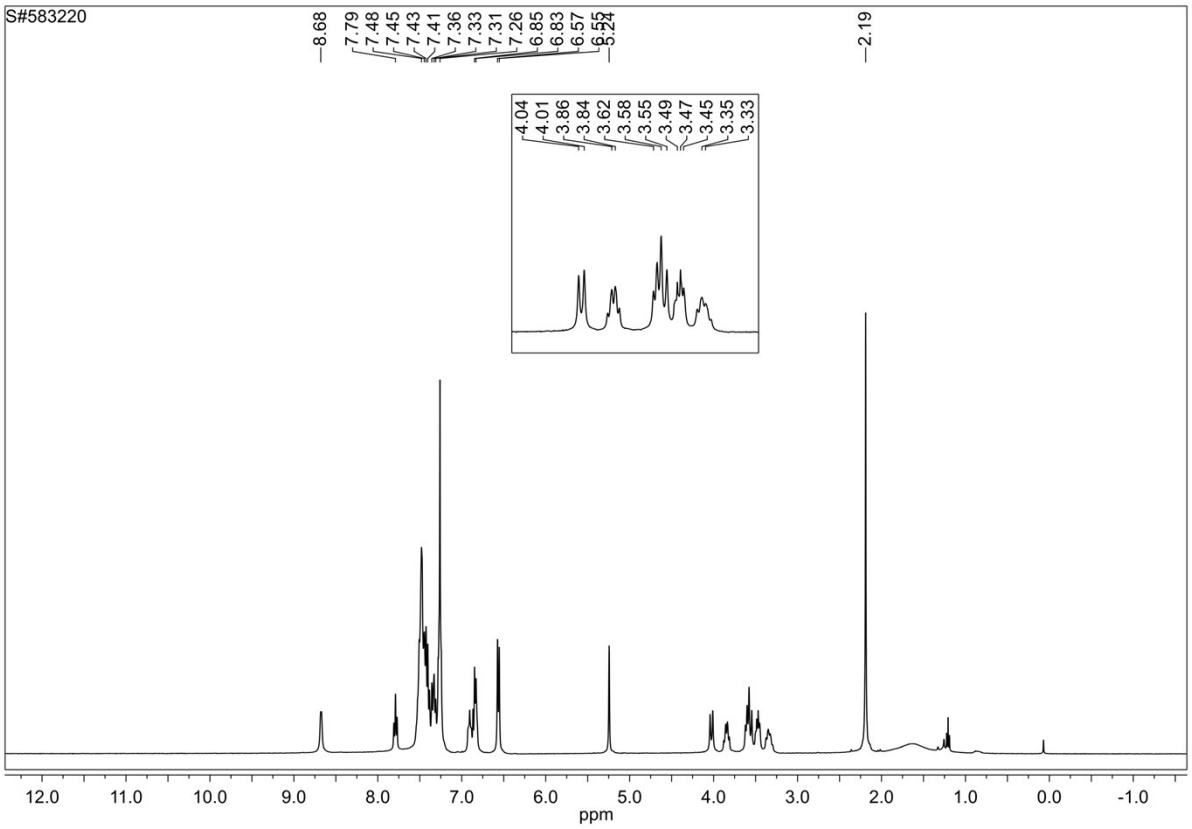

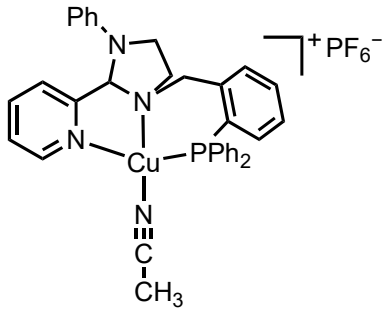

Figure S 77. ^{31}P NMR spectrum of the $[Cu(NNP)(CH_3CN)][PF_6]$ in $CDCl_3$ at 298 K.

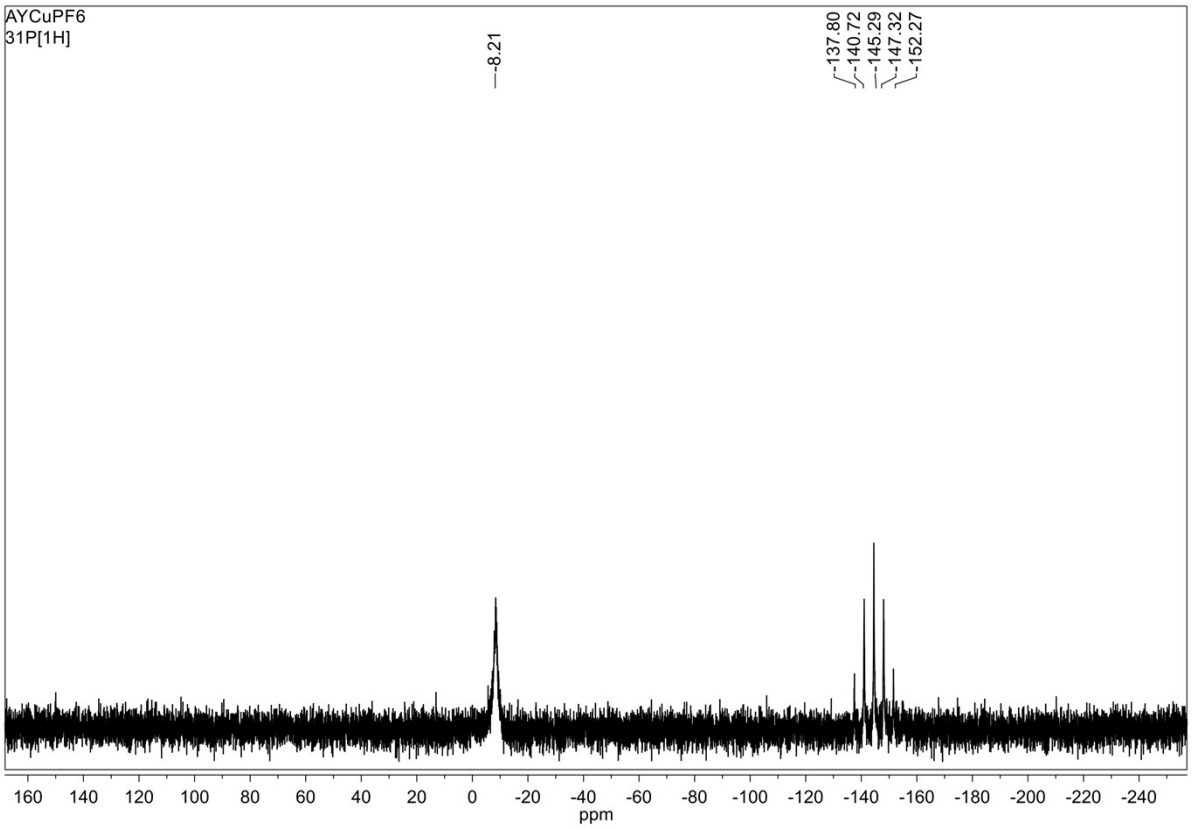

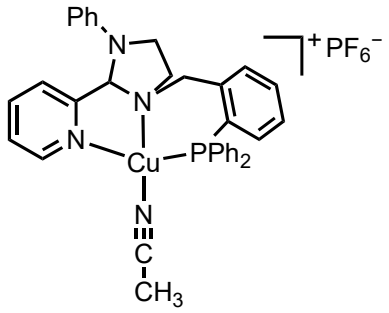

Figure S 78. ^{1}H NMR spectrum of the [Cu(NNP)(CH_3CN)][OTf] in $CDCl_3$ at 298 K.

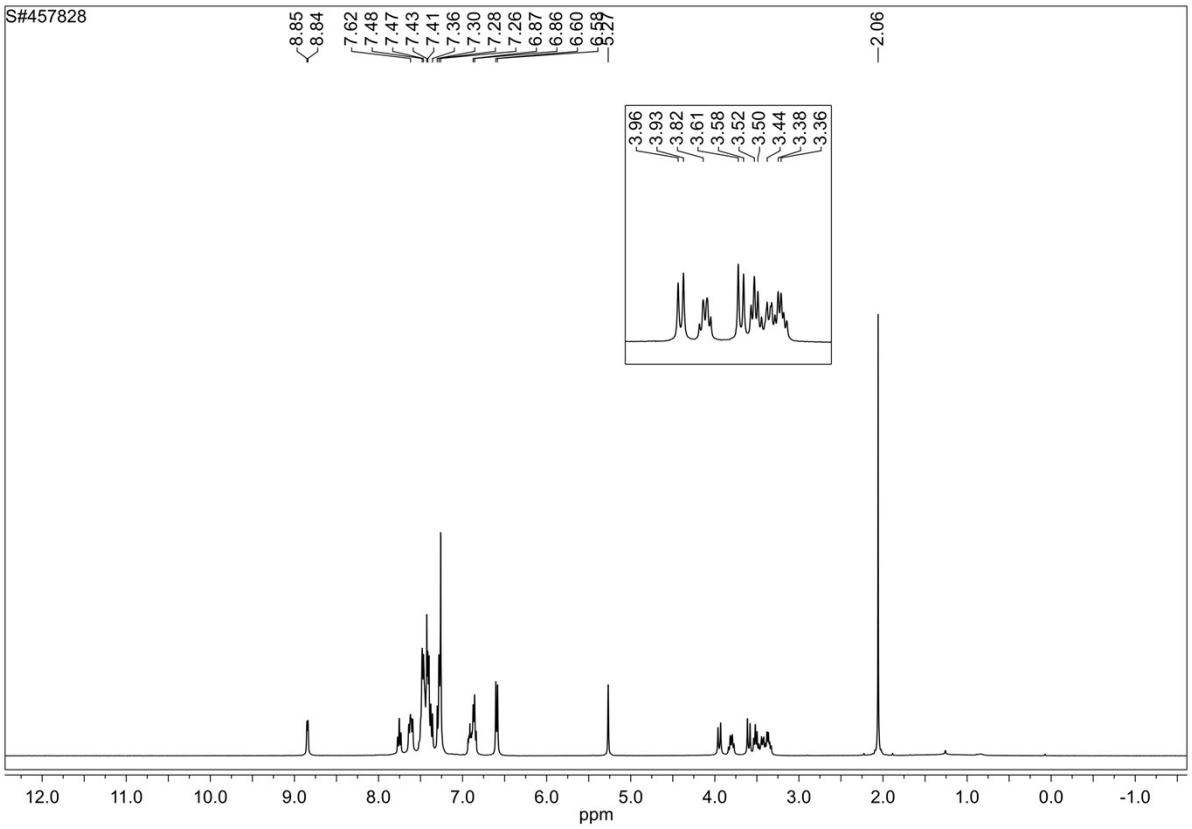

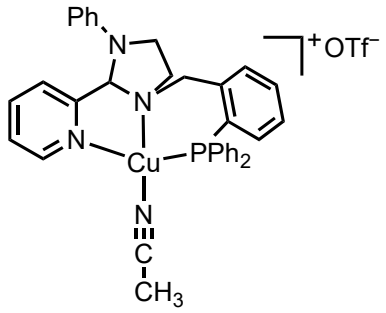

Figure S 79. ^{31}P NMR spectrum of the [Cu(NNP)(CH_3CN)](OTf) in $CDCl_3$ at 298 K.

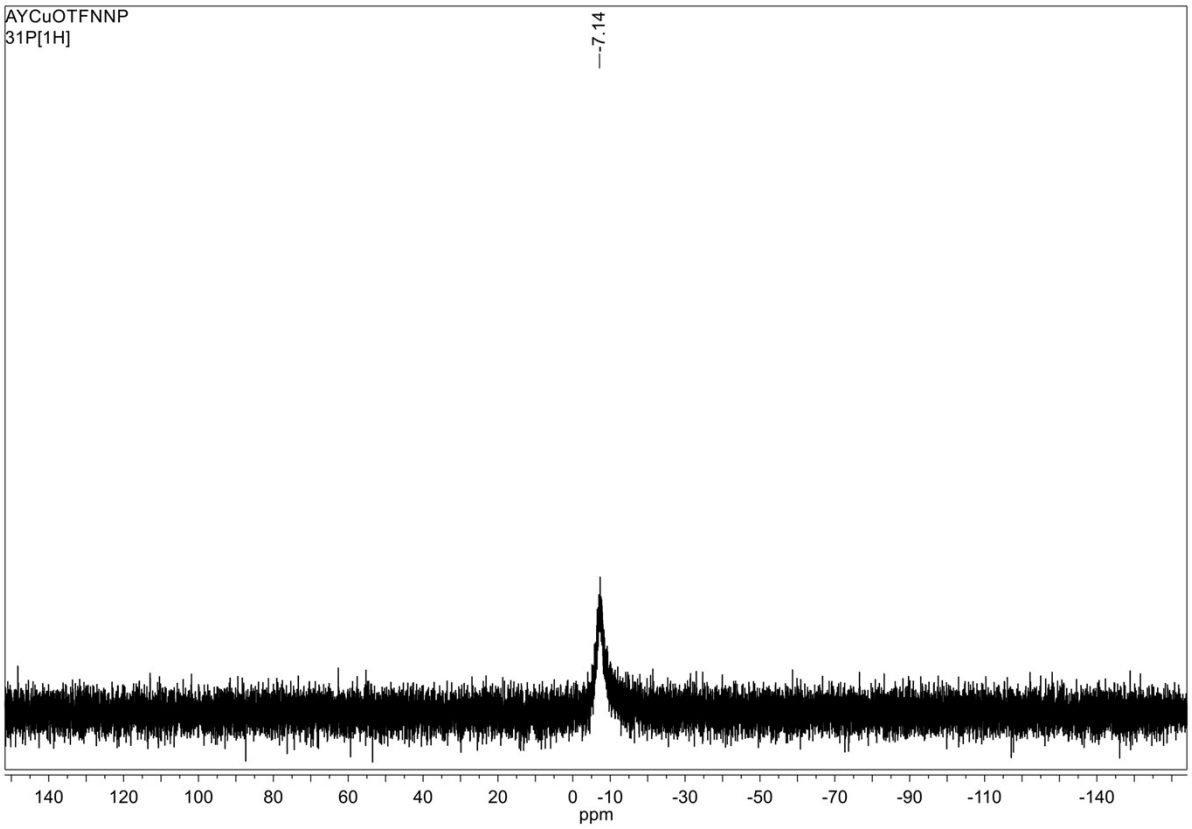

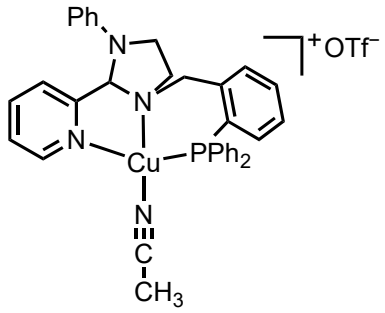

Figure S 80. ^{1}H NMR spectrum of the $[Cu(NNP)(PPh_3)][BF_4]$ in $CDCl_3$ at 298 K.

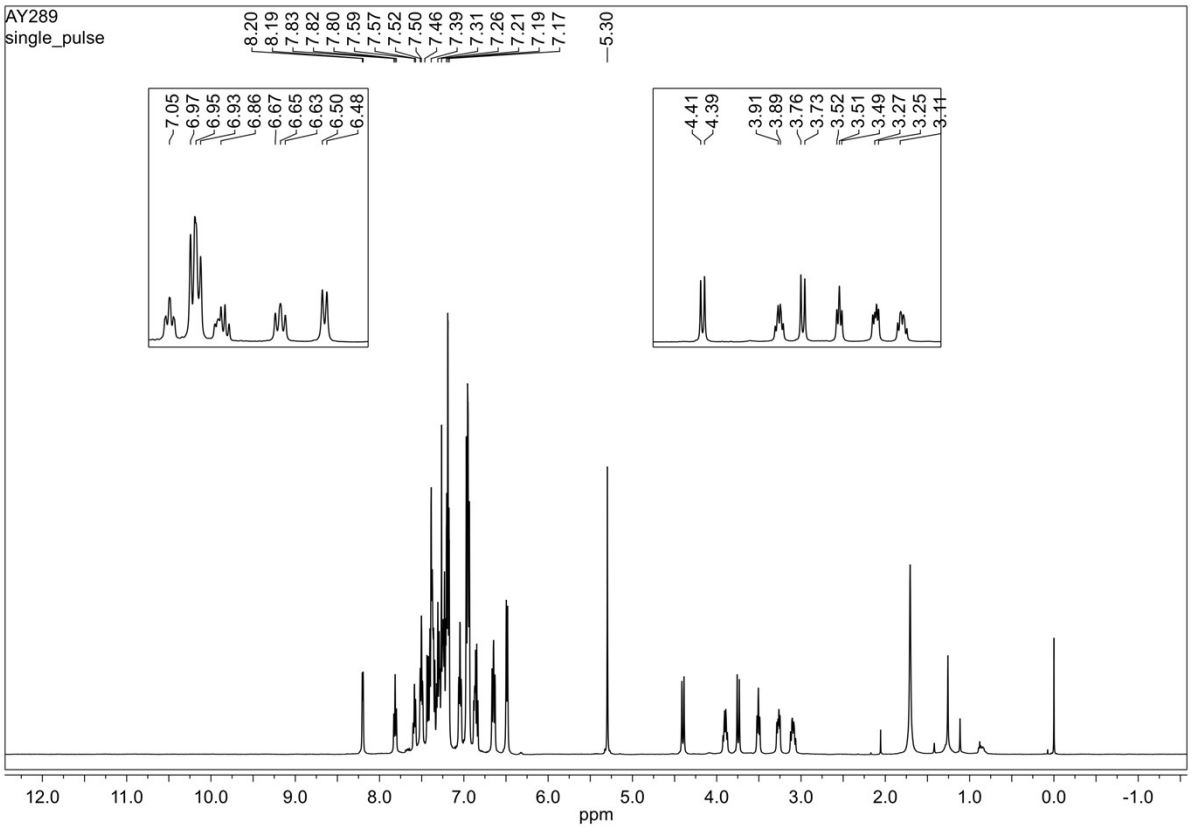

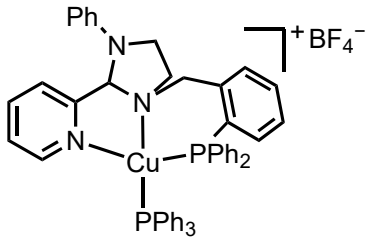

Figure S 81. ^{31}P NMR spectrum of the $[Cu(NNP)(PPh_3)][BF_4]$ in $CDCl_3$ at 298 K.

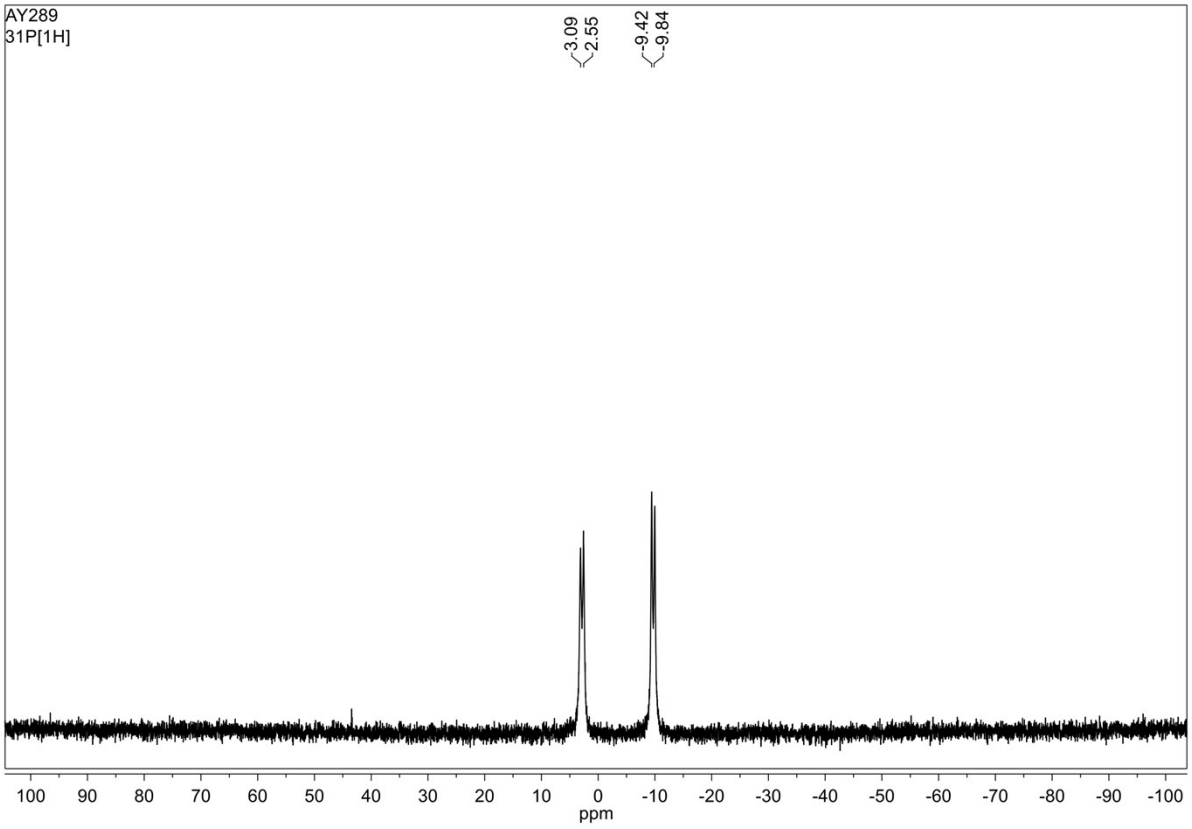

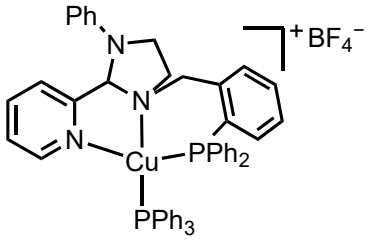

Figure S 82. ESI-MS of $[Cu_2(NNP)_2(\mu\text{-}Cl)Cl_2][CuCl_2]$

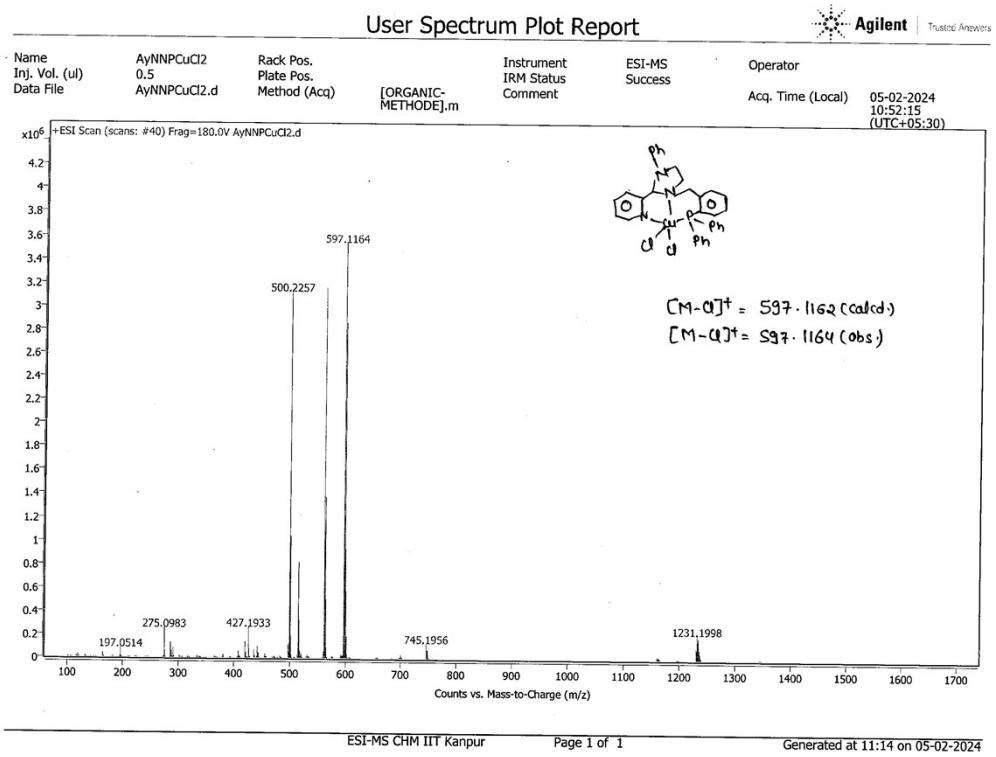

High resolution ESI-MS: *m/z* for $[M-Cl]^+$ = 597.1164 (calcd. 597.1162) = $[CuC_{33}H_{30}N_3PCl]^+$; $[M-2Cl]^+$ = 562.1472 (calcd. 562.1473) = $[CuC_{33}H_{30}N_3P]^+$; *m/z* = 500.2257 (calcd. 500.2256) = $[NNP+H]^+$; *m/z* = 1231.1998 (calcd. 1231.1983 (96.0%)) = $[Cu_2(NNP)_2(\mu\text{-}Cl)Cl_2]^+$.

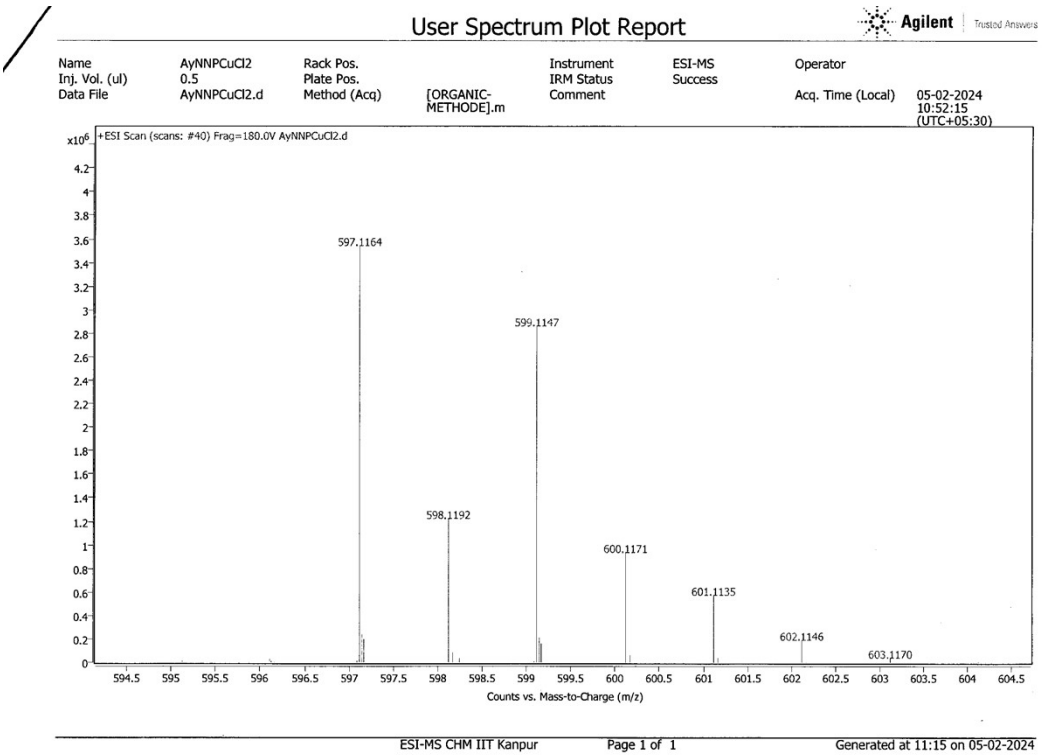

Figure S 83. Simulated ESI-MS of $[Cu_2(NNP)_2(\mu\text{-}Cl)Cl_2][CuCl_2]$,

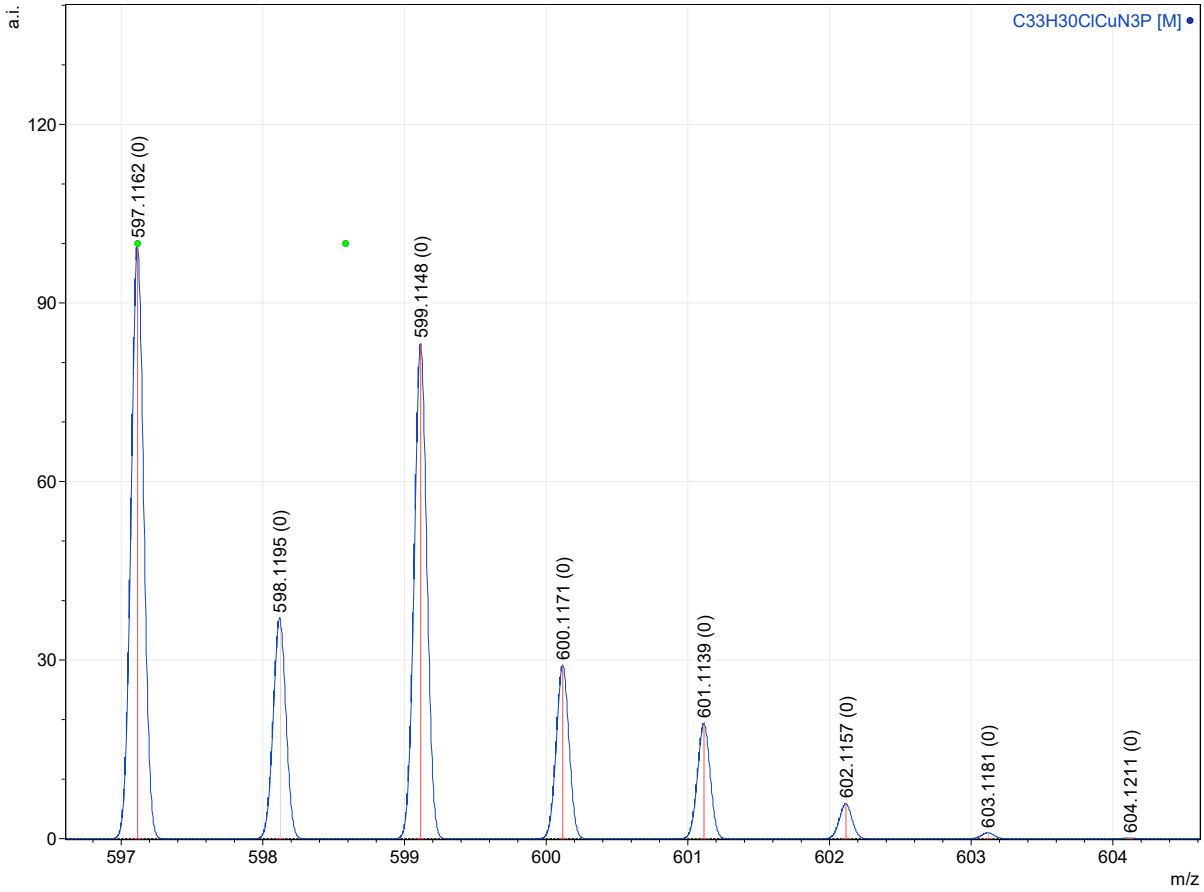

Figure S 84. Reduction of Cu(II) to Cu(I) using ascorbic acid

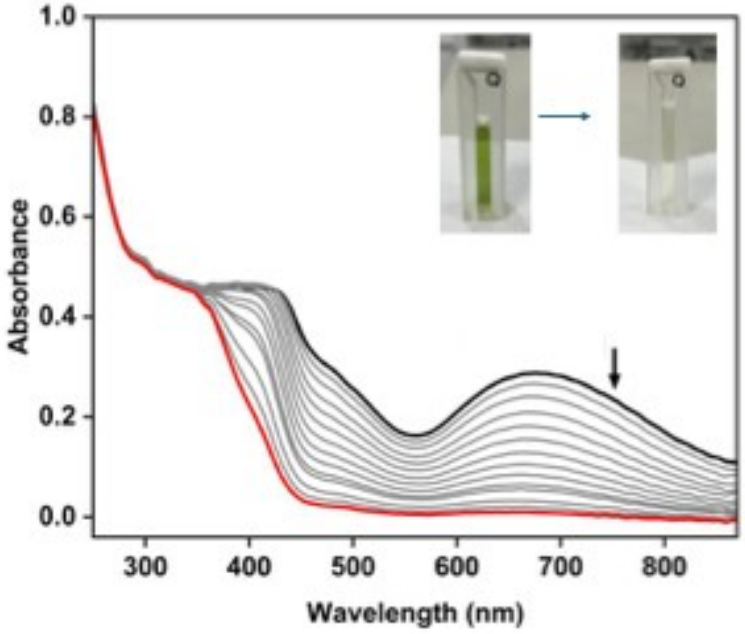

Absorbance spectra of $[Cu_2(NNP)_2(\mu\text{-}Cl)Cl_2][CuCl_2]$ complex (1mM) in CH_3CN in the presence of ascorbic acid (0-2.6 eq) (5mM) in 5% H_2O in CH_3CN.

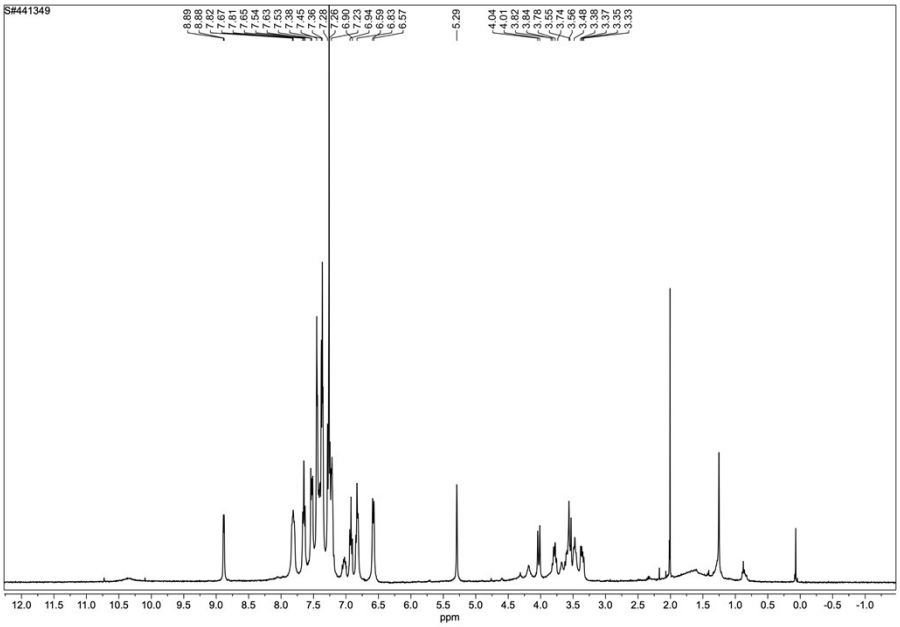

^1H NMR spectrum of the $[Cu_2(NNP)_2(\mu\text{-}Cl)Cl_2][CuCl_2]$ after adding ascorbic acid in $CDCl_3$ at 298 K.

Figure S 85. ^{1}H NMR titration for the transmetallation of Zn(II) by Cu(I) in $CDCl_3$:CD_3CN mixture at 298 K.

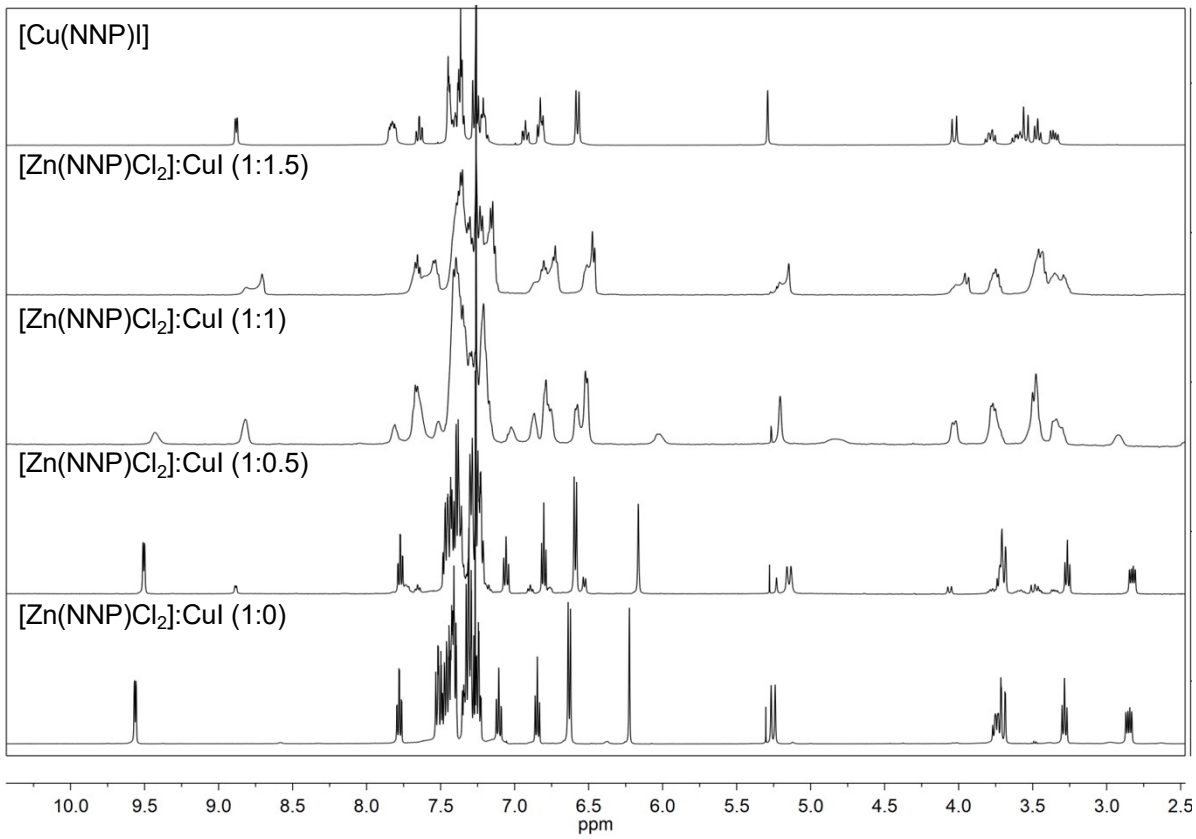

^{1}H NMR titration of [Zn(NNP)Cl_2] after addition of CuI (0-1.5eq) compared with directly prepared [Cu(NNP)I] complex (top).

Figure S 86. ^{31}P NMR titration for the transmetallation of Zn(II) by Cu(I) in $CDCl_3$:CD_3CN mixture at 298 K.

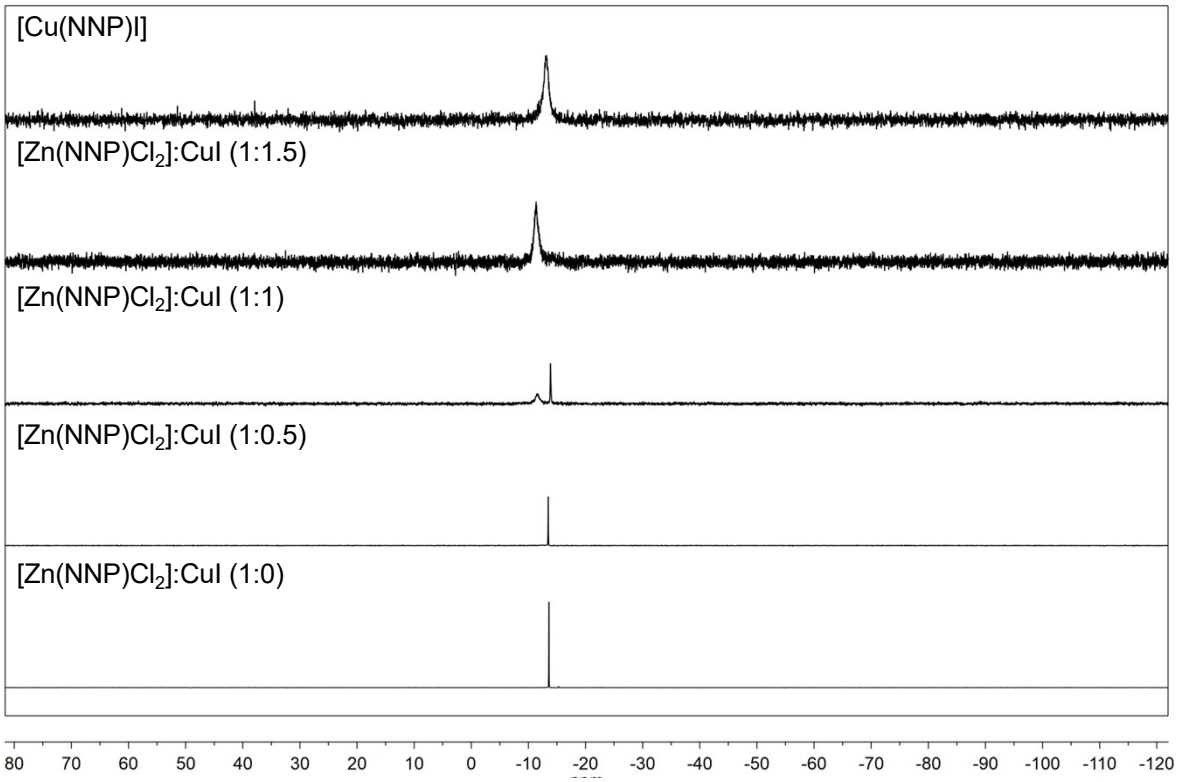

^{31}P NMR titration of [Zn(NNP)Cl_2] after addition of CuI (0-1.5eq) compared with directly prepared [Cu(NNP)I] complex (top).

Figure S 87. ESI-MS for the transmetallation of Zn(II) by Cu(I).

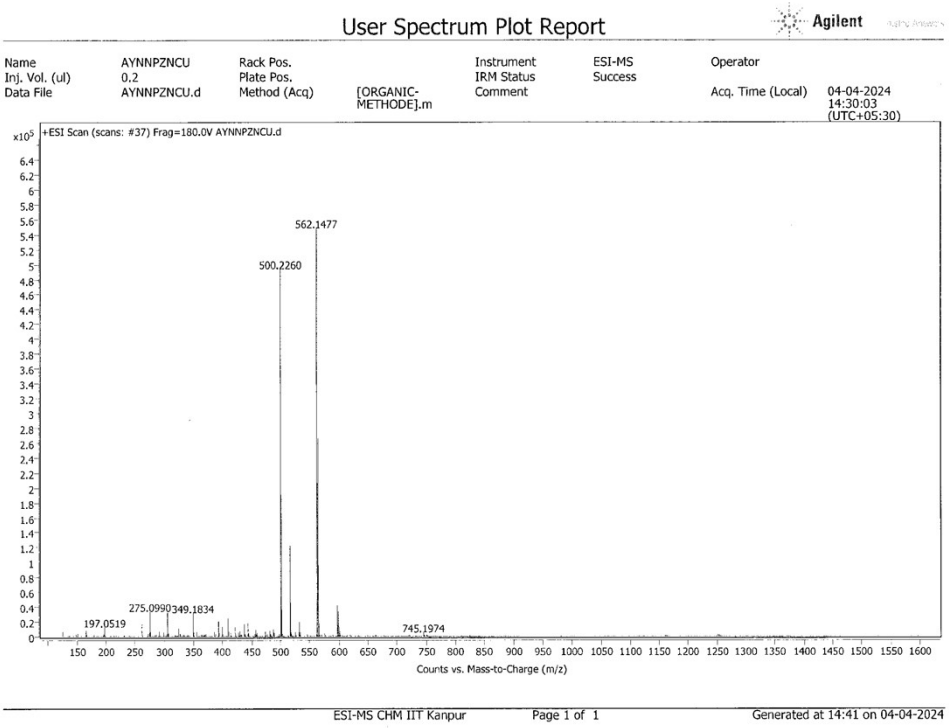

High resolution ESI-MS: *m/z* for $[M-I]^+$ = 562.1477 (calcd. 562.1473) = $[CuC_{33}H_{30}N_3P]^+$.

User Spectrum Plot Report

Agilent

Name	AYNNPZNCU	Rack Pos.		Instrument	ESI-MS	Operator	
Inj. Vol. (ul)	0.2	Plate Pos.		IRM Status	Success		
Data File	AYNNPZNCU.d	Method (Acq)	[ORGANIC-METHODE].m	Comment		Acq. Time (Local)	04-04-2024 14:30:03 (UTC+05:30)

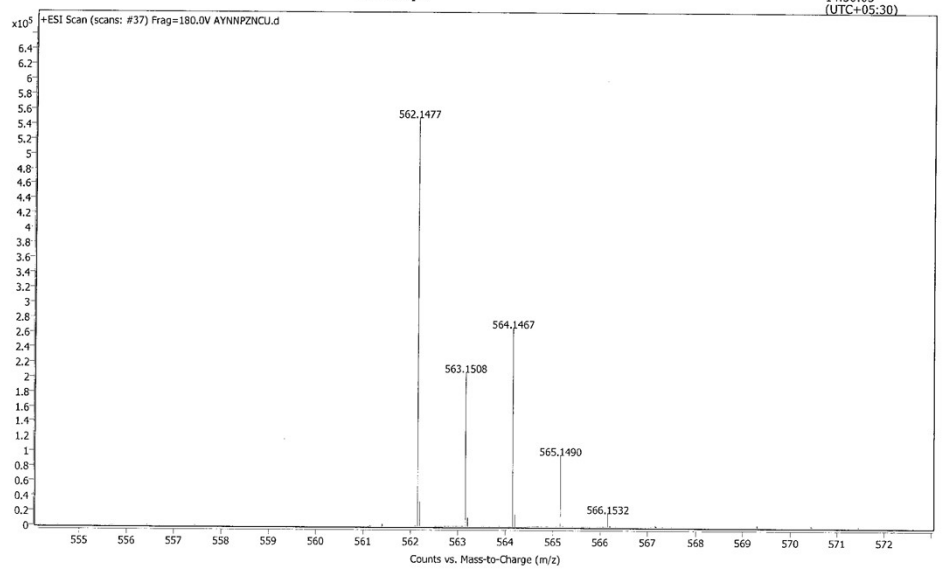

Figure S 88. Cyclic Voltammogram of [Cu(NNP)(CH_3CN)][OTf]

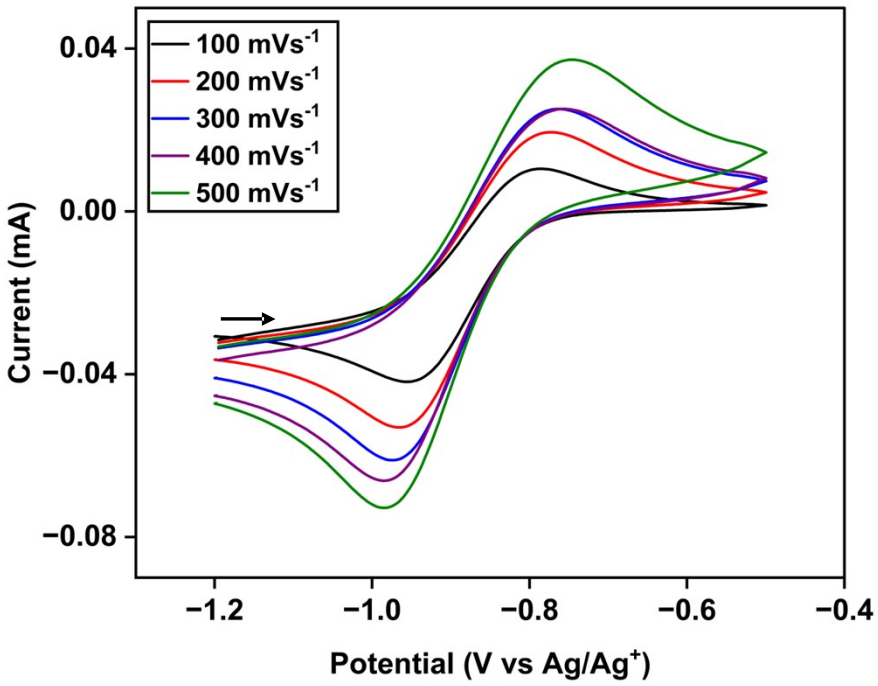

Cyclic Voltammograms of 1mM of [Cu(NNP)(CH_3CN)][OTf] complex at a static glassy Carbon working electrode with Ag/AgCl reference electrode, and a Pt wire auxiliary electrode at 25 °C in CH_3CN solution containing 0.1 M $TBAPF_6$ (supporting electrolyte) at different scan rates under nitrogen atmosphere.

Figure S 89. Cyclic Voltammogram of [Cu(NNP)(CH_3CN)][PF_6]

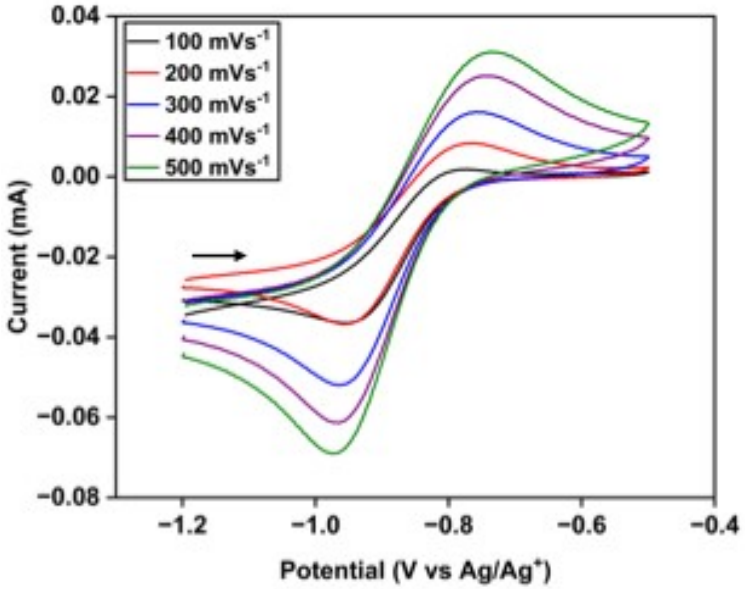

Cyclic Voltammograms of 1mM of [Cu(NNP)(CH_3CN)][PF_6] complex at a static glassy Carbon working electrode with Ag/AgCl reference electrode, and a Pt wire auxiliary electrode at 25 °C in CH_3CN solution containing 0.1 M $TBAPF_6$ (supporting electrolyte) at different scan rates under nitrogen atmosphere.

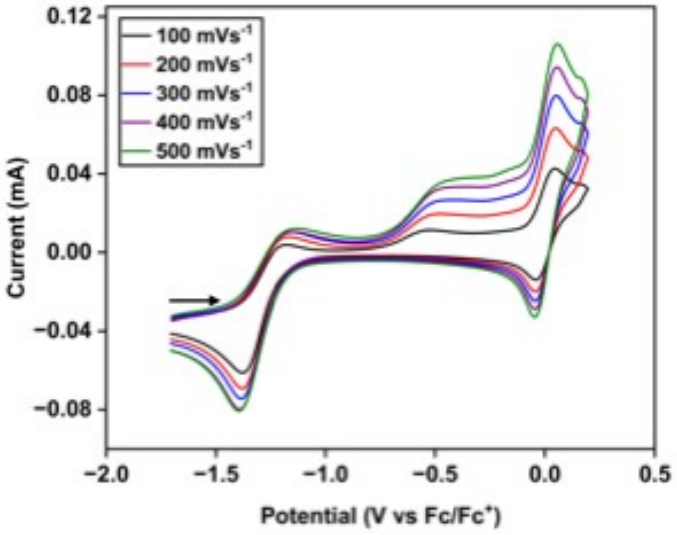

Cyclic Voltammograms of 1mM of [Cu(NNP)(CH_3CN)][PF_6] complex after the addition of 1 mM ferrocene at a static glassy Carbon working electrode with Ag/AgCl reference electrode, and a Pt wire auxiliary electrode at 25 °C in CH_3CN solution containing 0.1 M $TBAPF_6$ (supporting electrolyte) at different scan rates under nitrogen atmosphere.

Figure S 90. Cyclic Voltammogram of [Cu(NNP)I]

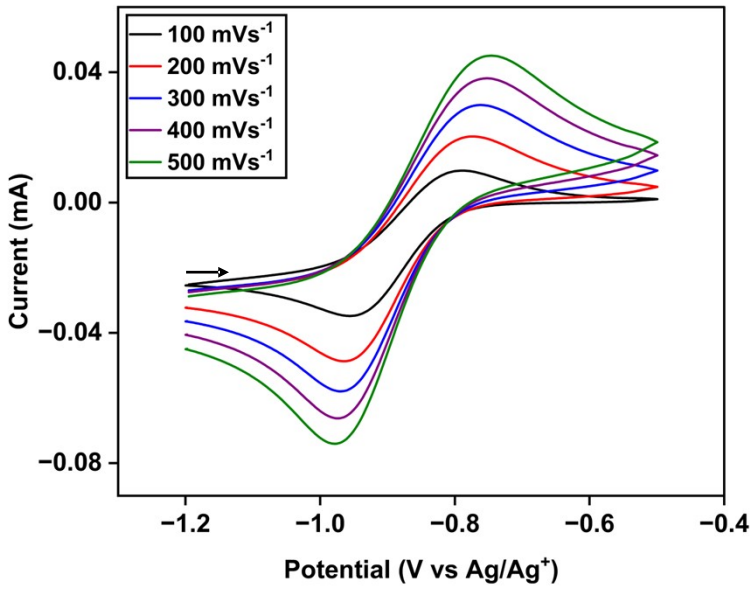

Cyclic Voltammograms of 1mM of [Cu(NNP)I] complex at a static glassy Carbon working electrode with Ag/AgCl reference electrode, and a Pt wire auxiliary electrode at 25 °C in CH_3CN solution containing 0.1 M $TBAPF_6$ (supporting electrolyte) at different scan rates under nitrogen atmosphere.

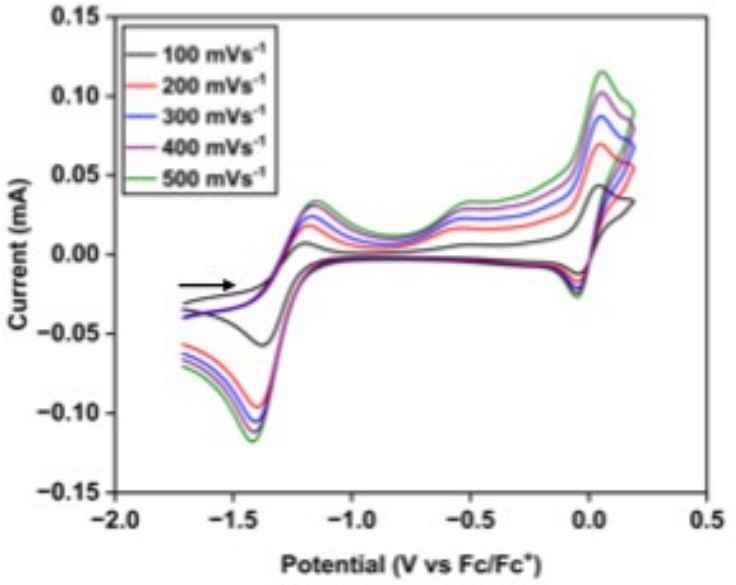

Cyclic Voltammograms of 1mM of [Cu(NNP)I] complex after the addition of 1 mM ferrocene at a static glassy Carbon working electrode with Ag/AgCl reference electrode, and a Pt wire auxiliary electrode at 25 °C in CH_3CN solution containing 0.1 M $TBAPF_6$ (supporting electrolyte) at different scan rates under nitrogen atmosphere.

Figure S 91. Cyclic Voltammogram of [Cu(NNP)Cl]

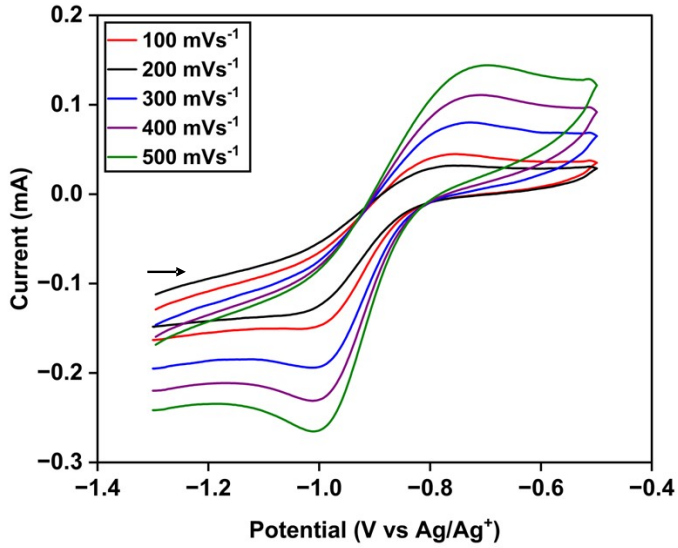

Cyclic Voltammograms of 1mM of [Cu(NNP)Cl] complex at a static glassy Carbon working electrode with Ag/AgCl reference electrode, and a Pt wire auxiliary electrode at 25 °C in CH_3CN solution containing 0.1 M $TBAPF_6$ (supporting electrolyte) at different scan rates under nitrogen atmosphere.

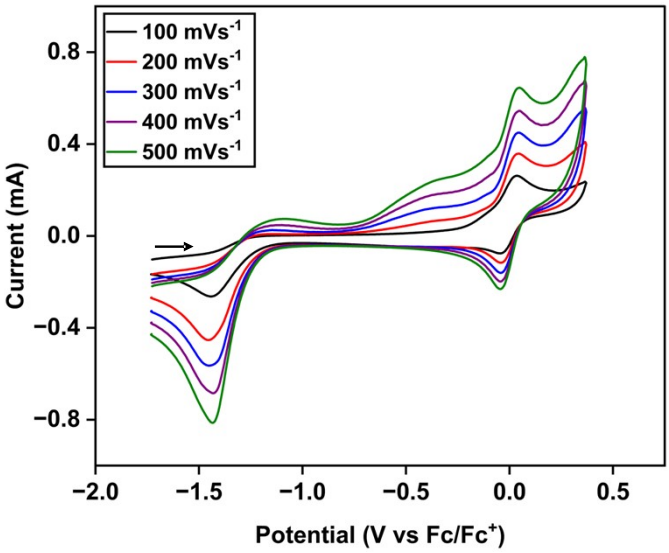

Cyclic Voltammograms of 1mM of [Cu(NNP)Cl] complex after the addition of 1 mM ferrocene at a static glassy Carbon working electrode with Ag/AgCl reference electrode, and a Pt wire auxiliary electrode at 25 °C in CH_3CN solution containing 0.1 M $TBAPF_6$ (supporting electrolyte) at different scan rates under nitrogen atmosphere.

Figure S 92. Cyclic Voltammogram of $[Cu_2(NNP)_2(\mu\text{-}Cl)Cl_2][CuCl_2]$

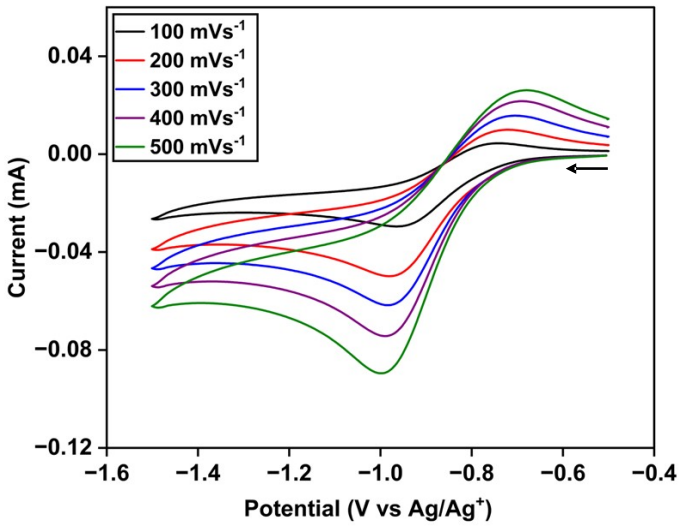

Cyclic Voltammograms of 1mM of $[Cu_2(NNP)_2(\mu\text{-}Cl)Cl_2][CuCl_2]$ complex at a static glassy Carbon working electrode with Ag/AgCl reference electrode, and a Pt wire auxiliary electrode at 25 °C in CH_3CN solution containing 0.1 M $TBAPF_6$ (supporting electrolyte) at different scan rates under nitrogen atmosphere.

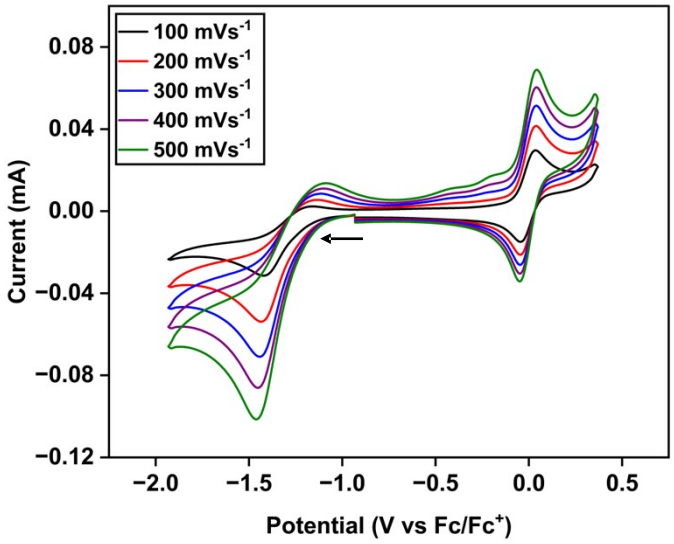

Cyclic Voltammograms of 1mM of $[Cu_2(NNP)_2(\mu\text{-}Cl)Cl_2][CuCl_2]$ complex after the addition of 1 mM ferrocene at a static glassy Carbon working electrode with Ag/AgCl reference electrode, and a Pt wire auxiliary electrode at 25 °C in CH_3CN solution containing 0.1 M $TBAPF_6$ (supporting electrolyte) at different scan rates under nitrogen atmosphere.

Figure S 93. ORTEP of NNP

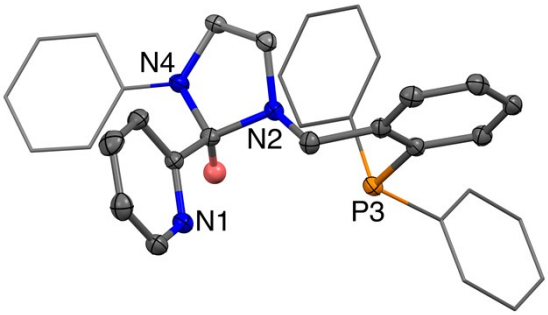

ORTEP of NNP at 50% probability level. Hydrogen (except C*H) and solvents are omitted for clarity.

Figure S 94. ORTEP of [Zn(NNP)Cl_2]

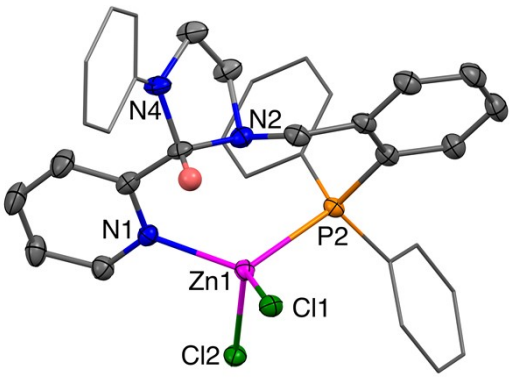

ORTEP of [Zn(NNP)Cl_2] at 50% probability level. Hydrogen (except C*H) and solvents are omitted for clarity. Selected bond distance [Å] and angle [°]: Zn(1)-Cl(1), 2.2685(7); Zn(1)-Cl(2), 2.2572(7); Zn(1)-P(3), 2.4224(7); Zn(1)-N(1), 2.075(2); Cl(2)-Zn(1)-Cl(1), 111.85(3); P(3)-Zn(1)-Cl(1), 101.03(3); P(3)-Zn(1)-Cl(2), 111.86(3); N(1)-Zn(1)-Cl(1), 99.98(6); N(1)-Zn(1)-Cl(2), 109.54(6); N(1)-Zn(1)-P(3), 121.41(6).

Figure S 95. ORTEP of $[Ni(NNP)Cl_2]\cdot CH_3CN$

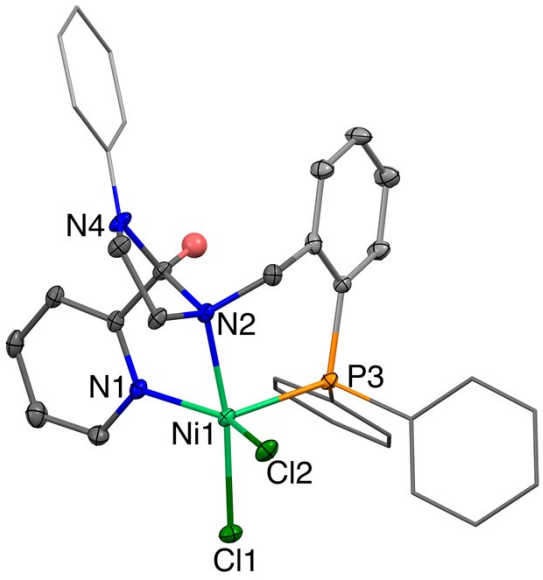

ORTEP of $[Ni(NNP)Cl_2]\cdot CH_3CN$ at 50% probability level. Hydrogen (except C*H) and solvents are omitted for clarity. Selected bond distance [Å] and angle [°]: Ni(1)-Cl(1), 2.3460(9); Ni(1)-Cl(2), 2.2870(9); Ni(1)-P(3), 2.3252(9); Ni(1)-N(1), 2.070(3); Ni(1)-N(2), 2.137(2); Cl(2)-Ni(1)-Cl(1), 93.78(3); P(3)-Ni(1)-Cl(1), 94.11(3); P(3)-Ni(1)-Cl(2), 103.83(3); N(1)-Ni(1)-Cl(1), 93.84(7); N(1)-Ni(1)-Cl(2), 145.50(7); N(1)-Ni(1)-P(3), 109.10(7); N(2)-Ni(1)-Cl(2), 89.69(7); N(2)-Ni(1)-Cl(1), 171.31(7); N(2)-Ni(1)-P(3), 92.78(7); N(2)-Ni(1)-P(3), 78.89(10).

Figure S 96. ORTEP of [Pd(NNP)Cl][Cl]

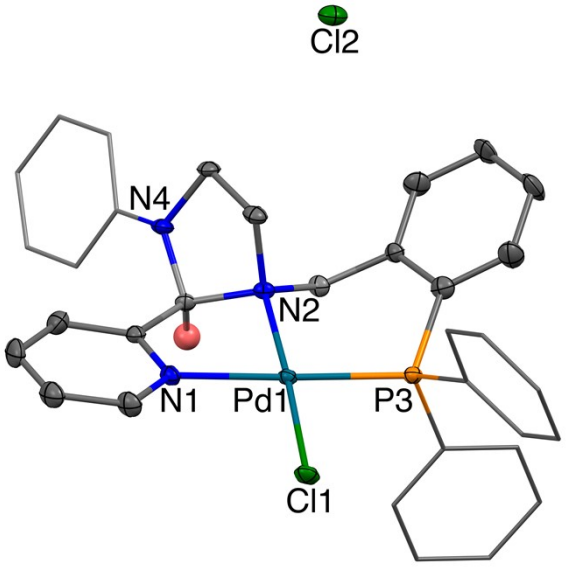

ORTEP of [Pd(NNP)Cl][Cl] at 50% probability level. Hydrogen (except C*H) and solvents are omitted for clarity. Selected bond distance [Å] and angle [°]: Pd(1)-Cl(1), 2.2918(10); Pd(1)-P(3), 2.2401(11); Pd(1)-N(1), 2.080(3); Pd(1)-N(2), 2.060(3); P(3)-Pd(1)-Cl(1), 87.47(4); N(1)-Pd(1)-Cl(1), 96.12(9); N(1)-Pd(1)-P(3), 176.12(9); N(2)-Pd(1)-Cl(1), 176.99(9); N(2)-Pd(1)-P(3), 95.47(9); N(2)-Pd(1)-N(1), 80.92(12).

Figure S 97. ORTEP of [Pd(NNP)(SPhCH$_3$)][PF$_6$]

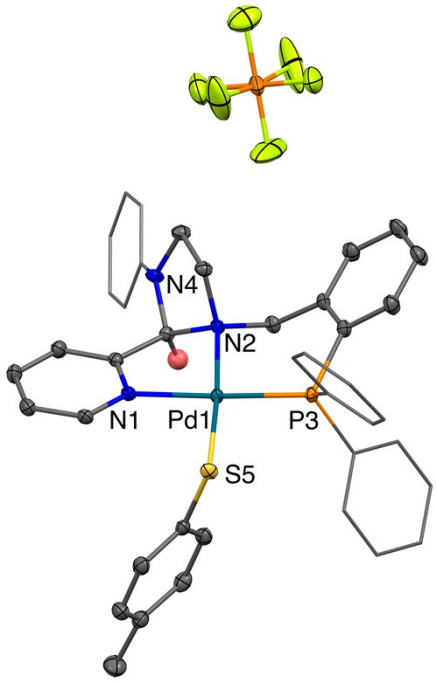

ORTEP of [Pd(NNP)(SPhCH$_3$)][PF$_6$] at 50% probability level. Hydrogen (except C*H) and solvents are omitted for clarity. Selected bond distance [Å] and angle [°]: Pd(1)-N(1), 2.099(2); Pd(1)-P(3), 2.2313(6); Pd(1)-S(5), 2.2899(6); Pd(1)-N(2), 2.1061(19); P(3)-Pd(1)-S(5), 87.45(2); N(1)-Pd(1)-S(5), 95.29(6); N(1)-Pd(1)-P(3), 177.22(6); N(2)-Pd(1)-S(5), 175.78(5); N(2)-Pd(1)-P(3), 96.68(5); N(2)-Pd(1)-N(1), 80.58(7).

Figure S 98. ORTEP of [Ru(NNP)(PPh_3)Cl_2]

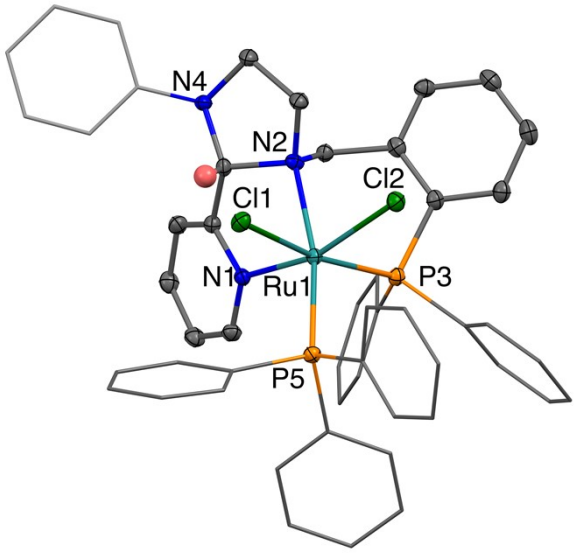

ORTEP of [Ru(NNP)(PPh_3)Cl_2] at 50% probability level. Hydrogen and solvents are omitted for clarity. Selected bond distance [Å] and angle [°]: Ru(1)-Cl(1), 2.4958(8); Ru(1)-Cl(2), 2.4173(8); Ru(1)-P(5), 2.3403(9); Ru(1)-P(3), 2.2924(9); Ru(1)-N(1), 2.133(2); Ru(1)-N(2), 2.221(2); Cl(2)-Ru(1)-Cl(1), 84.79(3); P(5)-Ru(1)-Cl(1), 83.53(3); P(5)-Ru(1)-Cl(2), 100(17); P(3)-Ru(1)-Cl(1), 168.55(3); P(3)-Ru(1)-Cl(2), 83.80(3); P(3)-Ru(1)-P(5), 99.50(3); N(1)-Ru(1)-Cl(1), 97.09(7); N(1)-Ru(1)-Cl(2), 161.51(7); N(1)-Ru(1)-P(5), 98.32(7); N(1)-Ru(1)-P(3), 93.41(7); N(2)-Ru(1)-Cl(1), 85.79(7); N(2)-Ru(1)-Cl(2), 85.39(7); N(2)-Ru(1)-P(5), 167.44(7). N(2)-Ru(1)-P(3), 92.26(7); N(2)-Ru(1)-N(1), 76.43(9).

Figure S 99. ORTEP of *anti-rac*-[Ru(NNP)(H)Cl(CO)]

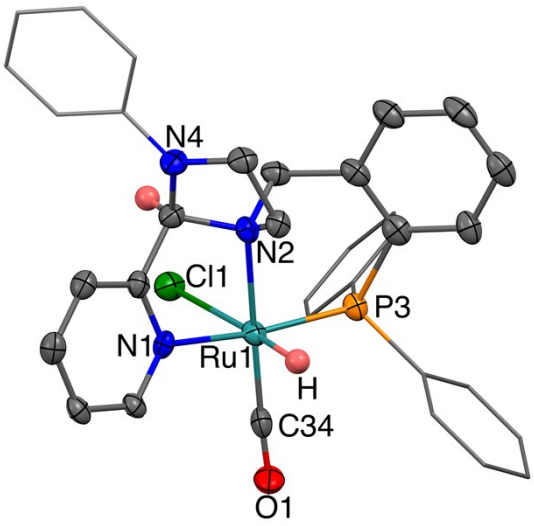

ORTEP of *anti-rac*-[Ru(NNP)(H)Cl(CO)] at 50% probability level. Hydrogen (except Ru-H and C*H) and solvents are omitted for clarity. Selected bond distance [Å] and angle [°]: Ru(1)-P(3), 2.2525(10); Ru(1)-Cl(1), 2.5092(10); Ru(1)-N(1), 2.127(3); Ru(1)-N(2), 2.199(3); Ru(1)-C(34), 1.830(4); Cl(1)-Ru(1)-P(3), 98.87(4); N(1)-Ru(1)-P(3), 170.19(9); N(1)-Ru(1)-Cl(1), 84.80(8); N(2)-Ru(1)-P(3), 93.18(8); N(2)-Ru(1)-Cl(1), 86.51(8); N(2)-Ru(1)-N(1), 77.90(12); C(34)-Ru(1)-P(3), 88.65(12); C(34)-Ru(1)-Cl(1), 98.04(12); C(34)-Ru(1)-N(1), 99.89(14); C(34)-Ru(1)-N(2), 174.78(14).

Figure S 100. ORTEP of *syn-rac*-[Ru(NNP)(H)Cl(CO)]

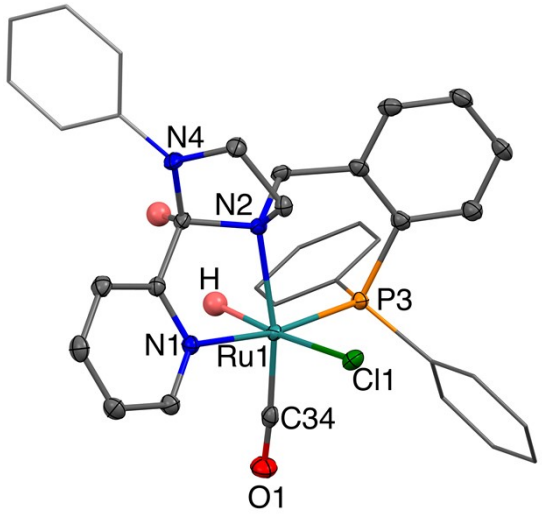

ORTEP of *syn-rac*-[Ru(NNP)(H)Cl(CO)] at 50% probability level. Hydrogen (except Ru-H and C*H) and solvents are omitted for clarity. Selected bond distance [Å] and angle [°]: Ru(1)-P(3), 2.2646(6); Ru(1)-Cl(1), 2.5318(6); Ru(1)-N(1), 2.1142(18); Ru(1)-N(2), 2.2172(18); Ru(1)-C(34), 1.825(2); Cl(1)-Ru(1)-P(3), 95.59(2); N(1)-Ru(1)-P(3), 170.76(5); N(1)-Ru(1)-Cl(1), 87.36(5); N(2)-Ru(1)-P(3), 93.80(5); N(2)-Ru(1)-Cl(1), 90.66(5); N(2)-Ru(1)-N(1), 77.38(7); C(34)-Ru(1)-P(3), 89.60(7); C(34)-Ru(1)-Cl(1), 100.79(7); C(34)-Ru(1)-N(1), 98.47(8); C(34)-Ru(1)-N(2), 167.69(8).

Figure S 101. ORTEP of *anti-rac*-[Ru(NNP)(H)(η^1-BH_4)(CO)]

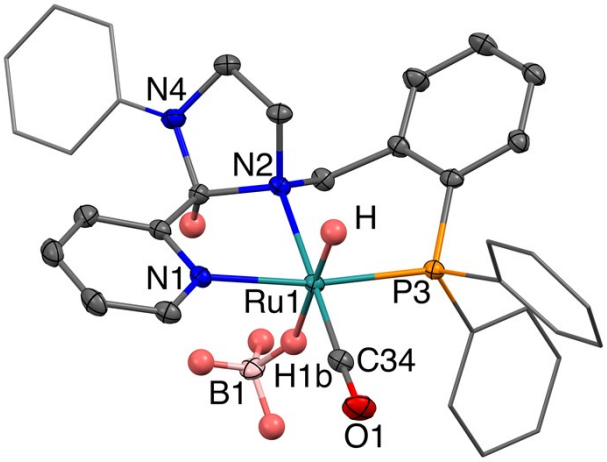

ORTEP of *anti-rac*-[Ru(NNP)(H)(η^1-BH_4)(CO)].at 50% probability level. Hydrogen (except Ru-H, BH_4 and C*H) and solvents are omitted for clarity. Selected bond distance [Å] and angle [°]: Ru(1)-P(3), 2.2567(5); Ru(1)-H, 1.551; Ru(1)-H1b, 1.913; Ru(1)-N(1), 2.1120(16); Ru(1)-N(2), 2.1792(16); Ru(1)-C(34), 1.829(2); N(2)-Ru(1)-P(3), 92.99(4); N(1)-Ru(1)-P(3), 170.27(5); N(2)-Ru(1)-N(1), 78.33(6); C(34)-Ru(1)-P(3), 89.04(7); C(34)-Ru(1)-N(1), 99.28(8); C(34)-Ru(1)-N(2), 175.12(8).

Figure S 102. ORTEP of [Ru(NNP)(CS_2H)$_2$(CO)]

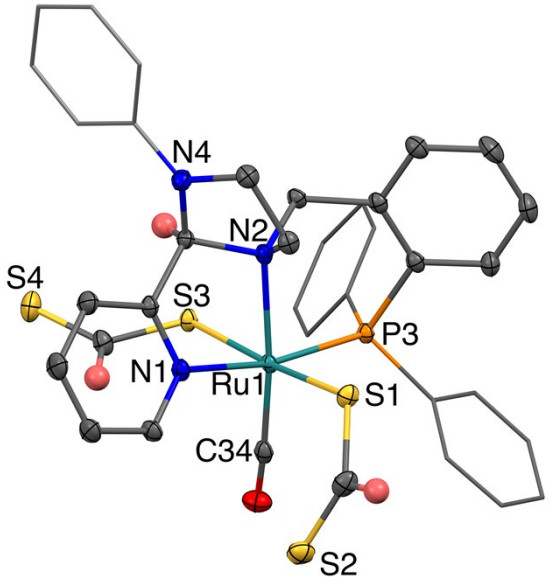

ORTEP of [Ru(NNP)(CS_2H)$_2$(CO)]at 50% probability level. Hydrogen (except CS_2H and C*H) and solvents are omitted for clarity. Selected bond distance [Å] and angle [°]: Ru(1)-P(3), 2.3045(6); Ru(1)-S(3), 2.4042(6); Ru(1)-S(1), 2.3951(7); Ru(1)-N(1), 2.123(2); Ru(1)-N(2), 2.243(2); Ru(1)-C(34), 1.862(3); P(3)-Ru(1)-S(3), 89.98(2); S(1)-Ru(1)-S(3), 174.46(2); S(1)-Ru(1)-P(3), 91.16(2); N(2)-Ru(1)-S(3), 87.58(5); N(2)-Ru(1)-P(3), 92.99(5); N(2)-Ru(1)-S(1), 86.94(5); N(1)-Ru(1)-S(3), 88.45(6); N(1)-Ru(1)-P(3), 168.82(6); N(1)-Ru(1)-S(1), 89.38(6); N(1)-Ru(1)-N(2), 75.88(7); C(34)-Ru(1)-S(3), 86.51(8); C(34)-Ru(1)-P(3), 89.61(7); C(34)-Ru(1)-S(1), 98.92(8); C(34)-Ru(1)-N(1), 101.34(9); C(34)-Ru(1)-N(2), 173.54(9).

Figure S 103. ORTEP of [Cu(NNP)I]

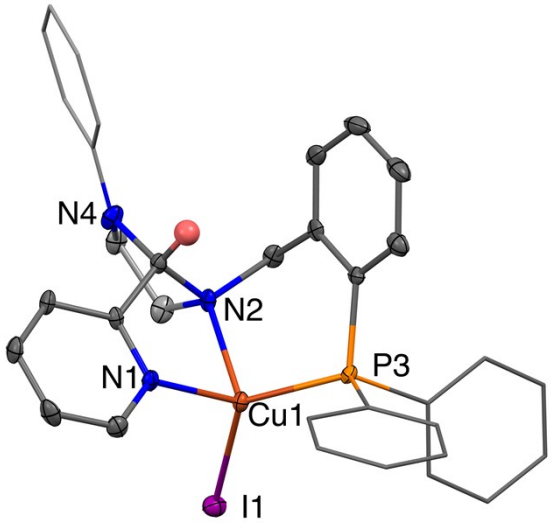

ORTEP of [(NNP)CuI] at 50% probability level. Hydrogens (except C*H) and solvents are omitted for clarity. Selected bond distance [Å] and angle [°]: Cu(1)-I(1), 2.5490(5); Cu(1)-P(3), 2.1800(9); Cu(1)-N(1), 2.072(3); Cu(1)-N(2), 2.160(3); P(3)-Cu(1)-I(1), 123.42(3); N(1)-Cu(1)-I(1), 109.99(8); N(1)-Cu(1)-P(3), 121.02(9); N(2)-Cu(1)-I(1), 110.36(8); N(2)-Cu(1)-P(3), 100.76(8); N(2)-Cu(1)-N(1), 80.79(11).

Figure S 104. ORTEP of [Cu(NNP)(PPh_3)][BF_4]

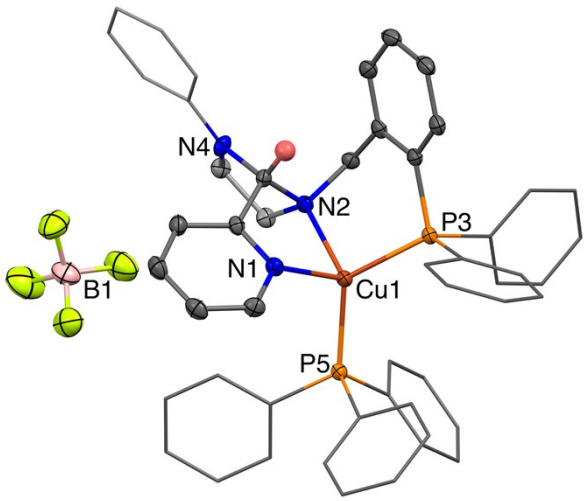

ORTEP of [Cu(NNP)(PPh_3)][BF_4] at 50% probability level. Hydrogens (except C*H) and solvents are omitted for clarity. Selected bond distance [Å] and angle [°]: Cu(1)-P(5), 2.2396(7); Cu(1)-P(3), 2.2489(7); Cu(1)- N(1), 2.103(2); Cu(1)-N(2), 2.1428(19); P(3)-Cu(1)-P(5), 122.62(2); N(1)-Cu(1)-P(5), 105.99(6); N(1)-Cu(1)-P(3), 116.28(6); N(2)-Cu(1)-P(5), 126.82(6); N(2)-Cu(1)-P(3), 97.01(6); N(2)-Cu(1)-N(1), 81.88(7).

Figure S 105. ORTEP of [Cu(NNP)Cl]

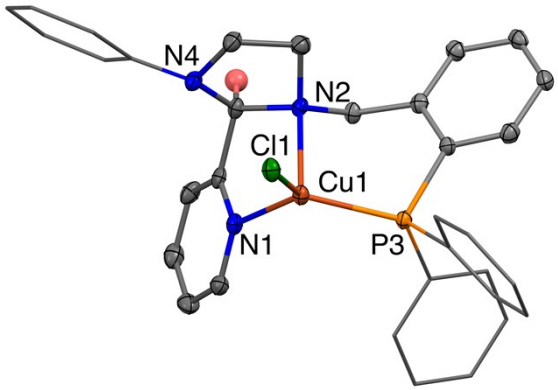

ORTEP of [Cu(NNP)Cl] at 50% probability level. Hydrogens (except C*H) and solvents are omitted for clarity. Selected bond distance [Å] and angle [°]: Cu(1)-Cl(1), 2.2672(7); Cu(1)-P(3), 2.1959(7); Cu(1)-N(1), 2.076(2); Cu(1)-N(2), 2.230(2); P(3)-Cu(1)-Cl(1), 114.49(3); N(1)-Cu(1)-Cl(1), 122.59(6); N(1)-Cu(1)-P(3), 119.67(6); N(2)-Cu(1)-Cl(1), 110.79(6); N(2)-Cu(1)-P(3), 97.76(5); N(2)-Cu(1)-N(1), 79.87(8).

Figure S 106. ORTEP of $[Cu_2(NNP)_2(\mu\text{-}Cl)Cl_2][CuCl_2]$

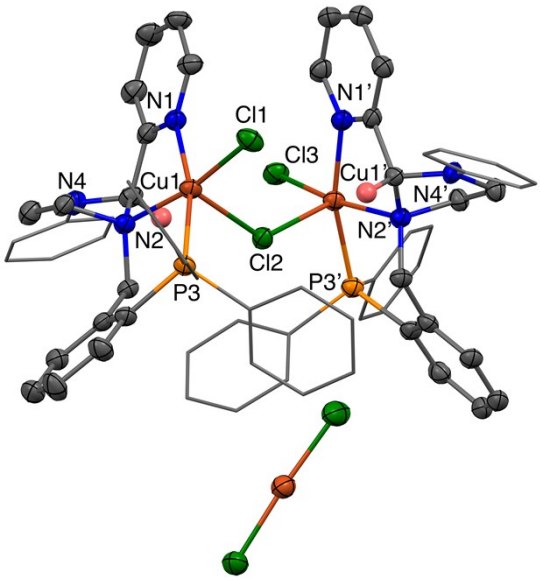

ORTEP of $[Cu_2(NNP)_2(\mu\text{-}Cl)Cl_2][CuCl_2]$ at 50% probability level. Hydrogens (except C*H) and solvents are omitted for clarity. Selected bond distance [Å] and angle [°]: Cu(1)-Cl(1), 2.2655(12); Cu(1)-P(3), 2.3216(12); Cu(1)- N(1), 2.018(3); Cu(1)-N(2), 2.087(4); P(3)-Cu(1)-Cl(1), 90.46(4); P(3)-Cu(1)-Cl(2), 94.43(4); N(1)-Cu(1)-Cl(2), 96.99(11); N(1)-Cu(1)-Cl(1), 94.87(11); N(1)-Cu(1)-P(3), 166.23(11); N(2)-Cu(1)-Cl(2), 88.64(10); N(2)-Cu(1)-Cl(2), 88.64(10); N(2)-Cu(1)-Cl(1), 169.84(10); N(2)-Cu(1)-P(3), 91.88(9); N(2)-Cu(1)-N(1), 80.75(14); Cu(1)-Cl(2)-Cu(1'), 132.27(5).

Identification code	10febc_0m	CCDC2472269
Empirical formula	$C_{33}H_{30}N_3P$	
Formula weight	499.600	
Temperature	273.15 K	
Crystal system	orthorhombic	
Space group	Pbca	
Unit cell dimensions	a = 12.2438(3) Å	α = 90º
	b = 24.9067(7) Å	β = 90º
	c = 35.1266(9) Å	γ = 90º
Volume	10711.9(5) $Å^3$	
Z	16	
Density (calculated)	1.239 g/cm^3	
Absorption coefficient	0.130 mm^{-1}	
F(000)	4227.8	
Crystal size	0.25 × 0.21 × 0.16 mm^3	
Radiation	Mo Kα (λ = 0.71073)	
2Θ range for data collection	5.08 to 56.64	
Index ranges	$-16 \leq h \leq 16$, $-33 \leq k \leq 33$, $-46 \leq l \leq 46$	
Reflections collected	167147	
Independent reflections	13318 [R_{int} = 0.0981, R_{sigma} = 0.0463]	
Completeness of theta = 28.310º	99.8 %	
Absorption correction	Semi-empirical from equivalents	
Max. and min. transmission	0.746 and 0.685	
Refinement method	Full-matrix least-square on F^2	
Data/restraints/parameters	13318/0/667	
Goodness-of-fit on F^2	1.107	
Final R indexes [I>=2σ (I)]	R_1 = 0.0472, wR_2 = 0.0949	
Final R indexes [all data]	R_1 = 0.0835, wR_2 = 0.1208	
Largest diff. peak/hole	0.51/-0.55 e $Å^{-3}$	

Table S 1. Crystal data and structure refinement for 10febc_0m (NNP)

Identification code	27octf	CCDC2472270
Empirical formula	$C_{33}H_{30}Cl_2N_3PZn$	
Formula weight	635.90	
Temperature	273.15 K	
Crystal system	monoclinic	
Space group	$P2_1/n$	
Unit cell dimensions	a =10.6154(9) Å	α = 90º
	b =17.3832(15) Å	β = 90.263(3)º
	c =15.9872(16) Å	γ = 90º
Volume	2950.1(5) $Å^3$	
Z	4	
Density (calculated)	1.432 g/cm^3	
Absorption coefficient	1.096 mm^{-1}	
F(000)	1315.5	
Crystal size	0.25 × 0.21 × 0.16 mm^3	
Radiation	Mo Kα (λ = 0.71073)	
2Θ range for data collection	4.5 to 56.62º	
Index ranges	$-14 \leq h \leq 14$, $-23 \leq k \leq 23$, $-21 \leq l \leq 21$	
Reflections collected	47036	
Independent reflections	7343 [R_{int} = 0.0639, R_{sigma} = 0.0403]	
Completeness of theta = 28.310º	99.9 %	
Absorption correction	Semi-empirical from equivalents	
Max. and min. transmission	0.746 and 0.701	
Refinement method	Full-matrix least-square on F^2	
Data/restraints/parameters	7343/0/361	
Goodness-of-fit on F^2	1.070	
Final R indexes [I>=2σ (I)]	R_1 = 0.0434, wR_2 = 0.0946	
Final R indexes [all data]	R_1 = 0.0594, wR_2 = 0.1074	
Largest diff. peak/hole	2.32/-0.92 e $Å^{-3}$	

Table S 2. Crystal data and structure refinement for 27octf [Zn(NNP)Cl_2]

Identification code	26maya_0m	CCDC2472271
Empirical formula	$C_{35}H_{33}Cl_2N_4NiP$	
Formula weight	670.251	
Temperature	273.15	
Crystal system	triclinic	
Space group	P-1	
Unit cell dimensions	a = 9.3630(19)Å	α = 77.395(5)º
	b = 11.082(2)Å	β = 88.124(5)º
	c = 17.163(3)Å	γ = 66.360(6)º
Volume/Å^3	1589.1(5)	
Z	2	
Density (calculated)	1.401 g/cm^3	
Absorption coefficient	0.860 mm^{-1}	
F(000)	697.9	
Crystal size	0.26 × 0.25 × 0.21 mm^3	
Radiation	Mo Kα (λ = 0.71073)	
2Θ range for data collection /°	5.22 to 56.8	
Index ranges	-12 ≤ h ≤ 12, -14 ≤ k ≤ 14, -22 ≤ l ≤ 22	
Reflections collected	23988	
Independent reflections	7863 [R_{int} = 0.0624, R_{sigma} = 0.0663]	
Completeness of theta = 28.310º	98.5%	
Absorption correction	Semi-empirical from equivalents	
Max. and min. transmission	0.746 and 0.674	
Refinement method	Full-matrix least-square on F^2	
Data/restraints/parameters	7863/0/520	
Goodness-of-fit on F^2	1.083	
Final R indexes [I>=2σ (I)]	R_1 = 0.0546, wR_2 = 0.1104	
Final R indexes [all data]	R_1 = 0.0721, wR_2 = 0.1211	
Largest diff. peak/hole	1.47/-0.73e Å^{-3}	

Table S 3. Crystal data and structure refinement for 26maya_0m [Ni(NNP)Cl_2]·CH_3CN

Table S 4. Crystal data and structure refinement for 3febd [Pd(NNP)Cl][Cl].

Identification code	3febd	CCDC2472560
Empirical formula	$C_{37}H_{40}Cl_2N_3OPPd$	
Formula weight	787.074	
Temperature	273.15 K	
Crystal system	monoclinic	
Space group	$P2_1/c$	
Unit cell dimensions	a = 19.162(4) Å	α = 90º
	b = 9.563(2) Å	β =101.933(7)º
	c = 20.013(5) Å	γ = 90 º
Volume	3588.2(15) $Å^3$	
Z	4	
Density (calculated)	1.457 g/cm^3	
Absorption coefficient	0.751 mm^{-1}	
F(000)	1622.4	
Crystal size	0.25 × 0.21 × 0.16 mm^3	
Radiation	Mo Kα (λ = 0.71073)	
2Θ range for data collection	5.04 to 57.08	
Index ranges	-25 ≤ h ≤ 25, -12 ≤ k ≤ 12, -26 ≤ l ≤ 26	
Reflections collected	70299	
Independent reflections	9045 [R_{int} = 0.1196, R_{sigma} = 0.0667]	
Completeness of theta = 28.310º	99.0 %	
Absorption correction	Semi-empirical from equivalents	
Max. and min. transmission	0.746 and 0.578	
Refinement method	Full-matrix least-square on F^2	
Data/restraints/parameters	9045/0/433	
Goodness-of-fit on F^2	1.046	
Final R indexes [I>=2σ (I)]	R_1 = 0.0591, wR_2 = 0.1131	
Final R indexes [all data]	R_1 = 0.0773, wR_2 = 0.1203	
Largest diff. peak/hole	1.05/-2.01 e $Å^{-3}$	

Table S 5. Crystal data and structure refinement for 1augb_0m [Pd(NNP)($SPhCH_3$)][PF_6].

Identification code	1augb_0m	CCDC2472273
Empirical formula	$C_{42}H_{41}Cl_4F_6N_3P_2PdS$	
Formula weight	1044.043	
Temperature	273.15 K	
Crystal system	triclinic	
Space group	P-1	
Unit cell dimensions	a = 9.4411(3) Å	α = 83.854(1) º
	b = 13.4278(4) Å	β = 76.261(1) º
	c = 17.6952(5) Å	γ = 78.513(1) º
Volume	2131.23(11) $Å^3$	
Z	2	
Density (calculated)	1.627 g/cm^3	
Absorption coefficient	0.873 mm^{-1}	
F(000)	1056.5	
Crystal size	0.21 × 0.19 × 0.17 mm^3	
Radiation	Mo Kα (λ = 0.71073)	
2Θ range for data collection	5.54 to 56.72	
Index ranges	-12 ≤ h ≤ 12, -17 ≤ k ≤ 17, -23 ≤ l ≤ 23	
Reflections collected	45301	
Independent reflections	10628 [R_{int} = 0.0383, R_{sigma} = 0.0344]	
Completeness of theta = 28.310º	99.8%	
Absorption correction	Semi-empirical from equivalents	
Max. and min. transmission	0.746 and 0.669	
Refinement method	Full-matrix least-square on F^2	
Data/restraints/parameters	10628/0/506	
Goodness-of-fit on F^2	1.045	
Final R indexes [I>=2σ (I)]	R_1 = 0.0374, wR_2 = 0.0851	
Final R indexes [all data]	R_1 = 0.0447, wR_2 = 0.0906	
Largest diff. peak/hole	1.92/-1.24 e $Å^{-3}$	

Identification code	23dece_0m	CCDC2472272
Empirical formula	$C_{56}H_{56}Cl_5N_3OP_2Ru$	
Formula weight	1127.363	
Temperature	273.15 K	
Crystal system	monoclinic	
Space group	$P2_1/n$	
Unit cell dimensions	a = 19.123(4) Å	α = 90º
	b = 13.942(3) Å	β = 109.988(6)º
	c = 20.518(4) Å	γ = 90º
Volume	5140.7(16) $Å^3$	
Z	4	
Density (calculated)	1.457 g/cm^3	
Absorption coefficient	0.671 mm^{-1}	
F(000)	2319.8	
Crystal size	0.25 × 0.21 × 0.16 mm^3	
Radiation	Mo Kα (λ = 0.71073)	
2Θ range for data collection	5 to 56.6º	
Index ranges	$-25 \leq h \leq 25$, $-18 \leq k \leq 18$, $-27 \leq l \leq 27$	
Reflections collected	81526	
Independent reflections	12731 [R_{int} = 0.0885, R_{sigma} = 0.0572]	
Completeness of theta = 28.310º	99.6 %	
Absorption correction	Semi-empirical from equivalents	
Max. and min. transmission	0.746 and 0.676	
Refinement method	Full-matrix least-square on F^2	
Data/restraints/parameters	12731/0/615	
Goodness-of-fit on F^2	1.118	
Final R indexes [I>=2σ (I)]	R_1 = 0.0421, wR_2 = 0.0855	
Final R indexes [all data]	R_1 = 0.0725, wR_2 = 0.1071	
Largest diff. peak/hole	1.25/-1.07 e $Å^{-3}$	

Table S 6. Crystal data and structure refinement for 23dece_0m [$Ru(NNP)(PPh_3)Cl_2$].

Table S 7. Crystal data and structure refinement for 12mayd_0m *anti-rac*-[Ru(NNP)(H)Cl(CO)].

Identification code	12mayd_0m	CCDC2472462
Empirical formula	$C_{34}H_{31}ClN_3OPRu$	
Formula weight	506.809	
Temperature	273.15 K	
Crystal system	triclinic	
Space group	P-1	
Unit cell dimensions	a = 10.0277(14) Å	α =113.653(3)º
	b = 14.344(2) Å	β = 96.348(3)º
	c = 14.788(2) Å	γ = 108.767(3)º
Volume	1773.0(4) $Å^3$	
Z	2	
Density (calculated)	0.949 g/cm^3	
Absorption coefficient	0.319 mm^{-1}	
F(000)	531.3	
Crystal size	0.25 × 0.21 × 0.16 mm^3	
Radiation	Mo Kα (λ = 0.71073)	
2Θ range for data collection	5.58 to 56.68	
Index ranges	-13 ≤ h ≤ 13, -19 ≤ k ≤ 19, -19 ≤ l ≤ 19	
Reflections collected	32660	
Independent reflections	8826 [R_{int} = 0.0566, R_{sigma} = 0.0547]	
Completeness of theta = 28.310º	99.5%	
Absorption correction	Semi-empirical from equivalents	
Max. and min. transmission	0.746 and 0.621	
Refinement method	Full-matrix least-square on F^2	
Data/restraints/parameters	8826/0/374	
Goodness-of-fit on F^2	1.083	
Final R indexes [I>=2σ (I)]	R_1 = 0.0543, wR_2 = 0.1383	
Final R indexes [all data]	R_1 = 0.0753, wR_2 = 0.1574	
Largest diff. peak/hole	1.79/-1.22 e $Å^{-3}$	

Table S 8 Crystal data and structure refinement for 5jula_O_0m *syn-rac*-[Ru(NNP)(H)Cl(CO)].

Identification code	5jula_O_0m	CCDC2472461
Empirical formula	$C_{35}H_{33}Cl_3N_3OPRu$	
Formula weight	751.869	
Temperature	296.15	
Crystal system	triclinic	
Space group	P-1	
Unit cell dimensions	a = 11.7616(6) Å	α = 89.683(2)º
	b = 11.7873(5) Å	β = 85.783(2) º
	c = 12.0837(6) Å	γ = 78.997(2) º
Volume	1639.94(14) $Å^3$	
Z	2	
Density (calculated)	1.523 g/cm^3	
Absorption coefficient	0.805 mm^{-1}	
F(000)	764.9	
Crystal size	0.25 × 0.21 × 0.16 mm^3	
Radiation	Mo Kα (λ = 0.71073)	
2Θ range for data collection	4.48 to 56.64	
Index ranges	-13 ≤ h ≤ 15, -15 ≤ k ≤ 15, -16 ≤ l ≤ 16	
Reflections collected	28382	
Independent reflections	8145 [R_{int} = 0.0446, R_{sigma} = 0.0442]	
Completeness of theta = 28.310º	99.7	
Absorption correction	Semi-empirical from equivalents	
Max. and min. transmission	0.746 and 0.673	
Refinement method	Full-matrix least-square on F^2	
Data/restraints/parameters	8145/0/408	
Goodness-of-fit on F^2	1.030	
Final R indexes [I>=2σ (I)]	R_1 = 0.0331, wR_2 = 0.0810	
Final R indexes [all data]	R_1 = 0.0407, wR_2 = 0.0847	
Largest diff. peak/hole	1.17/-1.22 e $Å^{-3}$	

Table S 9. Crystal data and structure refinement for 31augb_a *anti-rac*-[Ru(NNP)(H)(η^1-BH_4)(CO)].

Identification code	31augb_a	CCDC2472463
Empirical formula	$C_{34}H_{35}BN_3OPRu$	
Formula weight	647.722	
Temperature	273.15	
Crystal system	monoclinic	
Space group	$P2_1/c$	
Unit cell dimensions	a = 9.8128(4)Å	α = 90 º
	b = 17.7134(8)Å	β = 101.136(1) º
	c = 17.5485(8)Å	γ = 90 º
Volume	2992.8(2) $Å^3$	
Z	4	
Density (calculated)	1.438 g/cm^3	
Absorption coefficient	0.611 mm^{-1}	
F(000)	1332.1	
Crystal size	0.21 × 0.18 × 0.16 mm^3	
Radiation	Mo Kα (λ = 0.71073)	
2Θ range for data collection	4.74 to 56.7	
Index ranges	-13 ≤ h ≤ 13, -23 ≤ k ≤ 23, -23 ≤ l ≤ 23	
Reflections collected	46991	
Independent reflections	7466 [R_{int} = 0.0470, R_{sigma} = 0.0304]	
Completeness of theta = 28.310º	99.9	
Absorption correction	Semi-empirical from equivalents	
Max. and min. transmission	0.746 and 0.712	
Refinement method	Full-matrix least-square on F^2	
Data/restraints/parameters	7466/0/390	
Goodness-of-fit on F^2	1.076	
Final R indexes [I>=2σ (I)]	R_1 = 0.0287, wR_2 = 0.0651	
Final R indexes [all data]	R_1 = 0.0365, wR_2 = 0.0723	
Largest diff. peak/hole	0.63/-0.65 e $Å^{-3}$	

Identification code	9marb_0m	CCDC2472464
Empirical formula	$C_{38}H_{36}Cl_4N_3OPRuS_4$	
Formula weight	952.842	
Temperature	273.15	
Crystal system	triclinic	
Space group	P-1	
Unit cell dimensions	a = 10.3188(12) Å	α = 100.491(3)º
	b = 12.7542(15) Å	β = 97.584(3) º
	c = 17.1219(19) Å	γ = 112.179(3)º
Volume	2001.3(4) $Å^3$	
Z	2	
Density (calculated)	1.581 g/cm^3	
Absorption coefficient	0.944 mm^{-1}	
F(000)	968.3	
Crystal size	0.26 × 0.21 × 0.18 mm^3	
Radiation	Mo Kα (λ = 0.71073)	
2Θ range for data collection	5.32 to 56.9	
Index ranges	-13 ≤ h ≤ 13, -17 ≤ k ≤ 17, -22 ≤ l ≤ 22	
Reflections collected	43076	
Independent reflections	10039 [R_{int} = 0.0409, R_{sigma} = 0.0329]	
Completeness of theta = 28.310º	99.4	
Absorption correction	Semi-empirical from equivalents	
Max. and min. transmission	0.746 and 0.656	
Refinement method	Full-matrix least-square on F^2	
Data/restraints/parameters	10039/0/477	
Goodness-of-fit on F^2	1.052	
Final R indexes [I>=2σ (I)]	R_1 = 0.0351, wR_2 = 0.0891	
Final R indexes [all data]	R_1 = 0.0411, wR_2 = 0.0950	
Largest diff. peak/hole	2.48/-1.62 e $Å^{-3}$	

Table S 10. Crystal data and structure refinement for 9marb_0m [Ru(NNP)$(CS_2H)_2$(CO)].

Table S 11. Crystal data and structure refinement for 25mayb [Cu(NNP)I].

Identification code	25mayb	CCDC2472465
Empirical formula	$C_{33}H_{30}CuIN_3P$	
Formula weight	690.050	
Temperature	273.15 K	
Crystal system	orthorhombic	
Space group	$Pna2_1$	
Unit cell dimensions	a = 19.6143(9) Å	α = 90º
	b = 15.1465(7) Å	β = 90º
	c = 10.1231(5) Å	γ = 90º
Volume	3007.5(3) $Å^3$	
Z	4	
Density (calculated)	1.524 g/cm^3	
Absorption coefficient	1.832 mm^{-1}	
F(000)	1384.9	
Crystal size	0.25 × 0.21 × 0.18 mm^3	
Radiation	Mo Kα (λ = 0.71073)	
2Θ range for data collection	4.94 to 56.68	
Index ranges	$-26 \leq h \leq 26$, $-20 \leq k \leq 20$, $-13 \leq l \leq 13$	
Reflections collected	44685	
Independent reflections	7505 [R_{int} = 0.0544, R_{sigma} = 0.0367]	
Completeness of theta = 28.310º	1.89/1.00	
Absorption correction	Semi-empirical from equivalents	
Max. and min. transmission	0.746 and 0.502	
Refinement method	Full-matrix least-square on F^2	
Data/restraints/parameters	7505/1/352	
Goodness-of-fit on F^2	1.042	
Final R indexes [I>=2σ (I)]	R_1 = 0.0313, wR_2 = 0.0657	
Final R indexes [all data]	R_1 = 0.0333, wR_2 = 0.0667	
Largest diff. peak/hole	0.59/-0.88 e $Å^{-3}$	
Flack parameter	-0.460(7)	

Table S 12. Crystal data and structure refinement for 13junb [(NNP)Cu(PPh_3)][BF_4].

Identification code	13junb	CCDC2472467
Empirical formula	$C_{102}H_{90}B_2Cu_2F_8N_6P_4$	
Formula weight	2164.242	
Temperature	273.15 K	
Crystal system	triclinic	
Space group	P-1	
Unit cell dimensions	a = 13.501(1) Å	α = 101.962(3)º
	b = 15.6110(11) Å	β = 103.969(2)º
	c = 25.256(2) Å	γ = 98.689(2)º
Volume	4938.9(7) $Å^3$	
Z	2	
Density (calculated)	1.455 g/cm^3	
Absorption coefficient	0.779 mm^{-1}	
F(000)	2229.8	
Crystal size	0.21 × 0.18 × 0.16 mm^3	
Radiation	Mo Kα (λ = 0.71073)	
2Θ range for data collection	3.8 to 56.64	
Index ranges	$-18 \leq h \leq 18$, $-20 \leq k \leq 20$, $-33 \leq l \leq 33$	
Reflections collected	107944	
Independent reflections	24521 [R_{int} = 0.0589, R_{sigma} = 0.0523]	
Completeness of theta = 28.310º	99.8	
Absorption correction	Semi-empirical from equivalents	
Max. and min. transmission	0.746 and 0.694	
Refinement method	Full-matrix least-square on F^2	
Data/restraints/parameters	24521/0/1117	
Goodness-of-fit on F^2	1.076	
Final R indexes [I>=2σ (I)]	R_1 = 0.0468, wR_2 = 0.1178	
Final R indexes [all data]	R_1 = 0.0719, wR_2 = 0.1371	
Largest diff. peak/hole	0.66/-0.69 e $Å^{-3}$	

Table S 13. Crystal data and structure refinement for 16maya_0m_a [Cu(NNP)Cl]

Identification code	16maya_0m_a	CCDC2472466
Empirical formula	$C_{33}H_{30}ClCuN_3P$	
Formula weight	598.598	
Temperature	273.15 K	
Crystal system	monoclinic	
Space group	$P2_1/c$	
Unit cell dimensions	a = 14.7065(15) Å	α = 90º
	b = 9.5484(10) Å	β = 98.113(3)º
	c = 19.838(2) Å	γ = 90º
Volume	2757.8(5)Å^3	
Z	4	
Density (calculated)	1.442 g/cm^3	
Absorption coefficient	0.975 mm^{-1}	
F(000)	1243.0	
Crystal size	0.21 × 0.18 × 0.16 mm^3	
Radiation	Mo Kα (λ = 0.71073)	
2Θ range for data collection	5.96 to 56.58	
Index ranges	$-16 \leq h \leq 19$, $-12 \leq k \leq 12$, $-26 \leq l \leq 15$	
Reflections collected	14356	
Independent reflections	6830 [R_{int} = 0.0444, R_{sigma} = 0.0684]	
Completeness of theta = 28.310º	99.6	
Absorption correction	Semi-empirical from equivalents	
Max. and min. transmission	0.746 and 0.652	
Refinement method	Full-matrix least-square on F^2	
Data/restraints/parameters	6830/0/352	
Goodness-of-fit on F^2	1.051	
Final R indexes [I>=2σ (I)]	R_1 = 0.0435, wR_2 = 0.0948	
Final R indexes [all data]	R_1 = 0.0665, wR_2 = 0.1074	
Largest diff. peak/hole	0.78/-0.73 e Å^{-3}	

Identification code	5mayc_sq	CCDC2472468
Empirical formula	$C_{67}H_{62}Cl_7Cu_3N_6P_2$	
Formula weight	1452.032	
Temperature	100.00 K	
Crystal system	monoclinic	
Space group	$P2_1/c$	
Unit cell dimensions	a = 15.946(2) Å	α = 90°
	b = 22.473(3) Å	β = 112.647(3)°
	c = 20.544(3) Å	γ = 90°
Volume	6794.4(15) $Å^3$	
Z	4	
Density (calculated)	1.420 g/cm^3	
Absorption coefficient	1.297 mm^{-1}	
F(000)	2978.	
Crystal size	0.21 × 0.18 × 0.16 mm^3	
Radiation	Mo Kα (λ = 0.71073)	
2Θ range for data collection	5.48 to 52.74	
Index ranges	$-19 \leq h \leq 19$, $-28 \leq k \leq 28$, $-25 \leq l \leq 25$	
Reflections collected	88825	
Independent reflections	13866 [R_{int} = 0.0928, R_{sigma} = 0.0609]	
Completeness of theta = 28.310°	99.8%	
Absorption correction	Semi-empirical from equivalents	
Max. and min. transmission	0.813 and 0.762	
Refinement method	Full-matrix least-square on F^2	
Data/restraints/parameters	13866/0/739	
Goodness-of-fit on F^2	1.142	
Final R indexes [I>=2σ (I)]	R_1 = 0.0519, wR_2 = 0.1415	
Final R indexes [all data]	R_1 = 0.0869, wR_2 = 0.1768	
Largest diff. peak/hole	0.71/-0.80e $Å^{-3}$	

Table S 14. Crystal data and structure refinement for 25mayb $[Cu_2(NNP)_2(\mu\text{-}Cl)Cl_2][CuCl_2]$.

Table S 15. MIC (µg/mL) of metal salts and hydride precursors against *S. aureus* ATCC29213.

Compounds	MIC (µg/mL)
$ZnCl_2$	>64
$[Pd(CH_3CN)_2Cl_2]$	>64
$[Ru(H)Cl(CO)(PPh_3)_3]$	>64
$[Ru(PPh_3)_3Cl_2]$	>64
$[Cu(CH_3CN)_4][BF_4]$	>64
$[Cu(CH_3CN)_4][PF_6]$	>64
$[Cu(CH_3CN)_4][OTf]$	>64
$CuCl_2$	>64
CuCl	>64
CuI	>64

Table S 16. MIC (µg/mL) of NNP copper complexes against *S. aureus* ATCC29213.

Compounds	MIC (µg/mL)
[Cu(NNP)I]	>64
$[Cu(NNP)(PPh_3)][BF_4]$	8
$[Cu(NNP)(CH_3CN)][BF_4]$	16
$[Cu(NNP)(CH_3CN)][OTf]$	16
$[Cu(NNP)(CH_3CN)][PF_6]$	16
[Cu(NNP)Cl]	>64
$[Cu_2(NNP)_2(\mu\text{-}Cl)Cl_2][CuCl_2]$	16

Figure S 108. Cytotoxicity profiles

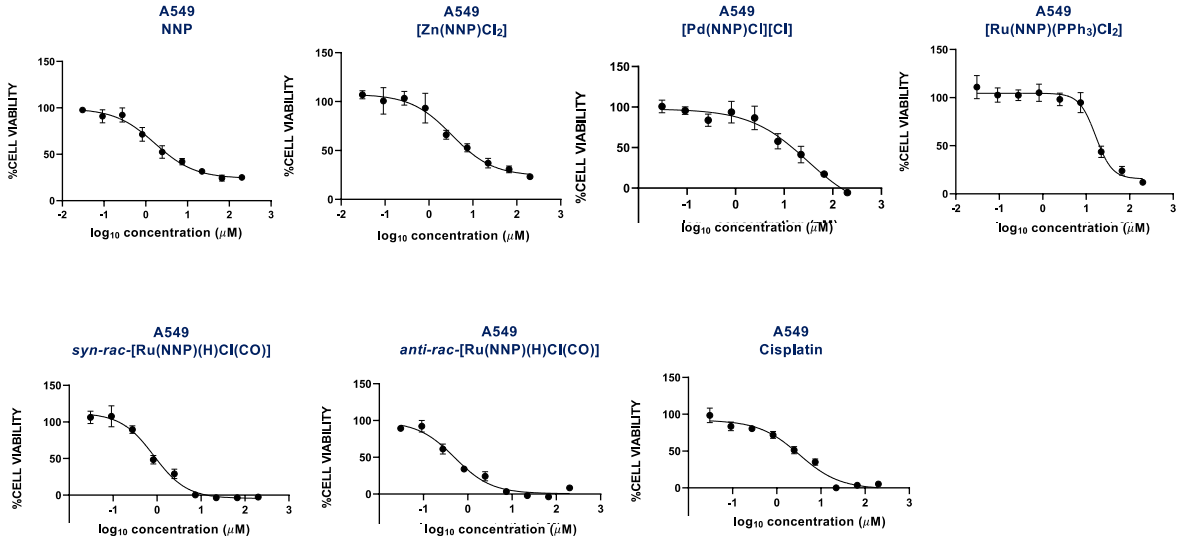

Cytotoxicity profile in A549 cell line by MTT Assay

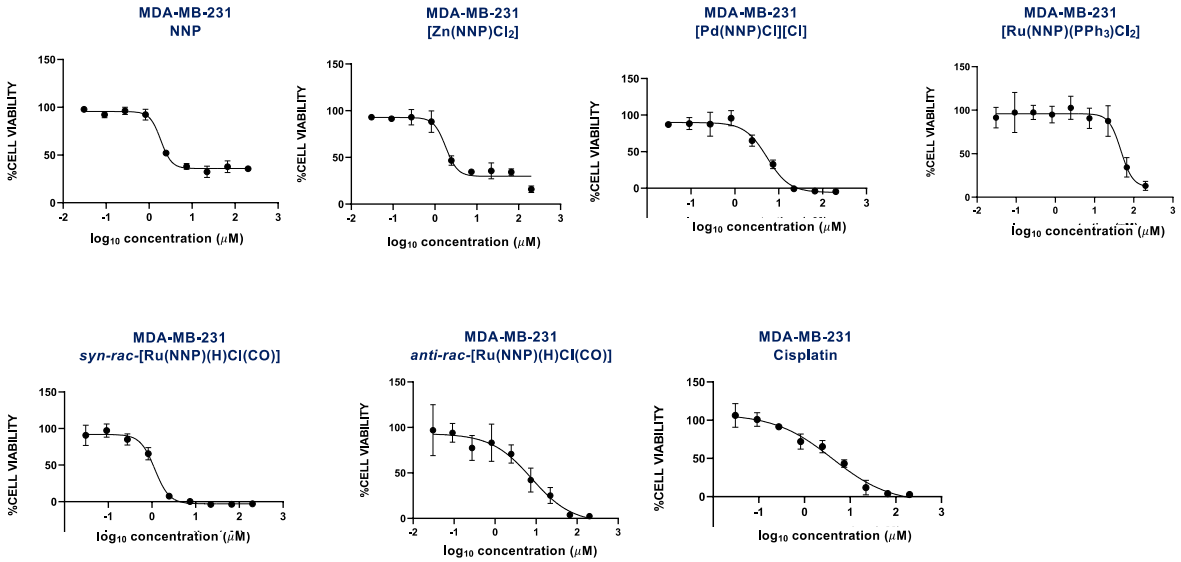

Cytotoxicity profile in MDA-MB-231 cell line by MTT Assay

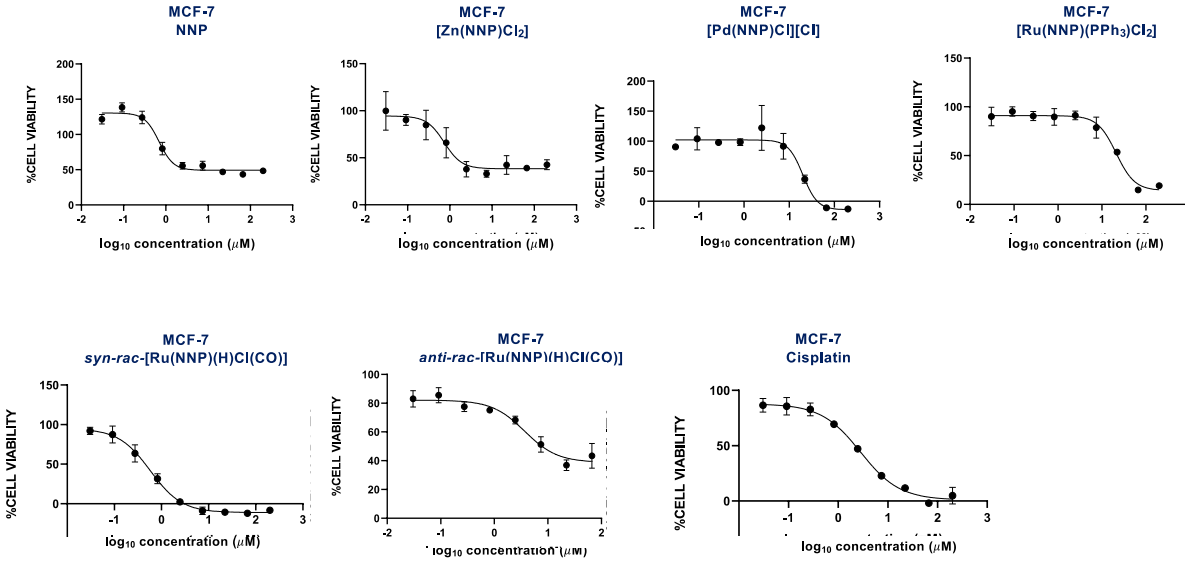

Cytotoxicity profile in MCF-7 cell line by MTT Assay

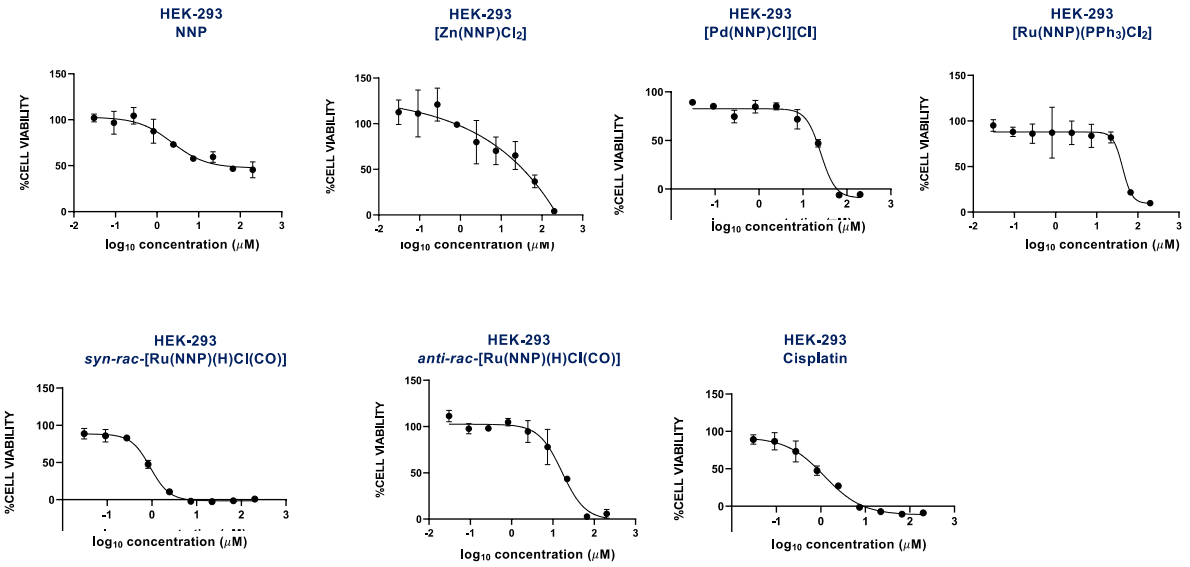

Cytotoxicity profile in HEK-293 cell line by MTT Assay